UNIVERSITAT POLITÈCNICA DE VALÈNCIA

Departamento de Máquinas y Motores Térmicos

DOCTORAL THESIS:

Modelling and analysis methodology of SI IC engines turbocharged by VGT

Presented by: D. Alejandro Gómez Vilanova
Supervised by: Dr. D. José Ramón Serrano Cruz

in fulfillment of the requirements for the degree of

Doctor of Philosophy

Valencia, October 2021

Doctoral Thesis

Modelling and analysis methodology of SI IC engines turbocharged by VGT

Presented by: D. Alejandro Gómez Vilanova
Supervised by: Dr. D. José Ramón Serrano Cruz

THESIS EXAMINERS

Dr. D. Fabio Bozza
Dr. D. Miguel Ángel Reyes Belmonte
Dr. D. Sam Akehurst

DEFENSE COMMITTEE

Chairman: Dr. D. José Galindo Lucas
Secretary: Dr. D. Fabio Bozza
Member: Dr. D. Francisco Vera García

Valencia, October 2021

Abstract

The new generation of spark ignition (SI) engines is expected to represent most of the future market share in the context of power-train with or without hybridization. Nevertheless, the current technology has still critical challenges in front to meet incoming CO2 and pollutant emissions standards. Consequently, new technologies are emerging to improve engine efficiency and meet new pollutant regulations. Among others, one of the most followed trends is engine size reduction, known as downsizing, based on the turbocharging technique. New turbocharger technologies, such as variable geometry turbines (VGT), are evaluated for their application under the demanding operating conditions of SI engines.

In this work, from experimental data obtained in an engine test cell, a 1-D complete engine model calibration methodology was conducted: a theoretical analysis aimed at ensuring full control on any aspect of the simulation. In other words, the 1-D engine model was fully fitted with respect to the experimental engine data.

Furthermore, it is evidenced the requirement of post-processing and validating the experimental data dealing with turbocharger maps, since phenomena such as heat transfer and friction losses are required to be decoupled from the so-called experimental turbocharger maps. Accordingly, a methodology for turbocharger maps obtention is presented, based on an experimental campaign divided into several test typologies and followed by the modelling stage. The modelling stage is carried out making usage of already developed integral turbocharger models available in the literature. Additionally, the improvement in the accuracy of the simulations when post-processed turbocharger maps are compared against purely experimental maps is addressed.

Taking advantage of the highly validated and physically representative 1-D gas-dynamics engine model and turbocharger validated maps, it is discussed how experimental uncertainties or "out-of-control" variables may impact the experimental results. A methodology is proposed to overcome this point from the modelling perspective. The previous allows performing exclusively turbine technologies/units comparison. In addition, taking as a basis the already developed model, it is possible to explore different optimization calculations, control strategies and provide turbine technology comparisons at engine full and partial loads in a wide range of engine speed. Also, the altitude impact

is addressed and load transients are evaluated for two analysed turbine technologies: VGT and WG.

In all, it was found that VGT technology shows fewer limitations in extreme working conditions, such as full load curve, where the WG technology represents a limitation in terms of the maximum power output. Full load differences become even more evident in altitude working conditions. When it comes to partial loads, differences in fuel consumption are minor but potentially beneficial for VGTs.

Keywords: Turbochargers; variable geometry turbines; waste-gate; 1-D engine model; experimental data

Resumen

Se espera que la nueva generación de motores de encendido provocado represente la mayor parte del mercado en el contexto de la propulsión de vehículos con o sin hibridación. Sin embargo, la tecnología actual todavía tiene desafíos críticos por delante para cumplir con los nuevos estándares de emisiones de CO2 y contaminantes. Consecuentemente están surgiendo nuevas tecnologías para mejorar la eficiencia de los motores y que estos cumplan con las nuevas normativas anti-contaminación. Entre otras, una de las tendencias más seguidas en la actualidad es la reducción de tamaño de los motores, concepto conocido como "downsizing", bajo la técnica de la turbosobrealimentación. Las nuevas tecnologías de turbocompresores, como las turbinas de geometría variable (TGV), se empiezan a considerar para su aplicación en las exigentes condiciones de funcionamiento de los nuevos motores de encendido provocado.

En este trabajo, a partir de datos experimentales obtenidos en la sala de ensayos del motor, se propone una metodología de calibración del modelo completo de motor 1-D: se realiza un análisis teórico dirigido a asegurar el control total sobre cualquier aspecto de la simulación. En otras palabras, el modelo de motor 1-D se ajustó completamente con respecto a los datos experimentales del motor.

Además, se demuestra la necesidad del postprocesamiento y validación de datos experimentales relacionados con mapas de turbocompresores, ya que se requiere desacoplar fenómenos como la transferencia de calor y las pérdidas por fricción de los denominados mapas experimentales de turbocompresores. De acuerdo con esto, se presenta una metodología para la obtención de mapas de turbocompresores, basada en una campaña experimental dividida en varias tipologias de ensayos y seguida de la etapa de modelado. La etapa de modelado se lleva a cabo utilizando modelos de turbocompresores integrales ya desarrollados o disponibles en la literatura. Adicionalmente se aborda la mejora en la precisión de las simulaciones cuando se comparan mapas de turbocompresores postprocesados con mapas puramente experimentales.

Aprovechando el modelo de motor 1-D altamente validado y físicamente representativo así como los mapas validados del turbocompresor, se discute cómo las incertidumbres experimentales o las variables "fuera de control"pueden afectar los resultados experimentales. Se propone una metodología para superar este punto desde la perspectiva del modelado. Lo anterior permite realizar

comparativas que en las se analiza exclusivamente el impacto de diferentes tecnologías de turbina o unidades de turbinas. Además, tomando como base el modelo ya desarrollado, es posible explorar diferentes cálculos de optimización, estrategias de control y proporcionar comparaciones de tecnología de turbinas en plenas cargas y cargas parciales de motor en un amplio rango de revoluciones. También se aborda el impacto de la altitud y se evalúan los transitorios de carga para dos tecnologías de turbinas analizadas: VGT y WG.

Como conclusión, se demuestra que la tecnología VGT muestra menos limitaciones en condiciones de trabajo extremas, como en la curva de plena carga, donde la tecnología WG representa una limitación en términos de máxima potencia. Las diferencias a plena carga se vuelven aún más evidentes en condiciones de trabajo en altitud. Cuando se trata de cargas parciales, las diferencias en el consumo de combustible son menores, pero potencialmente beneficiosas para los VGT.

Resum

S'espera que la nova generació de motors d'encesa per espurna representi la major part del mercat en el context de la propulsió de vehicles amb o sense hibridació. No obstant això, la tecnologia actual encara té reptes crítics per davant per complir amb els nous estàndards d'emissions de CO2 i contaminants. Conseqüentment estan sorgint noves tecnologies per millorar l'eficiència dels motors i que aquests compleixin amb les noves normatives anti-contaminació. Entre d'altres, una de les tendències més seguides en l'actualitat és la reducció de grandària dels motors, concepte conegut com "downsizing", sota la tècnica de la turbosobrealimentación. Les noves tecnologies de turbocompressors, com les VGT, es comencen a considerar per la seva aplicació en les exigents condicions de funcionament dels nous motors d'encesa per espurna.

En aquest treball, a partir de dades experimentals obtingudes a la sala d'assajos de l'motor, es proposa una metodologia de calibratge del model complet de motor 1-D: es realitza una anàlisi teòrica dirigit a assegurar el control total sobre qualsevol aspecte de la simulació. En altres paraules, el model de motor 1-D es va ajustar completament respecte a les dades experimentals del motor.

A més, es demostra la necessitat del posprocesamiento i validació de dades experimentals relacionats amb mapes de turbocompressors, ja que es requereix desacoblar fenòmens com la transferència de calor i les pèrdues per fricció dels denominats mapes experimentals de turbocompressors. D'acord amb això, es presenta una metodologia per a l'obtenció de mapes de turbocompressors, basada en una campanya experimental dividida en diverses tipologies d'assajos i seguida de l'etapa de modelatge. L'etapa de modelatge es porta a terme utilitzant models de turbocompressors integrals ja desenvolupats disponibles a la literatura. A més a s'aborda la millora en la precisió de les simulacions quan es comparen mapes de turbocompressors postprocessats amb mapes purament experimentals.

Aprofitant el model de motor 1-D validat i físicament representatiu així com els mapes validats del turbocompressor, es discuteix com les incerteses experimentals o les variables "fora de control"poden afectar els resultats experimentals. Es proposa una metodologia per superar aquest punt des de la perspectiva de la modelització. L'anterior permet realitzar exclusivament la comparació de tecnologies / unitats de turbines. A més, prenent com a base el model ja desenvolupat, és possible explorar diferents càlculs d'optimització,

estratègies de control i proporcionar comparacions de tecnologia de turbines a càrregues completes i parcials del motor en un ampli rang de revolucions del motor. També s'aborda l'impacte de l'altitud i s'avaluen els transitoris de càrrega per a dues tecnologies de turbines analitzades: VGT i WG.

com a conclusió, es demostra que la tecnologia VGT mostra menys limitacions en condicions de treball extremes, com en la corba de plena càrrega, on la tecnologia WG representa una limitació en termes de màxima potència. Les diferències a plena càrrega es tornen encara més evidents en condicions de treball en altitud. Quan es tracta de càrregues parcials, les diferències en el consum de combustible són menors, però potencialment beneficioses per als VGT.

List of publications

Alejandro Gómez-Vilanova is co-author of the publications detailed in this section, with the supervision of other members of the I.U. CMT-Motores Térmicos (CMT), and specially by Prof. José Ramón Serrano Cruz. The publications in this section are merely the publications resulting from the researching activities performed during the candidate's doctorate. The respondent carried out several experimental activities, which were analysed and processed in order to back up the studies and assumptions pretended, as well as the development of models presented in the publications. The analysis and discussion of results and procedures were done in collaboration with the thesis director (Prof. José Ramón Serrano Cruz) and with the co-authors of each publication. Each author's contribution to each study is specified in the "contributions description section" in the different studies. Any requirement to guarantee the fulfilment of the Ph.D. works, such as materials, software licenses and test benches were provided by the UPV and CMT.

The results of the works cited in this section have been improved, ordered, linked, completed, and further discussed in the present thesis manuscript. The aforementioned or whatever other publications, have been appropriately referred to, in the document itself. However, for the sake of readiness and avoidance of reiterative structure at each chapters' beginning, the publications of this list may not have been specifically cited every time, as part of the contents, figures and discussions have been partially taken from my publications.

This section compensates and justifies that the basis of the innovative component has already been presented in the publications specified in this section, therefore constituting my thesis document.

In any case, the PhD candidate becomes the last signer of the CMT members in every study/publication according to CMT members seniority signing order protocol.

[1] J. R. Serrano, F. J. Arnau, L. M. García-Cuevas, A. Gómez-Vilanova, S. Guilain, and S. Batard. "A Methodology for Measuring Turbocharger Adiabatic Maps in a Gas-Stand and Its Usage for Calibrating Control Oriented and One-Dimensional Models at Early ICE Design Stages". *Journal of Energy Resources Technology* 143.(4) (2021), pp. 1–11. ISSN: 0195-0738. DOI: 10.1115/1.4048229
Awarded as the most valuable technical paper in its track at the ICEF 2019

[2] J. R. Serrano, P. Piqueras, J. De la Morena, A. Gómez-Vilanova, and S. Guilain. "Methodological analysis of variable geometry turbine technology impact on the performance of highly downsized spark-ignition engines". *Energy* 215 (2021). ISSN: 03605442. DOI: 10.1016/j.energy.2020.119122

[3] J. R. Serrano, F. J. Arnau, P. Bares, A. Gomez-Vilanova, J. Garrido-Requena, M. J. Luna-Blanca, and F. J. Contreras-Anguita. "Analysis of a novel concept of 2-stroke rod-less opposed pistons engine (2S-ROPE): Testing, modelling, and forward potential". *Applied Energy* 282.(PA) (2021), p. 116135. ISSN: 03062619. DOI: 10.1016/j.apenergy.2020.116135. URL: https://doi.org/10.1016/j.apenergy.2020.116135

[4] J. R. Serrano, R. Payri, B. Tormos, and A. Gómez-Vilanova. "¿ Por qué es necesario seguir desarrollando motores de combustión para luchar contra la crisis climática global desde la perspectiva del transporte?" *Dyna Ingeniería e Industria* (2019), pp. 48–54. DOI: 10.23800/10329

[5] J. R. Serrano, F. J. Arnau, J. De la Morena, A. Gómez-Vilanova, S. Guilain, and S. Batard. "A methodology to calibrate Gas-Dynamic Models of turbocharged petrol egines with variable geometry turbines and with focus on dynamics prediction during tip-in load transient tests". In: *Volume 8: Industrial and Cogeneration; Manufacturing Materials and Metallurgy; Marine; Microturbines, Turbochargers, and Small Turbomachines*. Vol. 2020-june. American Society of Mechanical Engineers, 2020, pp. 22–26. ISBN: 978-0-7918-8419-5. DOI: 10.1115/GT2020-15169. URL: https://asmedigitalcollection.asme.org/GT/proceedings/GT2020/84195/Virtual,Online/1095133

[6] J. R. Serrano, F. J. Arnau, L. M. G.-C. González, A. Gómez-Vilanova, and S. Guilain. "Impact of a holistic turbocharger model in the prediction of engines performance in transient operation and in steady state with LP-EGR". in: *Volume 2: Emissions Control Systems; Instrumentation, Controls, and Hybrids; Numerical Simulation; Engine Design and Mechanical Development*. San Diego, California, USA: American Society of Mechanical Engineers, 2018, pp. 1–16. ISBN: 978-0-7918-5199-9. DOI: 10.1115/ICEF2018-9550. URL: https://asmedigitalcollection.asme.org/ICEF/proceedings/ICEF2018/51999/SanDiego,California,USA/273145

[7] J. R. Serrano, F. J. Arnau, L. M. G.-C. González, A. Gómez-Vilanova, and S. Guilain. "An experimental methodology and model for characterizing radial centrifugal compressors of turbocharged engines from diathermal perspective". In: *Advances in Mechanism and Machine Science*. Krakow, Poland: Springer International Publishing, 2019, pp. 883–892. ISBN: 978-3-030-20130-2. DOI: 10.1007/978-3-030-20131-9_88. URL: https://link.springer.com/chapter/10.1007/978-3-030-20131-9_88

Acknowledgments

Firstly, I wish to thank Dr. José Ramón Serrano for his precious time, dedication and the hundreds of meetings and hours of technical discussion and incredibly valuable guidance. I would also like to thank all the staff in CMT-Motores Térmicos that make from the researching department, an amazing researching institute and home from Monday to Friday. Special remark to José María Desantes and Francisco Payri, who opened the doors for me from the first day, and welcomed me in the researching institute, I will always remember that day.

I would also like to grate my desk colleges, who made from the PhD period, an enjoyable trip that I will always keep in mind. Especially to Roberto, Vishnu, David and Barbara with whom I have shared most of my time during the last years.

And, of course, to my parents, Jesús and Inmaculada, my sister Patricia and my girlfriend Estela to whom I owe all my achievements and the happiness and motivation with which I live every day, I am infinitely grateful to you all.

Valencia, October 2021.

"Just do it."

Nike Inc.

Contents

List of Tables

List of Figures

List of symbols

Latin characters

A	area	m^2
Air	air	$-$
CN	compressor metal thermal equivalent node	-
CO	compressor outlet	-
c_p	isobaric specific heat capacity	$J \cdot kg^{-1} \cdot K^{-1}$
H1	housing metal thermal equivalent node close to turbine	-
H2	housing metal thermal equivalent intermedium node	-
H3	housing metal thermal equivalent node close to compressor	-
h	convective coefficient	$W \cdot m^{-2} \cdot K^{-1}$
I	moment of inertia	kgm^2
h_{jb}	correcting factor for journal bearing	-
K_{jb}	correcting factor for journal bearing	-
l	characteristic length	m
$\dot{m}$	mass flow rate	$kg \cdot s^{-1}$
n	compressor rotational speed	rpm
$\dot{n}$	compressor rotational acceleration	$rev \cdot s^{-2}$
p	pressure	bar
Pr	Prandtl number	$-$
$\dot{Q}$	heat per unit of time	W
R	Radius	m
Re	Reynods number	$-$
rps	Revolutions per second	$rev \cdot s^{-1}$
s	entropy	$J \cdot K^{-1}$
TN	turbine metal thermal equivalent node	-
TO	turbine outlet	-
TURB	turbine	-
$sqrt$	square root	$-$
T	temperature	žC
$\dot{W}$	work per unit of time	W
x	coordinate in dominant direction	
$\overline{Y}$	variable Y averaged value	

Greek characters

Δ	absolute difference	$-$
ϵ	relative difference	%
η	efficiency	%
γ	politropic process exponent	$-$
κ	thermal conductivity	$W \cdot K^{-1}$
μ	dynamic viscosity	$Pa \cdot s$

Sub- and Superscripts

0	stagnation variable
1	environmental boundaries
2	compressor outlet conditions
3	turbine inlet conditions
4	turbine outlet conditions
air	dry air
cond	conduction
conv	convection
exp	experimental
mod	modelled
i	whatever thermal node or considered fluid
$i+1$	node following node i
in	intake flow
jb	journal bearing
opt	optimized
out	outlet flow
red	reduced
ref	reference value
rel	relative
s	isentropic
stoich	stoichiometric mixture
$t-s$	total to static evolution
$t-t$	total to total evolution
oil	lubricating oil
water	liquid water

Acronyms

0D	Zero dimensional
1D	One dimensional
2D	Two dimensional
2S	Two stroke
3D	Three dimensional
4S	Four stroke
AE	Adiabatized and extrapolated
AFR	Air to fuel ratio
BEV	Battery electric vehicle
BSFC	Break specific fuel consumption
BSR	Blade to speed ratio
CA10	Crank angle for 10% mixture burnt
CA50	Crank angle for 50% mixture burnt
CA90	Crank angle for 90% mixture burnt
CAD	Crank angle degrees
CFD	Computational fluid dynamics
CI	Compression ignited
CNN	Combustion neural network
CPA	Cylinder pressure analysis
CO	Carbon monoxide
CO_2	Carbon dioxide
ECU	Engine control unit
EGR	Exhaust gas recirculation
EM	Exhaust manifold
e-REX	Electric range extender
ETE	Effective turbocharger efficiency
EVC	Exhaust valve closing
FDC	Forward discharge coefficient
FMEP	Friction mean effective pressure
GWP	Global Warming Potential
HP-EGR	High pressure EGR
HT	Heat transfer
HTM	Heat transfer Multiplier
ICE	Internal combustion engine
IMEP	Indicated mean effective pressure
IVO	Intake valve opening
LP-EGR	Low pressure EGR
LPC	Low pressure compressor

ML	Mechanical losses
NNW	Neural Network
NO_x	Mono-nitrogen oxides
OC	Overall cylinder
PID	Proportional integral derivative
PMEP	Pumping mean effective pressure
PR	Pressure ratio
RDE	Real driving emissions
ROPE	Rod-less opposed piston engine
SI	Spark ignited
TC	Turbocharger
TCM	Turbocharger model
TOC	Time of combustion
TR	Trapping ratio
UHCs	Un-burnt hydrocarbons
VGT	Variable geometry turbine
VVT	Variable valve timing
WCAC	Water charge air cooling
WG	Waste gate

Chapter 1

Introduction

Contents

1.1 Background

Internal combustion engines (ICE) are the main propulsion systems in road transport nowadays. However, news call to question this fact shortly soon in favour of battery electric vehicles (BEV). Is it the end of the ICE for road transportation in favour of pure electric vehicles? Or is it necessary to further develop the ICE? May ICE's continuous improvement and latest developments help in the fight against the climate crisis from transport perspective? In this introductory section, it is discussed the impossibility of replacing ICE as power plants in most vehicles which is the main motivation of this work.

Until now, the continuous improvement of ICE (in terms of efficiency and pollutant emissions) coupled to the cheap and high-power density fuels availability, was enough to support the ICE industry medium-to-long term viability [8]. The main point that calls into question ICE's usage in the future, lies in the fact that BEV have just become an actual product in the market's catalogue. Having reached this point, at a first sight, one may be tempted to consider electric cars [9],[10] as the perfect replacement for the previous and older technology: The ICE. The last, in combination with several scandals such as diesel-gate [11] has been taken by the media as "the end of ICE" indistinctly for diesel and gasoline engines.

However, aiming to lighten this topic from an objective perspective, some research has been done, to consider all the potential drawbacks directly linked to the BEV: The first problem is that the electric motor does not use an energy source, but an energy vector. In other words, electricity does not exist as a source and cannot be accumulated in large quantities; it must be generated at the time that it is consumed. If we think of batteries as accumulators of electrical energy, they were invented a long time ago and they are still cells of chemicals that can easily be transformed into electricity as required. Despite the progress observed, batteries are an immature technology in the range of power and energy required for land transport. Therefore, they cannot compete successfully with liquid fuels. And why is it such an immature technology? There are four reasons:

- First, battery level replenishment is unacceptably long for users [12].
- Secondly, the energy density is unacceptably low. With real ranges below the desired ones [13].

- Thirdly, battery life is limited and shorter than the life of the vehicle itself. Studies such as Tang et al. [14] and Polzin et al. [15] are a good proof of this problem associated with more electronic waste than recycling.

- Fourthly, the supply of raw materials for their manufacture (nickel, lithium, cobalt, copper, manganese, etc.) is a pressing problem since they are reaching exorbitant prices [16]. As an example, the main problem today is the supply of cobalt, necessary for the cathode of lithium-ion batteries. This mineral is extracted mainly in the Democratic Republic of Congo, where human rights are violated through child labour and the lack of safety in mines, among many other realities. Then it reaches international markets, and its origin is diluted due to the scarce existing traceability. Finally, it is primarily refined in China, adding geopolitical problems to the insecurity of supply. In all, this makes the final product more expensive and less accessible to be distributed to the overall population [17]. As an example, a Tesla Model X needs 7 kg per vehicle and a Tesla Model 3 about 4.5 kg. Recent studies confirm that the price of an electric car is about 75.5% more expensive (at initial cost) compared to traditional vehicles, even with regional subsidies promoting BEV [18].

The second problem lies in the fact that electricity is produced in most cases from non-renewable energy sources (with around 60% losses) and transported afterwards (with additional losses of about 20%). Unfortunately, renewable sources account for barely 12% of the world's energy consumption mix and we do not have a medium-term forecast that this figure will increase significantly. The previous is clearly reflected in Figure 1.1, from Our world in data [19]. The data from Figure 1.1 comprises of a combination of data from [20] and [21]. This analysis is highly relevant as it is a global analysis and not a state or urban one.

In some countries such as the US, China, Russia, Poland, South Korea and Germany, fossil fuels, including a good percentage of coal, remain the largest source of energy as a raw material for electricity production. Among G8 countries with real alternatives to technologies that emit CO2, there is only one: France, and this is due to its continued commitment to nuclear energy. Therefore, with the current energy mix and with a complete life cycle analysis, the so-called cradle-to-grave analysis, the alternative of electric motors will not eliminate global CO2 emissions. Keeping in mind that CO2 emissions are a

global problem, not particular from Europe, moving from ICE to batteries-based technology would not solve the problem at all in the medium-term.

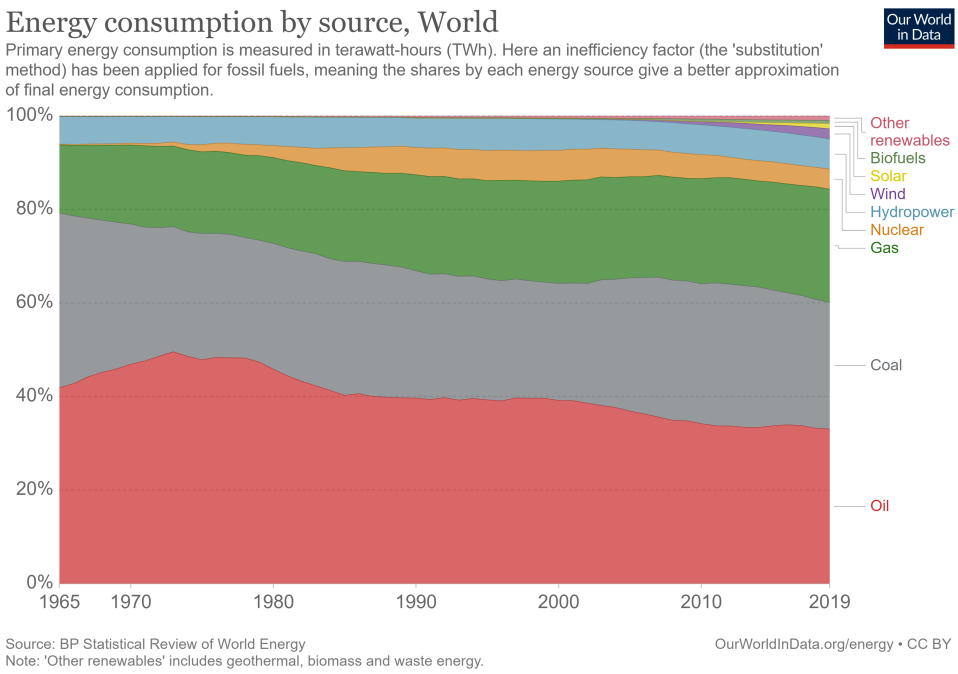

Figure 1.1: World energy consumption by source

In April 2019, Prof. Dr. Hans-Werner Sinn et al. from the German IFO (Institute Center for Economic Studies, CESifo GmbH) concluded that with the German energy mix, a Tesla Class 3 emits in its useful life from 156 to 180 gCO2 / km. This is between 11% and 28% more than modern Diesel E6d Temp [22]. At this time, an analysis from the cradle-to-the-grave of the process of total electrification of transport shows that gaseous emissions would only be relocating from the cities to the surroundings of large thermal power plants and production centres, as Dr. Maarten Messagie, from the Universiteit Brussel - MOBI research group pointed out [23].

Unfortunately, the problem of global warming cannot be "relocated". In short, with the massive electrification of the car fleet and with the current world energy mix, it is only possible to aspire to relocate the CO2 emitted. But what is worse, no substantial changes are foreseen in the current elec-

tricity mix between now and 2030 so that the electrification of transport is not a clear solution to the problem of climate change. Regarding greenhouse gas emissions and the Global Warming Potential (GWP), the contribution of transport to global GWP emissions in equivalent tons of CO2 remains at 16% (road transport about 11.9%). This can be seen in Figure 1.2, produced by Our World in Data [24]. Industry, buildings, agriculture, resource extraction, garbage processing, energy production (for among other things heating systems and air conditioning in homes) do the rest. Therefore, a massive global change to electric vehicles would mean a global potential reduction of 11.9% in the equivalent emitted tons of CO2. This potential reduction would only be possible if every BEV charges its battery from "free-of-CO2-energy", basically renewable and nuclear, which is an unrealistic situation nowadays, as well as in the medium-term.

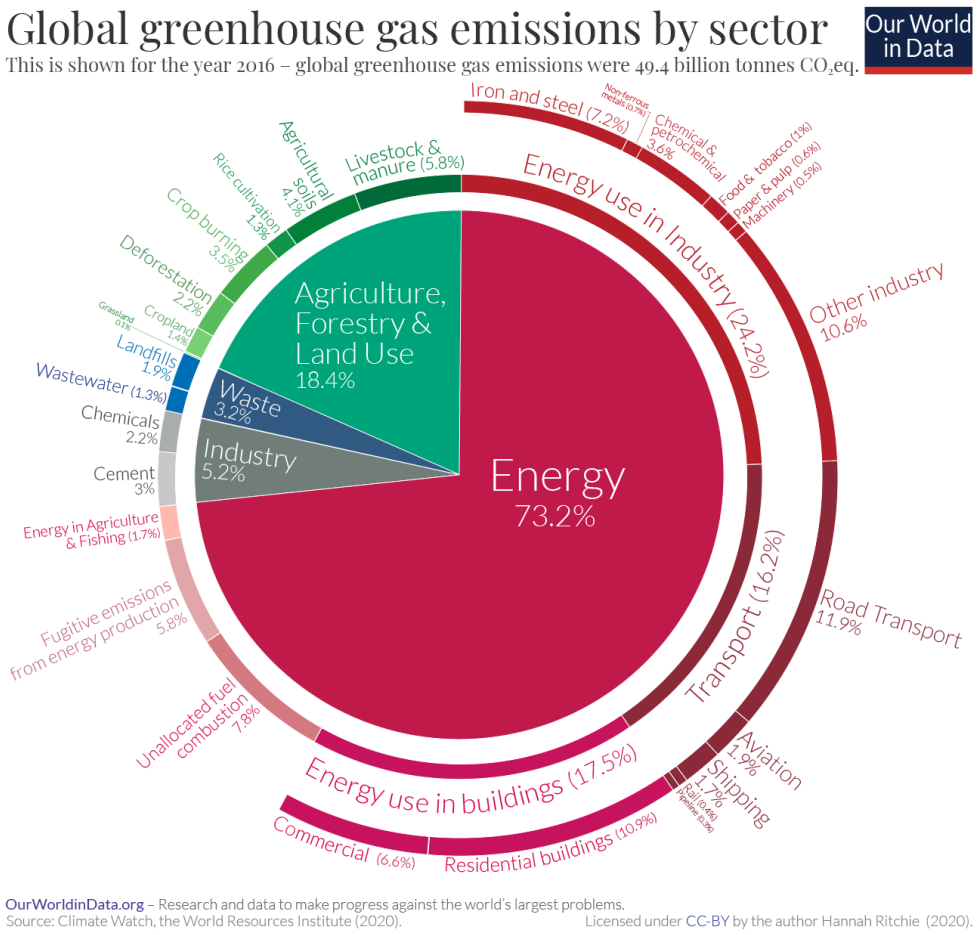

Figure 1.2: Greenhouse gas emissions by sector in 2016. Road transport 11.9%

Finally, the following example clarifies the interest in further developing ICE: One of the latest sport utility vehicles (SUV) and purely electric, has been equipped with a 99kWh battery. Attending to the study developed by [25] each kWh of battery is associated with 177kg equivalent CO2 emissions. Accordingly, the analysed 99kWh battery vehicle results in 17523kg equivalent CO2 emissions, for just building the battery. In conjunction with the rest of the electrical systems and the rest of the vehicle, the overall emissions reach approximately 24700Kg of equivalent CO2 emissions. Assuming an energy consumption of 21kWh each 100km and in the context of the Spaniard energy

mix, where the electricity production is about 240g/kWh, the equivalent CO2 emissions each 100km result in 5.04kg. Parallelly, building an equivalent ICE vehicle would require 5500Kg of equivalent CO2 emissions (again, according to [25] 4200km coming from the chassis and 1300 from the gasoline engine production). Assuming a fuel consumption of 7l/100Km, the equivalent CO2 emissions would be around 16.63kg each 100km. In all, it would take around 165700km until the CO2 emissions of both vehicles equal each other. If one considers a diesel engine, building the power unit takes approximately 20.8% more than the gasoline choice (in terms of CO2). However, assuming that fuel consumption is about 6l/100km, the CO2 emissions of the diesel vehicles would be lower than the ones of the BEV during the first 205000km. To the previous, it should be added the battery disposal problems.

1.2 Motivation

Nowadays, moving from traditional cars to electric cars (not paying attention to the subsequent CO2 emissions that such a massive transformation would imply) would mean a reduction in GWP gas emissions of less than 12% (the portion of renewable energy generation in the world mix) times the 11.9% (road transport contribution to CO2 emissions) that results in approximately a 1.4% of CO2 emissions reduction.

Future limitations on greenhouse gases (CO2), gaseous pollutants, and noise emissions will be more severe as it has happened in the last years with new regulations [26], [27]. Real Driving Emissions (RDE) regulations are being adopted in the main economic zones worldwide [28], [29]. Aspects such as cold start [30] and actual fuel consumption [31] are more deeply studied since real driving cycles include such working conditions. The last, forces engine manufacturers and the automotive industry to invest and research in more innovative and sophisticated technologies, such as passive pre-chambers in combination with lower carbon content fuels [32], additives for diesel [33] and better understanding and modelling of turbocharger concepts for more sophisticated engine boosting [34]. Research in catalyst chemistry offers interesting possibilities for the exhaust gases after-treatment [35].

Also, hybridization takes an important role, [36] and [37] are an example of traditional engines adapted to hybrid configurations. Apart from the "traditional" engines and working operation principles, new/innovative engine

architectures, specifically developed for hybrid configurations, as the range-extender, take place. In comparison to traditional spark/compression ignition engines, range extenders' operative area is drastically reduced. Hence, the range extender engines call for a higher simplicity and compactness. These engines are conceived to work in a reduced operative range, with the duty of recharging a battery, as in [38], based on the engine studied in [3], for series-hybrid configuration in the automotive field. [3] deals with an SI-ICE, based on a 2-stroke cycle and on a rod-less opposed-piston engine (2S-ROPE), which consists of a rotative mechanism based in a crank-shaft with faced cams perpendicular to the opposed pistons skirts, see Figure 1.3. Its electric range-extender layout is known as e-REX, Figure 1.4.

In other words, the homologation cycles pose additional challenges for auto-makers and lead to new technologies, as this vastly expands the operational range of the ICE in which pollutant emissions must be kept below type approval limits. Today, nothing is too innovative or risky to meet the expected medium-term pollutants' reduction demand. Finally, fossil fuels are still cheap and readily available. Oil depletion is no longer a topic of discussion, as fracking technology has offered a new paradigm, making the United States the world's largest producer of fossil fuels [21].

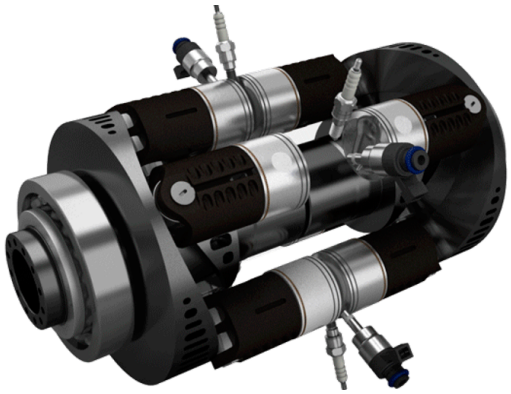

Figure 1.3: 2S-ROPE engine

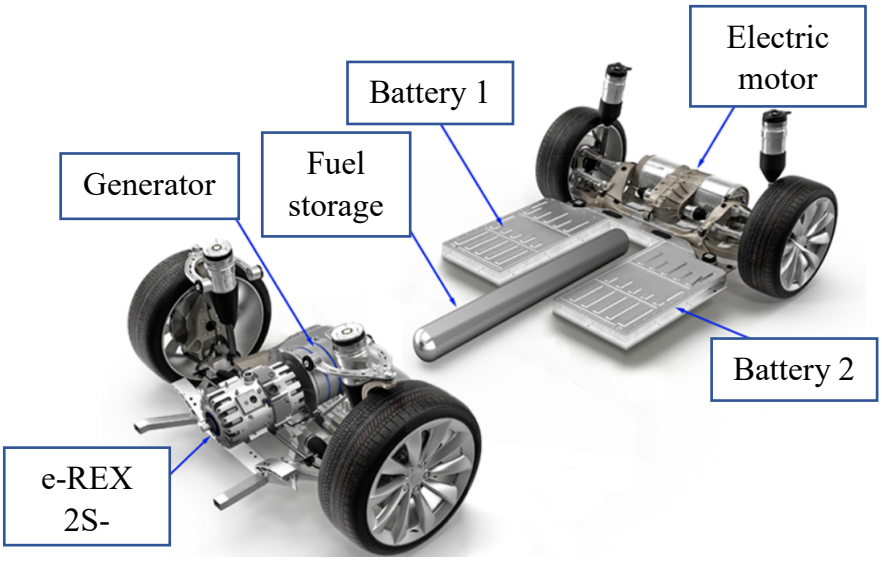

Figure 1.4: 2S-ROPE engine in an hybrid architecture: e-REX version

A revolution is coming from traditional gasoline and diesel engines, and the boundaries between both are rapidly blurring as a deeper understanding and greater control of any aspect is gained. Furthermore, it is not only about fuel consumption and pollutant emissions, but also about improving the engine response for safety and driving experience reasons, for example new turbocharger technologies [39] and hybridization [40] which are part of the ICE environment, all dedicated to further optimize and improve nowadays engines.

Among all the engine aspects stated in the previous section, it is turbocharging the SI engine the main phenomenon to be studied in this thesis.

Thanks to turbocharging, it is possible to downsize and down-speed the ICE [41], the reduction of mechanical and heat losses is guaranteed, thus contributing to further reduce the BSFC and, hence, the CO2 emissions. This point has led the vast majority of nowadays engine manufacturers to turbocharge their ICE catalogue.

Smaller engine architectures imply higher engine boosting if the performance is attempted to be kept. Consequently, the turbocharger operation and its interaction with the rest of the engine hardware becomes a critical

point and has led to invest and consider new turbocharger technologies, going from fixed compressor and turbines, to variable geometry compressor and turbines [42] to guarantee the most suitable "turbocharger size" at each engine operative area. The previous shows the importance of the TC-ICE interaction for proper engine output figures.

In other words, new turbocharger technologies in the context of series ICE engines become potential solutions when improving nowadays' fuel consumption and power figures. Some examples of nowadays efforts in improving the turbocharger units themselves are:

- Twin-scroll turbocharging [43] for pulse interaction avoidance.
- Self-recirculating case treatment [44] for surge margin retard.
- Ball-bearing technologies [45] in order to diminish friction losses in the turbocharger shaft.
- Combinations of variable geometry and twin-scroll [46].
- Dual-stage turbocharger systems with the target of optimizing engine performance and transient response simultaneously [47].
- Hybrid turbochargers and their management optimization [48].

In the current study, variable geometry turbines (VGT), are compared to the SI ICE standard turbine: the waste-gate (WG). In WG turbines, part of the exhaust gas flow by-passes a fixed turbine geometry. Therefore, the amount of by-passed flow becomes the boost-level controlling parameter. By-passing the turbine as a boost pressure control strategy, partially wastes the available exhaust gas flow enthalpy, damaging the turbocharger efficiency. By contrast, VGT technology modifies the vanes' passage geometry to fulfil the boost demand. Since all the exhaust mass flow goes through the turbine, VGT provides higher efficiency and result in a better matching throughout a wider operative range [42].

Nevertheless, the VGT technology can suffer from deformation and the eventual stack of the mechanism when exposed at high temperatures. For this reason, its usage has been widely extended in the context of compression-ignition engines, where the maximum turbine inlet temperatures are lower

than the ones in SI engines: In diesel engines, turbine inlet temperature rarely overcomes the barrier of 870ºC, while in gasoline engines, the value of 960ºC can be surpassed at full load. However, material technology improvements (partially motivated by SI engines requirements) led to the first VGT prototypes for SI application.

1.3 Objectives

In this work, it is compared the VGT against WG turbine technology, in the context of highly downsized SI engines. For this purpose, an experimental campaign is developed, making usage of several experimental facilities in the CMT-Motores térmicos Researching Institute. Taking advantage of these experimental campaigns, a well-calibrated model is obtained to proceed with an accurate technology comparison in which no experimental uncertainty implies any bias. Also, the differences in terms of compressors (in any turbocharger assembly) performance can be avoided by configuring "iso-compressor" simulations for example. The procedure followed in this work is the one that follows:

- In the current chapter 1, it is discussed the relevance and the necessity of developing and improving ICE nowadays. As well, some recent studies dealing with engine improvements and new engine architectures are included. Finally, the importance of turbocharging the ICE is evidenced in the new turbocharger technologies arising and being implemented in the automotive market and researching field.

- Literature review and state of the art is included in chapter 2. In this chapter, the importance of heat transfer and mechanical losses effects in turbochargers are discussed. As well, a brief review of previous works dealing with the complete TC modelling is presented. The state of the art also includes a brief review of nowadays implementation and studies dealing with VGT and SI engines.

- The experimental campaign and modelling methodology focused on obtaining a validated 1-D engine model is included in chapter 3. Here, the complete engine model is fitted according to the experimental campaign carried out. However, in chapter 3 it is also evidenced that it is required

to carry out a specific experimental and modelling methodology to well-reproduce the TC units performance. The previous results in a complete engine-turbocharger validated model which can be used for prospective modelling and theoretical studies such as in chapter 4 is presented.

- In chapter 4, the validated 1D model is used for a comparison between VGT and WG turbine technologies. This section also includes calculations dealing with full loads and partial loads, altitude working conditions, VVT optimization... Deep comparisons can be made between turbine technologies, without any kind of experimental uncertainty or compressor technology differences. To finish with chapter 4, it is proposed a control methodology for the VGT management under transient operation.

- Finally, the main conclusions, findings and most relevant items would be summarized in the conclusions dedicated chapter 5. Also, future works and potentially interesting studies are pointed out.

Chapter 1 Bibliography

[3] J. R. Serrano, F. J. Arnau, P. Bares, A. Gomez-Vilanova, J. Garrido-Requena, M. J. Luna-Blanca, and F. J. Contreras-Anguita. "Analysis of a novel concept of 2-stroke rod-less opposed pistons engine (2S-ROPE): Testing, modelling, and forward potential". *Applied Energy* 282.(PA) (2021), p. 116135. ISSN: 03062619. DOI: 10.1016/j.apenergy.2020.116135. URL: https://doi.org/10.1016/j.apenergy.2020.116135 (cit. on pp. xii, 8).

[8] J. R. Serrano. "Imagining the future of the internal combustion engine for ground transport in the current context". *Applied Sciences (Switzerland)* 7.(10) (2017). ISSN: 20763417. DOI: 10.3390/app7101001 (cit. on p. 2).

[9] T. Gnann, P. Plötz, S. Funke, and M. Wietschel. "What is the market potential of plug-in electric vehicles as commercial passenger cars? A case study from Germany". *Transportation Research Part D: Transport and Environment* 37.(2015) (2015), pp. 171–187. ISSN: 13619209. DOI: 10.1016/j.trd.2015.04.015. URL: http://dx.doi.org/10.1016/j.trd.2015.04.015 (cit. on p. 2).

[10] S. Bobeth and I. Kastner. "Buying an electric car: A rational choice or a norm-directed behavior?" *Transportation Research Part F: Traffic Psychology and Behaviour* 73 (2020), pp. 236–258. ISSN: 13698478. DOI: 10.1016/j.trf.2020.06.009. URL: https://doi.org/10.1016/j.trf.2020.06.009 (cit. on p. 2).

[11] C. Brand. "Beyond 'Dieselgate': Implications of unaccounted and future air pollutant emissions and energy use for cars in the United Kingdom". *Energy Policy* 97 (2016), pp. 1–12. ISSN: 03014215. DOI: 10.1016/j.enpol.2016.06.036. URL: http://dx.doi.org/10.1016/j.enpol.2016.06.036 (cit. on p. 2).

[12] M. Neaimeh, S. D. Salisbury, G. A. Hill, P. T. Blythe, D. R. Scoffield, and J. E. Francfort. "Analysing the usage and evidencing the importance of fast chargers for the adoption of battery electric vehicles". *Energy Policy* 108.(December 2016) (2017), pp. 474–486. ISSN: 03014215. DOI: 10.1016/j.enpol.2017.06.033 (cit. on p. 2).

[13] M. E. López-Lambas, A. Monzón, and G. Pieren. "Analysis of using electric car for urban mobility, perceived satisfaction among university users." *Transportation Research Procedia* 27 (2017), pp. 524–530. ISSN: 23521465. DOI: 10.1016/j.trpro.2017.12.132. URL: https://doi.org/10.1016/j.trpro.2017.12.132 (cit. on p. 2).

[14] L. Tang, G. Rizzoni, and A. Cordoba-Arenas. "Battery Life Extending Charging Strategy for Plug-in Hybrid Electric Vehicles and Battery Electric Vehicles". *IFAC-PapersOnLine* 49.(11) (2016), pp. 70–76. ISSN: 24058963. DOI: 10.1016/j.ifacol.2016.08.011. URL: http://dx.doi.org/10.1016/j.ifacol.2016.08.011 (cit. on p. 3).

[15] I. Bloom et al. "An accelerated calendar and cycle life study of Li-ion cells". *Journal of Power Sources* 101.(2) (2001), pp. 238–247. ISSN: 03787753. DOI: 10.1016/S0378-7753(01)00783-2 (cit. on p. 3).

[16] B. Jones, R. J. Elliott, and V. Nguyen-Tien. "The EV revolution: The road ahead for critical raw materials demand". *Applied Energy* 280.(April) (2020), p. 115072. ISSN: 03062619. DOI: 10.1016/j.apenergy.2020.115072. URL: https://doi.org/10.1016/j.apenergy.2020.115072 (cit. on p. 3).

[17] J. Zhao, X. Xi, Q. Na, S. Wang, S. N. Kadry, and P. M. Kumar. "The technological innovation of hybrid and plug-in electric vehicles for environment carbon pollution control". *Environmental Impact Assessment*

Review 86.(October 2020) (2021). ISSN: 01959255. DOI: 10.1016/j.eiar.2020.106506 (cit. on p. 3).

[18] G. Milev, A. Hastings, and A. Al-Habaibeh. "The environmental and financial implications of expanding the use of electric cars - A Case study of Scotland". *Energy and Built Environment* 2.(2) (2021), pp. 204–213. ISSN: 26661233. DOI: 10.1016/j.enbenv.2020.07.005. URL: https://doi.org/10.1016/j.enbenv.2020.07.005 (cit. on p. 3).

[19] H. Ritchie and M. Roser. "Energy". *Our World in Data* (2020). URL: https://ourworldindata.org/energy (cit. on p. 3).

[20] V. Smil. *Energy Transitions: Global and National Perspectives (Expanded and updated edition)*. 2nd ed. Vol. 30. 4. Praeger; 2 edition (Dec 31 2016), 2017, p. 297. ISBN: 144085324X. URL: http://vaclavsmil.com/2016/12/14/energy-transitions-global-and-national-perspectives-second-expanded-and-updated-edition/ (cit. on p. 3).

[21] BP. *Statistical Review of World Energy globally consistent data on world energy markets . and authoritative publications in the field of energy The Statistical Review world of World Energy and data on world energy markets from is The Review has been providing.* Tech. rep. BP, 2020, p. 66. URL: https://www.bp.com/content/dam/bp/business-sites/en/global/corporate/pdfs/energy-economics/statistical-review/bp-stats-review-2020-full-report.pdf (cit. on pp. 3, 8).

[22] C. Buchal, H.-D. Karl, and H.-W. Sinn. "Kohlemotoren, Windmotoren und Dieselmotoren: Was zeigt die CO2-Bilanz?" *ifo Schnelldienst* 8.(April) (2019), pp. 40–54. URL: ifosd-v72-y2019-i08-p40-54.pdf (cit. on p. 4).

[23] Maarten Messagie. "Life Cycle Analysis of the Climate Impact of Electric Vehicles". *Transport and Environment* (2017), p. 14 (cit. on p. 4).

[24] H. Ritchie and M. Roser. "CO and Greenhouse Gas Emissions". *Our World in Dat* (2020). URL: https://ourworldindata.org/co2-and-other-greenhouse-gas-emissions (cit. on p. 5).

[25] R. Kawamoto, H. Mochizuki, Y. Moriguchi, T. Nakano, M. Motohashi, Y. Sakai, and A. Inaba. "Estimation of CO2 Emissions of internal combustion engine vehicle and battery electric vehicle using LCA". *Sus-*

tainability (Switzerland) 11.(9) (2019). ISSN: 20711050. DOI: 10.3390/su11092690 (cit. on pp. 6, 7).

[26] E. Massaguer, A. Massaguer, T. Pujol, M. Comamala, L. Montoro, and J. R. Gonzalez. "Fuel economy analysis under a WLTP cycle on a mid-size vehicle equipped with a thermoelectric energy recovery system". *Energy* 179 (2019), pp. 306–314. ISSN: 03605442. DOI: 10.1016/j.energy.2019.05.004. URL: https://doi.org/10.1016/j.energy.2019.05.004 (cit. on p. 7).

[27] J. Pavlovic, B. Ciuffo, G. Fontaras, V. Valverde, and A. Marotta. "How much difference in type-approval CO2 emissions from passenger cars in Europe can be expected from changing to the new test procedure (NEDC vs. WLTP)?" *Transportation Research Part A: Policy and Practice* 111.(October 2017) (2018), pp. 136–147. ISSN: 09658564. DOI: 10.1016/j.tra.2018.02.002 (cit. on p. 7).

[28] K. Kurtyka and J. Pielecha. "The evaluation of exhaust emission in RDE tests including dynamic driving conditions". *Transportation Research Procedia* 40 (2019), pp. 338–345. ISSN: 23521465. DOI: 10.1016/j.trpro.2019.07.050. URL: https://doi.org/10.1016/j.trpro.2019.07.050 (cit. on p. 7).

[29] R. Suarez-Bertoa, P. Mendoza-Villafuerte, F. Riccobono, M. Vojtisek, M. Pechout, A. Perujo, and C. Astorga. "On-road measurement of NH3 emissions from gasoline and diesel passenger cars during real world driving conditions". *Atmospheric Environment* 166 (2017), pp. 488–497. ISSN: 18732844. DOI: 10.1016/j.atmosenv.2017.07.056. URL: http://dx.doi.org/10.1016/j.atmosenv.2017.07.056 (cit. on p. 7).

[30] A. Zare et al. "Cold-start NOx emissions: Diesel and waste lubricating oil as a fuel additive". *Fuel* 286.(P2) (2021). ISSN: 00162361. DOI: 10.1016/j.fuel.2020.119430. URL: https://doi.org/10.1016/j.fuel.2020.119430 (cit. on p. 7).

[31] J. Pavlovic, G. Fontaras, S. Broekaert, B. Ciuffo, M. A. Ktistakis, and T. Grigoratos. "How accurately can we measure vehicle fuel consumption in real world operation?" *Transportation Research Part D: Transport and Environment* 90.(December 2020) (2021). ISSN: 13619209. DOI: 10.1016/j.trd.2020.102666. URL: https://doi.org/10.1016/j.trd.2020.102666 (cit. on p. 7).

[32] R. Novella, J. Gomez-Soriano, P. J. Martinez-Hernandiz, C. Libert, and F. Rampanarivo. "Improving the performance of the passive pre-chamber ignition concept for spark-ignition engines fueled with natural gas". *Fuel* 290.(November 2020) (2021). ISSN: 00162361. DOI: 10.1016/j.fuel.2020.119971. URL: https://doi.org/10.1016/j.fuel.2020.119971 (cit. on p. 7).

[33] T. Kegl, A. Kovač Kralj, B. Kegl, and M. Kegl. "Nanomaterials as fuel additives in diesel engines: A review of current state, opportunities, and challenges". *Progress in Energy and Combustion Science* 83 (2021). ISSN: 03601285. DOI: 10.1016/j.pecs.2020.100897 (cit. on p. 7).

[34] J. Galindo, J. R. Serrano, L. M. García-Cuevas, and N. Medina. "Using a CFD analysis of the flow capacity in a twin-entry turbine to develop a simplified physics-based model". *Aerospace Science and Technology* 112 (2021). ISSN: 12709638. DOI: 10.1016/j.ast.2021.106623. URL: https://doi.org/10.1016/j.ast.2021.106623 (cit. on p. 7).

[35] F. Dong and K. Yamazaki. "The Pt-Pd alloy catalyst and enhanced catalytic activity for diesel oxidation". *Catalysis Today* (July) (2020). ISSN: 09205861. DOI: 10.1016/j.cattod.2020.08.019. URL: https://doi.org/10.1016/j.cattod.2020.08.019 (cit. on p. 7).

[36] A. F. Abdul-Manan, H. W. Won, Y. Li, S. M. Sarathy, X. Xie, and A. A. Amer. "Bridging the gap in a resource and climate-constrained world with advanced gasoline compression-ignition hybrids". *Applied Energy* 267.(April) (2020), p. 114936. ISSN: 03062619. DOI: 10.1016/j.apenergy.2020.114936. URL: https://doi.org/10.1016/j.apenergy.2020.114936 (cit. on p. 7).

[37] H. Dong, J. Fu, Z. Zhao, Q. Liu, Y. Li, and J. Liu. "A comparative study on the energy flow of a conventional gasoline-powered vehicle and a new dual clutch parallel-series plug-in hybrid electric vehicle under NEDC". *Energy Conversion and Management* 218.(March) (2020). ISSN: 01968904. DOI: 10.1016/j.enconman.2020.113019. URL: https://doi.org/10.1016/j.enconman.2020.113019 (cit. on p. 7).

[38] J. R. Serrano, A. García, J. Monsalve-Serrano, and S. Martínez-Boggio. "High efficiency two stroke opposed piston engine for plug-in hybrid electric vehicle applications: Evaluation under homologation and real driving conditions". *Applied Energy* 282.(October 2020) (2021). ISSN: 03062619. DOI: 10.1016/j.apenergy.2020.116078 (cit. on p. 8).

[39] Q. Tang, J. Fu, J. Liu, B. Boulet, L. Tan, and Z. Zhao. "Comparison and analysis of the effects of various improved turbocharging approaches on gasoline engine transient performances". *Applied Thermal Engineering* 93 (2016), pp. 797–812. ISSN: 13594311. DOI: 10.1016/j.applthermaleng.2015.09.063 (cit. on p. 9).

[40] W. Geng, D. Lou, C. Wang, and T. Zhang. "A cascaded energy management optimization method of multimode power-split hybrid electric vehicles". *Energy* 199 (2020), p. 117224. ISSN: 03605442. DOI: 10.1016/j.energy.2020.117224. URL: https://doi.org/10.1016/j.energy.2020.117224 (cit. on p. 9).

[41] H. Hiereth and P. Prenninger. *Charging the Internal Combustion Engine*. Springer, Vienna, 2007, pp. 1–268. ISBN: 978-3-211-47113-5. DOI: 10.1007/978-3-211-47113-5 (cit. on pp. 9, 32).

[42] A. J. Feneley, A. Pesiridis, and A. M. Andwari. "Variable Geometry Turbocharger Technologies for Exhaust Energy Recovery and Boosting-A Review". *Renewable and Sustainable Energy Reviews* 71.(September 2015) (2017), pp. 959–975. ISSN: 18790690. DOI: 10.1016/j.rser.2016.12.125. URL: http://dx.doi.org/10.1016/j.rser.2016.12.125 (cit. on pp. 10, 32).

[43] N. Brinkert, S. Sumser, S. Weber, K. Fieweger, A. Schulz, and H.-J. Bauer. "Understanding the Twin Scroll Turbine: Flow Similarity". *Journal of Turbomachinery* 135.(2) (2012), p. 021039. ISSN: 0889-504X. DOI: 10.1115/1.4006607 (cit. on p. 10).

[44] Y. Mingyang, M. botas Ricardo, D. Kangyao, Z. Yangjun, and Z. Xinqian. "Unsteady influence of Self Recirculation Casing Treatment (SRCT) on high pressure ratio centrifugal compressor". *International Journal of Heat and Fluid Flow* 58 (2016), pp. 19–29. ISSN: 0142727X. DOI: 10.1016/j.ijheatfluidflow.2015.12.004 (cit. on p. 10).

[45] D. Zeppei, S. Koch, and A. Rohi. "Ball Bearing Technology for Passenger Car Turbochargers". *MTZ worldwide* 77.(11) (2016), pp. 26–31. DOI: 10.1007/s38313-016-0109-z (cit. on pp. 10, 31).

[46] S. Rajoo, A. Romagnoli, and R. F. Martinez-Botas. "Unsteady performance analysis of a twin-entry variable geometry turbocharger turbine". *Energy* 38.(1) (2012), pp. 176–189. ISSN: 03605442. DOI: 10.1016/j.energy.2011.12.017. URL: http://dx.doi.org/10.1016/j.energy.2011.12.017 (cit. on p. 10).

[47] B. Lee, D. Jung, D. Assanis, and Z. Filipi. "Dual-stage turbocharger matching and boost control options". In: *Proceedings of the Spring Technical Conference of the ASME Internal Combustion Engine Division*. January. 2008, pp. 267–277. ISBN: 0791848132. DOI: 10.1115/ICES2008-1692 (cit. on p. 10).

[48] H. Dong, Z. Zhao, J. Fu, J. Liu, J. Li, K. Liang, and Q. Zhou. "Experiment and simulation investigation on energy management of a gasoline vehicle and hybrid turbocharger optimization based on equivalent consumption minimization strategy". *Energy Conversion and Management* 226.(August) (2020). ISSN: 01968904. DOI: 10.1016/j.enconman.2020.113518. URL: https://doi.org/10.1016/j.enconman.2020.113518 (cit. on p. 10).

Chapter 2

State of the art

Contents

2.1 Introduction

In this chapter, it is provided a review of turbochargers' modelling approaches and key points state of the art. There are several uncertainties, physical phenomena and experimental limitations which were not considered in the past. However, with the forward ICE downsizing, the role of the turbocharger in the context of the ICE becomes more relevant, in conjunction with all the collateral arising phenomena.

Therefore, physical phenomena such as heat transfer and mechanical losses become of high interest to properly model turbocharged engines at any operating point.

Also, a literature review about boosting the SI engine, specifically by means of VGT technology, is made.

Finally, a background section is provided, in order to highlight the starting point in this thesis and show an example in which is evidenced the potential of well-predicting engine-turbocharger variables when taking validated turbocharger models.

2.2 Turbocharger modelling

New coming policies dealing with pollutant emissions and fuel consumption, force engine developers to forward downsize the engines and take into consideration operative areas and physical phenomena that previously were not as important as nowadays.

Some examples of the previous can be found in studies like the one by Ding et al. [49], who employed a turbine 1D model for evaluating its performance at pulsating conditions such as those occurring in ICE. Bozza et al. [50] also explored exhaust gas recirculation to overcome turbine inlet temperature limitations through 1D engine modelling. In other works such as in Sandoval et al. [51], it was developed a methodology to characterize turbocharger performance on driving conditions.

The aforementioned studies, show the importance and efforts in this field, to better understand and overcome the technical problems arising nowadays

because of the new restrictions and market demands.To improve the ICE from the turbocharging activities perspective, a deeper knowledge is necessary from the earliest modelling stages. The key points in which researching efforts are being made can be divided into four: Heat transfer effects, TC maps limited experimental information, friction losses effects and pulsating and unsteady flow. The state of the art in the four mentioned researching fields corresponds to the next subsections.

2.2.1 Heat transfer effects

Turbocharger maps are recorded in gas stands, specifically designed, assembled and equipped for this purpose. Afterwards, the obtained data are used to build the look-up tables that constitute the so-called "turbocharger maps" for later modelling purposes i.e... The problem is that during the turbocharger testing, a set of forced working conditions are kept according to standards such as [52] and [53] (oil inlet temperature, cooling water, turbine inlet temperature...).

The working conditions at which the turbochargers are tested, influence the obtained maps: Several studies analyse the presence and the effect of heat transfer in the turbocharger. Casey et al.[54] concluded that even if there is no interaction between aerodynamics and heat transfer, the last may impact the recorded compressor and turbine efficiencies up to a 20% in small turbochargers for automotive applications. In [54], it was also stated that higher impact is expected in the lower speeds and mass flow operating areas. Romagnoli et al.[55] studied the impact of boundary conditions and the turbocharger architecture and finally concluded that measured compressor efficiency may vary from 17-30% with respect to the adiabatic efficiency.

In other studies, spatial wall temperature distributions are measured by means of an infra-red camera [56] for heat transfer analysis purposes and simplified semi-empirical correlations are proposed. Other researchers such as Burke et al. [57] concluded that heat losses in the turbine side represent systematically a 20% of the total turbine enthalpy drop if not even more in the lower power operative points. In [58] it was also pointed out the improvement in around 27ºC in terms of turbine outlet temperature prediction when heat transfer effects are considered. Salameh et al. [58] dealt with a lumped model in which the turbocharger was divided into three thermal nodes, for water-cooled turbochargers heat transfer effects calculation.

Before proceeding with the literature review, the term "adiabatization" shall be clarified: it is understood as adiabatization, the prediction of the heat transfer fluxes taking place in a given system (such as in a turbocharger) with the purpose of being able to decouple heat transfer effects, from other thermodynamic processes. In this line, Silvia Marelli et al. [59] considered three different heat transfer models for the compressor maps adiabatization and it was found that all of them provided consistent results. The impact of cooling water temperature and compressor inlet temperature was also assessed (in addition to turbine inlet temperature).

Other works [60] apply neural networks to correct heat transfer effects on turbine outlet temperature, as a function of several operating parameters. However, in these approaches, no corrections over the hot turbocharger maps themselves are made, and the heat transfer effects on the turbocharger performance are not considered, just a correction over turbine outlet temperature is made for after-treatment purposes.

Standards for gasoline engines' turbochargers testing state that turbine inlet temperature must be set up at 900 ºC [52]. One must realize that if instead of 900 ºC turbine inlet gas temperature (T3), the turbocharger test was done at 600 ºC T3, the heat transfer from the turbine to the environment and to the compressor side would be much lower. Since unfortunately, the turbomachinery is not fully adiabatic, the last would result in different maps if selected conditions had been 600 ºC or 900 ºC T3. Two different maps could be obtained for the turbine and compressor. The diathermic operation of the turbomachinery is the cause why just reducing maps with thermodynamic conditions of intake flow is not enough to universally represent a given turbocharger performance.

Depending on the approach taken into consideration, heat transfer in the turbocharger can be considered to happen at different locations. In this thesis work, the 1-dimensional heat transfer and mechanical losses turbocharger model (1D-HT-ML-TCM) developed by the CMT-Motores Térmicos Researching Institute is taken as the reference. This model considers that heat transfer from hot gas entering the turbine side takes place along the volute itself. Since turbine volute is heated up, heat transfer happens between the turbine volute and the environment by means of radiation and convection. Internal conduction between the turbine volute and central housing is computed as well. The heat reaching the central housing is at the same time: accumulated (raising the metal walls' temperature) and delivered to the cooling water, lubricat-

ing oil, and the compressor case (again by metal conduction). Finally, heat reaches compressed air and heats it up. In other words, the heat transfer model considers:

- Convective heat transfer between working fluids (hot gasses for example) and the turbo-machine walls (turbine volute for example). Figure 2.1 shows the enthalpy-entropy diagram evolution in the turbine side. Point 30 in Figure 2.1 corresponds to turbine inlet total temperature. Heat transfer is assumed to happen at turbine volute before the gas expansion. This energy lost is calculated by the model as in [61] is explained and gives as a result point 30'. Afterwards, it takes place, the actual turbine expansion with the corresponding irreversibility, giving as a result, point 40'. It is of high importance the fact that 30 is the measured temperature (not 30'), while it is 30 the temperature used for the turbine maps generation: in other words, heat transfer affects the turbine experimental aerodynamic maps. Heat transfer implications on the turbocharger predicted performance, are analysed in [62].

  On the compressor side, the heat is considered to happen after the air compression and may go into/from the compressed air, depending on the thermal gradient [7] (see Figure 2.2 air evolution from point 20 to 20'). For example, if there is cooling water, and the central housing is cooler than the compressed air, air would be cooled down according to the blue path, in the opposite situation, air would be heated up (red path).

- The model also considers heat transfer between the central housing and lubricating oil (and cooling water if it is present). More detail about convective coefficients can be found in [61]. Water and oil thermally interact with the central housing and contribute to the thermal balance.

- Concerning the external convection and radiation, the model estimates any interaction between the case and the environment to perform the energy balance for wall-thermal stabilization [63]. The model copes with forced and natural external convection as a function of the surrounding air velocity given as information.

- Metal thermal conductances and heat accumulation properties. This sub-model estimates heat through the metal and discretizes the turbocharger into five sections. Experimental methodologies to characterize the conductances and accumulative properties are included in [64].

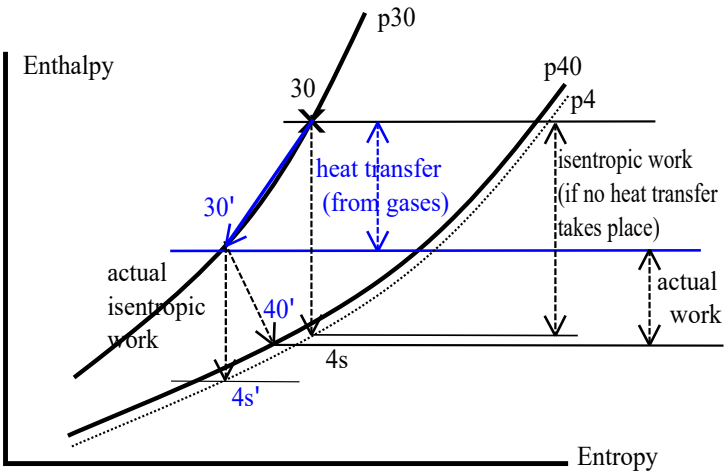

Figure 2.1: Effect of heat transfer in turbine enthalpy-entropy diagram

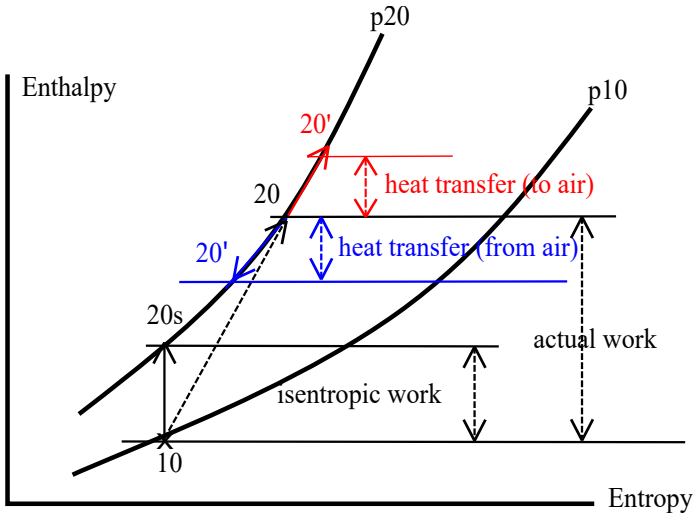

Figure 2.2: Effect of heat transfer in compressor enthalpy-entropy diagram

Figure 2.3 gathers the complete heat transfer model and shows the nodes: turbine (T), housing from the turbine to compressor sides (H1, H2, H3) and compressor (C), which correspond to the discretized nodes in which the TC is thermally divided. The connections between the different nodes are repre-

sented by thermal conductances (between interacting metal-to-metal nodes) and convective connections (metal-to-fluid couples). The overall capabilities of this model are explained on [62] for deeper understanding.

In summary, depending on the working conditions, and the operative area of the turbocharger, pretended to be studied, the effects of heat transfer may lead to modelling errors [65]. The fact of not decoupling heat effects from measured compressor/turbine diathermal efficiencies imply wrong energy balances along with the turbocharger, which leads to unrealistic results [5].

Therefore, having a holistic model that may consider all these phenomena, to pre-process the experimentally collected data, may result in a set of maps accounting for purely aerodynamic phenomena, which accurately represent air evolution, in combination with models able to predict heat transfer influence.

As evidenced in the previous studies, heat transfer effects are especially relevant in low mass flow and low power delivery working conditions. In highly downsized spark-ignited ICE this occurs in a wide range since stoichiometric mixture requires low air mass flow (hence, low power output from the turbocharger). Furthermore, thermal gradients along the turbocharger itself are even higher than in diesel engines: The stoichiometric mixture leads to higher turbine inlet temperatures, while the requirement of cooling water in the housing (to avoid oil cooking i.e.), enhances heat transfer in the turbine side [1].

The previous, coupled to the fact of the high interest in accurately comparing turbocharger technologies under transient operation, partial loads... evidence the importance of properly modelling the TC unit, in combination with the rest of engine elements (1-D pipes, combustion process, heat transfer phenomena, valve timing, friction losses...).

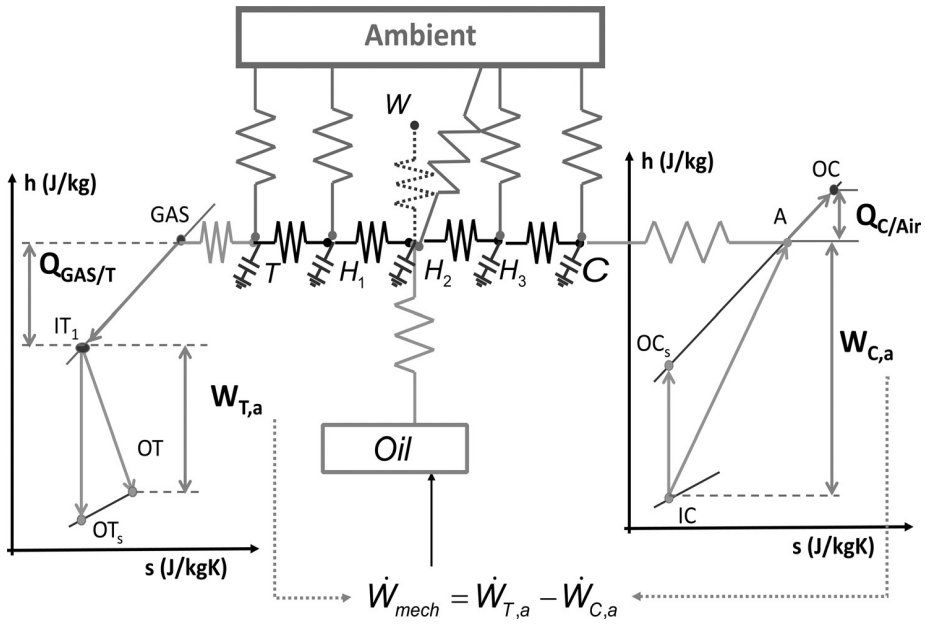

Figure 2.3: Nodal turbocharger heat transfer model

2.2.2 Obtaining complete TC maps

Another problem of just taking experimental information for the turbocharger modelling is the amount of collected data limitation on the turbine side: since the compressor working range is much reduced than the one for the turbine, turbine measurable operative area is limited by compressor surge and choke areas as well as by maximum compressor outlet temperature and maximum turbocharger speed.

To further illustrate this point, Figure 2.4 shows for a given turbine, the amount of experimental data that was obtained at the CMT-Motores Térmicos Researching Institute. Circles correspond to the experimental information while continuous lines correspond to the result of the turbine maps extrapolation model.

Figure 2.4 (A) deals with turbine mass flow maps and Figure 2.4 (B) with efficiency maps. As it can be appreciated, a large range of maps is required to

be extrapolated without any type of experimental information. If one looks at each iso-speed line separately, it can be seen how the pressure ratio range is about 0.4 in the best of the cases.

Figure 2.5, shows the corresponding obtained compressor map (for the same turbocharger), experimental data corresponds to circles and extrapolated information to the continuous lines. As it can be observed, the compressor map is much more complete: surge limit was reached and the only extrapolated area in terms of mass flow corresponds to the shaded triangle in Figure 2.5(A). Furthermore, peak efficiency was measured for all the speeds as in Figure 2.5(B) is shown. Consequently, for complete 1D engine simulations, known turbine operative areas may be insufficient. Studies such as [66] try to widen and measure turbine maps under extreme working conditions, which are hard to force in traditional gas stands, indeed, working areas in which the turbine consumes power (coming from the compressor side), are identified and studied. Other studies such as [67] propose a mapping technique that accounts for pulsating component effects of flow as well as broadens turbine collected information.

Other approaches assume that from experimental campaigns it is hard to measure the complete turbocharger operative range. To solve this limitation, several studies such as the one by Salameh et al. [68] propose a semi-empirical mass-flow turbine model for mass flow extrapolation that accounts even for negative mass-flows at very low pressure ratios. Zhu et al. [69] proposes a physical-based model for turbine mass flow maps extrapolation. In other studies models that simultaneously extrapolate turbine mass flow and efficiency maps are proposed [70].

In this context, researchers have developed different numerical approaches over the last years to fully understand the implications of turbine operation on the engine. Serrano et al.[71] used a 3D-CFD tool to analyse tip losses at extreme blade-speed ratio conditions, and then used these learnings to develop a methodology for extrapolating turbine maps needed for engine 1D simulations [72].

Finally, even if the experimental information for compressor maps is more complete than for turbines, in some cases it is still necessary to develop pressure ratio [73] and efficiency [74] extrapolation models.

The main advantage of these extrapolation models relies upon the fact

that experimental campaigns can be substantially reduced, so there are less time-consuming. In addition, fewer failure risks are assumed, since extreme working conditions can be extrapolated from the developed models.

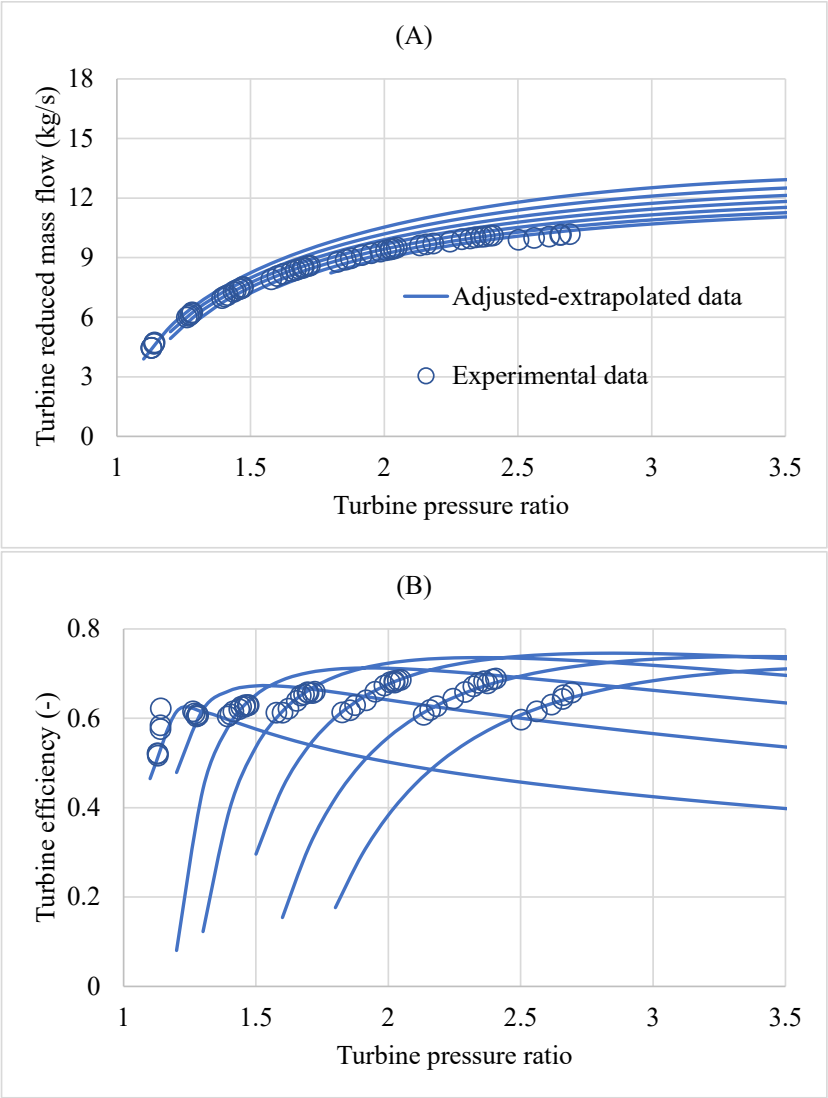

Figure 2.4: Turbine map from gas stand (experimental data) and extrapolated data. (A) Corresponds to mass flow maps. (B) Corresponds to turbine efficiency map

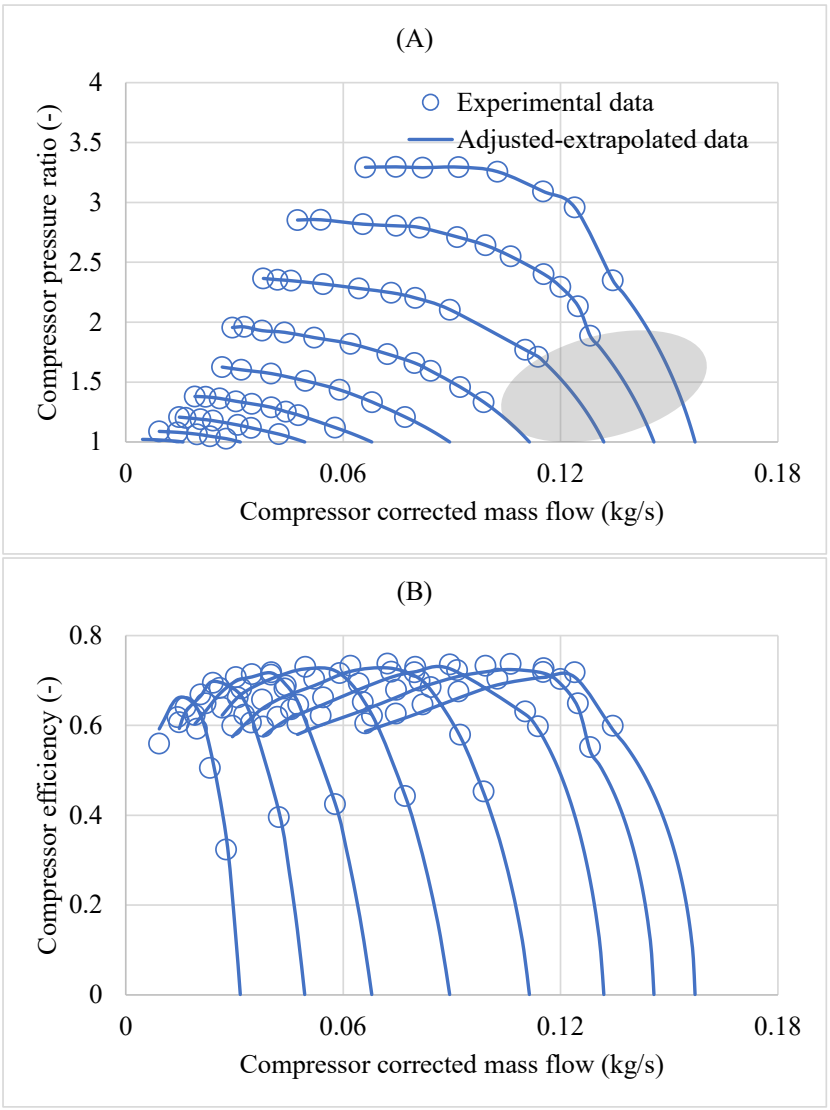

Figure 2.5: Compressor map from gas stand (experimental) and extrapolated data. (A) Corresponds to mass flow maps. (B) Corresponds to compressor efficiency map. Shaded triangle corresponds to extrapolated area

2.2.3 Friction losses effects

Friction losses in the shaft also have their impact. Especially in the low turbocharger rpm range, mechanical efficiency is identified to be between 50-60% [75]. Other studies deal with the influence of pulsating flow (such as the one in ICE) in the mechanical losses estimation and conclude that a constant value for mechanical efficiency overestimates the friction losses [76].

Deligant et al. [77] experimentally identified thrust and journal bearings contribution to the total amount of friction losses and concluded that more effort shall be made to improve thrust contribution. Accordingly, Novotný et al. [78] proposed a methodology to improve thrusts bearings for the turbocharger desired operative areas, with the drawback of reducing out-of-design performance. Other authors, backed by 3D CFD models and experiments identified the main physical processes that take place in thrusts bearings and proposed faster computational models to reproduce them [79]. Further studies state that by changing the layout of lubrication grooves in full-floating ring bearings, both: vibration and power losses can be diminished [80].

Simplified 0D models based on Navier-Stokes equations are pretended for thrust and journal bearing friction losses, as in [75], where, turbocharger speed, axial force, oil flow and temperature are taken into account in combination with several turbocharger geometrical parameters. Special remark is done in the oil temperature, since oil viscosity varies accordingly, influencing friction losses. After all the mathematical procedure developed in [75], Equation 2.1 estimates friction losses attributed to the journal bearing. The term "$\mu(\overline{T}_{oil})$" shows the direct impact of oil viscosity on journal bearing friction losses. The rest of parameters correspond to: Turbocharger rpm "n" to the power of two, the journal bearing radius to the power of three "R_{jb}", the journal bearing length "L_{jb}", the journal clearance "h_{jb}" and "K_{jb}" which is a correcting factor for tangential velocity speed gradient differences between central and extreme sections of the bearing.

$$\dot{W}_{jb} = 2\pi R_{jb}^3 K_{jb} \frac{L_{jb}}{h_{jb}} \mu(\overline{T}_{oil}) n^2 \tag{2.1}$$

In traditional look-up tables, the effect of mechanical losses are directly implemented in the called net or Effective Turbine Efficiency "ETE", see Equation 2.2, that evaluates the total power consumed by the compressor side

"$\dot{W}^{actual}_{compressor}$", respect of the theoretical maximum power that the turbine side may provide "$\dot{W}^{isentropic}_{turbine}$". In all, this definition of "ETE" evaluates how much power reaches the compressor in comparison to the available power on the turbine side. The difference between both corresponds to turbine efficiency and mechanical efficiency. In other words, (and neglecting heat transfer effects previously explained), the term "$\dot{W}^{actual}_{compressor}$" can be defined, as the actual turbine power"$\dot{W}^{actual}_{turbine}$" times the mechanical efficiency "$\eta_{mechanic}$", as stated in Equation 2.3.

Applying Equation 2.3 in Equation 2.2, results in Equation 2.4. The issue with the definition of "ETE" is: if mechanical efficiency varies as a consequence of working conditions (an engine cold start for example) the turbine map, constituted by the "ETE", would be hardly representing the turbine-shaft efficiency, since the term "$\eta_{mechanic}$" included in the maps would not be representative of the actual mechanical efficiency.

$$ETE = \frac{\dot{W}^{actual}_{compressor}}{\dot{W}^{isentropic}_{turbine}} \tag{2.2}$$

$$\dot{W}^{actual}_{compressor} = \dot{W}^{actual}_{turbine}\eta_{mechanic} \tag{2.3}$$

$$ETE = \frac{\dot{W}^{actual}_{turbine}}{\dot{W}^{isentropic}_{turbine}}\eta_{mechanic} = \eta_{turbine}\eta_{mechanic} \tag{2.4}$$

In other words, mechanical losses may vary with working conditions and operative areas of the TC, therefore, a mechanical loses model, independent from the turbine maps would be required if one attempts to well model all the physical phenomena under any working conditions. More evidence about the impact of mechanical losses is the arising of new technologies such as ball bearings [45], which are specially developed to compensate the friction losses during the engine warm-up, when oil is still cold, or hardly reaching the turbocharger shaft and bearings.

2.2.4 Pulsating and unsteady flow

When turbocharger maps are measured, steady-state is assured before collecting any working point. However, in engine working conditions, pulsating flow happens due to the volumetric-displacement element: the cylinders, particularly during exhaust and intake strokes. To identify the impact of the flow unsteadiness, 1-D turbine [49] and compressor [81] models have been developed. The 1-D simplified model is employed to account for pulsating flow effects and air evolution along with the different elements through which Strouhal number is significant enough (compressor and turbine volutes presumably). The aforementioned studies concluded that both: turbine and compressor operative maps could be measured and considered as quasi-steady, despite of the engine pulsating flow, for example, at turbine stator inlet (or compressor stator outlet) and from the point of view of mass flow parameter and efficiency calculation [82].

Slightly more sophisticated quasi-2D models have also been studied to well-reproduce acoustics in the turbine side [83]. Other authors attempt to simplify the compressor side into a 0-D element [84] for mass flow estimation under uniform and fluctuating flow conditions.

2.3 Turbocharging the SI engine by means of VGT

Knock used to be the major limitation for the boosting activities in the context of SI [85] engines. Indeed, turbocharging a given port injection gasoline engine would imply decreasing the engine compression ratio from 9:1 to around 6.7:1. However, with the arising of the direct injection technology, in combination with the already extended charge cooling and spark-plug retarding technique, knock could be retarded and turbocharging the gasoline engine started to become another way to achieve better power density and BSFC figures. However, due to the time lapse between diesel-gasoline turbocharging activities, it can be found in the available literature that while VGT was the standard for diesels, gasoline engines turbocharging discussion was mainly focused on WG technology [41].

In comparison to fixed geometry turbines, it is considered that the VGT offers (presumably) a better transient response, improved torque delivery at

full load, as well as better figures of BSFC [42]. However, the implementation in series gasoline ICE is regulated by the cost/benefit and cost/necessity ratios. Nowadays thanks to the extensive application and the investment in new materials (able to cope with higher temperatures), the costs are less, the benefit is being analysed and quantified (for example in this thesis itself), and the necessity increases with new CO2 reduction policies.

However, the lack of hardware availability targeted for SI engines has also limited the number of studies about this topic in the literature. Sjeric et al. [86] used engine 1D simulations to evaluate the potential of the VGT coupled with exhaust gas recirculation for fuel consumption improvements on SI engines. Andersen et al. [87] evaluated six different samples of VGT, confirming performance advantages for most of them compared to a fixed geometry turbocharger, especially at low speeds.

Shimizu et al. [88] pointed out that the fuel enrichment needed to be implemented to protect the variable nozzle turbine (VNT) mechanism induced a severe increase of unburnt hydrocarbons (UHCs) and CO emissions. Noga [89] applied VGT technology to an over-expanded engine, thanks to the higher temperature reduction, evidencing the potential to significantly increase wide-open throttle performance.

Tang et al. [90] evaluated the performance of such turbochargers in transient operation, highlighting the challenges of achieving a proper compromise between turbocharger acceleration and engine volumetric efficiency loss, due to excessive turbine inlet pressure.

Valve timing and VGT synergies were also of high interest. Ericsson et al. [91] studied the interaction between VGT and variable valve timing to optimize the transient response. Wang et al. [92] studied the potential benefits of VGT combined with early intake valve closing (IVC) to reduce knocking tendency and fuel enrichment.

2.4 Background

2.4.1 1D-HT-ML-TCM usage

In this section, the aforementioned 1D-HT-ML-TCM has been taken as the tool to model the complete turbocharger system according to all the previous points. This model does not only account for mechanical losses and heat transfer but also extrapolates turbine and compressor maps once the experimental data has been properly processed and the adiabatization has been carried out.

To provide with an idea of the capabilities and benefits that may be expected from the model, a comparison between hot maps (constituted by lookup tables) and the 1D-HT-ML-TCM is included. For this purpose, 1-D complete engine simulations, (dealing with a VGT turbocharged 1.6 L diesel engine) are performed, making usage of both TC approaches.

The 1-D ICE model is fitted and matches experimental data. Simulations are performed with both turbocharger approaches. Differences between experimental and each calculation sets output are purely attributed to the TC modelling approach and not to spurious ICE modelling errors. This brief study includes:

- Partial load, steady-state, low-pressure exhaust gas recirculation (LP-EGR) points. This results in a matrix of 51 points distributed between five engine speeds: 1250, 1500, 1750, 2000 and 2250. Only LP-EGR is set up while high pressure (HP) EGR is always closed. Most remarkable variables' error summary is included in [6] and summarized in Table 2.1. The impact of the TC model approach, on main variables such as torque and BSFC, is around 1.2% better for the holistic model. Directly involved turbocharger variables are even better for the holistic model as well as in Table 2.1 is evidenced.

- Transient sudden tip-in response from very low load to 100% load at 1750 engine rpms. During these tests, with the purpose of simplifying model results analysis, both LP-EGR and HP-EGR valves were kept closed. The load-transient test has been intentionally made slower than in production engines. The intention was to make the recording procedure easier. In addition, a slightly slower transient also forces a longer interaction between the different sub-models. Results for compressor outlet temperature (T2) and intake manifold temperature (T2') are shown in Figure 2.6. Turbine inlet temperature evolution is included in Fig-

ure 2.7(A) and turbine outlet in Figure 2.7(B), T3 and T4 respectively.

In any case, the experimental data corresponds to the blue and black series (low and high thermal inertia thermocouples respectively). Here, it is evidenced the requirement of installing low inertia thermocouples in order to properly catch the actual fluid temperature evolution. The low inertia thermocouple consists of a 5 μm diameter sensor while the high inertia one consists of a 1.5 mm. In the case of the data coming from the modelling: T2, T2', T3 and T4 deal with predicted mass-averaged fluid temperatures.

Compressor outlet temperature differences between modelling approaches are hard to find. From the second three in advance, a 10^{o}C improvement is found, in favour of the 1D-HT-ML-TCM. In terms of exhaust gases temperature, while T3 is equally accurate for both sets of calculations, turbine outlet temperature (T4) prediction by means of the 1D-HT-ML-TCM results in a much better prediction. Hot maps result in a consistent 100^{o}C over-prediction in terms of T4, see Figure 2.7.

In any case, the better prediction of the holistic model is evidenced along with the complete transient and steady-state cases. These calculations are an example of the capabilities and improvements that may be expected from the 1D-HT-ML-TCM.

What is more by further improvement of the model, fine-tuning of the model fitted parameters, and individual adjustment of the turbocharger properties (depending on the turbocharger unit analysed), better results may be expected, and more trustful models may be developed.

Table 2.1: Mean quadratic error for Low-to-medium load LP-EGR steady state points with different turbocharger approaches (Look-up table and 1D-HT-ML-TCM)

Variable	ϵTorque(%)	ϵBSFC	ϵT1 (K)	ϵT2 (K)	ϵT4 (K)	ϵp3 (pa)	ϵp4 (pa)
Hot maps	9.9	6.5	10.6	15	50.8	96.5	9.5
1D-HT-ML-TCM	8.7	5.7	7.2	7.2	20.8	58.6	2.9

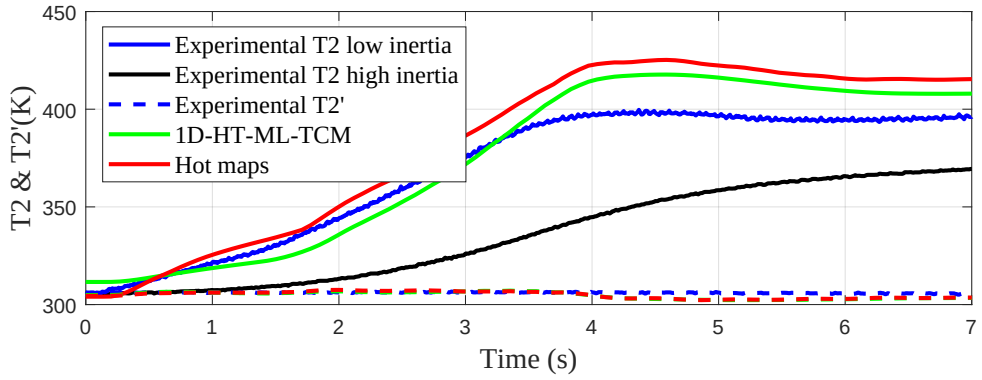

Figure 2.6: 1750 engine rpm compressor outlet temperatures (experimental and models), during transient sudden tip-in

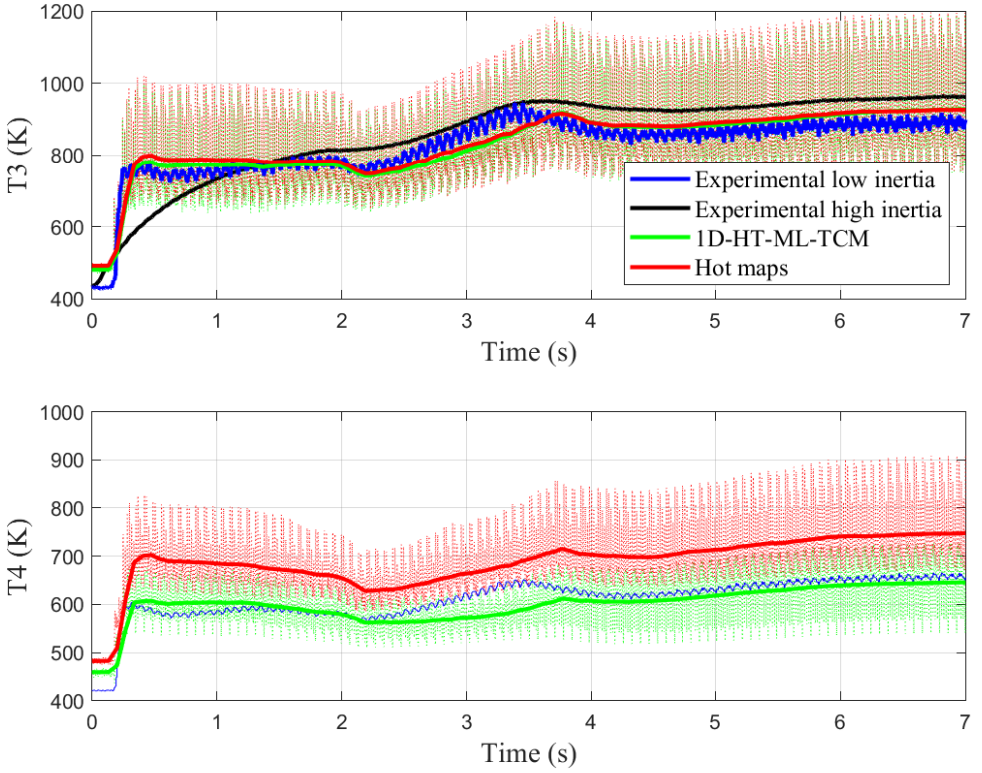

Figure 2.7: 1750 engine rpm turbine outlet temperatures (experimental and models), during transient sudden tip-in

2.4.2 Model update for actively-cooled turbochargers

As in [6], the 1D-HT-ML-TCM was mainly developed and used for diesel engines and non-water-cooled turbochargers. On the contrary, SI-ICE turbocharger housings are actively cooled by water, with the aim of placing a thermal barrier between the compressor and turbine sides, avoid oil cooking and evacuate some heat in the turbine side. In some cases, even the compressor housing is actively cooled with a water-jacket, which introduces a new heat flow path.

A collateral effect of placing this cooling water lies in the fact that compressed air, may exchange heat with the coolant, following the blue path, indicated by the blue arrow in Figure 2.2. In the case of non-cooled turbochargers, the working conditions in which the compressed air is cooled down in the compressor volute, happens hardly ever, since the normal "heat flux path" goes from turbine to compressor side (from hot to cold node respectively). However, this situation is dramatically different when cooling water is forced through the housing. In consequence, very little amount of experimental information was used to feed the models' correlation for heat transfer estimation, when the compressor outlet air, is cooled down in the compressor case, as a consequence of cooling water presence.

To solve this problem at the very early stages of this thesis, the 1D-HT-ML-TCM heat transfer correlation was fitted to well-predict heat transfer under the aforementioned working conditions, on the compressor side. This work corresponds to the one in [7].

In this study, two compressor units were tested:

- An electric booster, with a water jacket between the electric motor and the compressor itself, see Figure 2.8(A).

- A cooled compressor case turbocharger unit with a water jacket, coming from a two-stage compression system, and which corresponds to the low-pressure compressor unit (LPC), see the light blue component in Figure 2.8(B).

Figure 2.8: (A) E-booster for the study. (B) LPC in light blue, in a 2-stage compression system

In summary, an experimental campaign specifically developed for each turbocharger unit was carried out to identify the heat transfer fluxes coming/going from/to the compressed air. The main advantage of both depicted turbocharger units, lies in the fact that cooling water could be adjusted in a wide range, which allowed to force a net heat transfer in the compressor case, furthermore, in the desired "direction" (towards or from the compressed air).

After that, and making the correspondent assumptions, Equation 2.5 is obtained for the heat transfer prediction in the compressor volute: the target parameters to be fitted, in Equation 2.5 are "a", "b". The selected combination of values is the one that shows the minimum square root error in the "$\dot{Q}_{CN/Air}$" prediction, which corresponds to the experimental heat transfer between the compressor node (CN) and the compressed air. The term "Re" corresponds to the Reynolds number, "Pr" to the Prandtl number. The term "T_{CN}" corresponds to the wall temperatures of the compressor node, and "T_2" to the compressor outlet air temperature, both of them coming from the experimental campaign. Finally "k_{air}" corresponds to the air conductivity and "L" to a characteristic length. More details about the mathematical procedure and the experimental campaign can be found in [7].

$$\dot{Q}_{CN/Air} = \frac{aRe^{b}Pr^{c}k_{air}}{L}A(T_{CN} - T_2) \tag{2.5}$$

The obtained result of the fitting for the parameter "b", is constant and takes a value of "0.7", while parameter "a" value is "0.883" when compressed air

is heated up, and "0.829" when compressed air is cooled down. Applying the obtained correlation with the fitted coefficients, to predict heat transfer, gives back the results in Figure 2.9. As in Figure 2.9 is shown, the validation of the correlation is done not only for both units taken for the correlation development (the e-booster and the LPC) but also for a series of data corresponding to the CMT-Database, which is constituted by several non-water-cooled turbochargers, in which heat fluxes (especially in the negative area), are located in a smaller range than for the other two data sets. This is the main motivation why the e-booster and the LPC were taken as the basis for the correlation fitting: with higher values of net heat transfer, experimental uncertainties become of less relevance and the fitting results in a more robust correlation.

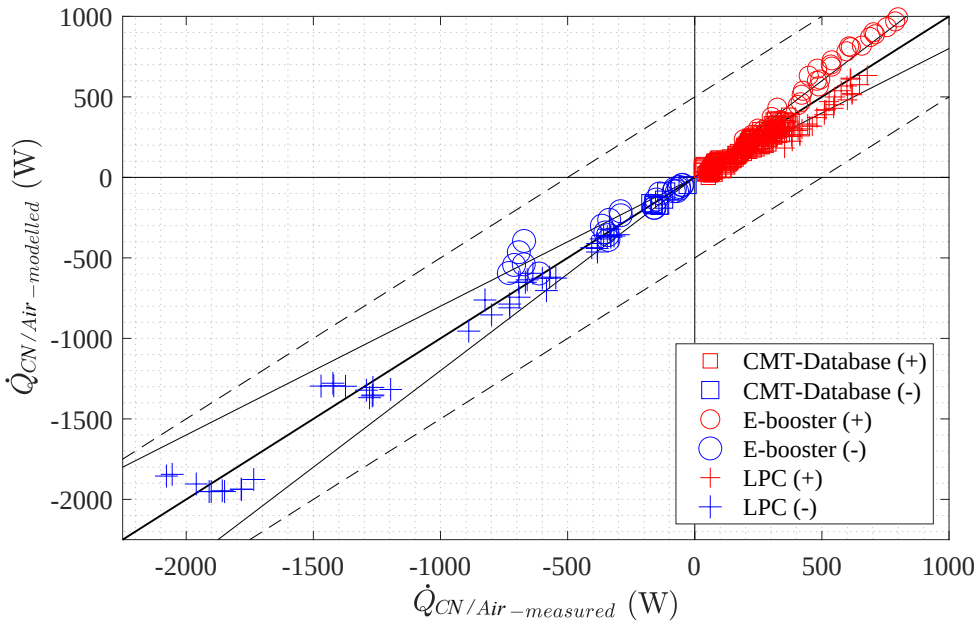

Figure 2.9: Compressor case node/Compressed air modelled VS experimental heat flux. Three series of data: CMT-Database, E-booster and LPC. Dashed lines correspond to +-500Watts and continuous lines to a +-20% dispersion

2.5 Summary and conclusions

In this chapter, it is presented a literature review about researching efforts in order to properly model and understand the physical phenomena taking place around turbochargers.

Nowadays, motivated by new homologating cycles, further downsizing of the ICE is required. Hence, turbochargers' role becomes more relevant, and its performance is considered in a wider range (and out of design) of working conditions than it used to be evaluated. The previous calls into question the usage of common look-up tables as it has been done previously in [62].

In other words, just correcting the effect of pressure and temperature with the aim of obtaining reduced/corrected universal maps does not account for the effect of heat transfer, unsteady flow, and mechanical losses variability. If realistic results are desired to be predicted, a deeper analysis is worth and a more sophisticated process of the data is required, such as in 1-D holistic models is done. Among other benefits, it could be stated that relatively simple data and low computational cost are required for these models.

Furthermore, due to turbocharger limitations (and turbine-to-compressor matching), recorded data is limited and relatively incomplete maps are normally delivered by manufacturers. Thus, more sophisticated maps-extrapolation methods are proposed by researchers in the field.

In this chapter, it has also been carried out a literature review dealing with the implementation of variable geometry turbochargers in SI engines. Most of the studies are focused on modelling activities rather than experimental ones, due to the lack of hardware availability. However, because of the market request, some studies and experiments start to flourish.

In this chapter, it is discussed the capabilities/benefits of using a holistic integral turbocharger model, in comparison with the old look-up table approach. This is done for partial loads with low-pressure EGR as well as load transients.

Finally, as a consequence of the review, the model which was taken as a reference for this thesis work: the 1D-HT-ML-TCM, required to be updated with a more robust correlation for the compressor side convective heat transfer prediction. The last is especially relevant in the context of SI turbocharged

engines since cooling water is present in the housing, forcing either positive or negative heat fluxes in the compressor side. This situation hardly happened in the context of turbochargers for diesel engines application, this is why the model had to be upgraded, calling for accuracy in terms of heat transfer prediction on the compressor side.

As a conclusion of the review, the novelty of this thesis with respect to the available works and knowledge will lie in several points: Firstly, this thesis takes advantage of an already built integral and holistic turbocharger model to cope with the turbocharger experimental maps uncertainties. In this line, it will be proposed an experimental-modelling straightforward methodology, in order to calibrate the turbocharger model itself, independently from the engine-test campaign. The target is to obtain high-quality maps for which there is no requirement of efficiency multipliers for example. The robustness of the study is backed up by the fact that two VGT are called into question, as well as a WG unit.

Secondly, an innovative component is the amount of experimental information dealing with VGT turbochargers in the context of spark-ignited engines. As it was shown in the literature review, most of the studies were theoretical and very little experimental data was included.

Thirdly, a sensibility study is proposed, taking advantage of the high-quality and validated model. In this study, the impact of the experimental uncertainties as well as the "out-of-control" variables is assessed.

Fourthly, it is proposed a novel methodology in which a complete engine model is calibrated with the collected experimental information. The 1-D engine code calibration methodology, fits a series of parameters along the complete engine block and piping, while any turbocharger uncertainty is neglected.

Finally, the obtained and validated turbocharger maps and engine model, for prospective analysis, represent some of the novelty of this work. It is possible to develop a strategy for purely turbine technologies comparison under diverse working conditions and engine operation areas. Thanks to the previous, it is possible to obtain main conclusions when comparing waste-gate turbines (nowadays standard in SI engines) versus variables geometry turbines.

Chapter 2 Bibliography

[1] J. R. Serrano, F. J. Arnau, L. M. García-Cuevas, A. Gómez-Vilanova, S. Guilain, and S. Batard. "A Methodology for Measuring Turbocharger Adiabatic Maps in a Gas-Stand and Its Usage for Calibrating Control Oriented and One-Dimensional Models at Early ICE Design Stages". *Journal of Energy Resources Technology* 143.(4) (2021), pp. 1–11. ISSN: 0195-0738. DOI: 10.1115/1.4048229 (cit. on pp. xii, 25, 105).

[5] J. R. Serrano, F. J. Arnau, J. De la Morena, A. Gómez-Vilanova, S. Guilain, and S. Batard. "A methodology to calibrate Gas-Dynamic Models of turbocharged petrol egines with variable geometry turbines and with focus on dynamics prediction during tip-in load transient tests". In: *Volume 8: Industrial and Cogeneration; Manufacturing Materials and Metallurgy; Marine; Microturbines, Turbochargers, and Small Turbomachines*. Vol. 2020-june. American Society of Mechanical Engineers, 2020, pp. 22–26. ISBN: 978-0-7918-8419-5. DOI: 10.1115/GT2020-15169. URL: https://asmedigitalcollection.asme.org/GT/proceedings/GT2020/84195/Virtual,Online/1095133 (cit. on pp. xii, 25, 105).

[6] J. R. Serrano, F. J. Arnau, L. M. G.-C. González, A. Gómez-Vilanova, and S. Guilain. "Impact of a holistic turbocharger model in the prediction of engines performance in transient operation and in steady state with LP-EGR". In: *Volume 2: Emissions Control Systems; Instrumentation, Controls, and Hybrids; Numerical Simulation; Engine Design and Mechanical Development*. San Diego, California, USA: American Society of Mechanical Engineers, 2018, pp. 1–16. ISBN: 978-0-7918-5199-9. DOI: 10.1115/ICEF2018-9550. URL: https://asmedigitalcollection.asme.org/ICEF/proceedings/ICEF2018/51999/SanDiego,California,USA/273145 (cit. on pp. xiii, 34, 36, 51, 64).

[7] J. R. Serrano, F. J. Arnau, L. M. G.-C. González, A. Gómez-Vilanova, and S. Guilain. "An experimental methodology and model for characterizing radial centrifugal compressors of turbocharged engines from diathermal perspective". In: *Advances in Mechanism and Machine Science*. Krakow, Poland: Springer International Publishing, 2019, pp. 883–892. ISBN: 978-3-030-20130-2. DOI: 10.1007/978-3-030-20131-9_88. URL: https://link.springer.com/chapter/10.1007/978-3-030-20131-9_88 (cit. on pp. xiii, 23, 37, 38, 98).

[41] H. Hiereth and P. Prenninger. *Charging the Internal Combustion Engine*. Springer, Vienna, 2007, pp. 1–268. ISBN: 978-3-211-47113-5. DOI: 10.1007/978-3-211-47113-5 (cit. on pp. 9, 32).

[42] A. J. Feneley, A. Pesiridis, and A. M. Andwari. "Variable Geometry Turbocharger Technologies for Exhaust Energy Recovery and Boosting-A Review". *Renewable and Sustainable Energy Reviews* 71.(September 2015) (2017), pp. 959–975. ISSN: 18790690. DOI: 10.1016/j.rser.2016.12.125. URL: http://dx.doi.org/10.1016/j.rser.2016.12.125 (cit. on pp. 10, 32).

[45] D. Zeppei, S. Koch, and A. Rohi. "Ball Bearing Technology for Passenger Car Turbochargers". *MTZ worldwide* 77.(11) (2016), pp. 26–31. DOI: 10.1007/s38313-016-0109-z (cit. on pp. 10, 31).

[49] Z. Ding, W. Zhuge, Y. Zhang, H. Chen, R. Martinez-Botas, and M. Yang. "A one-dimensional unsteady performance model for turbocharger turbines". *Energy* 132 (2017), pp. 341–355. ISSN: 03605442. DOI: 10.1016/j.energy.2017.04.154. URL: http://dx.doi.org/10.1016/j.energy.2017.04.154 (cit. on pp. 20, 32).

[50] F. Bozza, V. De Bellis, and L. Teodosio. "Potentials of cooled EGR and water injection for knock resistance and fuel consumption improvements of gasoline engines". *Applied Energy* 169 (2016), pp. 112–125. ISSN: 03062619. DOI: 10.1016/j.apenergy.2016.01.129. URL: http://dx.doi.org/10.1016/j.apenergy.2016.01.129 (cit. on p. 20).

[51] O. R. Sandoval, M. V. Fonda, V. R. Roso, R. B. R. da Costa, R. M. Valle, and J. G. Baêta. "Computational technique for turbocharger transient characterization using real driving conditions data". *Energy* 186 (2019). ISSN: 03605442. DOI: 10.1016/j.energy.2019.07.152 (cit. on p. 20).

[52] Society of Automotive Engineers. *Turbocharger Gas Stand Test Code - SAE Standards*. 1995. DOI: 10.4271/J1826_199503. URL: http://standards.sae.org/wip/j1826/ (cit. on pp. 21, 22, 84, 110).

[53] SAE J1723. *Supercharger testing standard*. 1995. DOI: J1723_199508. URL: https://saemobilus.sae.org/content/J1723_199508 (cit. on pp. 21, 89, 91, 105).

[54] B. Sirakov and M. Casey. "Evaluation of Heat Transfer Effects on Turbocharger Performance". *Journal of Turbomachinery* 135.(2) (2012). ISSN: 0889504X. DOI: 10.1115/1.4006608 (cit. on pp. 21, 97).

[55] A. Romagnoli and R. Martinez-Botas. "Heat transfer analysis in a turbocharger turbine: An experimental and computational evaluation". *Applied Thermal Engineering* 38 (2012), pp. 58–77. ISSN: 13594311. DOI: 10.1016/j.applthermaleng.2011.12.022. URL: http://dx.doi.org/10.1016/j.applthermaleng.2011.12.022 (cit. on pp. 21, 97).

[56] G. Tanda, S. Marelli, G. Marmorato, and M. Capobianco. "An experimental investigation of internal heat transfer in an automotive turbocharger compressor". *Applied Energy* 193 (2017), pp. 531–539. ISSN: 03062619. DOI: 10.1016/j.apenergy.2017.02.053. URL: http://dx.doi.org/10.1016/j.apenergy.2017.02.053 (cit. on p. 21).

[57] R. D. Burke, C. R. Vagg, D. Chalet, and P. Chesse. "Heat transfer in turbocharger turbines under steady, pulsating and transient conditions". *International Journal of Heat and Fluid Flow* 52 (2015), pp. 185–197. ISSN: 0142727X. DOI: 10.1016/j.ijheatfluidflow.2015.01.004. URL: http://dx.doi.org/10.1016/j.ijheatfluidflow.2015.01.004 (cit. on p. 21).

[58] G. Salameh, G. Goumy, and P. Chesse. "Water cooled turbocharger heat transfer model initialization: Turbine and compressor quasi-adiabatic maps generation". *Applied Thermal Engineering* 185.(June 2020) (2021). ISSN: 13594311. DOI: 10.1016/j.applthermaleng.2020.116430. URL: https://doi.org/10.1016/j.applthermaleng.2020.116430 (cit. on p. 21).

[59] S. Marelli, G. Marmorato, M. Capobianco, and A. Rinaldi. "Heat Transfer Effects on Performance Map of a Turbocharger Compressor for Automotive Application". In: *SAE Technical Papers*. Vol. 2015-April. April. 2015. DOI: 10.4271/2015-01-1287. URL: http://papers.sae.org/2015-01-1287/ (cit. on pp. 22, 84, 97).

[60] L. Huang, C. Ma, Y. Li, J. Gao, and M. Qi. "Applying neural networks (NN) to the improvement of gasoline turbocharger heat transfer modeling". *Applied Thermal Engineering* 141.(November 2017) (2018), pp. 1080–1091. ISSN: 13594311. DOI: 10.1016/j.applthermaleng.2018.06.062 (cit. on p. 22).

[61] J. R. Serrano, P. Olmeda, F. J. Arnau, M. A. Reyes-Belmonte, and H. Tartoussi. "A study on the internal convection in small turbochargers. Proposal of heat transfer convective coefficients". *Applied Thermal Engineering* 89 (2015), pp. 587–599. ISSN: 13594311. DOI: 10.1016/j.applthermaleng.2015.06.053 (cit. on pp. 23, 84).

[62] J. R. Serrano, P. Olmeda, F. J. Arnau, A. Dombrovsky, and L. Smith. "Turbocharger heat transfer and mechanical losses influence in predicting engines performance by using one-dimensional simulation codes". *Energy* 86 (2015), pp. 204–218. ISSN: 03605442. DOI: 10.1016/j.energy.2015.03.130 (cit. on pp. 23, 25, 39, 51).

[63] F. Payri, P. Olmeda, F. J. Arnau, A. Dombrovsky, and L. Smith. "External heat losses in small turbochargers: Model and experiments". *Energy* 71 (2014), pp. 534–546. ISSN: 03605442. DOI: 10.1016/j.energy.2014.04.096. URL: http://dx.doi.org/10.1016/j.energy.2014.04.096 (cit. on p. 23).

[64] J. R. Serrano, P. Olmeda, A. Páez, and F. Vidal. "An experimental procedure to determine heat transfer properties of turbochargers". *Measurement Science and Technology* 21.(3) (2010). ISSN: 13616501. DOI: 10.1088/0957-0233/21/3/035109 (cit. on p. 23).

[65] A. Romagnoli, A. Manivannan, S. Rajoo, M. S. Chiong, A. Feneley, A. Pesiridis, and R. F. Martinez-Botas. *A review of heat transfer in turbochargers*. 2017. DOI: 10.1016/j.rser.2017.04.119. URL: http://dx.doi.org/10.1016/j.rser.2017.04.119 (cit. on p. 25).

[66] J. R. Serrano, A. Tiseira, L. M. García-Cuevas, L. B. Inhestern, and H. Tartoussi. "Radial turbine performance measurement under extreme off-design conditions". *Energy* 125 (2017), pp. 72–84. ISSN: 03605442. DOI: 10.1016/j.energy.2017.02.118 (cit. on p. 27).

[67] Z. Liu and C. Copeland. "New method for mapping radial turbines exposed to pulsating flows". *Energy* 162 (2018), pp. 1205–1222. ISSN: 03605442. DOI: 10.1016/j.energy.2018.08.107. URL: https://doi.org/10.1016/j.energy.2018.08.107 (cit. on p. 27).

[68] G. Salameh, P. Chesse, and D. Chalet. "Mass flow extrapolation model for automotive turbine and confrontation to experiments". *Energy* 167 (2019), pp. 325–336. ISSN: 03605442. DOI: 10.1016/j.energy.2018.10.183. URL: https://doi.org/10.1016/j.energy.2018.10.183 (cit. on p. 27).

[69] S. Zhu, K. Deng, and S. Liu. "Modeling and extrapolating mass flow characteristics of a radial turbocharger turbine". *Energy* 87 (2015), pp. 628–637. ISSN: 03605442. DOI: 10.1016/j.energy.2015.05.032. URL: http://dx.doi.org/10.1016/j.energy.2015.05.032 (cit. on pp. 27, 98).

[70] F. Payri, J. R. Serrano, P. Fajardo, M. A. Reyes-Belmonte, and R. Gozalbo-Belles. "A physically based methodology to extrapolate performance maps of radial turbines". *Energy Conversion and Management* 55 (2012), pp. 149–163. ISSN: 01968904. DOI: 10.1016/j.enconman.2011.11.003 (cit. on pp. 27, 98).

[71] J. R. Serrano, F. J. Arnau, L. M. García-Cuevas, and L. B. Inhestern. "An innovative losses model for efficiency map fitting of vaneless and variable vaned radial turbines extrapolating towards extreme off-design conditions". *Energy* 180 (2019), pp. 626–639. ISSN: 03605442. DOI: 10.1016/j.energy.2019.05.062 (cit. on p. 27).

[72] J. R. Serrano, A. Tiseira, L. M. García-Cuevas, and T. R. Usaquén. "Adaptation of a 1-D tool to study transient thermal in turbocharger bearing housing". *Applied Thermal Engineering* 134.(June 2017) (2018), pp. 564–575. ISSN: 13594311. DOI: 10.1016/j.applthermaleng.2018.01.085. URL: https://doi.org/10.1016/j.applthermaleng.2018.01.085 (cit. on p. 27).

[73] J. Galindo, R. Navarro, L. M. García-Cuevas, D. Tarí, H. Tartoussi, and S. Guilain. "A zonal approach for estimating pressure ratio at compressor extreme off-design conditions". *International Journal of Engine Research* 20.(4) (2019), pp. 393–404. ISSN: 20413149. DOI: 10.1177/1468087418754899 (cit. on p. 27).

[74] J. Galindo, A. Tiseira, R. Navarro, D. Tarí, H. Tartoussi, and S. Guilain. "Compressor Efficiency Extrapolation for 0D-1D Engine Simulations". In: *SAE Technical Papers*. 2016. DOI: 10.4271/2016-01-0554 (cit. on pp. 27, 98).

[75] J. R. Serrano, P. Olmeda, A. Tiseira, L. M. García-Cuevas, and A. Lefebvre. "Theoretical and experimental study of mechanical losses inautomotive turbochargers". *Energy* 55 (2013), pp. 888–898. ISSN: 03605442. DOI: 10.1016/j.energy.2013.04.042. URL: http://dx.doi.org/10.1016/j.energy.2013.04.042 (cit. on pp. 30, 84, 97).

[76] J. R. Serrano, P. Olmeda, A. Tiseira, L. M. García-Cuevas, and A. Lefebvre. "Importance of Mechanical Losses Modeling in the Performance Prediction of Radial Turbochargers under Pulsating Flow Conditions". In: *SAE International Journal of Engines*. Vol. 6. 2. 2013, pp. 729–738. DOI: 10.4271/2013-01-0577. URL: http://saeeng.saejournals.org/content/6/2/729\%5Cnhttp://saeeng.saejournals.org/content/6/2/729.abstract (cit. on pp. 30, 84, 97).

[77] M. Deligant, P. Podevin, and G. Descombes. "Experimental identification of turbocharger mechanical friction losses". *Energy* 39.(1) (2012), pp. 388–394. ISSN: 03605442. DOI: 10.1016/j.energy.2011.12.049. URL: http://dx.doi.org/10.1016/j.energy.2011.12.049 (cit. on p. 30).

[78] P. Novotný, M. Jonák, and J. Vacula. "Evolutionary Optimisation of the Thrust Bearing Considering Multiple Operating Conditions in Turbomachinery". *International Journal of Mechanical Sciences* 195.(September 2020) (2021). ISSN: 00207403. DOI: 10.1016/j.ijmecsci.2020.106240 (cit. on p. 30).

[79] P. Novotný and J. Hrabovský. "Efficient computational modelling of low loaded bearings of turbocharger rotors". *International Journal of Mechanical Sciences* 174.(September 2019) (2020). ISSN: 00207403. DOI: 10.1016/j.ijmecsci.2020.105505 (cit. on p. 30).

[80] L. Smolík and Š. Dyk. "Towards efficient and vibration-reducing full-floating ring bearings in turbochargers". *International Journal of Mechanical Sciences* 175.(January) (2020). ISSN: 00207403. DOI: 10.1016/j.ijmecsci.2020.105516 (cit. on p. 30).

[81] A. Torregrosa, F. Arnau, P. Piqueras, M. Reyes-Belmonte, M. Knutsson, and J. Lennblad. "Acoustic one-dimensional compressor model for integration in a gas-dynamic code". In: *SAE Technical Papers*. 2012. DOI: 10.4271/2012-01-0834. URL: http://papers.sae.org/2012-01-0834/ (cit. on p. 32).

[82] J. Galindo, P. Fajardo, R. Navarro, and L. M. García-Cuevas. "Characterization of a radial turbocharger turbine in pulsating flow by means of CFD and its application to engine modeling". *Applied Energy* 103 (2013), pp. 116–127. ISSN: 03062619. DOI: 10.1016/j.apenergy.2012.09.013. URL: http://dx.doi.org/10.1016/j.apenergy.2012.09.013 (cit. on p. 32).

[83] J. Galindo, F. J. Arnau, L. M. García-Cuevas, and P. Soler. "Experimental validation of a quasi-two-dimensional radial turbine model". *International Journal of Engine Research* 21.(6) (2020), pp. 915–926. ISSN: 20413149. DOI: 10.1177/1468087418788502 (cit. on p. 32).

[84] K. Song, B. Zhao, H. Sun, and W. Yi. "A physics-based zero-dimensional model for the mass flow rate of a turbocharger compressor with uniform/distorted inlet condition". *International Journal of Engine Research* 20.(6) (2019), pp. 624–639. ISSN: 20413149. DOI: 10.1177/1468087418773673 (cit. on p. 32).

[85] N. Watson and M. Janota. *Turbocharging the Internal Combustion Engine*. Basingstok. Macmillan, 1982. ISBN: 0333242904 (cit. on p. 32).

[86] M. Sjerić, I. Taritaš, R. Tomić, M. Blažić, D. Kozarac, and Z. Lulić. "Efficiency improvement of a spark-ignition engine at full load conditions using exhaust gas recirculation and variable geometry turbocharger – Numerical study". *Energy Conversion and Management* 125 (2016), pp. 26–39. ISSN: 01968904. DOI: 10.1016/j.enconman.2016.02.047 (cit. on p. 33).

[87] J. Andersen, E. Karlsson, and A. Gawell. "Variable turbine geometry on SI engines". In: *SAE Technical Papers*. Vol. 2006. 724. 2006, pp. 776–790. DOI: 10.4271/2006-01-0020 (cit. on pp. 33, 158).

[88] K. Shimizu, W. Sato, H. Enomoto, and M. Yashiro. "Torque control of a small gasoline engine with a variable nozzle turbine turbocharger". In: *SAE Technical Papers*. 2009, pp. 1–7 (cit. on p. 33).

[89] M. Noga. "Application of VNT turbocharger in spark ignition engine with additional expansion of exhaust gases". *Tehnicki Vjesnik* 25.(6) (2018), pp. 1575–1580. ISSN: 18486339. DOI: 10.17559/TV-20160211230747 (cit. on p. 33).

[90] H. Tang, C. Copeland, S. Akehurst, C. Brace, P. Davies, L. Pohorelsky, L. Smith, and G. Capon. "A novel predictive semi-physical feed-forward turbocharging system transient control strategy based on mean-value turbocharger model". *International Journal of Engine Research* 18.(8) (2017), pp. 765–775. ISSN: 20413149. DOI: 10.1177/1468087416670052 (cit. on p. 33).

[91] G. Ericsson, H. E. Angstrom, and F. Westin. "Optimizing the transient of an SI-engine equipped with variable cam timing and variable turbine". In: *SAE Technical Papers*. Vol. 3. 1. 2010, pp. 903–915. DOI: 10.4271/2010-01-1233 (cit. on pp. 33, 63, 163, 165).

[92] Y. Wang, G. Conway, J. McDonald, and A. Birckett. "Predictive GT-power simulation for VNT matching to EIVC strategy on a 1.6 L turbocharged gdi engine". In: *SAE Technical Papers*. Vol. 2019-April. April. 2019, pp. 1–12. DOI: 10.4271/2019-01-0192 (cit. on p. 33).

Chapter 3

Turbocharged 4-S SI ICE experimental and modelling activities

Contents

3.1 Introduction

The purpose of this chapter is to detail step by step the proposed procedure and methodology in order to obtain high-quality 1-D turbocharged engines models. Both, the engine unit as well as the turbochargers are tested, modelled and validated according to a straightforward proposed methodology. The main target is to obtain a model from which valuable information may be obtained, with a special focus on turbocharging activities.

Lots of uncertainties may be faced when trying to model a given engine. From the modelling perspective, even if the air mass flow (and fuel) are well-reproduced... a lack/excess of predicted torque may be attributed to several wrongly modelled sources, among others:

- Combustion proper prediction;
- Volumetric efficiency;
- Engine pressure ratio, valve timing;
- Injection timing;
- Heat transfer in the cylinders during the combustion phase;
- Friction losses;

Furthermore, a lack or an excess of air mass flow may also arise during complete engine simulations. Mass flow error may be attributed to errors in volumetric efficiency due to various wrongly modelled phenomena: valves discharge coefficients; valves timing; instantaneous back-pressure; heat transfer during open-loop part of the cycle; ...

In addition to all the previous, when a given turbocharger is coupled to the virtual engine, errors in the turbocharger map may also appear and impact the results. A wrong turbine and/or compressor map may lead to model instabilities or incorrect boundaries to the engine block and high-pressure lines. For example, if the turbocharger maps under-predict the efficiency, then both scenarios may happen:

- Back-pressure to the engine block may be under/over-predicted. In this case, some effect on the pumping losses and average air mass flow take place (impacting in a lower or higher degree the engine output). However, it can be expected a good approximation as it is analysed in [62] and [6].
- Boost pressure may not be achieved even if boost control actuators saturate during the simulation time.

To further show the previous scenarios, Figure 3.1 shows a complete engine simulation, trying to reproduce a steady-state working point, in a 1.3L Spark-Ignited, VGT turbocharged ICE. Left Y-axis deals with boost pressures (black series and blue series), while the right axis corresponds to the VGT position adjusted by means of a PID implemented into the GT-Power software. Figure 3.1(A) shows the scenario in which even if the VGT mechanism forces the maximum closure position, (0% VGT opening), however, the targeted boost pressure is never reached. What is more, the extremely closed resulting VGT, implies an excessive back-pressure, this fact that contributes to the lack of air mass flow, torque.... On the contrary, Figure 3.1(B) shows a simulation in which the VGT control was successfully targeting the boost pressure. The only difference between both simulations was the turbocharger maps to represent turbocharger.

In other words, not only the engine block and piping shall be accurately modelled, but also turbocharger maps have their impact in a larger or smaller degree depending on the working point. The work in this section is structured into three main different sub-sections:

- The engine in question is tested in combination with three different turbochargers, labelled as VGT-1, VGT-2 and WG. With the experimental information, a complete engine model is fitted following a proposed methodology that neglects any possible uncertainty coming from the turbochargers' maps. Afterwards, TC supplier maps (measured under standard conditions) are called into question. Hot maps are evaluated, and some limitations are found section 3.2.
- To solve the turbocharger maps limitations, a straightforward methodology in which an experimental campaign is used to calibrate the 1D-HT-ML-TCM is proposed. This work is detailed in section 3.3 and it is

independent from the work in section 3.2. The result is a complete set of almost validated maps for each turbine and compressor analysed.

- Finally in this chapter, the obtained TC maps are implemented in the already developed 1-D engine model, for complete engine simulations. All this procedure is carefully described in section 3.4.

The idea is that section 3.2 and section 3.3 represent independent procedures, hence a 1-D engine model as well as a set of well-predictive turbocharger maps are obtained. In such a proposed methodology, turbocharger and/or engine modelling uncertainties are decoupled and not affecting each other procedures. Finally, a validation in which both sub-systems modelling accuracy is simultaneously assessed in section 3.4.

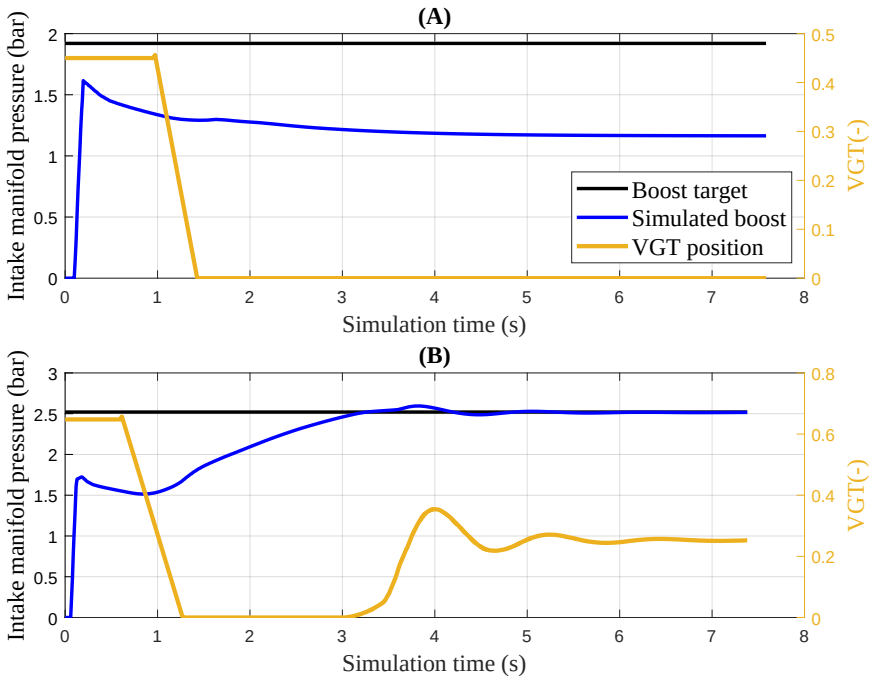

Figure 3.1: Steady state simulation: (A) Not well-targeted boost pressure simulation. (B) Well targeted boost pressure

3.2 1-D Turbocharged ICE model obtention

3.2.1 ICE Experimental campaign

The SI ICE of this study is one with 4 cylinders, 1.3 Litres (L) of displaced volume, variable valve timing (VVT), direct injection, waste gate (WG) turbocharged and EU6d-Temp calibration. Even if it is equipped with EGR, it is not used in this work. Some of the more relevant engine specifications are gathered in Table 3.1.

Table 3.1: Main engine features

Type of engine	1.3L Gasoline Spark-Ignited
Number of cylinders	4
Bore/Stroke	72.2mm/81.35mm
Compression ratio	9.6
Maximum engine speed	6200
Number of valves per cylinder	4 with variable timing
Injection system	Direct injection
Turbocharger	Yes
Charger cooling	Yes
Pollutant normative	EU6d-Temp

Three turbocharger units are assembled and tested in the described ICE, the baseline WG turbocharger and two other turbocharger units which were specifically selected and manufactured making usage of variable geometry turbine technology (from now in advance VGT-1 and VGT-2) and corresponding to two different suppliers. The engine and turbochargers were tested during this thesis in the laboratories of the UPV research institute CMT-Motores Térmicos. Recorded variables are summarized in the engine diagram available in Figure 3.2.

Main variables are registered within a frequency of 10 to 20 Hz. High-frequency pressure sensors for the intake manifold, exhaust manifold and cylinders were also instrumented. High-frequency information samples each 0.5 crank angle degrees. Additionally, other variables such as the VGT/WG position, throttle position, VVT and spark advance were recorded and directly taken from the engine control unit (ECU). A summary of the sensors used and their accuracy is included in Table 3.2. All the previous is applied to

the three turbocharger units and the several steady-state points and transients described in this section as follows.

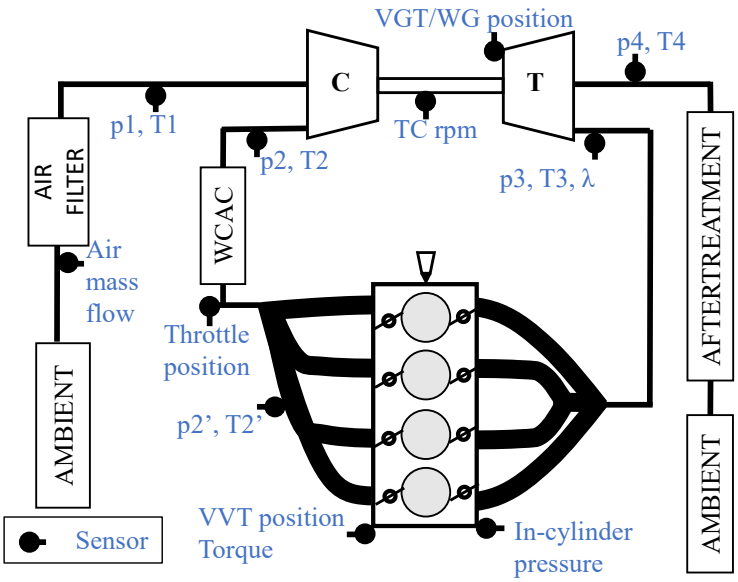

Figure 3.2: Engine diagram and recorded variables

Table 3.2: Engine test bench instrumentation

Variable	**Equipment**	**Range**	**Accuracy**
Speed	Dynamometer	6000rpm	0.03% fs
Torque	Dynamometer	±450Nm	0.05% fs
Cylinder pressure	AVL ZI33	0 to 250bar	0.3% lin.
Amplifier	Kistler 5011B	±10V	-
Air flow	AVL Flowsonix Air	20 to 720kg/h	2%
Fuel flow	AVL 733S Fuel Meter	0-150kg/h	0.2%
Temperature	K-type Thermocouples	-200 to 1250ºC	1.5ºC
Mean pressure	Kistler Piezo-Resistive Transmitters	0-10 bar	0.2% lin.
Gases analysis	Horiba mexa 7100 DEGR	-	1-4 fs.

3.2.1.1 Full loads

Nine full load points covering a wide engine speed range were tested for each turbocharger unit. The target was to reach the maximum engine performance for each point and engine-turbocharger combination. VGT mechanism and WG position were controlled externally to the (ECU) using a PXI™ system from National Instruments. Simultaneously, the spark advance was optimized to keep knock under control by means of a homemade knock detection and combustion diagnosis software based on the in-cylinder pressure analysis described in [93].

Air-to-Fuel Ratio (AFR) was managed by the engine control unit (ECU). The ECU estimates turbine inlet temperature and modifies the AFR accordingly to protect the turbine from overheating. Engine and turbocharger thermo-mechanic limits were provided by manufacturers and during the experimental campaign were kept under these limits, but as close as possible. Table 3.3 gathers these limits and Figure 3.3 shows the experimental results.

Table 3.3: Turbocharger limits

Variable	Limit	Controlled by
Maximum compressor outlet temperature	170ºC	WG or VGT
Maximum boost pressure	2.55bar	WG or VGT
Maximum TC speed	225krpm	WG or VGT
Maximum turbine inlet temperature	950ºC	AFR
Maximum turbine inlet pressure	3bar	WG or VGT

Full loads experimental campaign results are gathered in Figure 3.3. Before the analysis, "lambda" definition is required in order to properly describe the results. Lambda represents the engine Air-to-fuel-ratio (AFR) with respect to the Stoichiometric-Air-to-fuel-ratio ($AFR_{stoichiometric}$) as in Equation 3.1 is described. If Equation 3.1 is simplified, Equation 3.2 is obtained, and as a conclusion, an excess of injected fuel (operating under rich mixture conditions) provides with lambda<1.

$$Lambda = \frac{AFR}{AFR_{stoichometric}} = \frac{Air/Fuel_{injected}}{Air/Fuel_{stoichiometric}} \tag{3.1}$$

$$Lambda = \frac{Fuel_{stoichometric}}{Fuel_{injected}} \tag{3.2}$$

As a general conclusion, it could be stated that even if there are no appreciable differences in terms of air mass flow Figure 3.3(A), VGTs provide systematically, with a higher level of torque Figure 3.3(B), since the higher boost pressure level Figure 3.3(C). A particular analysis explaining the aforementioned differences is made for three considered operative regions:

- In the low-end-torque region (1250-1500 rpm), the WG turbocharger unit is limited by the turbine size and performance. No more WG mechanism closure is possible. For VGTs, the limitation was compressor surge, while there was still left some VGT closure margin. In other words, the WG turbine-engine matching is not suitable for the low-end-torque region.

  T3 differences between VGTs series, see Figure 3.3(D), are attributed to the T3 thermocouple location differences: While very similar values of air mass flow and lambda, see Figure 3.3(E) are obtained, T3 is higher for the WG than both VGTs at 1500rpm (and higher than VGT-2 at 1250). The last hardly makes any sense: since higher boost pressure is achieved by VGTs, which furthermore leads to some spark advance retard to avoid knock, see Figure 3.3(F). From the last, one expects T3 to be higher for the VGTs in any case, while this does not happen. In consequence T3 unrealistic differences are attributed to T3 thermocouple location.

- Medium range (2000-4000 rpm): In this range, the turbocharger limit is the maximum boost pressure Figure 3.3(C) of approximately 2.55 bar. Figure 3.3(G) reveals the WG higher turbine inlet pressure required for the same or even lower boosting pressure (in comparison to VGT-1 and VGT-2). This is a symptom of turbocharger efficiency differences in favour of the VGT turbochargers.

  Turbine inlet pressure is lower for the VGTs even if turbine inlet temperature in Figure 3.3(D) is lower (far from the 950^{o}C limit). Apart from the sensor location issue previously detailed, T3 differences are originated by the ECU management of the AFR. Mixture enrichment is not equally controlled for the three turbochargers, leading to unfavourable turbine inlet conditions in the case of the VGTs, especially for VGT-2, see Figure 3.3(G).

2000 rpm working point confirms the T3 thermocouple location issue: even if all turbocharger series are working under stoichiometric conditions, and higher boost is achieved by the VGTs, (again leading to some spark advance retard), T3 is higher for the WG.

- In the high-end speed range (4500-5000 rpm) WG limitation is the turbine inlet pressure, which was even overcome, see Figure 3.3(D), while Turbocharger's speed Figure 3.3(H) is also close to the limit. For both the VGT units the limitation is also turbine inlet pressure, which was very close to the maximum allowed. Special remark shall be done in the 5000rpm working point, in which, both VGT turbochargers, despite the lower p3 and T3, provide with the same or even higher boost pressure than the WG unit. This directly impacts the engine torque output.

  Additionally, in the case of the VGTs, the higher boost pressure observed leads to a higher compressor outlet temperature, or T2 in Figure 3.3(I), which at the same time, is very close to the limit provided by the turbocharger supplier.

It shall also be highlighted the fact that boundary conditions may be affecting the experimental results. For example, Figure 3.3(J) shows that compressor inlet pressure differences reach the value of 0.6 mbar at some points.

Finally, a second full load experimental campaign is performed, however, in this case, the stoichiometric mixture was fixed in the complete engine speed range. The main motivation for this experimental campaign is collecting as much information as possible, for the model development stage robustness.

The engine torque output is limited, see Figure 3.4(A), motivated by the forced almost-stoichiometric mixture Figure 3.4(B). The key point here lies in the fact that turbine inlet temperature limitation -of about 950^{o}C- is achieved, see Figure 3.4(C). Accordingly, the only way to surpassing the aforementioned thermo-mechanic limit is by means of a boost pressure level restriction Figure 3.4(D).

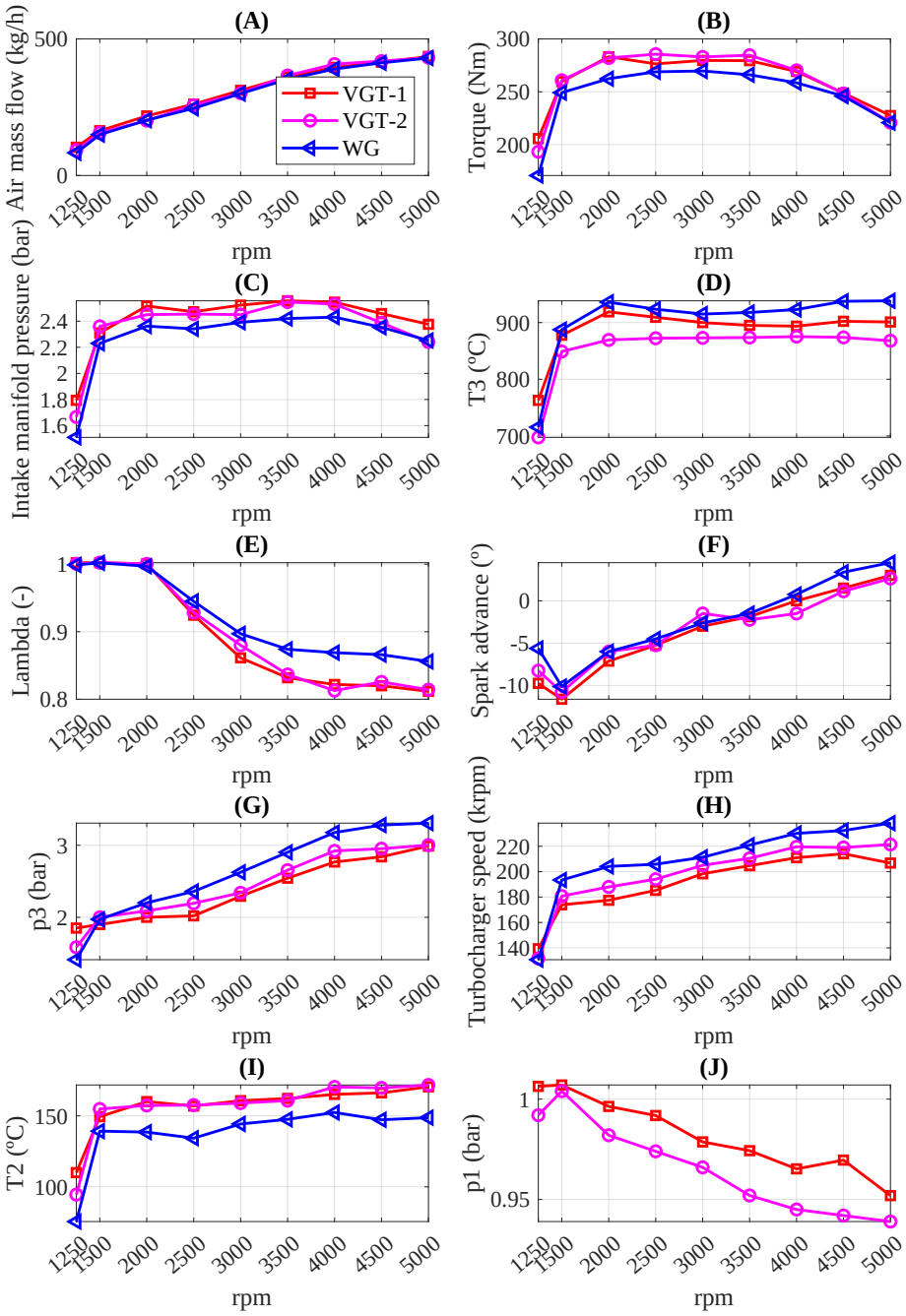

Figure 3.3: Full load experimental campaign for three turbocharger units

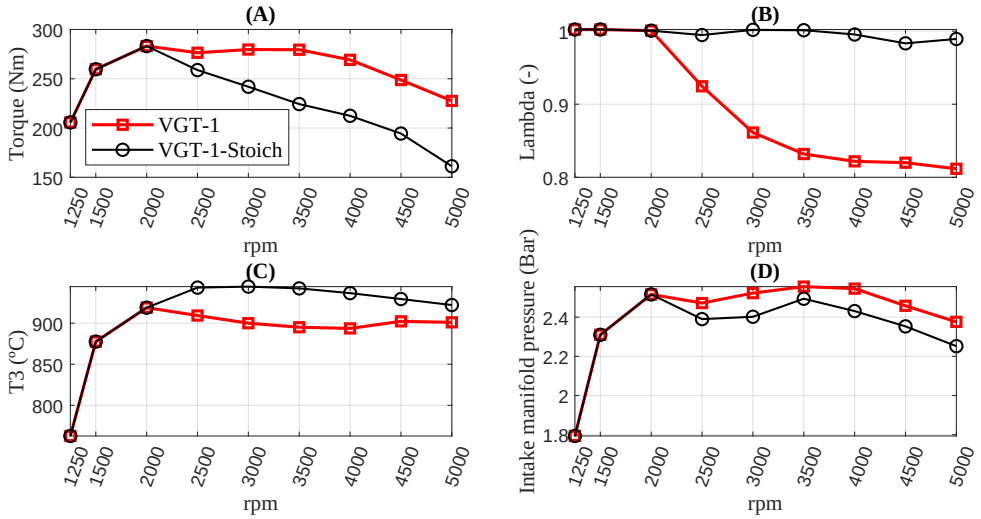

Figure 3.4: VGT-1 stoichiometric mixture experimental campaign

3.2.1.2 Partial loads

Moving to the partial loads, six working points have been tested for each turbocharger. Two points correspond to 16 bar of BMEP (165 Nm) and the rest to 12 bar BMEP (125 Nm). The reason for the 16 bar BMEP section is the one that follows: it is in this area, where the transition to throttle closure is required for the VGT units. Accordingly, 12 bar BMEP is selected following the same criteria but for the WG unit. This way, the amount of steady-state information covers the area in which the turbocharger unit has some impact (unlike very low loads, where all the turbocharger boost is throttled, and the engine behaves as a naturally aspirated throttled one).

Some of the main recorded variables are included in Figure 3.5. Torque differences are hard to detect in Figure 3.5(A) since torque was the target. Turbine inlet pressure differences are (also) hardly noticeable, see Figure 3.5(B). Looking at p2, in Figure 3.5(C) one can observe that higher compressor outlet pressure results in the VGTs, particularly in the 125 Nm line, in which the VGT-2 compressor outlet pressure is about 0.1-0.175 bar higher. However, differences are damped by the throttle, see p2' in Figure 3.5(D). It is detected a slightly higher p2' in the VGT-2, caused by the higher test cell temperature, see Figure 3.5(E) and its impact in intake manifold temperature, see

Figure 3.5(F). In other words, the higher inlet temperature is compensated by a slightly higher boost, in order to assure the same air mass flow level.

In all, it can also be concluded that the effects of boundary conditions affect the experimental results: Figure 3.5(G) shows how BSFC for the VGT-1 results in a 5-10 g/kWh better BSFC than VGT-2. The WG differences in comparison with VGT-1 are in the same range. Turbocharger speed is shown in Figure 3.5(H), differences hardly reach the 5 krpm between the three turbocharger units.

In conclusion from the experimental data analysis, experimental uncontrolled variability may prevent turbine technologies comparisons. This is one of the main reasons why obtaining proper 1-D calibrated models may be of high interest since all these issues could be avoided.

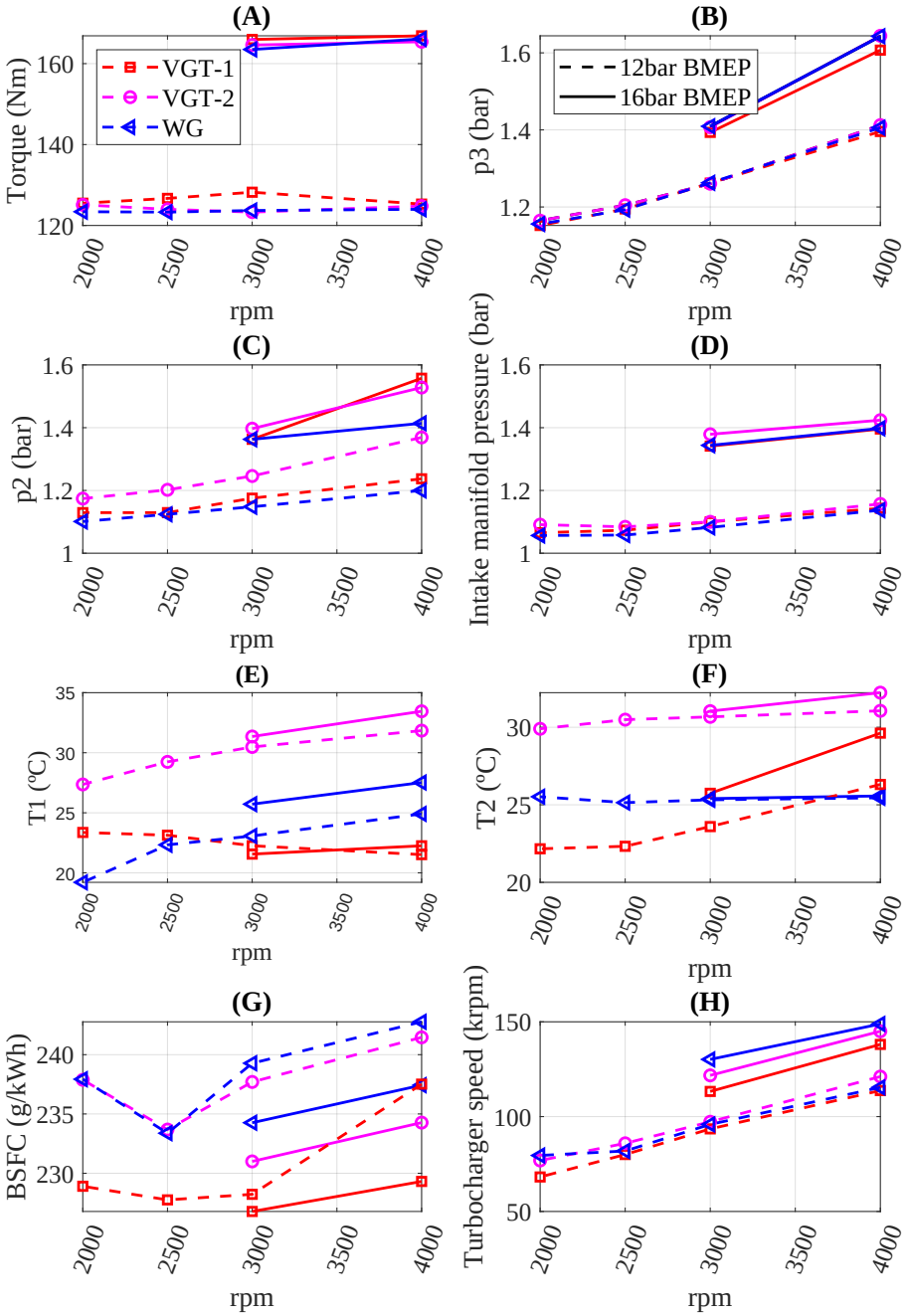

Figure 3.5: Partial loads experimental campaign results

3.2.1.3 Transient tests

Transient tests are performed for the three analysed turbocharger units as well. These transient tests consist of constant speed sudden load demand. For the transient tests, the same information as for the steady states is available.

The only difference lies in the iterative procedure that had to be carried out to reach the optimum solution in terms of transient response. This procedure was carried out for each VGTs and engine speed individually. The parameter to be optimized is the VGT position. The control optimization for the VGT follows two stages:

- In the earliest instants (during the sudden demand), an imposed offset to the VGT position is necessary to be applied. This corresponds to the so-called open-loop control stage. The initial offset is one of the parameters to be optimized for a proper engine response.
- Afterwards the open loop, a PI controller pursues the target boost pressure through the transient. Over the experimental campaign, the value of the “P” and “I” was targeting the closest to optimal transient response possible. However, P/I ratio was kept constant.

Figure 3.6 shows three different tip-ins for the same turbocharger and engine speed (VGT-1 and 1500 rpm). The difference between the three series is caused by the VGT control parameters. Boost pressure is included in Figure 3.6(A) and VGT position in Figure 3.6(B). The series labelled as "Slow" corresponds to one of the earliest tip-ins with very poor engine response. The “Over-oscillating” case, corresponds to a case in which the open-loop was not still optimized while the VGT PI parameters (during the closed-loop control stage) lead to an unsteady situation. The over-oscillation in boost pressure is caused by the VGT unsteadiness. Finally, the “Good” series corresponds to a close-to-optimum and stable combination of controlling parameters. It is remarkable how in the "Over-oscillating" series, a few % of the variation in terms of VGT position, lead to a heavily unsteady boost pressure fluctuation.

For the Waste-Gate, the control parameters were already calibrated and optimized in the production engine ECU, so it was not required further optimization during the experimental activities.

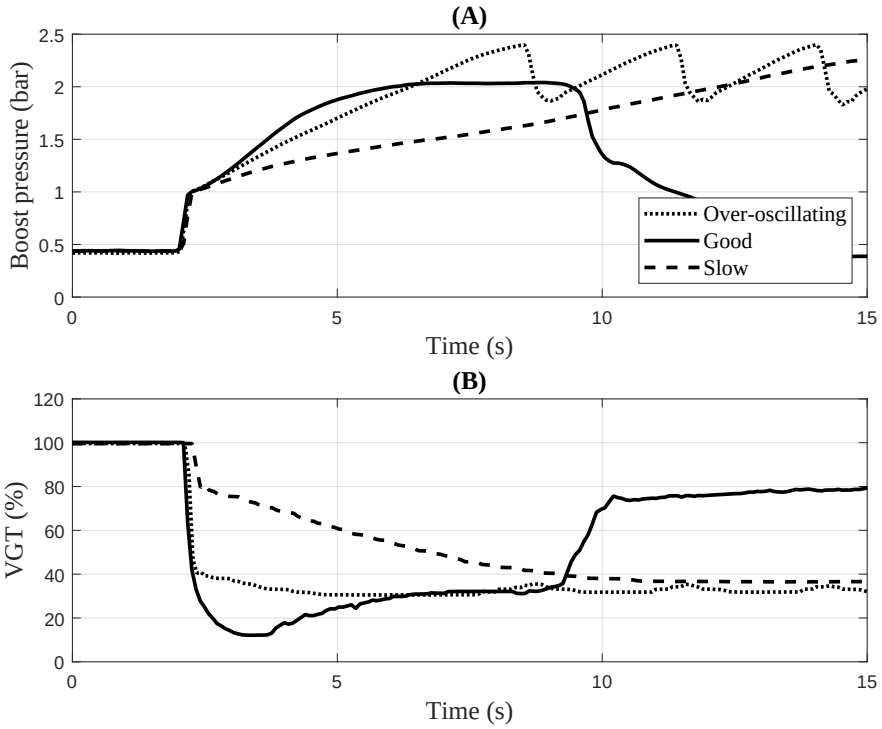

Figure 3.6: (A) Boost pressure and (B) VGT evolution for VGT-1, 1500 rpm and 3 different control strategies

Figure 3.7 gathers some of the main recorded variables governing the load transient response under a sudden engine torque demand, keeping a constant engine speed of 1500rpm. Figure 3.7(A) shows how for the VGT-2 it was able to increase the air flow rate faster than for the other two units, however, hardly any difference is observed in terms of torque Figure 3.7(B). Concerning the manifold pressure, it could be stated that VGT-2 builds it faster, however, the last is achieved by increasing p3 higher than for the other two series, see Figure 3.7(C) and Figure 3.7(D). In consequence, the volumetric efficiency deteriorates, and the engine output is almost the same as for the WG turbocharger. This goes in line with the conclusions obtained by Ericsson et al. [91], who concluded that a balance shall be kept between turbine power and engine volumetric efficiency when controlling the VGT closure.

The WG turbocharger response presents a similar boost pressure built,

while p3 is substantially smaller (reaching differences up to 0.65 bar). Turbocharger speed, in Figure 3.7(E), is similar in the earliest stages, although the resulting turbochargers' speed is different, even though p2 converges to the same value for all three series. The sudden drops in TC rpms, in the turbocharger speed, are merely a wrong sensor measurement which was happening randomly in the transient tests performed with the VGT-2. These drops do not represent the actual TC speed evolution. It is assumed that the inductive sensor misses eventually some of the blades of the impeller, leading to punctual speed under-predictions.

In terms of VGT or WG opening, the evolution of the mechanisms is presented in Figure 3.7(F) and shows how the WG mechanism closes as much as possible during most of the transient, while the VGT's still had some margin for further closure.

Finally, low inertia thermocouples (for thermal fast response) were assembled in the exhaust manifold and turbine outlet. For fast load transients (as the ones in this study) it is necessary to avoid/minimize the thermocouple thermal inertia [6]. In Figure 3.8 it is evidenced the difference in the temperature evolution response between 3mm and 0.3 mm thermocouples. Particularly, Figure 3.8 deals with VGT-1 sudden tip-in under constant engine speed (1500 rpm). This experimental information is of high importance for further modelling purposes. The low inertia thermocouples are highly sensitive to the actual fluid thermal evolution, but two main drawbacks shall be considered, they are much expensive than 3mm ones, and last for few minutes or even seconds depending on the engine operative area. In fact, the transient shown in Figure 3.8 is the only one with such relevant information.

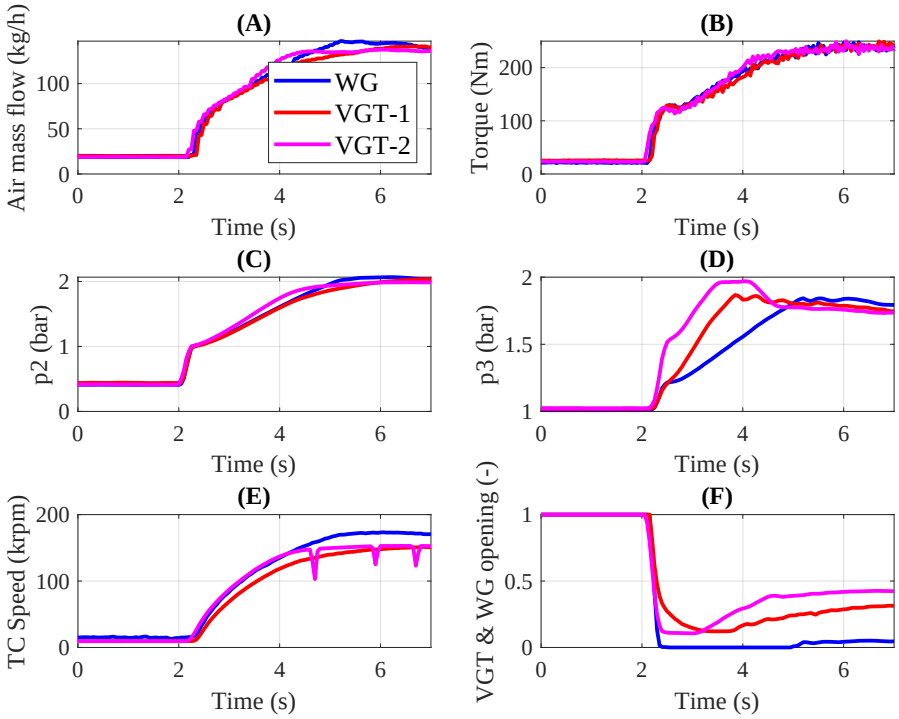

Figure 3.7: Transient tests for the three analysed turbochargers. Sudden tip-in under constant engine speed (1500rpm)

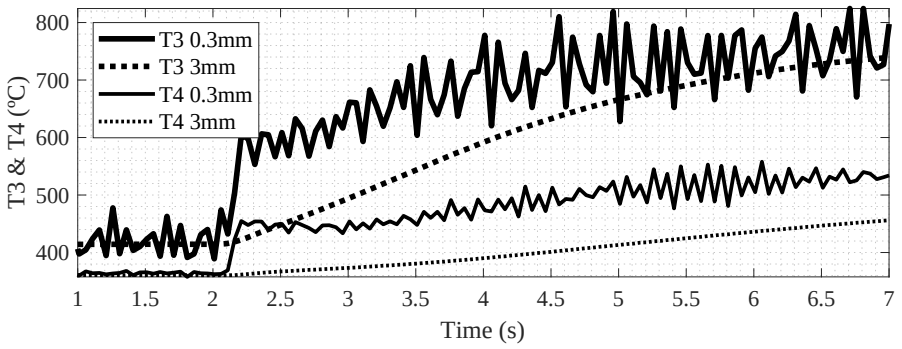

Figure 3.8: 1500rpm experimental transient evolution for T3 and T4 variables, measured with two different thermocouples, high inertia (3mm) and low inertia ones (0.3mm)

Figure 3.9 gathers the same amount of information dealing with the engine speed of 3000rpm load transients. Air mass flow and torque differences are hardly noticeable during the transient. In any case, air mass flow, boost pressure and the torque built take about 1s until steady-state conditions are reached.

The issue dealing with VGT-2 turbocharger sudden speed drops is found here as well, see Figure 3.9(E). Lastly, it is shown the VGT and WG positions in Figure 3.9(F). VGTs never reach the 0% opening position, while the WG does until 90% of the pressure demand is achieved. The last calls into question whether the WG mechanism would be capable of compensating the effect of adverse working conditions such as for example altitude or extremely hot weather.

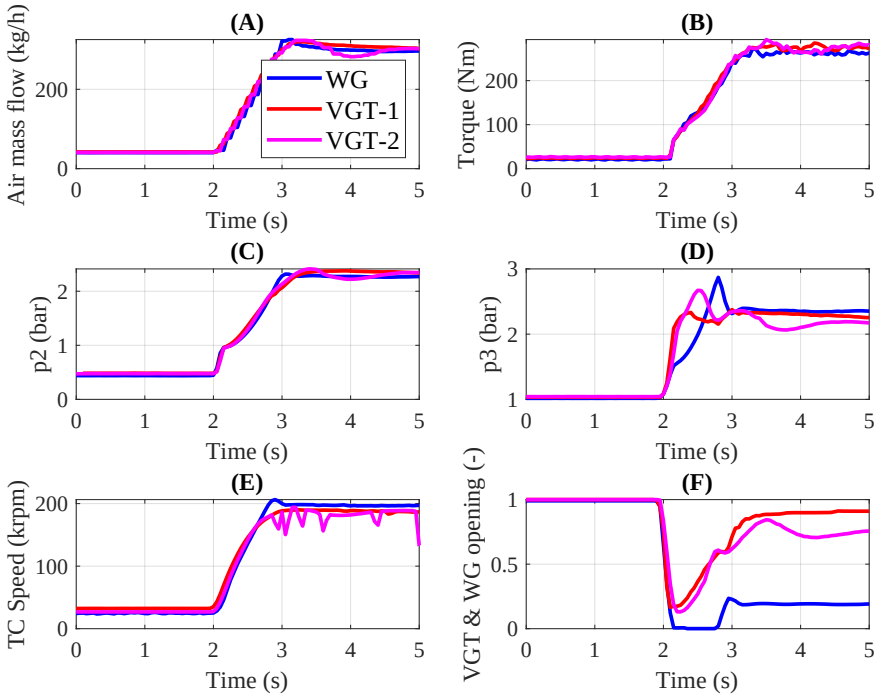

Figure 3.9: Transient tests for the three analysed turbochargers. Sudden tip-in under constant engine speed (3000rpm)

3.2.2 Model fitting

Once accepted the several crossed factors leading to modelling uncertainties, a calibration procedure was developed. During this virtual engine calibration procedure (or engine model fitting), the experimental data from full load tests is taken as a reference. In all, each fitting parameter targets only one experimental engine variable, with direct physical relation between both. If there are several possibilities the one with the strongest physical relationship is selected. The main purpose is to develop a procedure that is bi-univocal enough to be automatized. Therefore, it will provide clear guides to artificial intelligence (AI) codes or systems to be used for calibrating autonomously digital-twin like software.

- First, test cell working conditions and AFR for each point are imposed to be the experimental ones. Furthermore, VVT set-up shall be implemented for each point individually. Slight discrepancies in the VVT may affect cylinder composition, volumetric efficiency, cylinder pressure evolution, and pulsating behaviour in both exhaust and intake manifolds.
- Secondly, during this fitting procedure, the energy loop between the intake air and exhaust gas flows (linked to turbocharger unit) is avoided: the compressor and turbine are decoupled from each other. This way, the compressor speed is targeted to guarantee the intake manifold pressure (p2') using a PI controller. On the other side, the turbine speed is fixed (imposed to be the experimental one) while the VGT position pursues the exhaust manifold pressure (p3). This way, the impact of the turbocharger uncertainties on the engine response is avoided at the fitting stage. Simultaneously, the heat transfer multiplier (HTM) of the water charge-air-cooler (WCAC), fits the intake manifold temperature (T2'). From now in advance, the fitted HTM for the WCAC is labelled as WCAC-HTM.
- In third place, the overall cylinder heat transfer multiplier (OC-HTM) corrects the in-cylinder heat transfer model and fits the engine volumetric efficiency (intake charge flow). Fitting the volumetric efficiency, requires guaranteeing intake and exhaust boundary conditions. This is possible since the intake boost pressure and exhaust back-pressure have been previously imposed by compressor and turbine (as explained in previous paragraph). This is the main point why the decoupling between

compressor and turbine is necessary. In addition, thanks to the technique of decoupling the mechanical connection between compressor and turbine, a rough set of TC maps is enough in this phase, since turbine and compressor efficiencies are not governing the working point at all. In other words, during this phase the target is calibrating the engine block systems, hence, a suboptimal turbocharger (from the point of matching) would be enough. But a turbocharger object is still needed since the pressure wave reflective properties of the compressor and turbine maps are required for a proper modelling of gas-dynamics in the engine exhaust and intake manifolds.

Once all the previous is carried out, the different simulations converge to the experimental data, since all the PIDs are simultaneously forcing the simulation to do so. Furthermore, instantaneous pressure evolution along the exhaust and intake manifold can be called to question, since, added to the previous, the turbocharger has been implemented (and not a simple boundary, forcing constant p2' or p3 for example). What is more the fact of controlling the compressor and turbine separately, to assure intake and exhaust pressures (instead of directly implementing the pressure as a fixed boundary) is purposely done for pressure pulse propagation check. Finally, this enables the variable valve timing check.

After all, Figure 3.10 shows for the 1250 rpm, full load point, instantaneous pressure evolution for exhaust and intake manifolds as well as for the cylinder. 1250rpm has been selected since the low-end torque corresponds to the most interesting area and is more complex to properly simulate. Figure 3.10(A) corresponds to cylinder pressure evolution, Figure 3.10(B) corresponds to exhaust pressure evolution, and Figure 3.10(C) to intake. Figure 3.10 shows a high degree of agreement between experimental and modelled instantaneous pressure signals.

It is remarkable the exhaust valve opening (EVO) preciseness. This is evidenced in the sudden cylinder pressure drop (just before the 200º), see Figure 3.10(A) and also in the high degree of agreement in terms of p3 built (in both, pressure and timing). In all, Figure 3.10 reveals the accurately modelled timing and pressure pulses propagation. Furthermore, the intake manifold pressure evolution agreement is an indicator of a proper 0D/1D intake system modelling practice (including the intake manifold and the compressor).

After checking the pressure pulses and valve timing, as well as guaranteeing intake pressure and temperature, as well as exhaust manifold pressure, the overall cylinder heat transfer multiplier converged to a value of 0.59. Some simulations claimed a slightly higher value, some others slightly smaller ones, but since no clear trend was obtained, the fluctuations on the converged value are attributed to inherent experimental dispersion (sensor calibration i.e...) and assumptions/simplifications made during the modelling.

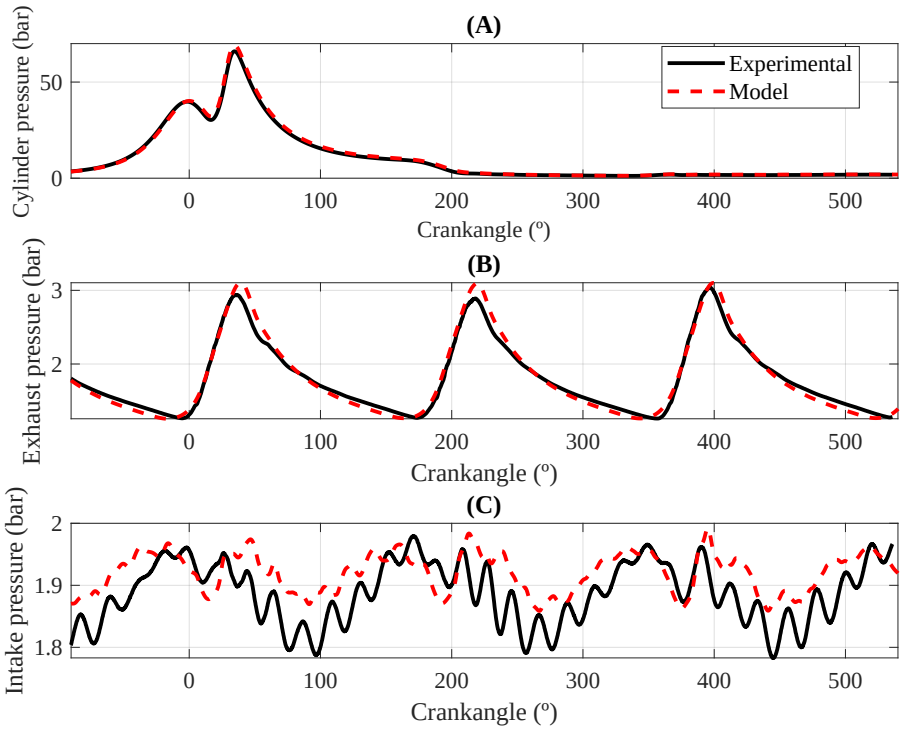

Figure 3.10: 1250 rpm experimental and model instantaneous pressure evolution for cylinder (A) exhaust (B) and intake (C)

Regarding combustion modelling, a Wiebe function is implemented. The parameters to be obtained are the combustion phasing (characterized by the CA50) and the Time of Combustion (TOC). The last is evaluated as the difference between CA90 and CA10. These parameters are obtained as the experimental instantaneous cylinder pressure is attempted to be reproduced by the simulation, during the called "cylinder pressure analysis" (CPA) proce-

dure. The CPA is a tool available in the GT-Power software for combustion modelling purposes. In other words, the instantaneous cylinder pressure evolution is adjusted by the GT-Power. However, before this procedure is carried out, the experimental air mass flow shall be well-reproduced by the model. Therefore, the previously discussed actions are a must, i.e.: decoupling compressor from turbine side, fitting the volumetric efficiency, and guaranteeing the correct VVT. In all, cylinder pressure evolution (focusing on combustion process) is shown for 5000 rpm in Figure 3.11.

Also, injection timing becomes a key point. Normally little effort is made in well-reproducing injection timing in 1-D simulations. As far as the injected fuel mass and TOC are well-targeted, injection timing is erroneously considered a second-order variable. However, in this modelling campaign, it was detected the influence of the injection timing. Figure 3.11 shows for 5000 rpm full load, how a wrong modelling strategy leads to a wrong estimation on the instantaneous in-cylinder pressure. Particularly, in this picture, the "wrong injection" series was done too early, hence, the gasoline evaporation effect on decreasing the mixture temperature (and pressure) during compression stroke was not well-reproduced. Particularly for the analysis of this modelling aspect, 5000rpm point has been selected since the wrong injection modelling practice effect is more noticeable with engine load and speed. Firstly, the higher the load, the more the injected fuel, hence, fuel evaporation effects are greater. Secondly, the higher the speed, the more relevant effect of fuel evaporation is, since overall heat to the walls decreases in relative terms. This is shown in Figure 3.12(A) for the full load modelling campaign: even if the total heat power transferred to the walls is greater, Figure 3.12(B).

In other words with high load and speed, fuel evaporation effect on fresh mixture temperature and pressure evolution become more relevant. Special care shall be applied to this modelling aspect, to well-reproduce the experimental cylinder evolution.

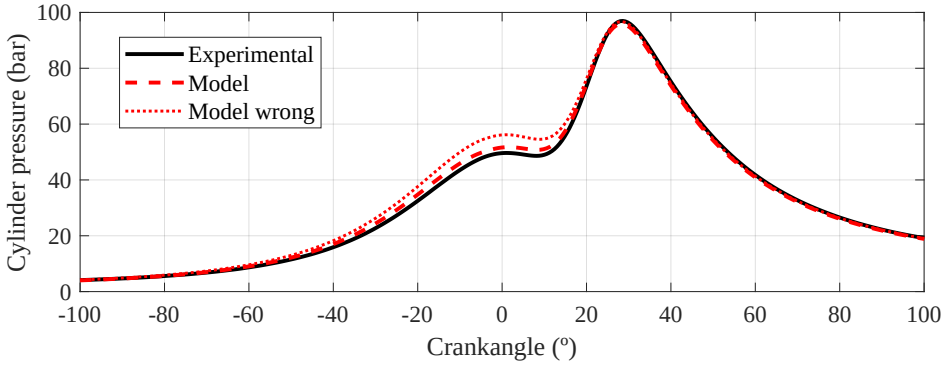

Figure 3.11: 5000 engine rpm instantaneous cylinder pressure evolution for experimental and model series of data Model wrong corresponds to an intentioned error in injection timing for the same TOC and fuel mass

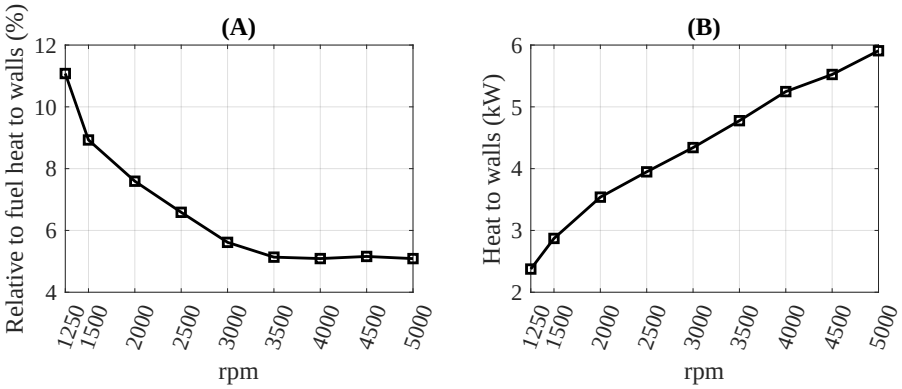

Figure 3.12: (A) Relative heat to the walls and (B) total heat to the walls from modelling fitting campaign

In addition, and simultaneously to the model fitting, injection strategy check and the combustion analysis utilizing the CPA, a neural network (NNW) is trained for combustion prediction. In other words, taking advantage of the calculated combustion parameters, these are correlated to directly related variables, through a neural network, so that for future prospective studies, one can predict the combustion parameters. Figure 3.13 shows a screen caption of the NNW structure developed in GT-Power: The idea is to train the NNW following the next sequence:

- The inputs to the NNW (from the left-top to the left-bottom of Figure 3.13) are the following four in-cylinder variables at intake valve closing (IVC): pressure, temperature, trapped residuals and trapped mass.

- Afterwards, the CPA calculated output, is provided to the NNW.

- The NNW is trained according to the previous two sets of data: given the inputs (engine variables in the first point on this list), the combustion is predicted (the NNW outputs).

The most interesting point of this methodology is the fact that the neural network is trained along with a wide range of operative areas, combining full and partial loads, for almost the complete engine rpm range. Consequently, the NNW shown in Figure 3.13 can be used afterwards in the training methodology, in order to predict the combustion process. As it is shown, the variables which are influencing combustion timing in a deeper way are taken into account for the training process. The target is to build a predictive and robust combustion system, by relating the aforementioned parameter (temperature, pressure, residuals...) with the TOC and CA50.

The box called "limiters" in Figure 3.13 appeals to input variables to NNW. This is required in order to avoid unstable/undesirable behaviour during the simulation initialization, when some variables input may have nonsense. The limits for the input variables should be the maximum and minimum values provided to the NNW during the training.

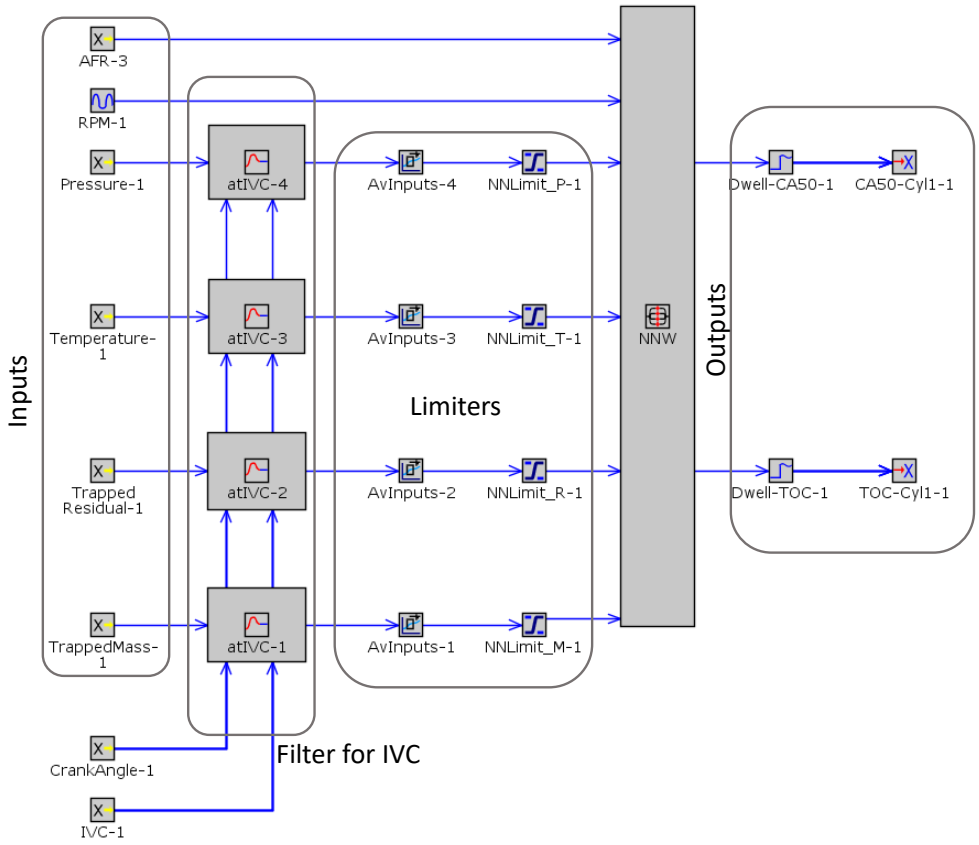

Figure 3.13: Neural network caption from GT-Power. From left to right: input variables, filter for variables at IVC, variables limits and NNW output

The (FMEP) is obtained as the difference between the indicated mean effective pressure (IMEP) and the brake mean effective pressure (BMEP). BMEP comes from the experimental torque while IMEP comes from the model (which as stated, reproduces in-cylinder pressure evolution). As a result of the complete experimental and modelling campaign fitting, the FMEP map in Figure 3.14 is obtained. As it is shown, FMEP is plotted versus engine speed and engine torque.

In all, it could be pointed out the high impact of the load from 3000rpm in advance, while speed effect on FMEP appears to be more relevant in the range going from 1250-3000. Finally, in terms of FMEP, it is remarkable the two plateaus arising around the 3000 and 4000 rpm, under whatever load. This

can hardly be explained, and it is attributed to the interpolating method and the FMEP values obtained during the fitting procedure.

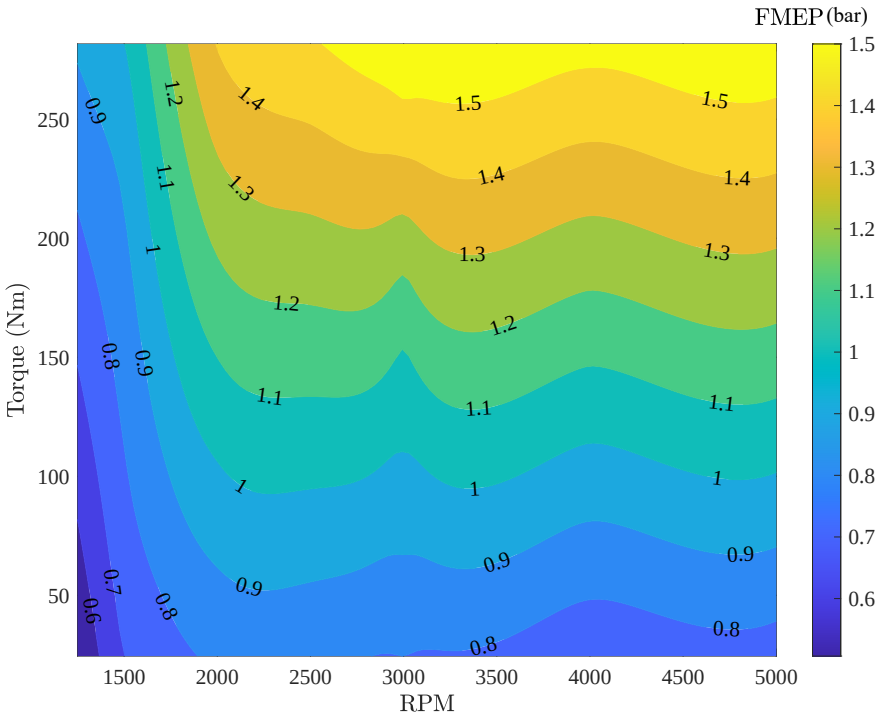

Figure 3.14: FMEP map as a function of torque and engine speed

Once the combustion, heat transfer to the cylinder walls, air mass flow and AFR are well-fitted, any error in the exhaust manifold temperature (T3) prediction comes necessarily from the exhaust line heat transfer. Experimental T3 is taken as a reference to adjust the exhaust ports and exhaust manifold heat transfer multiplier (EM-HTM). The turbine back-pressure (p4) is also fitted using a forward discharge coefficient located downstream the after-treatment, this discharge coefficient compensates the errors in the p4 committed by the model, and coming from the after-treatment wrong modelling practice, or the influence of the test-cell gasses-extraction system. This forward discharge coefficient is labelled from now in advance as (E-FDC). In conclusion, the E-FDC is highly dependent on the after-treatment line and also on the test cell, so it could vary accordingly.

The EM-HTM and WCAC-HTM trends are included in Figure 3.15(A) and Figure 3.15(B) respectively. For the EM-HTM, a third-degree polynomial correlation was found to fit better. The complete engine range, from the lower mass flow points up to the maximum mass flow points are of high interest in order to obtain a robust correlation along the complete operative area. The shape of the obtained trend could be attributed to several aspects, such as external boundaries, 3D phenomena which is not the target to be analysed in this work.

From the WCAC-HTM, in a first stage, it was obtained the light dotted third-degree curve shown in Figure 3.15(B). However, it was analysed the reason for the lowest mass flow points considerably higher HTM. For the following analysis it is taken as reference the lowest air mass flow point (but the same could be stated for the other). It was found that the p3>p2, leads to back-flows. The model estimated that back-flows, increased the predicted mass-averaged intake temperature. The model instantaneous mass-flows across the intake and exhaust valves as well as valve lifts, are included in Figure 3.16, where negative intake mass corresponds to back-flows.

Figure 3.17 shows the minimum air velocity in the intake manifold and pipes, until the intake valves (placed in the right side). As it can be seen, negative velocities (in the opposite direction of the normal flow) reach the intake manifold. In Figure 3.18 it is shown the intake air mass flow temperature distribution. In consequence the WCAC-HTM PID saturated to the maximum allowed level, trying to cold down the air, to compensate this effect.

In conclusion, these two low mass flows working points were not taken for the WCAC-HTM correlation, since the temperature over-prediction is not caused by a lack of the WCAC performance, but because of the back-flows originated by the extremely low air mass flows in both discussed working points. The air mass flow in these points it is approximately in the lower limit of the engine air mass flow sensor. The rest of working points were taken as a reference, and it was selected constant value for the WCAC-HTM, see the constant value dotted series in Figure 3.15(B).

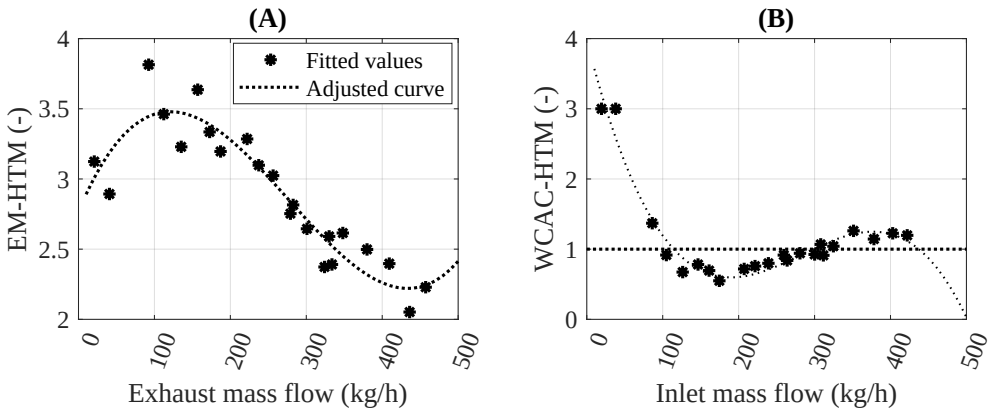

Figure 3.15: (A) EM-HTM and (B) WCAC-HTM as a function of exhaust and intake mass flow respectively. Dotted series correspond to adjusted curve and dots to fitted values

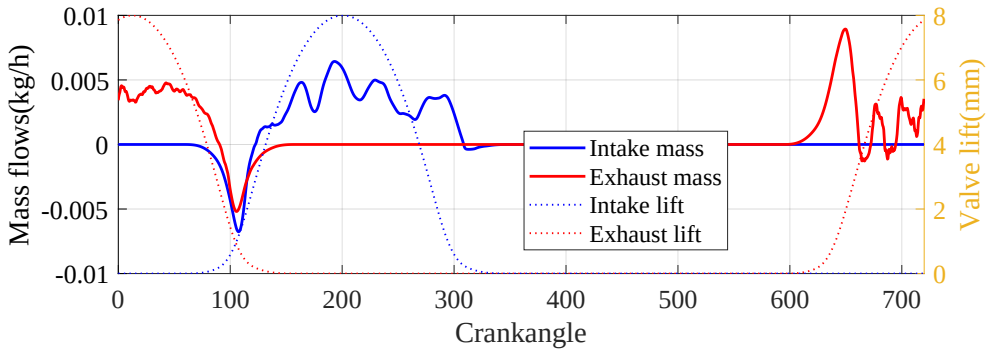

Figure 3.16: Lowest air mass flow point: Instantaneous mass flows though intake and exhaust valves and valve lifts

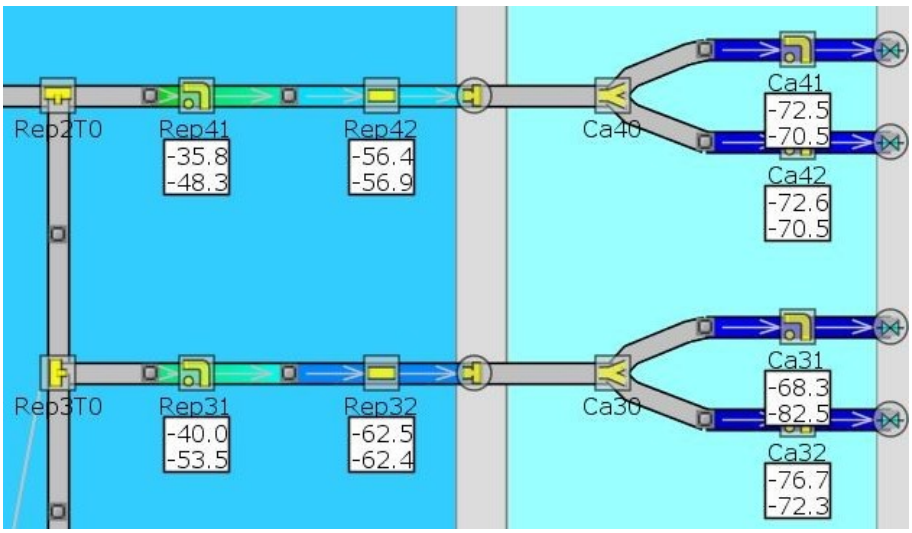

Figure 3.17: Intake manifold minimum air flow velocity for lowest air mass flow point in m/s

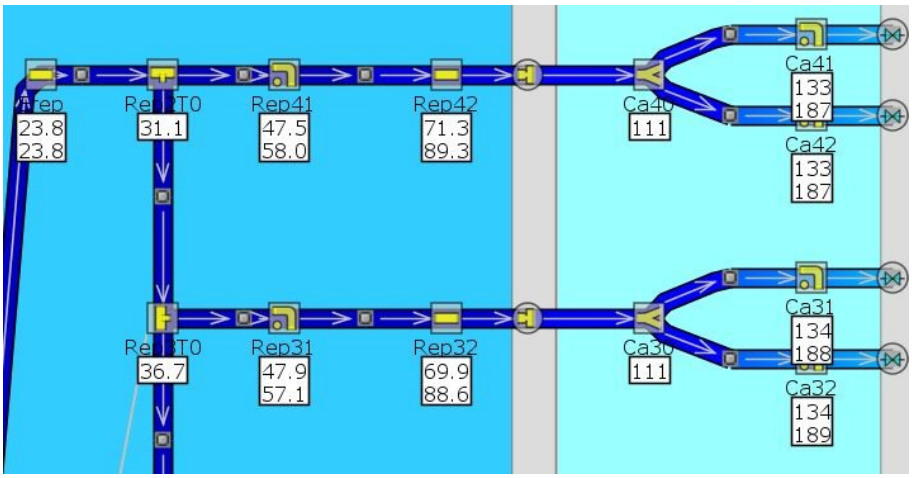

Figure 3.18: Intake manifold mass averaged temperature distribution (ºC) for lowest air mass flow point

Turbine outlet temperature (T4) is fitted employing the turbine heat transfer multiplier (TURB-HTM) located in the turbine volute and turbine diffuser pipes. For this reason additional pipes must be included to simulate these

tapered ducts of the turbine (they would be also convenient for wave dynamics simulation). In summary, for T4 calibration, a proper validated set of adiabatic turbine maps are necessary. If the turbine map corresponds to an experimental hot map, the heat transfer effects would be already included inside the effective turbine efficiency from these maps and then accounted twice. In consequence, heat transfer modelling for T4 adjustment can only be attempted making usage of adiabatic maps. When hot maps are used, then volute and diffuser heat transfer shall be neglected.

Moreover, logical sequence of PID activation was carried out. For example, after having targeted boost and exhaust pressure, as well as intake manifold temperature, volumetric efficiency PID actuates. In general the PID order actuation is the one in Table 3.4. The cylinder pressure analysis starts as soon as possible, trying to reproduce the cylinder pressure evolution from the very beginning. In any case, this set-up tries to follow a logic order, to earn as much time as possible and avoid unrealistic results. In all, the simulations are as long as required until all the PIDs converge to the selected experimental value (+-1% of discrepancy during 10 consecutive cycles).Figure 3.19 summarizes the explained methodology in a more schematic view.

To avoid interferences between several fitting parameters, physically representing limits are imposed during the calculation. The limits for each variable are summed up in Table 3.5. Table 3.5 also includes the results of the fitting for this engine.

Table 3.4: PID start order for fitting procedure

order	**Variable**	**Controlled by**
First	Ambient boundaries, lambda, VVT	FIXED
Second	Cylinder pressure evolution	Combustion analysis: CA50 and TOC
Third	p2' and p3	PID governing compressor speed and VGT/WG respectively
Fourth	T3 and T2'	PID governing EM-HTM and WCAC-HTM respectively
Fifth	Volumetric efficiency	PID governing OC-HTM
Sixth	p4, T4 and Torque	PID governing: E-FDC, TURB-HTM and FMEP respectively

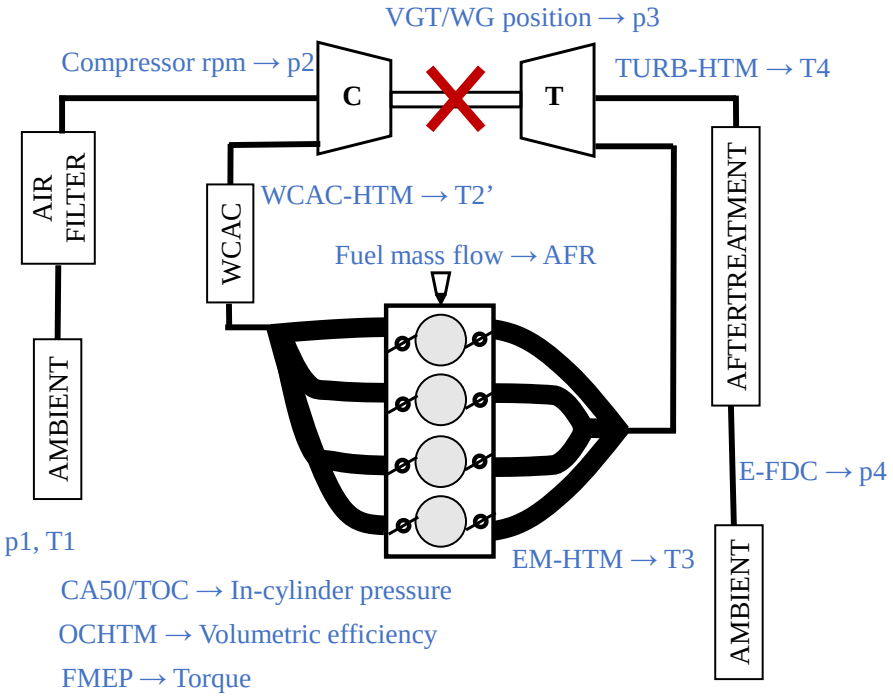

Figure 3.19: Model fitting schematic view

Table 3.5: PID limits for the fitting procedure and fitting results

Variable	**Limits**	**Result from fitting**
WCAC-HTM	0.5-1.5	Constant value of 1
OC-HTM	1-5	Constant value of 0.59
EM-HTM	1-5	Correlation in Figure 3.15(A)
TURB-HTM	1-5	Correlation in Figure 3.15(A)
E-FDC	0.1-1	Correlation in Equation 3.3
TC-RPM	10-275krpm	-

$$E-FDC = 1.448610^{-8}\dot{m}^3_{exhaust} - 1.577210^{-5}\dot{m}^2_{exhaust} + 0.0058\dot{m}_{exhaust} + 0.0999 \quad (3.3)$$

3.2.3 Model validation attempt with hot supplier turbocharger maps

After having obtained the set of coefficients and trained the NNW, the only potential uncertainty lies on the TC maps/modelling. In this subsection it is evidenced the lack of accuracy when using an engine-core model, previously calibrated following discussed methodology (with +/- 1% error in all relevant variables), and, coupled to turbocharger maps experimentally recorded under hot testing conditions (hot maps). The most controversial working areas (low and high engine rpm range) are analysed, and the wrong modelling is attributed and justified to take its origin in the turbocharger.

First, the turbocharger supplier hot maps are used for the turbine and compressor. These maps are recorded under hot conditions, which pretend to be close to the ones taking place in an engine context. In a second step, the connection between both (turbine and compressor) is restored. In other words, they are re-coupled to each other through the shaft. The last implies that the energy balance between the turbine and compressor, calls into question the turbocharger maps accuracy, hence, a wrong set of maps would lead to wrong predicted pressures and/or temperatures, as in this section is shown. In addition, two hints are worth to be explained:

- Mechanical efficiency in the TC shaft has been fixed to 100% (since mechanical efficiency, in theory, is already included in the "ETE" definition in Equation 2.4 of the turbine maps following SAE standards (as the suppliers do).
- TURB-HTM for heat transfer in the turbine volute and diffuser is set up to zero. This is done since hot maps include the effect of heat transfer by themselves, as previously stated.

As a result, VGT-1 simulation is shown in Figure 3.20. Main variables such as air mass flow in Figure 3.20(A), torque in Figure 3.20(B), turbocharger speed in Figure 3.20(C) and intake manifold pressure Figure 3.20(D) are shown. The most relevant fact is the lack of air mass flow in the low-end torque region of engine speeds. The last leads to a lack of torque and is attributed to the lack of intake manifold pressure, which at the same time comes from the lack of turbocharger speed. For the rest of the working area, one might detect

a slight lack of engine torque, even if intake manifold pressure is well-predicted by the model.

To lighten the low-end torque issue and the slight lack of torque in the 3000-5000 engine range, Figure 3.20 is further discussed.

- First, it is detected that the VGT position in the low-end torque region is set up to 0%, see Figure 3.20(E). This provides the key point for the low-end torque wrongly modelled point explanation: Turbocharger efficiency. In the low end-torque, the relatively closed VGT position and low mass flow call into question this specific area of the look-up table that constitutes the turbine map. Indeed it is in this area, where heat transfer effects are more important according to the available literature, as in subsection 2.2.1 was discussed. In all, turbine efficiency is under-predicted, to compensate for this effect more VGT closure is applied by the PI, until a point in which an extremely closed VGT turbine position, leads to an efficiency deterioration effect, which that further contributes to the extra VGT closure. This snowball effect leads to a p3 over-prediction, diminishing and a volumetric efficiency deterioration.

- The lack of turbine efficiency is evidenced for the rest of the engine range since the systematic over-prediction of p3 as in Figure 3.20(F) is depicted. However, from 2000rpm in advance, the resulting higher p3, has a limited impact on the volumetric efficiency, leading to a slight lack of air mass flow, which at the same time leads to the lack of torque, observed in Figure 3.20. Finally, it is worth mentioning the model accuracy in p4 prediction in Figure 3.20(F). T3 is depicted in Figure 3.20(G), with the only exception of the low-end torque (due to the lack of air and fuel), it is well-predicted. T4 is also shown in Figure 3.20(G) and results are slightly overestimated (up to 35^{o}), even if the predicted turbine pressure ratio is higher than it should, as previously stated.

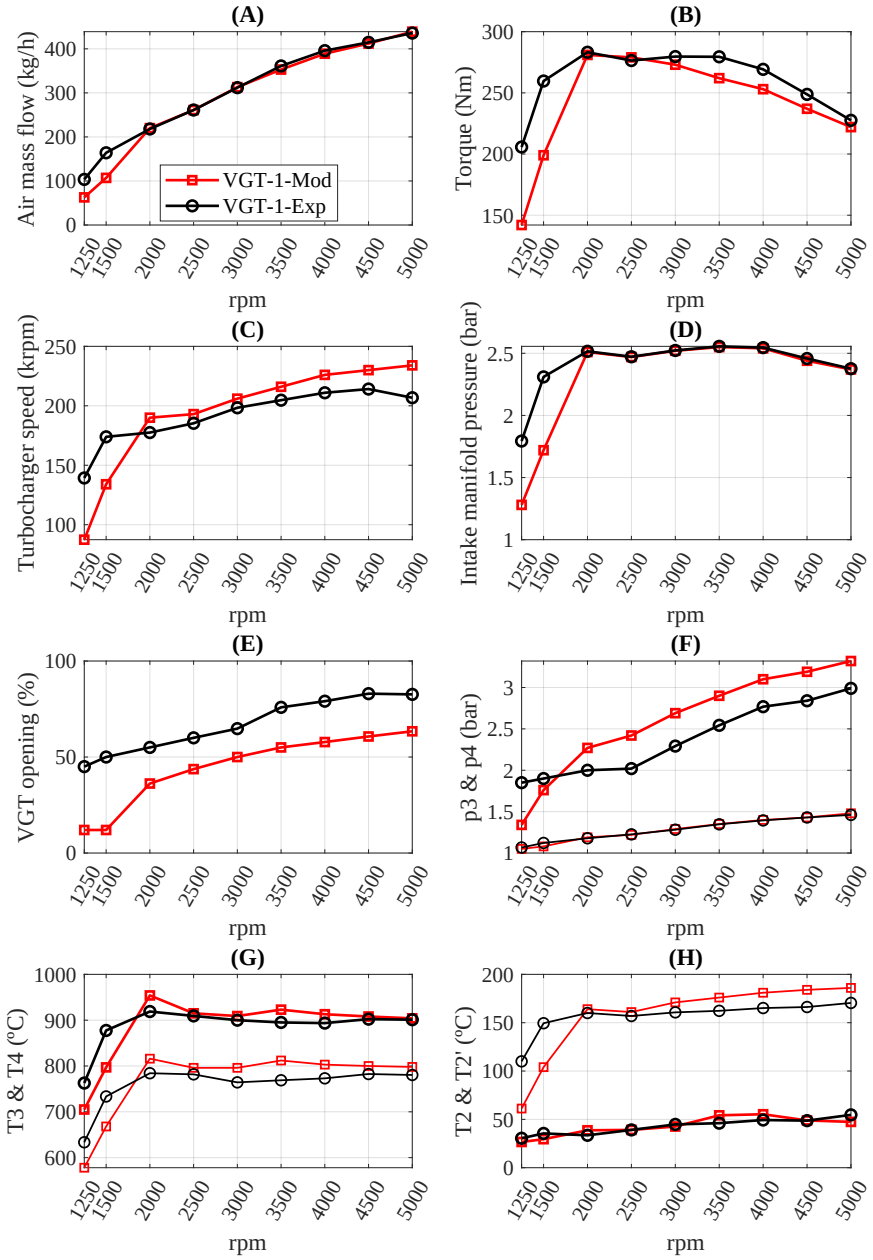

Figure 3.20: VGT-1 Full load engine variables experimental vs. modelling campaign comparison

For more robust conclusions, the same validation was followed for the WG unit and results are depicted in Figure 3.21. Conclusions are pretty much the same as for the VGT-1. Low-end torque boost under-prediction leads to a lack of air mass flow and torque, see Figure 3.21(A) and Figure 3.21(B). As for VGT-1, the last is directly related to the turbocharger performance, since the lack of turbocharger speed Figure 3.21(C) leads to a lack of boost pressure Figure 3.21(D) even if the WG diameter is set to the closest position Figure 3.21(E).

For the rest of the engine range, p3 over-prediction directly impacts the volumetric efficiency, which disturbs the air mass flow through the engine itself, causing a lack of torque. p3 results are shown in Figure 3.21(F).

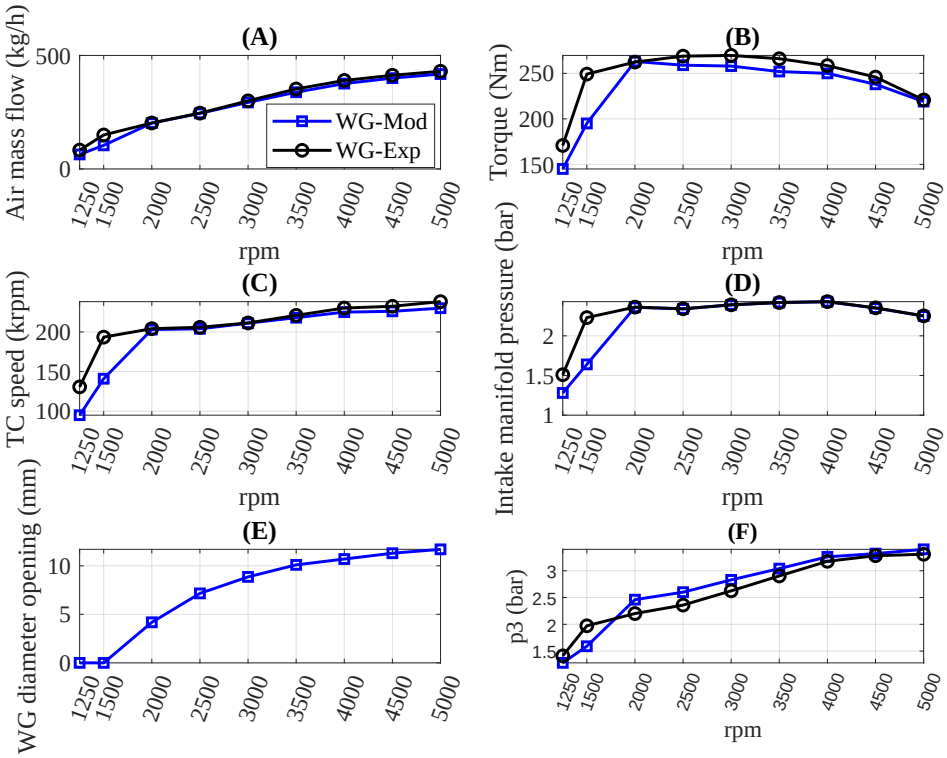

Figure 3.21: WG Full load engine variables experimental vs. modelling campaign comparison

In conclusion, even if the engine-core model was fitted with errors within +/- 1%, errors in terms of predicted averaged variables are caused by a wrong turbocharger modelling practice. Hence, the selected way to proceed is to correct the turbocharger maps, avoiding SAE standard look-up tables that include heat transfer and mechanical losses effects within the maps [52]. It is required to decouple aerodynamic efficiency from aforementioned phenomena, as in the following section 3.3 is described. The last highlights the importance of proper turbocharger modelling whatever turbine technology is used.

3.3 Adiabatic TC maps methodology

In this subsection, both VGT turbochargers have been tested in a gas stand. Tests have been performed in several conditions called: almost-adiabatic, hot-exposed, and hot-insulated. Careful management and selection of the recorded data have been assessed. As well, an energy balance study has been performed to evaluate the quality of the recorded information and all the possible energy fluxes have been considered.

In combination with the previous, turbocharger geometrical properties were measured (if possible), or estimated (if disassembling was not an option). The geometrical parameters are required by the heat transfer (HT) [61], [94] and mechanical losses (ML) models [75], [76], for heat fluxes and friction losses power computation.

Having collected all the previous information, an iterative fitting procedure of the turbocharger model is proposed, to process the experimental collected information. From the previous, a calibrated Heat Transfer and Mechanical Losses Turbocharger Model (HT-ML-TCM) has been obtained for both VGT turbochargers. In other words, this procedure gives as a result a set of purely adiabatic maps.

3.3.1 Experimental campaign

The testing campaign has been carried out in the gas stand described in [59]. The followed strategy for testing the two VGT turbocharger units is the one described in this section. The turbochargers are tested under three different configurations: Almost-adiabatic, Hot-insulated conditions and Hot-exposed

conditions (as per SAE standards).

On the one hand, Figure 3.22 shows the turbocharger installed in the gas stand and covered by thermal insulating material for Hot-insulated and almost-adiabatic working conditions configuration. On the other hand Figure 3.23 shows the SAE standard Hot-exposed conditions.

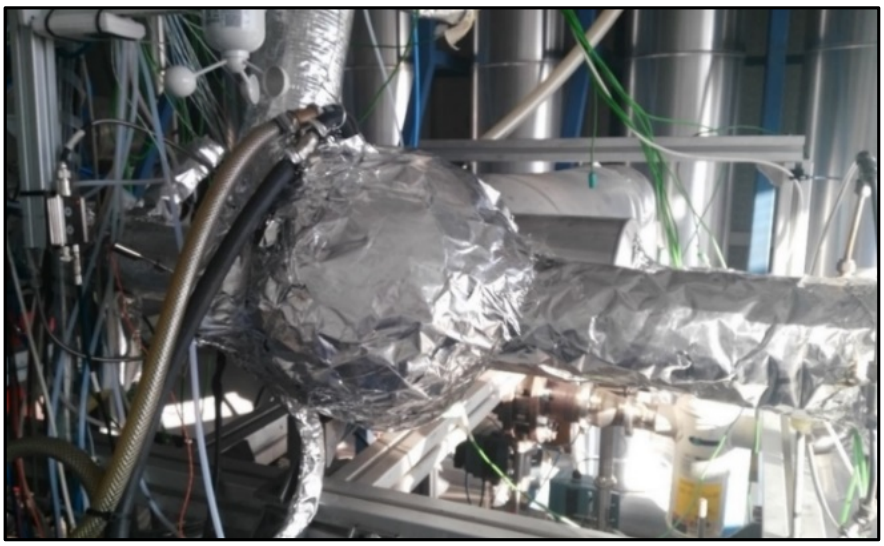

Figure 3.22: Gas stand under thermally insulated configuration for turbocharger testing

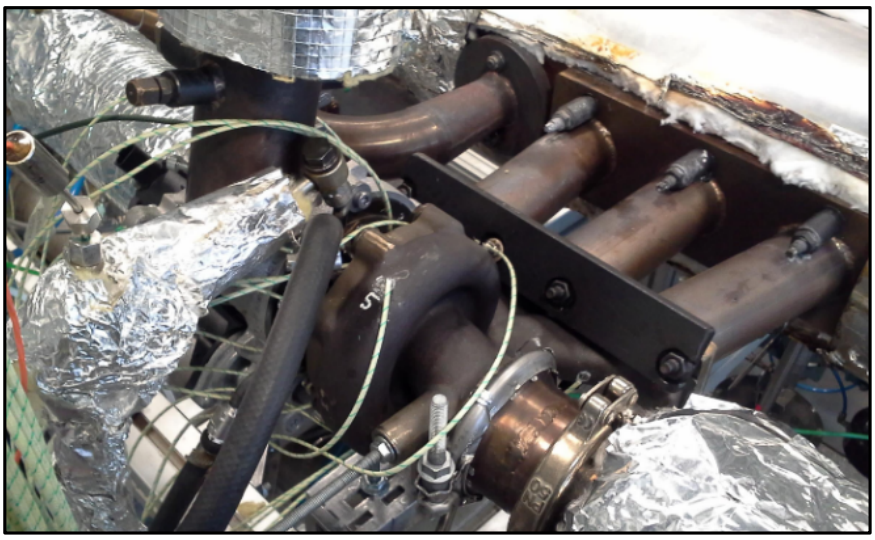

Figure 3.23: Gas stand under thermally exposed configuration for turbocharger testing

In the first stage, almost-adiabatic maps were recorded. These maps are obtained under a methodology that allows for a severe heat transfer reduction. The full turbocharger is insulated and no cooling water is used. In the same line, compressor air, turbine gas, and lubricating oil were kept at temperatures as similar as possible between them. The last is necessary to minimize internal heat fluxes between the different fluids. There are several approaches in the available literature for almost-adiabatic test fulfilment, they have been explored for benchmarking purposes in this thesis. One of the approaches consists of keeping constant fluids mean working temperatures other approaches state that the compressor outlet, turbine inlet, and oil inlet temperatures should be the ones considered. In other words, depending on the approach followed, if heat transfer in the turbocharger is aimed to be reduced during tests:

- Compressor outlet air, oil inlet flow, and turbine inlet gas temperatures are those variables to be controlled/monitored and to be kept as similar as possible. Figure 3.24(A) is a good example of this approach VGT-2.

- Compressor, oil, and turbine mean flow temperatures (average between inlet and outlet) are kept as similar as possible. This approach is harder to achieve from the point of view of control and has been the one selected for VGT-1.

It was decided that 10 °C was the maximum temperature difference between the controlled variables. This temperature difference presented a good compromise between testing time consumption and heat reduction. Regardless of the selected strategy for almost-adiabatic measurements, the target was to stabilize the monitored temperatures as close as possible to the desired target. Some safety issues were kept in mind during these tests, and may pose a conflict with the rule of the 10ºC of maximum temperature differences previously discussed:

- Oil temperature was adjusted within a range of 35 ºC to 110 °C. Even if maximum temperature differences are not well-targeted. This point is crucial to avoid oil cocking and properties deterioration (abnormally high oil viscosity).
- Minimum turbine inlet temperature was controlled to avoid water condensation. In the test bench, the software calculated on-live the dew temperature and turbine outlet temperature was always kept above.
- Pressure difference between the compressor outlet and turbine inlet shall be limited to avoid excessive turbine pulling. As a general rule, 1.5 bars was the maximum accepted pressure difference. This point is of high importance during almost-adiabatic measurements since much higher turbine inlet pressure is systematically required, as a consequence of the lower turbine inlet temperatures. Figure 3.24(B) shows the pressure differences along the rotational speed recorded range for VGT-2.

No water was used in almost-adiabatic tests, to avoid extra heat sinks/sources. The temperatures for each recorded point were set up using several PID controllers in the gas stand. Any of the turbocharger measuring stations has two to four probes, depending on the space available, i.e., the compressor inlet and outlet temperatures were registered by four thermocouples. All pressures were recorded by two sensors in the same piezometric ring. In the case of the turbine inlet temperature, and due to space constraints (turbine case and

exhaust manifold were welded and was not allowed to drill additional holes for this purposes), only one sensor was assembled. However, for checking purposes, the static temperature in a small tank upstream of the exhaust manifold inlet (turbine inlet) was also installed.

Mass flows were recorded twice (at inlet and outlet) for leakages or infiltration detection in both circuits, either turbine or compressor. Figure 3.24(C) shows turbine recorded mass flows. Figure 3.24(D) shows the same information for the compressor mass flow. As it is shown, for the lowest turbine mass flows, there is a discrepancy between inlet and outlet measurements. In summary, the range of the turbine inlet flow meter was exceeded. In these points, the average between both sensors was not used for further calculations and inlet flow sensor measurements were discarded.

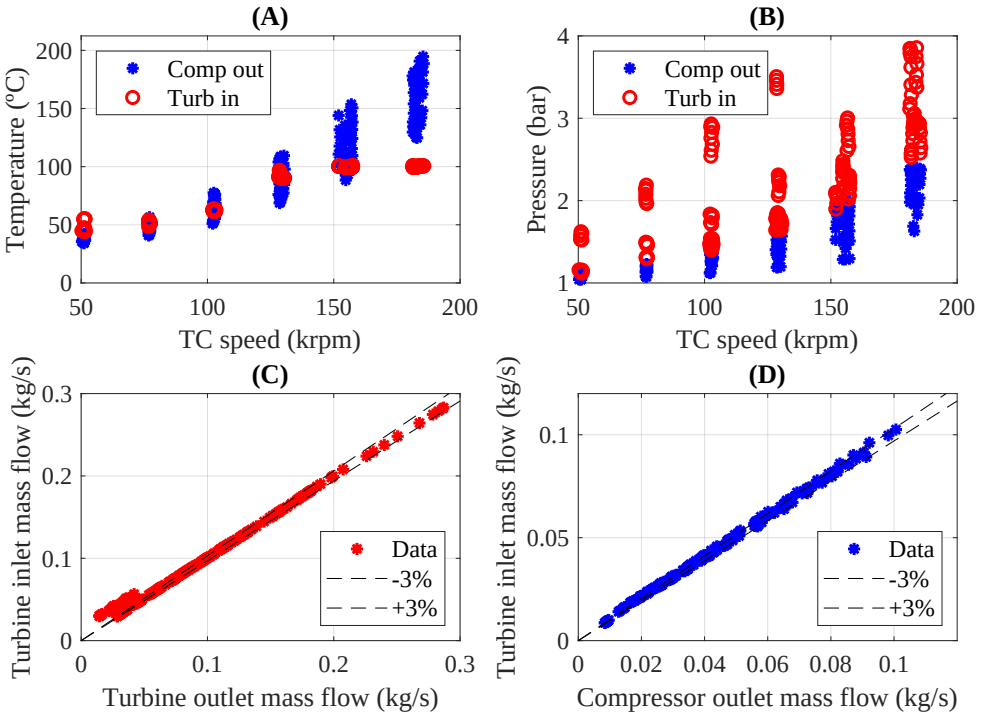

Figure 3.24: Gas stand almost-adiabatic tests experimental data check corresponding to VGT-2. (A) Corresponds to temperatures, (B) to pressures, (C) and (D) to turbine and compressor mass flows respectively

Lubricating oil temperature and mass flow were additionally recorded. For all the experimental campaigns, standard thermal stabilization criteria [53] were followed.

For this study, since heat transfer was one of the phenomena to be analysed, wall temperatures were also recorded. Wall thermocouples were installed in several locations: turbine volute and backplate, central housing and compressor back-plate and volute as well. Three thermocouples per location were assembled, afterwards, the averaged value for each turbocharger section is obtained. The previous is done to ensure consistent measurement and compensate for possible azimuthal thermal variations.

For hot-insulated and hot-exposed cases, the major time-consuming aspect corresponds to the thermal stabilization criteria for steadiness assurance, this is, waiting for all the temperatures to reach steady criteria. For example, when testing the turbocharger in hot conditions, wall and fluid temperatures may vary considerably depending on the point/working region. This is, when moving from low-power points to high-power output points, the thermal stabilization requires a considerable amount of time, not only from the fluids' perspective but also from the walls' one. The hot-insulated tests were performed to avoid external heat transfer. The complete turbocharger is surrounded by a wool rock layer to avoid external convection and radiation. Surrounding the wool rock layer, there is a second aluminium paper layer. Moving to the exposed tests, environmental conditions such as surrounding air velocity and temperature were monitored. For both tests type, oil and water inlet/outlet temperatures were recorded, as well as mass flows in any case. In the case of oil, the selected temperature was 100ºC, while for water, 50ºC were set up.

As final validation of the recorded data quality, the energy balance was performed. Figure 3.25(A1) shows the energy balance study for VGT-1 in absolute values, while Figure 3.25(A2) shows the energy balance in relative terms. Figure 3.25(B1) and Figure 3.25(B2) show the same information for VGT-2.

Unbalance was calculated according to Equation 3.4. The involved terms are the experimental turbine power as input and the rest of the fluids power as output. The second term is decoupled in experimental water, oil and compressed air absorbed power as Equation 3.5 specifies: "$\dot{W}_{water}$", "$\dot{W}_{oil}$" and "$\dot{W}_{compressor}$" respectively. Each of these terms is calculated according to Equation 3.6. Aiming to clarify the observed results, the analysis shall be

divided by the different series of data:

- Hot-exposed, red series in Figure 3.25: Turbine and compressor external heat transfer become the main reasons why a high unbalance arises for hot-exposed tests (since external heat transfer is not recorded, neither added to the energy balance). Relative energy unbalance reach values of about 89%. In other words, external heat transfer is the governing phenomenon for the low power working points. According to the available literature, the relative impact of heat transfer, is higher in the low power working areas, as it is evidenced in Figure 3.25(A2) and Figure 3.25(B2) for VGT-1 and VGT-2 respectively.

- Almost-adiabatic: On the one hand, it should be recalled that VGT-1 stabilization criteria considered the mean fluids working temperatures. This criterion is the one that takes more time to stabilize since turbine and oil outlets are being considered for thermal stabilization. Accordingly experimental unbalance for VGT-1 is closer to zero. On the other hand, for the VGT-2 testing procedure, it was considered compressor outlet air, oil inlet flow, and turbine inlet gas temperatures, like the ones for heat reduction purposes. In all, trying to evaluate the differences, Figure 3.26 provides with the energy balance particularly for the almost-adiabatic tests. It is evidenced that a close-to-zero energy balance is obtained for the approach followed by VGT-1. The last is attributed to the fact that the average temperature approach requires much more time until the thermal steadiness is acquired since turbine and oil outlet temperatures imply extra time. The last happens since turbine and oil outlet temperatures are affected to a high degree by the turbocharger thermal inertia, which takes its role, especially in the low power points, such as the ones below 3000kW, where major differences are found between both series of data. In conclusion, from the adiabatic test campaign, it has been detected the importance of not only assuring the steadiness of the considered variables but also the rest of variables, since the quality of the recorded data may lead to energy unbalances up to a 24%.

- Hot-insulated tests: As expected from the externally insulated tests, the external heat transfer (the only unaccounted variable) has been diminished as much as possible. The last is the main explanation why a closer-to-zero balance is reached in comparison to hot-exposed series. The non-

perfect insulation could explain the slight unbalance in the hot-insulated tests for VGT-2, Figure 3.25(B2). On the contrary, VGT-1 hot-insulated tests, result in a "negative" energy balance, Figure 3.25(A2). In other words, measured output power (compressed air, oil and water) is larger than the input (delivered by the hot gas). This is mainly attributed to two points: firstly to the experimental uncertainties, such as sensor locations and/or calibration. Secondly, to the electric heater's over-reaction during the thermal transient for the turbine inlet temperature accomplishment. The transient taking place before the steady-state is mainly governed by the gas-stand and turbocharger thermal inertia and the e-heaters PID. Even if the turbine inlet temperature was stabilized, the insulation material and the turbocharger metal themselves accumulated some heat during the thermal transient before the steady-state. Later, the accumulated heat was slowly released to lower temperature fluids: water, oil, and compressed air. Consequently, the later fluids' outlet temperatures were slightly raised, leading to the observed "negative energy balance". From the collected experience, stabilization criteria from [53] before data recording under hot-insulated conditions, does not satisfy the thermal steady-state condition. According to the analysis dealing with Figure 3.25(A2) it should be taken a longer time (than the one taken) to fully stabilize the hot-insulated cases. In the VGT-2 case, prevention of longer times was followed, and the negative unbalanced values disappeared, Figure 3.25(B2).

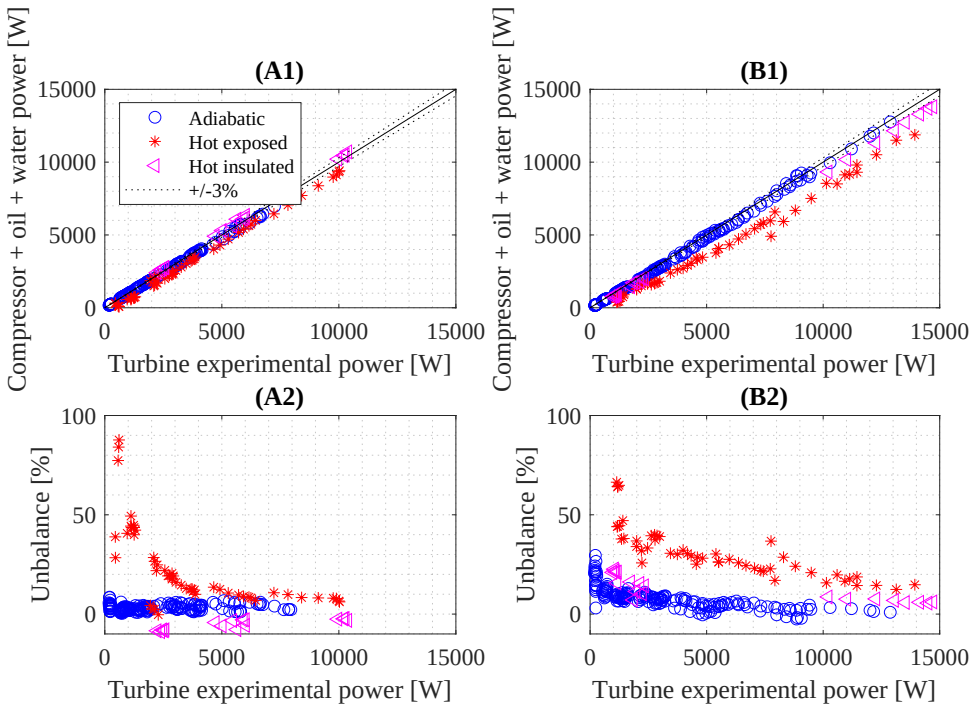

Figure 3.25: Energy balance for both turbochargers and all experiment types. VGT-1 tests(consirering with average fluid temperatures) correspond to (A1) and in relative terms to (A2). VGT-2 tests, (considering turbine inlet turbine, oil and compressor outlet temperature) correspond to (B1) and in relative terms to (B2)

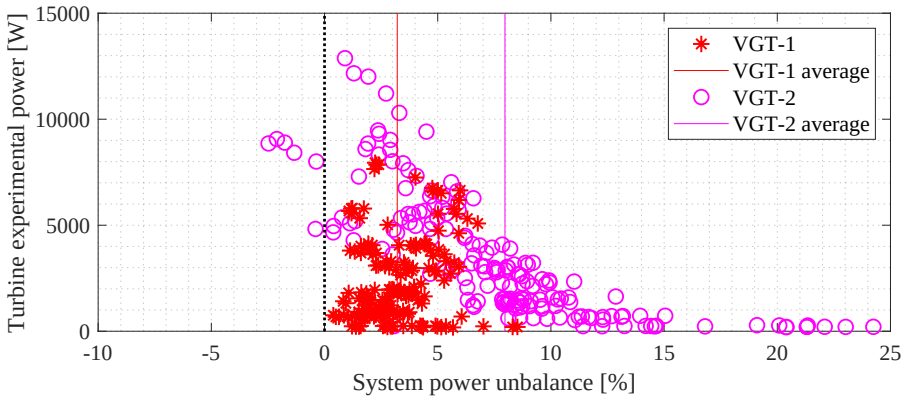

Figure 3.26: Adiabatic energy balance for VGT-1 and VGT-2

$$Unbalance = \frac{\dot{W}_{Turbine} - \dot{W}_{Output}}{\dot{W}_{Turbine}} \tag{3.4}$$

$$\dot{W}_{Output} = \dot{W}_{water} + \dot{W}_{oil} + \dot{W}_{compressor} \tag{3.5}$$

$$\dot{W}_i = \dot{m}_i \overline{cp}_i (T_{i-out} - T_{i-in}) \tag{3.6}$$

3.3.2 Modelling stage

To obtain the called adiabatic and purely isentropic turbocharger maps (dealing with purely aerodynamic information) the 1D-HT-ML-TCM is the one selected for the complete modelling of the three studied turbochargers. This model makes usage of basic geometrical data in combination with physical and semi-empirical equations. The mathematical explanation on the effect of heat transfer and mechanical losses in the experimental turbocharger maps (leading to wrongly predicted engine points in subsection 3.2.3) is the one that follows.

In any case, for the following equations, the sub-index "0" indicates total conditions. The terms without this sub-index specification, call for static conditions. In the turbine side, efficiency is considered as the total-to-static, as in "$\eta_{turbine,t-s}$", while in the compressor, as the total-to-total, "$\eta^{isentropic}_{compressor,t-t}$".

Firstly, it is required to define the experimental effective turbine efficiency "$ETE_{experimental}$" in Equation 3.7, from which one can realize that "$ETE_{experimental}$" is affected by friction losses, which are unknown and very complex to obtain from the experimental data. In Equation 3.7 it is made usage of the isentropic turbine efficiency considering the experimental data, "$\eta^{isentropic-experimental}_{turbine,t-s}$" and defined in Equation 3.8, which presents some problems:

- Firstly, "$\eta^{isentropic-experimental}_{turbine,t-s}$" is calculated using the experimental turbine outlet temperature "T'_{40}", which is difficult to measure properly. See "T'_{40}" location in Figure 3.27, which in addition, results from the "$30 - 30' - 40'$" evolution (heat transfer in the volute and later power extraction).

- Secondly, taking a look into Figure 3.27 again, and considering the "$\eta_{turbine,t-s}^{isentropic-experimental}$" definition in Equation 3.8, the resulting experimental isentropic efficiency may lead to values greater than one. The last happens since the experimental temperature difference, "$\triangle T_{turbine}^{experimental}$", calculated as "$T_{30} - T'_{40}$", may result in a value greater than the one in "$T_{turbine}^{isentropic,no-heat-considered}$", which represents the calculated isentropic temperature evolution "$T_{30} - T_{4s}$". The previous is purely attributed to the fact of not considering the heat losses between the "T_{30}" measurement and the actual "rotor inlet temperature" for the "T'_{30}" calculation, again, see Figure 3.27. Then, if by chance one could measure T'_{30}"(that would also imply re-defining the point "T_{4s}" as for "T'_{4s}") all this problem may be avoided: the turbine isentropic definition could be calculated as in Equation 3.9 is proposed, without the risk of obtaining anomalously high values (>1).

$$ETE_{experimental} = \eta_{turbine}^{isentropic-experimental}\eta_{mechanic} \tag{3.7}$$

$$\eta_{turbine,t-s}^{isentropic-experimental} = \frac{\dot{m}_t c_{p,t} \triangle T_{turbine}^{experimental}}{\dot{m}_t c_{p,t} \triangle T_{turbine}^{isentropic,no-heat-considered}} = \frac{\dot{m}_t c_{p,t}(T_{30} - T'_{40})}{\dot{m}_t c_{p,t}(T_{30} - T_{4S})} \tag{3.8}$$

$$\eta_{turbine,t-s}^{isentropic-theoretical} = \frac{\dot{m}_t c_{p,t}(T'_{30} - T'_{40})}{\dot{m}_t c_{p,t}(T'_{30} - T'_{4S})} \tag{3.9}$$

To partially solve the previous limitations, "$ETE_{experimental}$" re-definition is proposed from Equation 3.7. The mechanical efficiency is considered to be represented as the ratio between the recorded experimental compressor power and the turbine experimental one. The last results in Equation 3.10 and considers the experimental temperature variations for both: compressor "$T'_{20} - T_{10}$" and turbine "$T_{30} - T'_{40}$" which as explained, are not fully representative of the actual mechanical power balance (consumption-delivery) in the turbomachine rotor. See Figure 3.27 and Figure 3.28.

Applying Equation 3.10 and Equation 3.8 to Equation 3.7 results in Equation 3.11, which can be simplified to Equation 3.12. With respect to the first definition of the "$ETE_{experimental}$" in Equation 3.7, the main benefit of Equation 3.12 lies in the fact that there is no need to cope with the meaningless

term "$\eta_{turbine,t-s}^{isentropic-experimental}$", which as stated, may result in values greater than one.

By contrast, the main drawback of Equation 3.12, as said, it is the fact that actual mechanical power consumption-delivery is not properly accounted, it is just an approximation affected by heat transfer: see how after the simplification it is considered "$T'_{20}-T_{10}$", which results from the actual compressor work and the subsequent heat transfer (which is considered to happen afterwards the compressor volute, not affecting the shaft energy balance). Also the term "$T_{30}-T_{4s}$" is used for the "$ETE_{experimental}$", and represents the fluid evolution from 30 to 4s, aiming to describe the fluid evolution across the turbine impeller, while this is just a wrong assumption since for the isentropic fluid evolution through the turbine impeller, it shall be considered points "$30'-4s'$".

In all, the "$ETE_{experimental}$" definition for turbine modelling is affected by mechanical friction losses, heat transfer to the compressor side as well as heat losses in the turbine volute. Depending on the working conditions, heat flow in the compressor side may have one or another value (or even direction, as in Figure 3.28 is shown), hence, the obtained "$ETE_{experimental}$" from the experimental campaign as a way to model the turbine performance it is just a "snap-shot" of the "$ETE_{experimental}$" under very specific working conditions. It could also be concluded that "$ETE_{experimental}$" is not exclusively dealing with the energy balance in the turbocharger shaft, but also is being affected by the heat transfer effects that should not influence the TC shaft energy balance and that shall be accounted separately from it to well-predict the turbine and compressor rotors' actual boundaries.

$$\eta_{mechanic} = \frac{\dot{m}_c c_{p,c} \triangle T_{compressor}^{experimental}}{\dot{m}_t c_{p,t} \triangle T_{turbine}^{experimental}} = \frac{\dot{m}_c c_{p,c}(T'_{20}-T_{10})}{\dot{m}_t c_{p,t}(T_{30}-T'_{40})} \tag{3.10}$$

$$ETE_{experimental} = \frac{\cancel{\dot{m}_t c_{p,t}(T_{30}-T'_{40})}}{\dot{m}_t c_{p,t}(T_{30}-T_{4S})} \frac{\dot{m}_c c_{p,c}(T'_{20}-T_{10})}{\cancel{\dot{m}_t c_{p,t} T_{30}-T'_{40}}} \tag{3.11}$$

$$ETE_{experimental} = \frac{\dot{m}_c c_{p,c}(T'_{20}-T_{10})}{\dot{m}_t c_{p,t} T_{30}-T_{4s}} \tag{3.12}$$

On the compressor side, the analysis is slightly simpler, since heat transfer is considered to happen afterwards the actual compression (hence, the isentropic work is properly estimated, having recorded the experimental pressures

and inlet temperature). In all, compressor experimental isentropic efficiency, "$\eta^{isentropic-experimental}_{compressort-t}$" (directly obtained from recorded temperatures) it is defined in Equation 3.13. As one can see, "$\eta^{isentropic-experimental}_{compressort-t}$" is influenced by heat transfer, since "T'_{20}" represents compressor outlet temperature, downstream the compressor volute, Figure 3.28. If one could predict how much the compressor outlet temperature was raised by means of heat (evolution from 20-20'), one may attempt to obtain the purely isentropic compressor efficiency "$\eta^{isentropic}_{compressort-t}$", from Equation 3.14, which instead of "T'_{20}", directly considers "T_{20}", see again Figure 3.28.

$$\eta^{isentropic-experimental}_{compressor} = \frac{\triangle T^{isentropic}_{compressor}}{\triangle Tcompressor, t-t^{experimental}} = \frac{T_{20s}-T_{10}}{T'_{20}-T_{10}} \tag{3.13}$$

$$\eta^{isentropic}_{compressor,t-t} = \frac{T_{20s}-T_{10}}{T_{20}-T_{10}} \tag{3.14}$$

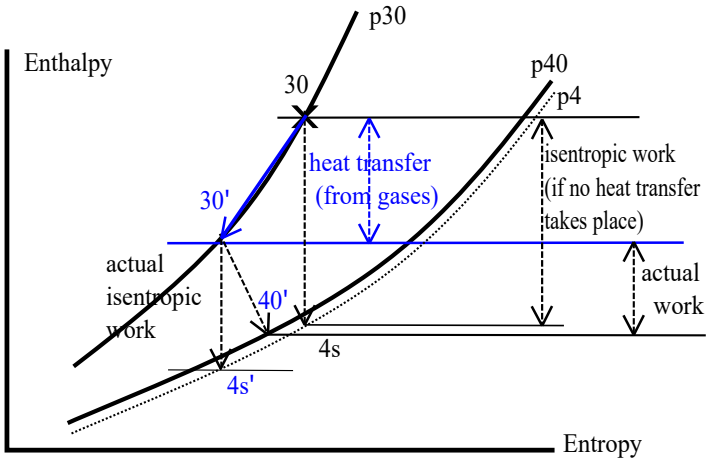

Figure 3.27: Effect of heat transfer in turbine enthalpy-entropy diagram

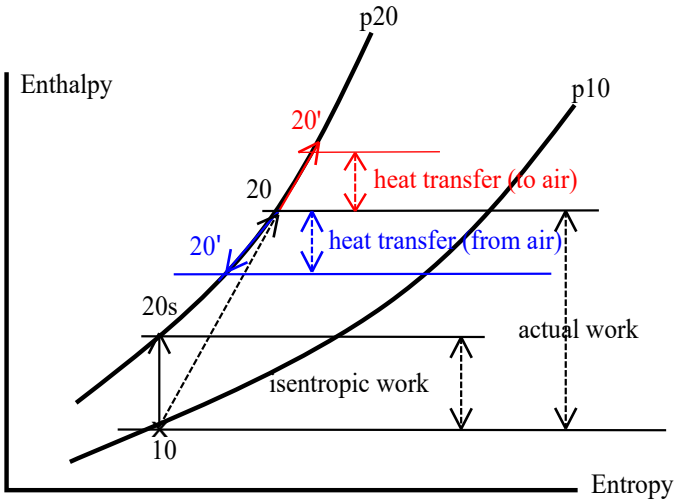

Figure 3.28: Effect of heat transfer in compressor enthalpy-entropy diagram

To summarize the previous, the HT-ML-TCM is used to take into consideration all the considered phenomena. The model is fed with the experimental obtained "$ETE_{experimental}$", which as explained, is deeply affected by resulting heat transfer and mechanical losses. Afterwards, employing the already developed models for heat transfer [94] and mechanical losses model [75], in combination with the experimental information provided to the model (pressures, temperatures and mass flow of each fluid) the heat transfer fluxes, such as the ones depicted in Figure 3.27 and Figure 3.28 can be estimated. As a result, purely isentropic efficiencies are calculated (not affected by other phenomena apart from aerodynamics). In Figure 3.29 according to the previous, it is shown how from experimental diathermal "$ETE_{experimental}$" the model obtained for each point, the isentropic turbine efficiency. The same methodology is simultaneously developed for the compressor side. Colour's criteria in any plot have been fixed as a function of turbine rotational speed, according to Table 3.6.

Previous works from several authors show the expected impact of the previously discussed phenomena in the turbocharger maps [76], [59][55][54].

Afterwards, turbine and compressor maps models are used. A series of physically-based parameters (the same for all VGT positions and all isospeeds) are adjusted to fit the purely adiabatic data and obtain the so-called

extrapolated turbine and compressor isentropic (aerodynamic) efficiency maps. This fitting is performed for the mass flow and efficiency as explained in [70] for the turbine and in [74] for the compressor. An example of the results for this fitting in the case of isentropic efficiency is shown in Figure 3.29. However, other models available in the literature for the same duty are proposed, such as the one in [69] and [7] for turbine and compressor respectively.

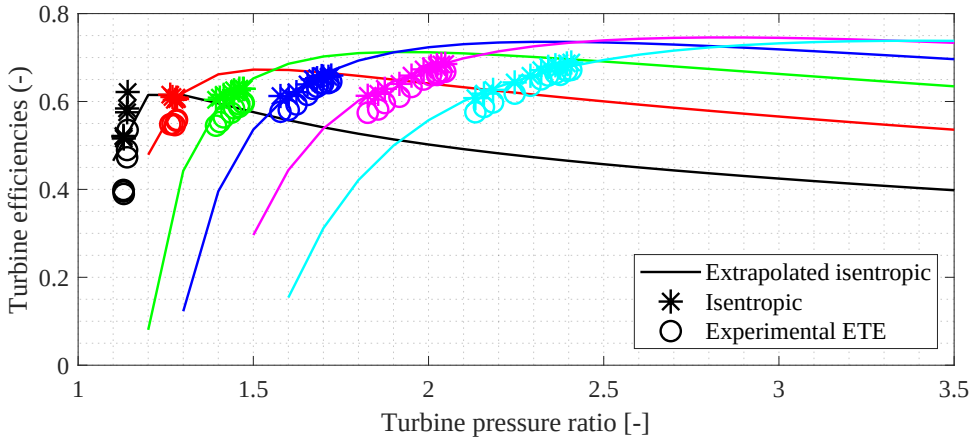

Figure 3.29: VGT-2 50% VGT opening iso-speed isentropic efficiency and $ETE_{experimental}$

Table 3.6: Iso-speed range-color criteria for turbine maps

Color	**Speed range [rps/sqrt(K)]**
Black	[0,50]
Red	]50,75]
Green	]75,100]
Blue	]100,125]
Magenta	]125,150]
Cyan	]150,160]

Having described the model capabilities and collected the previously described experimental information, the model calibration procedure can be summarized in the diagram of Figure 3.30. One of the major benefits of the proposed methodology lies in the fact that the different phenomena can be decoupled from the rest. This allows for aerodynamic maps, mechanical

losses, and heat transfer sub-models semi-independent calibration. As it can be deducted from the diagram in Figure 3.30, step by step, each of the model variables prediction is compared against the experimental data. Until the adjustment is satisfactory, the loop is repeated (red rows). Finally, when the quality of the analysed variable prediction is accepted, green lines show the next step to follow, and the calibration of the next turbocharger "sub-model" begins.

According to the diagram in Figure 3.30 thanks to the almost-adiabatic campaign, heat transfer to the oil was minimized: the major raise of oil enthalpy can be attributed to the mechanical losses. Presumably, any disagreement between the model results and the experimental data comes from the mechanical losses model. Parameter "K_{jb}" in Equation 3.15 is the one to be adjusted in. As it can be understood from Equation 3.15, mechanical losses "$\dot{W}_{jb}$" also depends on the bearing geometry, oil properties (dependant on working conditions) as well as turbocharger speed.

Once the mechanical losses model has been calibrated, a hot-insulated test campaign can be taken as a reference, neglecting the external heat transfer effects. The internal heat transfer model can be adjusted without any concern about external heat exchange. The calibration of internal conductances guarantees a good prediction of internal heat transfer. The term of internal conductance is represented by "$\kappa_{i-(i+1)}$" in Equation 3.16 for metal nodes heat power calculation "$\dot{Q}^{cond}_{i-(i+1)}$". Here, metal nodes heat power also depends on the temperature difference between two consecutive nodes: "$(T_i - T_{i+1})$". An example could be the temperature difference between the compressor backplate and the housing.

The final step corresponds to the external heat transfer model calibration making usage of the hot-exposed tests. At this point, model-to-experimental data discrepancies are attributed to the external heat transfer model (since all previous models have been validated). The iterative loop (red row number 9 in Figure 3.30) is repeated until a good solution is achieved. This step is clarified in Equation 3.17, where "A_i" represents the external surface or area of the element "i". The external surface is thermally divided into compressor case, central housing (3 sections), and turbine volute. In Equation 3.15 the term "h_{i-ext}" represents the external convective coefficient. The model estimates whether natural or forced convection is taking place. According to the previous, "h_{i-ext}" is calculated as a function of the surrounding air velocity.

$$\dot{W}_{jb} = 2\pi R_{jb}^3 K_{jb} \frac{L_{jb}}{h_{jb}} \mu(\overline{T}_{oil}) n^2 \tag{3.15}$$

$$\dot{Q}_{i-(i+1)}^{cond} = \kappa_{i-(i+1)}(T_i - T_{i+1}) \tag{3.16}$$

$$\dot{Q}_{i-ext}^{conv} = A_i h_{i-ext}(T_{ext} - T_i) HTM \tag{3.17}$$

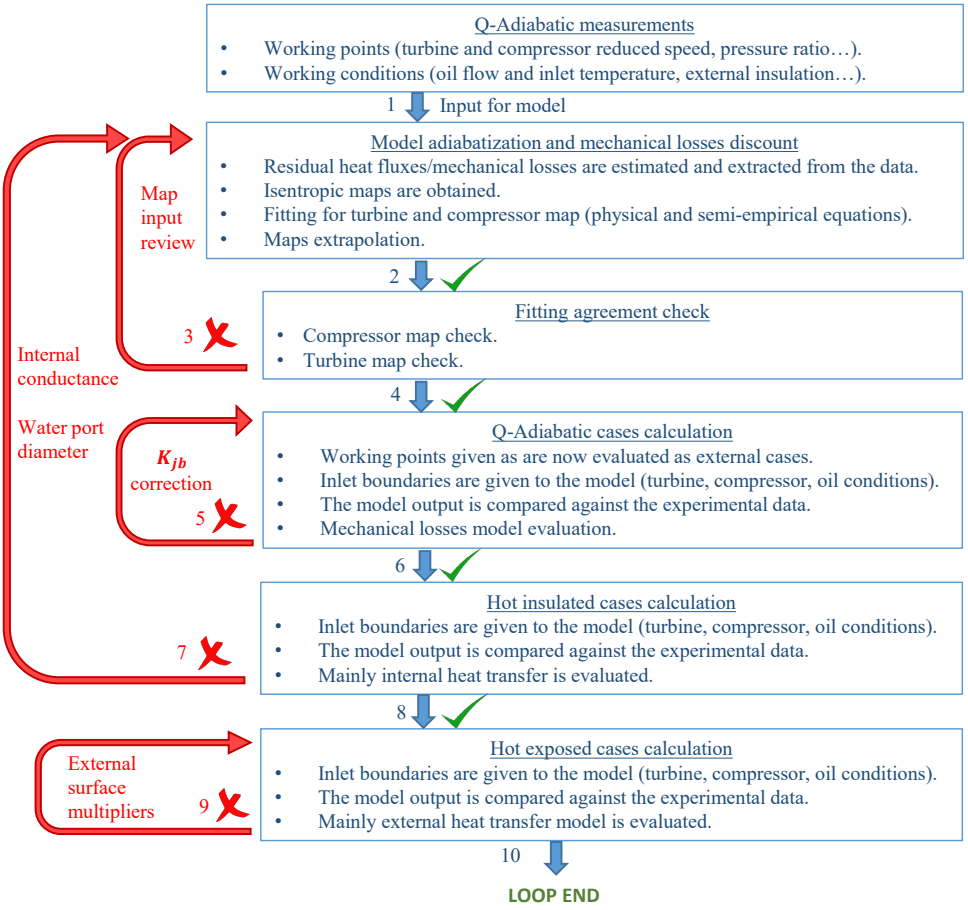

Figure 3.30: Diagram for HT-ML-TCM calibration procedure

3.3.3 Turbocharger model validation

It is of high importance, the quality of the obtained maps during the turbocharger model fitting procedure. Table 3.7 gathers the mean square root error committed during the mass flow and efficiency adjustment for both turbines. Errors during the fitting procedure do not reach 1% error in terms of mass flow and adiabatic efficiency curves adjustment. This check would correspond to the third box in the diagram in Figure 3.30.

Table 3.7: Mass flow and efficiency root mean square (RMS) error

VGT-1 ϵ mass	**VGT-1 ϵ efficiency**	**VGT-2 ϵ mass**	**VGT-2 ϵ efficiency**
0.25%	0.49%	0.88%	0.67%

The obtained maps for VGT-2 are shown in Figure 3.31. Three VGT positions have been chosen to ease the view of the fitting. Figure 3.31(A) deals with mas flow maps (in reduced units). Figure 3.31(B) corresponds to the 100%VGT position (maximum opening) isentropic turbine efficiency map. The model automatically extrapolates the isentropic efficiency points into a wide range of pressure ratio. This is highly useful for ICE turbocharger maps application since of the wide operative range and the pulsating flow component. Same information is shown for what it is called the 50%VGT opening in Figure 3.31(C) as well as 15% in Figure 3.31(D).

To show an example of the final model accuracy, after all previously described fitting procedures and validation methodology, some hot-exposed calculations were performed. During the gas stand simulations, turbocharger rotational speed was imposed, in combination with the several fluids experimental inlet temperatures. Finally, for these calculations, inlet and outlet pressures are guaranteed to be the experimental ones. In other words, pressure ratios are also imposed through turbomachine. In consequence, the predicted variables, given the aforementioned fixed boundaries are: outlet temperatures, mass flows and the energy balance.

Figure 3.32(A) shows the accuracy in terms of turbine and compressor outlet temperatures (always within ± 3 error). This is of high importance since the resulting temperatures are the result of the complete fluids' evolution along the turbomachine sides.

Mass flow prediction is compared to experimental data in Figure 3.32(B). Good agreement is shown by the calculations. It is of great importance to check out the mass flow prediction at this stage since hot experimental points were not provided as the basis for the turbine maps. Almost-adiabatic tests were the ones provided as information for the maps adjustment and later extrapolation: if mass flow maps were not correct, a wrong output of the mass flow would have resulted.

The highly accurate prediction of the oil friction losses power is noticeable in Figure 3.32(C). In these cases, oil enthalpy increases result from heat transfer and mechanical losses. A good prediction in terms of oil outlet temperature confirms that both: mechanical losses and heat from/to oil is well predicted. For the water enthalpy variation, it was considered that the obtained error in Figure 3.32(C) was satisfying the heat transfer to the water. Errors in the power to water hardly reach values of 200 W.

As far as the experimental rotational speed was imposed during the simulations, some energy unbalance is necessarily committed. Figure 3.32(D) shows the energy balance made by the model: turbine mechanical power is being compared against the mechanical losses and compressor consumed mechanical power. If the rotational speed was released, the error in energy balance will be translated into the turbocharger rpms (slightly increasing the speed since the turbine power is slightly higher than the consumed one).

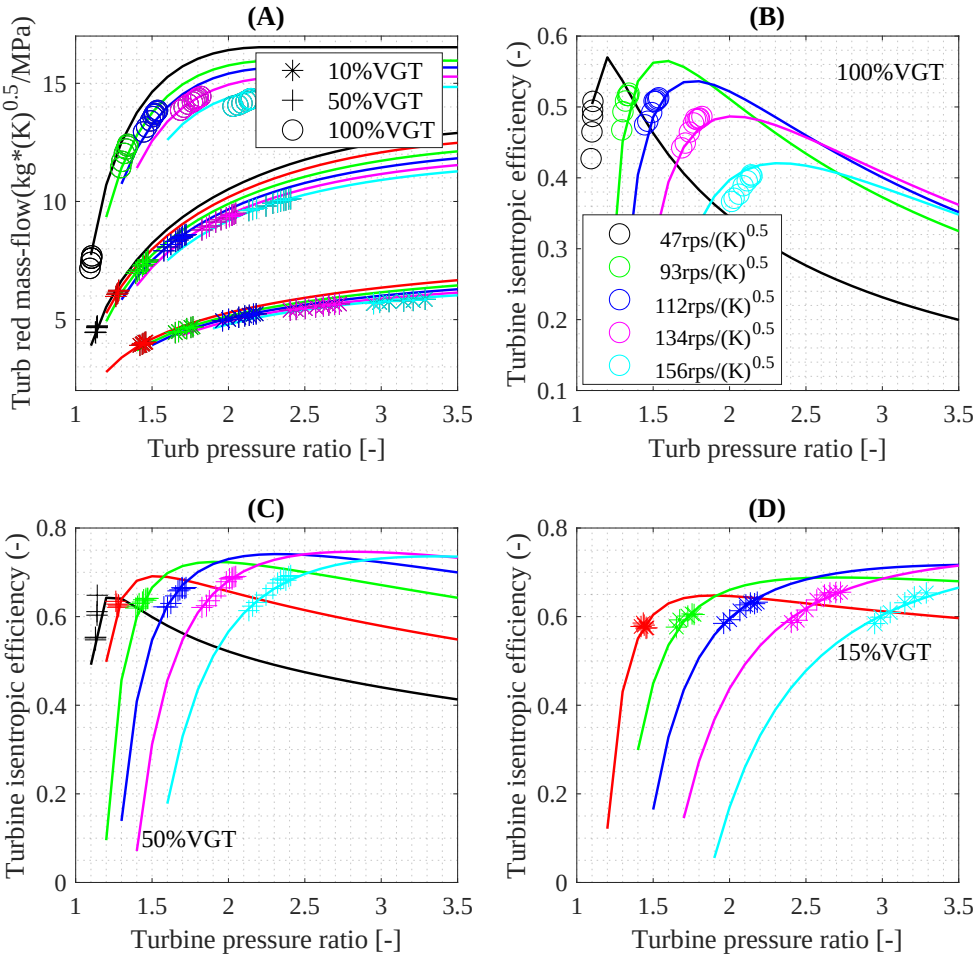

Figure 3.31: VGT-2 fitted and extrapolated maps for 100%, 50% and 15% VGT position

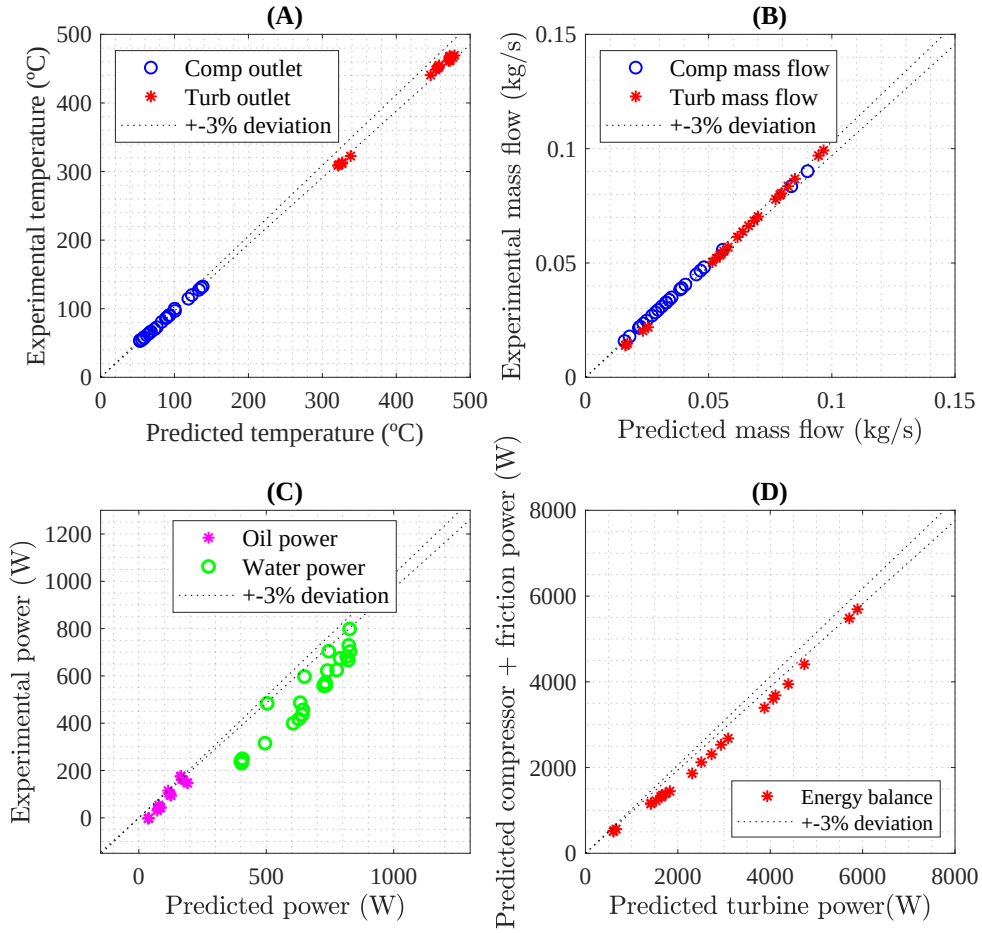

Figure 3.32: VGT-2 hot-exposed cases simulations (after model calibration procedure) VS experimental data

Wall temperature analysis is shown in Figure 3.33 for hot-exposed cases and two VGT positions (0% and 100%) in the VGT-2 unit. The working points selected for both VGT opening series go from choke to surge (minimum-maximum compressor outlet temperature respectively) and include a turbocharger rpm range between 75-150krpm. Good agreement between model and experimental has been achieved. The wall temperature distribution is a good indicator of proper heat fluxes estimation.

In Figure 3.33 x-axis, the information from left to right correspond to the

axial evolution from turbine inlet gas (TI) to compressor outlet gas (CO). In between, the turbocharger considered thermal nodes are: turbine wall temperature node (TN), first, second and third sections of the housing (H1, H2 and H3 respectively), as well as compressor wall node temperature (CN).

The predicted wall temperature is an output of the complete model: heat fluxes arising from the metal-to-fluids temperature differences imply metal temperature gradients. The last, in combination with metal nodes conductances, allows predicting the wall temperature distribution along with the turbocharger.

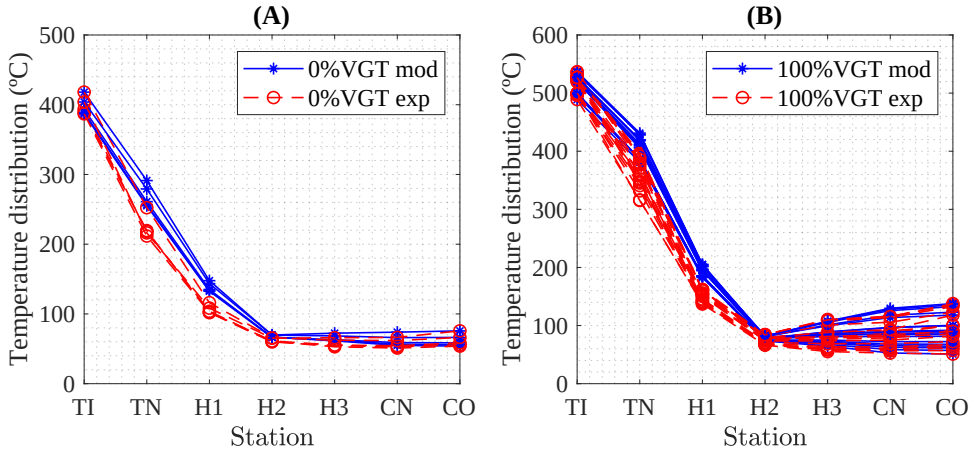

Figure 3.33: Hot-exposed simulations VS experiments. VGT-2, wall temperature distribution

3.4 Final turbocharged-engine model validation

Having reached this point a complete fitted and adjusted engine model has been obtained following the procedure in [5]. As it was highlighted in Figure 3.20 and Figure 3.21, there were several wrongly predicted variables when the engine model was used in combination with the called "hot turbocharger maps" measured and built following SAE standards [53]. The main motivation why all the work in section 3.3 was made is to get a complete set of validated turbocharger maps [1], in order to overcome the errors committed when modelling the turbocharger making usage of the aforementioned hot maps. Full loads, as well as transients, are modelled in this section. Accordingly, two sets

of calculations for each series of data are performed:

- Adiabatized-Extrapolated maps (AE series), corresponding to the ones obtained followed the procedure described in section 3.3.
- Hot-exposed SAE maps provided by the turbocharger supplier, which are Nor-Adiabatized-Neither-Extrapolated (NANE series).

3.4.1 Steady state model check

In these simulations, the followed strategy is the same as the one followed in the results shown in Figure 3.20 for example VGT/WG position targets the boost pressure as it is happening in the experimental campaign. Fitted parameters from the engine block fitting procedure are implemented and AFR is imposed to be the experimental one for each point.

Figure 3.34 deals with main engine variables and includes both: model and experimental results for full load and VGT-1 cases. Figure 3.35 shows for the same cases, the main turbocharger inputs and output variables. From Figure 3.34 one can infer that the AE series performs better than the NANE series does. As previously described, the main problem of NANE series lies in the low-end torque under-predicted turbocharger performance: Figure 3.34(A) shows the low air mass flow rate, leading to the noticeable torque under-prediction, shown in Figure 3.34(B), caused by the lack of turbocharger speed in Figure 3.34(C), which goes in hand with boost pressure, see Figure 3.34(D). This problem is solved with the validated AE maps. Low-end torque is well-predicted since boost pressure is achieved. What is more, the rest of the engine range modelling is improved in comparison to the NANE series: One can see how torque prediction is better from 3000 rpm engine speed in advance. The last is explained with Figure 3.35(A) that shows a systematic VGT wider opening, leading to a lower p3 Figure 3.35(B), implying fewer pumping losses as well as a slightly higher mass flow.

In terms of turbine inlet and outlet temperatures Figure 3.35(C), the most remarkable fact is the underprediction of temperature in the NANE series at low-end torque, however, it shall be highlighted that this is a snow-ball effect attributed to the lack of air (and fuel), not to combustion wrong modelling, neither to heat transfer effects in the exhaust manifold and turbocharger. In

the low-end torque, AE series predicts perfectly the experimental T4, and for the rest of the working points, it could be stated that exhaust temperatures are well-predicted slightly better than for the NANE series. It is only at 3500rpm where some error is committed.

Finally, when it comes to charging air evolution Figure 3.35(D), there is an error in terms of T2 prediction for both series: up to +14ºC in the NANE series and about -9ºC for the AE series. Even though, these errors are damped by the WCAC modelling.

In all, it could also be deducted that predicted volumetric efficiency is well-reproducing the actual one since for properly modelled engine core boundaries (p2', T2' and p3), air mass flow is well-predicted for the complete full load speed range. Finally, it is remarkable the accuracy of the torque prediction as well as T3, since both variables are deeply related to combustion prediction by the developed neural network.

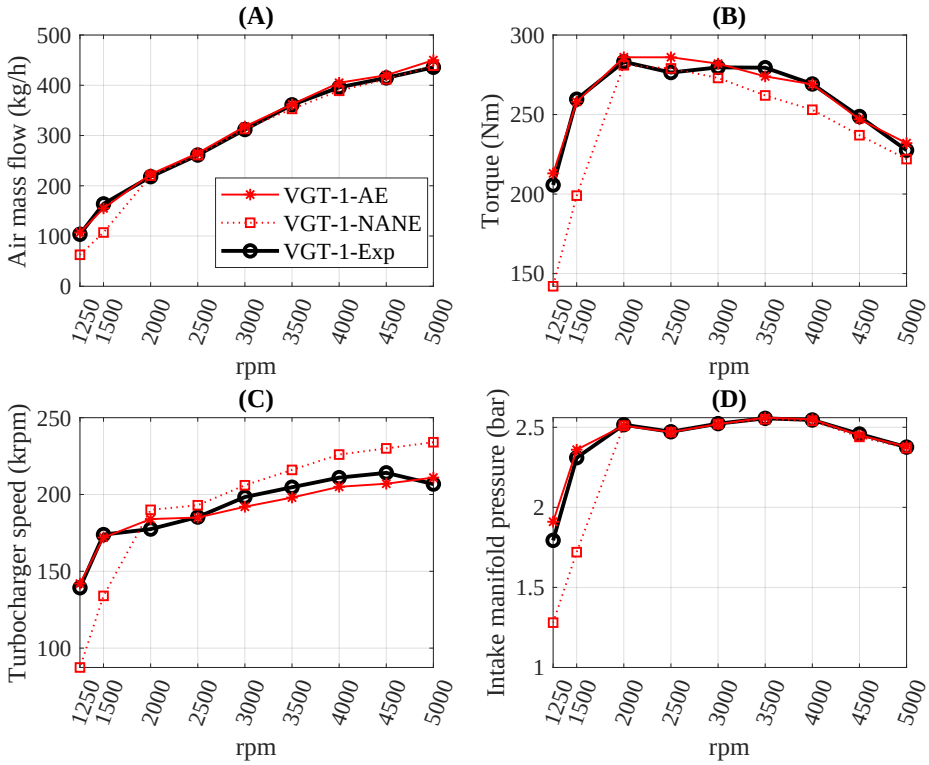

Figure 3.34: VGT-1 full loads, main engine variables: experimental, AE and NANE

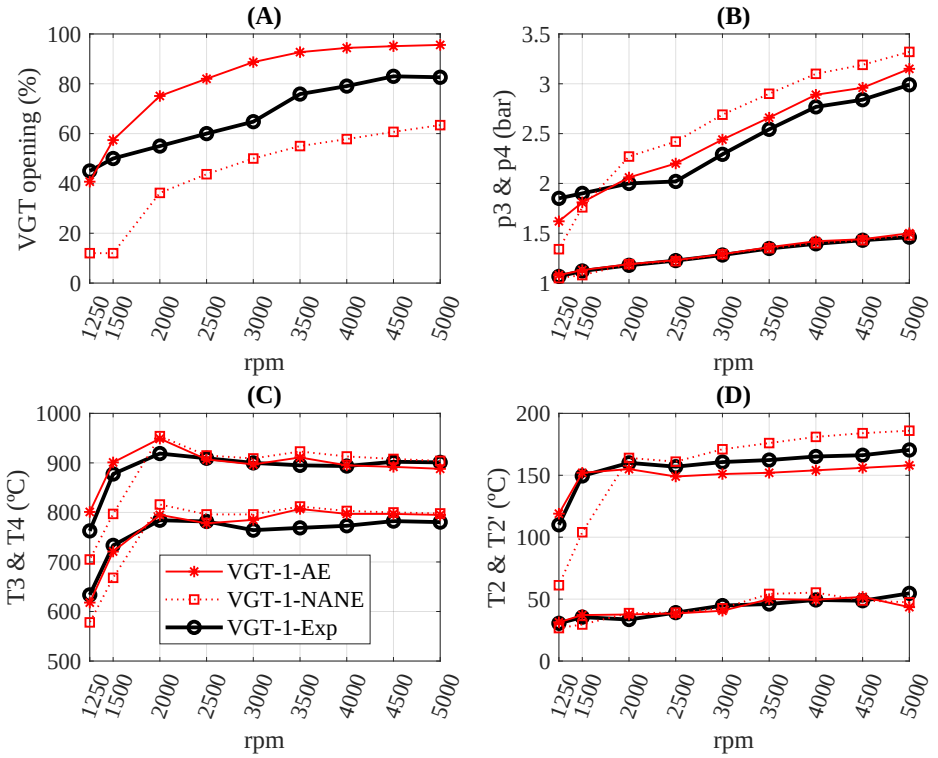

Figure 3.35: VGT-1 full loads, TC variables: experimental, AE and NANE

The same validation procedure is done for the VGT-2, for which adiabatic and extrapolated maps have also been obtained. Results are gathered in Figure 3.36 for VGT-2. The conclusions are almost the same as for the VGT-1 turbocharger: low-end torque is better predicted by means of the AE series, as far as air mass flow is properly modelled, see Figure 3.36(A). The last goes in hand with torque, Figure 3.36(B). In all, it is shown the importance of well-reproducing the turbocharger speed and boost pressure. Particularly in the case of the VGT-2, NANE series, the relatively low boost pressure in the 1250rpm working point (about 1.67bar) is achieved by the NANE series, while in the case of 1500rpm, the higher value of boost pressure (2.37 around) is not achieved by NANE series.

The second most remarkable aspect of these plots is the under-prediction of torque in the NANE series from 4000 in advance, even if boost pressure is well-targeted. The problem here is mainly attributed to the compressor

map: The supplier compressor map was an "estimated" one. In the high-speed area, the estimation is not as accurate as of the AE maps for example, which take as a basis, experimental information, before all the adiabatizing-extrapolating procedure. As a result, Figure 3.36(C) shows a turbocharger speed over-estimation ranging from 12krpm to 25krpm. To back-up the previous statement, Figure 3.37 is shown. Particularly, Figure 3.37(A) shows the VGT opening trend for each series. It is remarkable, how from 3500 to 5000rpm, the experimental and AE series tend to further open the VGT mechanism with speed, while the NANE series goes in the opposite direction, in order to speed up the turbocharger in the simulation, trying to compensate wrongly modelled compressor maps. The closed VGT operation results in an overestimated engine back-pressure, Figure 3.37(B). This has its direct impact in terms of air mass flow and engine torque, as in Figure 3.36 is shown from 3500 rpm in advance.

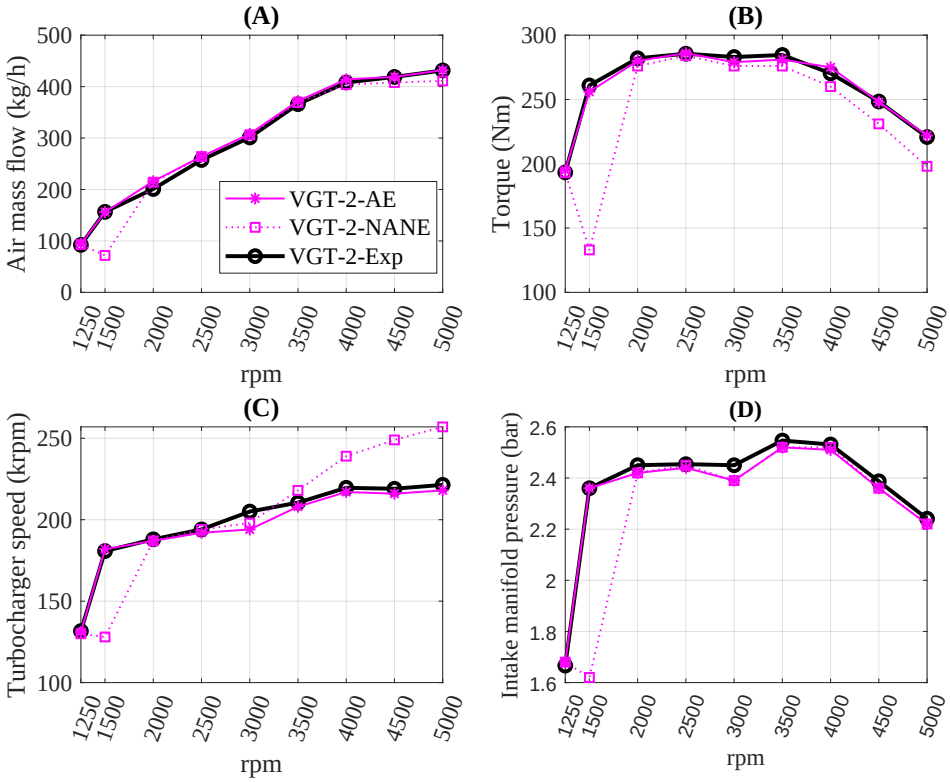

Figure 3.36: VGT-2 full loads, main engine variables: experimental, AE and NANE

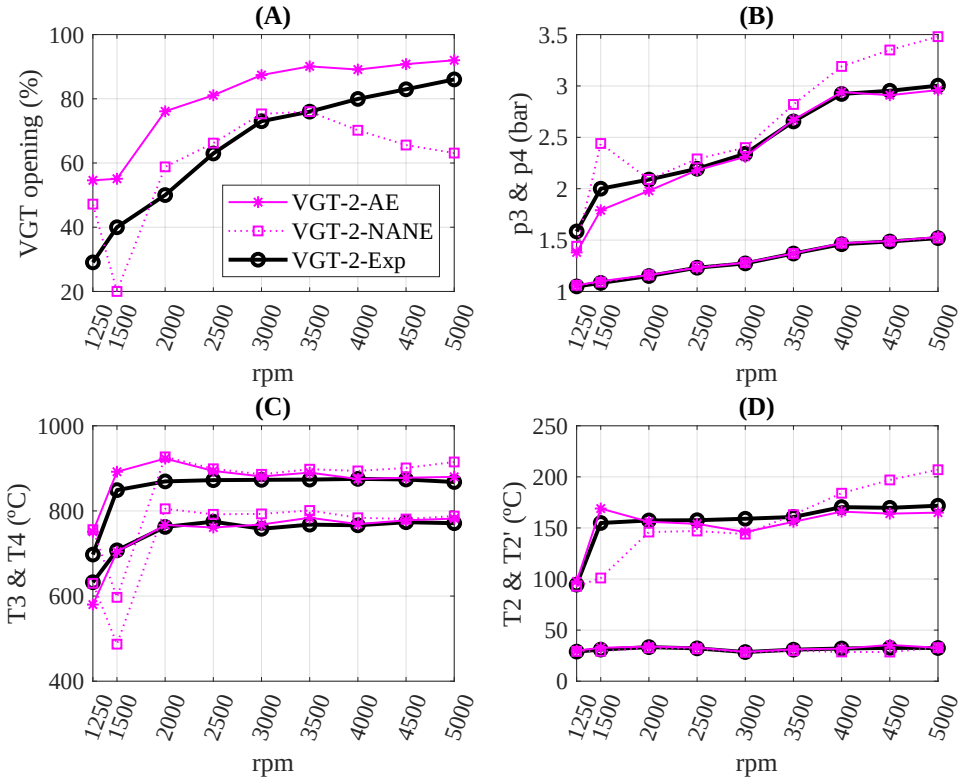

Figure 3.37: VGT-2 full loads, TC variables: experimental, AE and NANE

WG results are shown in Figure 3.38 and in Figure 3.39. In the case of the WG AE series, the turbocharger maps procedure is slightly different from the other two TC units, since the WG was not tested at CMT laboratories, contrary to the VGTs: Hot-exposed maps were provided by the turbocharger supplier who measured them following SAE standards. Afterwards, these maps were adiabatized making usage of the calibrated TC model and according to standard testing working conditions [52] (900 ºC at turbine inlet and 90 ºC as oil inlet, which are guessed to be the ones happening). That way it was checked CMT-TM effectiveness against SAE standards maps measured at other gas stands.

In all, conclusions are very similar to the ones in VGT-1 and VGT-2 in the low-end-torque and for the rest of the engine range: The lack of air mass flow Figure 3.38(A) and torque prediction Figure 3.38(B) in the NANE series are

motivated by the under-estimated turbocharger efficiency, which is evidenced by the lack of turbocharger rpm, in Figure 3.38(C), directly related to the lack of intake manifold pressure, as in Figure 3.38(D) is evidenced in the low-end torque.

Furthermore, the lack of TC efficiency can be observed in the full closure of the WG mechanism, as well as in the p3 overestimation in the range of 2000-4000 rpm, see Figure 3.39(A) and Figure 3.39(B). All the previous issues disappear in the AE series.

Turbine inlet and outlet temperatures (T3 and T4 respectively) are included in Figure 3.39(C). The turbine inlet temperature is in line with the prediction accuracy in the other two analysed turbochargers. Turbine outlet over-prediction in the NANE series is again attributed to the turbine wrongly predicted efficiency, especially in the range of 2500-4000 rpm.

Compressor outlet temperature under-prediction in the low-end torque NANE series, see Figure 3.39(D), results from the lack of compressor speed. In the range of 2000-2500, both modelled series show an offset of about 15-11ºC extra. On the one hand, in the case of the NANE series, this error is directly attributed to the impact of heat transfer in the compressor map. On the other hand, for the AE series, it is assumed that some error was committed during the adiabatization procedure since this turbocharger was not following the same procedure as for the rest.

However, Figure 3.39(D) shows that the WCAC damps the T2 error, so that intake manifold temperature (T2') is accurately predicted, within +-3ºC error when boost pressure is properly achieved.

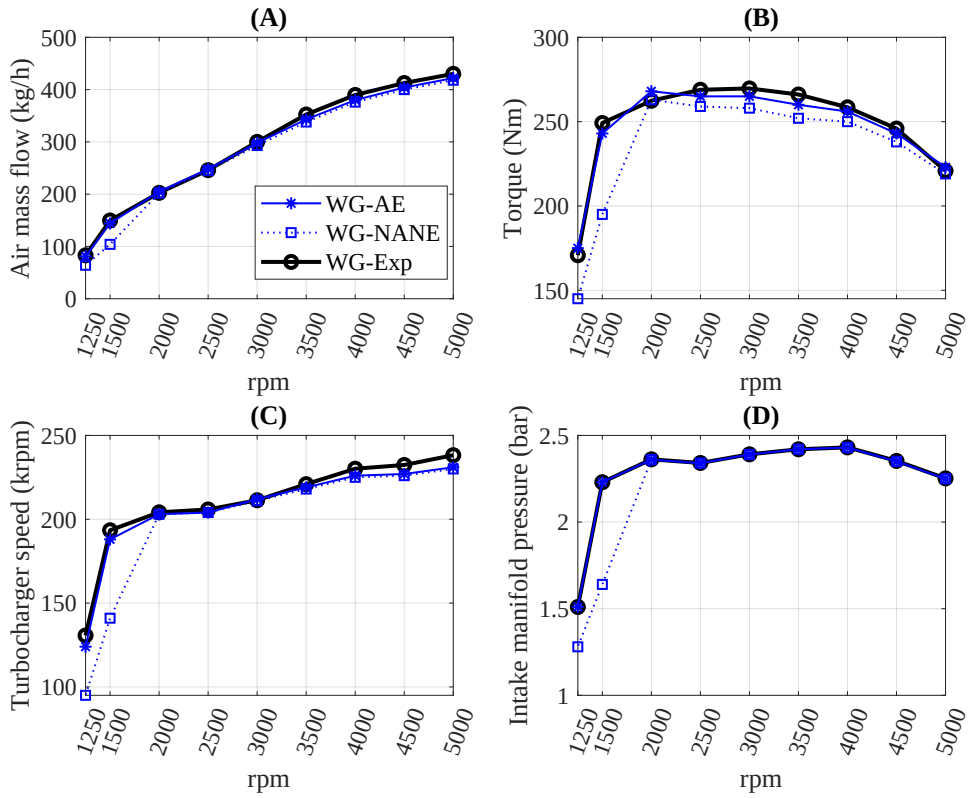

Figure 3.38: WG full loads, main engine variables: experimental, AE and NANE

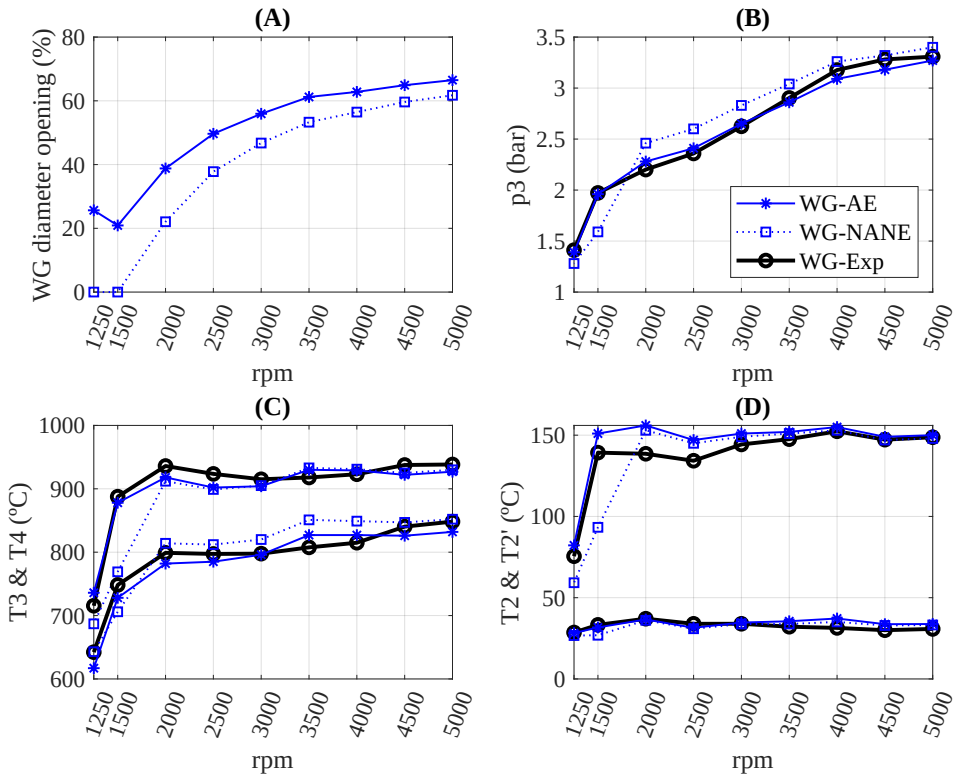

Figure 3.39: WG full loads, TC variables: experimental, AE and NANE

To conclude is shown that by using AE maps, coupled to the calibrated 1-D model, boost-pressure is always achieved, which in combination with a proper prediction of p3 and T2', leads to proper air mass flow modelling. Then the torque shows no significant mismatch against the experimental data. This is a symptom of proper modelling of the FMEP and combustion.

Robustness of the model and conclusions is assured since two different VGTs followed the same procedure. In addition, the WG provided the same feedback, taking as a basis a set of hot maps coming from the turbocharger supplier, and processing them with the calibrated turbocharger model. And in the three cases using the same engine-core previously calibrated model, following the procedure described in subsection 3.2.3 and using a sub-optimal turbocharger map.

3.4.2 Transient sudden tip-in check

For the transient response, two constant engine speeds have been selected for the analysis: 1500 and 3000 rpm. In both cases, making usage of AE and NANE maps. Some key points are the ones that follow:

- VVT and throttle signal evolution during the tip-in are recorded from the ECU source and imposed during the modelling stage. ECU, as previously stated, was already optimized by the engine manufacturer.

- Combustion parameters evolution during the complete load transient are predicted by the combustion NNW, which was trained in a wide range of load and engine speed from steady-state tests. Now is evaluated if it performs reasonably accurately or not.

- A VGT-position re-definition from a modelling point of view was necessary, to force the agreement between the VGT positions in the model (maps) and the engine tests. This task can be done by taking advantage of the previously analysed full load steady-state tests and simulations. Figure 3.40 shows the mismatch between the actual VGT mechanism and the definition of the map. This technique is recommendable if the percentage of VGT position is defined in the maps as a function of reduced air mass flow, rather than the measured voltage of the VGT mechanism actuator. AE maps were defined as a function of air mass flow, consequently, it was necessary to re-define the %VGT position for each VGT map, hence, guaranteeing to some degree, the agreement between the experimental and model definitions of %VGT position.

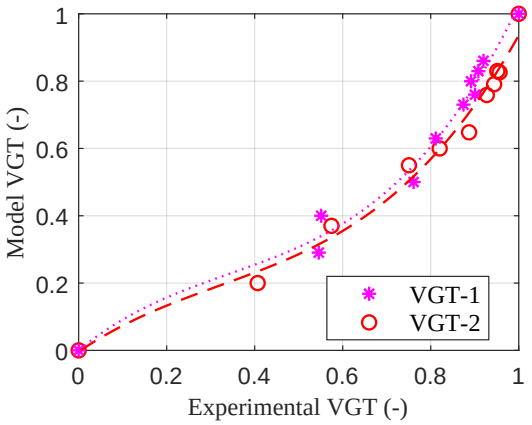

Figure 3.40: VGT-1 and VGT-2 model to experimental opening equivalence and adjusted curves for maps recalibration

- Once the previous point is accomplished, the experimental %VGT position evolution (which is recorded) can be taken as the reference for the simulation. The experimental signal is imposed as the initial condition during the first 0,5-1 second of load demand. Afterwards, a slight correction over the experimental signal is allowed in the model by just adding/subtracting a given % in terms of %VGT position. In other words, the correction over the experimental signal targets the intake manifold pressure (p2') accomplishment during the transient. The same methodology is applied to the WG mechanism. Figure 3.41(A) shows correction over experimental VGT-1, 1500rpm. It is evidenced that until second 3 (1 second after load demand), the experimental %VGT is imposed. Then, corrections hardly reach -7% as maximum deviation. In other words, in this simulation, a -7% is applied to the experimental %VGT position, so if the experimental signal was 40%, the model would correct this value and modify the VGT position to 33%. It is worth highlighting that experimental value is read from %VGT positioning mechanism, but correction value from model accomplishes to effective fluid dynamic %VGT position. Corrections arise due to VGT mechanism hysteresis, thermal dilatations, blade-to-blade dispersion and non-linearities; apart from model inaccuracy to fit experimental boost pressure (p2'). Figure 3.41(B) shows the same information for 3000rpms.

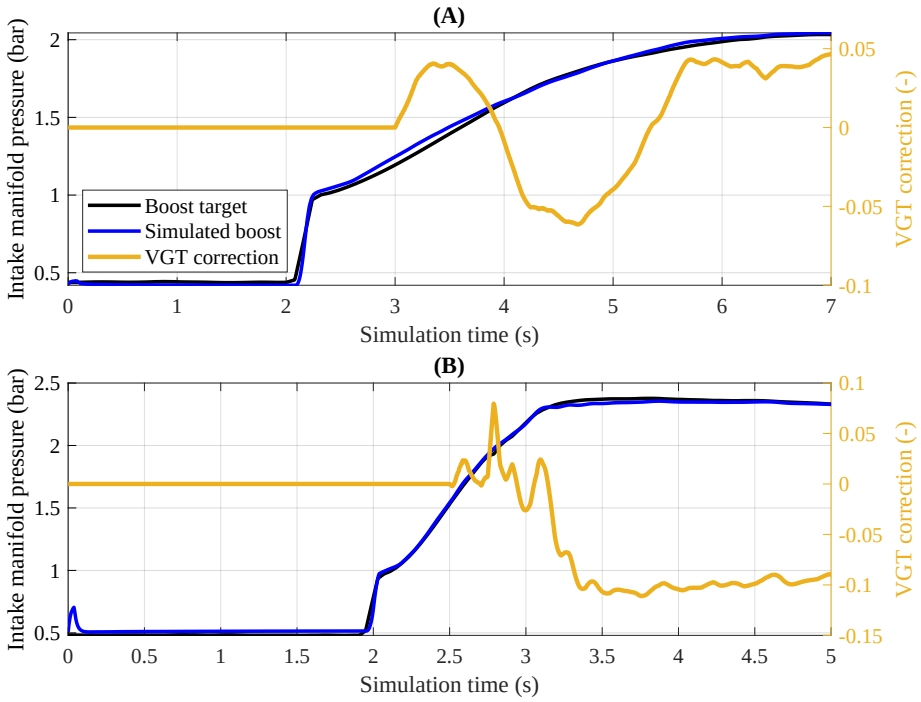

Figure 3.41: (A) VGT-1, 1500 sudden tip-in. VGT correction over experimental to target experimental boost pressure. (B) Corresponds to 3000rpm

Hence, it is of high importance the fact that experimental %VGT is taken as a reference for achieving the boost pressure. Considerable disagreements between the experiment and the model in terms of VGT opening maps definition may lead to wrong dynamic modelling practice.

In summary, Figure 3.42 shows a GT-power caption of the resulting model, detailing the engine block-exhaust manifold-turbocharger-after-treatment. The names for each engine part are included in the coloured boxes, as well as for the boost pressure control architecture: The experimental %VGT signal, which is corrected by the PID, according to the modelled-experimental difference in terms of boost pressure.

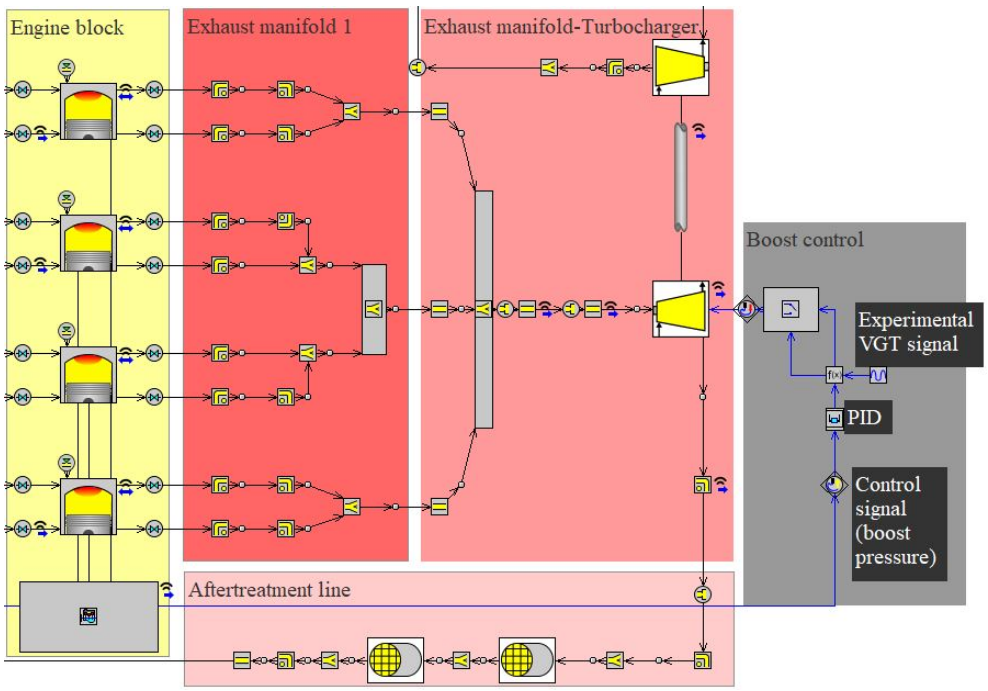

Figure 3.42: GT-Power engine model, detail on engine block, exhaust manifold, turbocharger, after-treatment and Boost control system

Figure 3.43, Figure 3.44 and Figure 3.45 show results for 3000rpm load transients, the information is shown comes from the experimental campaign and also from the 1-D model, in both developed configurations: AE and NANE turbocharger maps. Figure 3.43(A) shows how the AE series, perfectly follows the experimental air mass flow evolution during the complete engine transient, hence, torque is perfectly predicted Figure 3.43(B). The previous allows accepting the NNW performance, which even if it was trained in steady-state, it was well-reproducing combustion evolution during the transient test. The air mass flow goes in hand with p2' achievement through the complete tip-in, see Figure 3.43(C). The lack of p2' in the NANE series is the reason for the lack of air mass flow and torque.

Exhaust manifold pressure is shown in Figure 3.43(D), in the NANE series, as far as the air mass flow is not achieved, the lack of p3 is evident, while in the case of the AE series, there is only a lack of 0.2 bar in terms of p3, from seconds 2.2 until 2.9, for the rest of the time, the experimental evolution is

properly followed.

The TC speed evolution is shown in Figure 3.43(E), from the NANE maps, it could be concluded that during the very low-load steady-state initial point (until second 2), the turbocharger speed is accurately predicted, while for the transient itself this not true any-more. In the case of the AE series, the turbocharger speed discrepancy only appears at the very low-load steady-stated. The explanation for this is the one that follows: turbocharger maps are recorded normally in the range of 50-250krpm as for VGT-1 and VGT-2 was done, while under the (low load initial) engine operative point, the turbocharger speed hardly reaches the 10krpm. This is an out-off-design working speed for the turbocharger, in fact, the maps for both: compressor and turbine sides, are extrapolated for this working area. The discrepancy in this initial TC speed is attributed to the previously stated issue dealing with the turbomachinery maps.

Finally, VGT position is depicted in Figure 3.43(F). As it can be seen, the experimental VGT position evolution is completely imposed until second 2.5. Afterwards, a PID is enabled to perform a fast but subtle modification over the experimental signal, to fine-tune the boost pressure built. As it is shown, in the AE maps, this modification oscillates, increasing/reducing the experimental signal according to the simulation requirements. However, in the case of the NANE maps, even if there is a 12% of extra closure constantly applied, it was not enough for a successful boost pressure control.

The analysis in Figure 3.44 is consistent with the one carried out in Figure 3.43, although some differences are still identified. Firstly, the main conclusions dealing with models (AE vs. NANE) comparison, are almost the same in qualitative terms. Air mass flow and torque are perfectly reproduced by the AE maps since the boost pressure is achieved at any time, see Figure 3.44(A), Figure 3.44(B) and Figure 3.44(C). The most relevant fact in the NANE series, corresponds to the lack of air mass flow, torque, and p2, from seconds 2.5 to 3. The lack of boost pressure is directly attributed to a lack of turbocharger speed, as in Figure 3.44(E) is shown for the aforementioned time gap. The lack of boost pressure is directly compensated by an excessive p3, as a consequence of the extra VGT mechanism closure, see Figure 3.44(D) and Figure 3.44(F) for p3 and VGT respectively. At very closed VGT positions, slight modifications in the opening %, lead to important effective section variations.

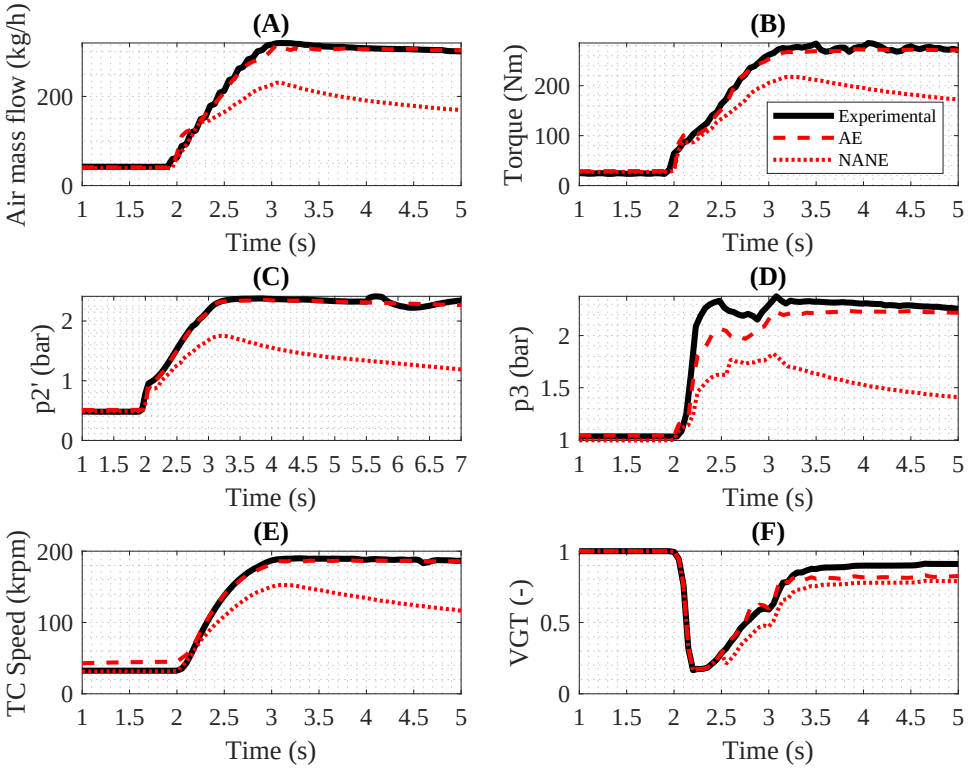

Figure 3.43: VGT-1, 3000rpms sudden tip-in, continuous series corresponds to experimental, dashed corresponds to model results with AE turbocharger maps, and dotted corresponds to NANE maps

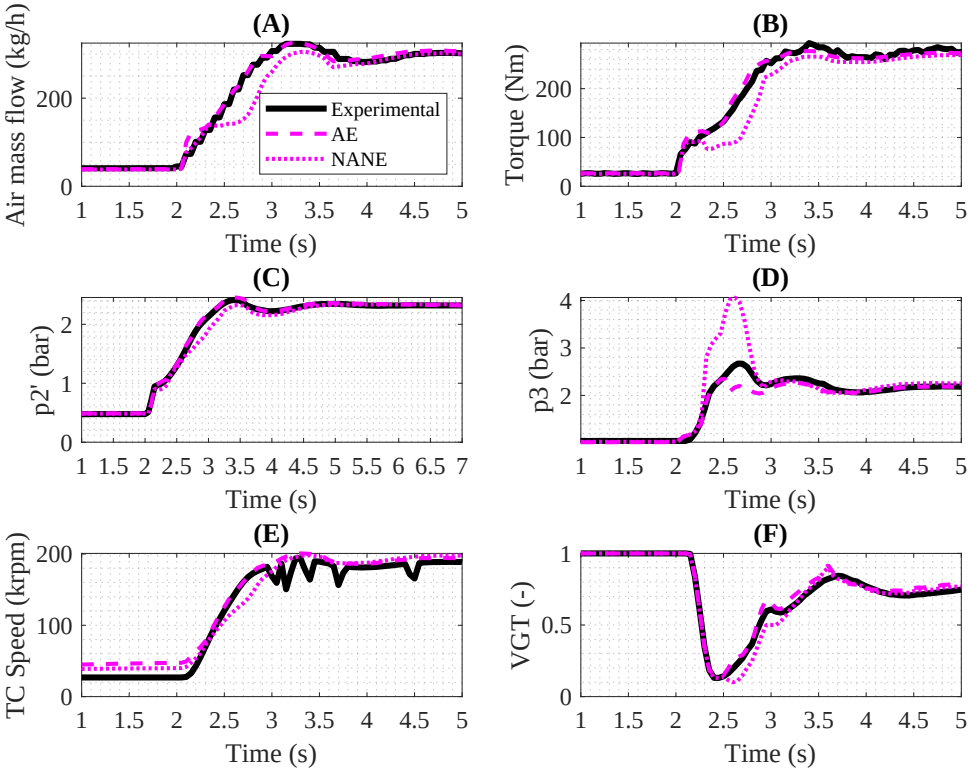

Figure 3.44: VGT-2, 3000rpms sudden tip-in, continuous series corresponds to experimental, dashed corresponds to model results with AE turbocharger maps, and dotted corresponds to NANE maps

Finally, dealing with the 3000rpm transient, Figure 3.45 shows the same information for the WG. In this TC unit, the differences are in line with the previously stated. In general words, conclusions would be summarized in the following sentence: AE maps accurately predict the transient, while the engine output in the NANE maps configuration, present some retard in terms of any engine variable: air mass flow and torque for example, in Figure 3.45(A) and Figure 3.45(B). This lag in the NANE simulation is also evidenced in terms of p3, see Figure 3.45(D), even if WG mechanism fully closure was forced, see Figure 3.45(F). The retard in p3 is attributed to the lack of boost pressure built, which directly impacts the amount of air. By contrast, the targeted final boost pressure is achieved in this case. It is remarkable the accuracy with which p3 is predicted using the AE series, until second 3.

It shall also be discussed the fact that experimental WG opening is estimated according to the experimental signal. The experimental signal for WG opening goes from 71.3 to 0%, which would correspond to an effective section of $17.3mm^2$ and $3mm^2$ respectively. However, the non-linearity between the signal voltage and the effective WG section is unknown since the orifice effective section was not calibrated. This is the main explanation for the disagreement between the experimental signal of the WG opening. However, the PID that was set up in the model, to correct these non-linear effects in the bypass section, effectively compensates for this. In consequence, boost pressure is well-targeted as shown, what is more, the high accuracy found in terms of p3 becomes another indicator of proper WG opening modelling practice.

Finally, for the WG turbocharger hardly any discrepancy is found in terms of turbocharger initial speed at the low-load initial condition. TC speed is perfectly predicted in this case for both TC map types, see Figure 3.45(D).

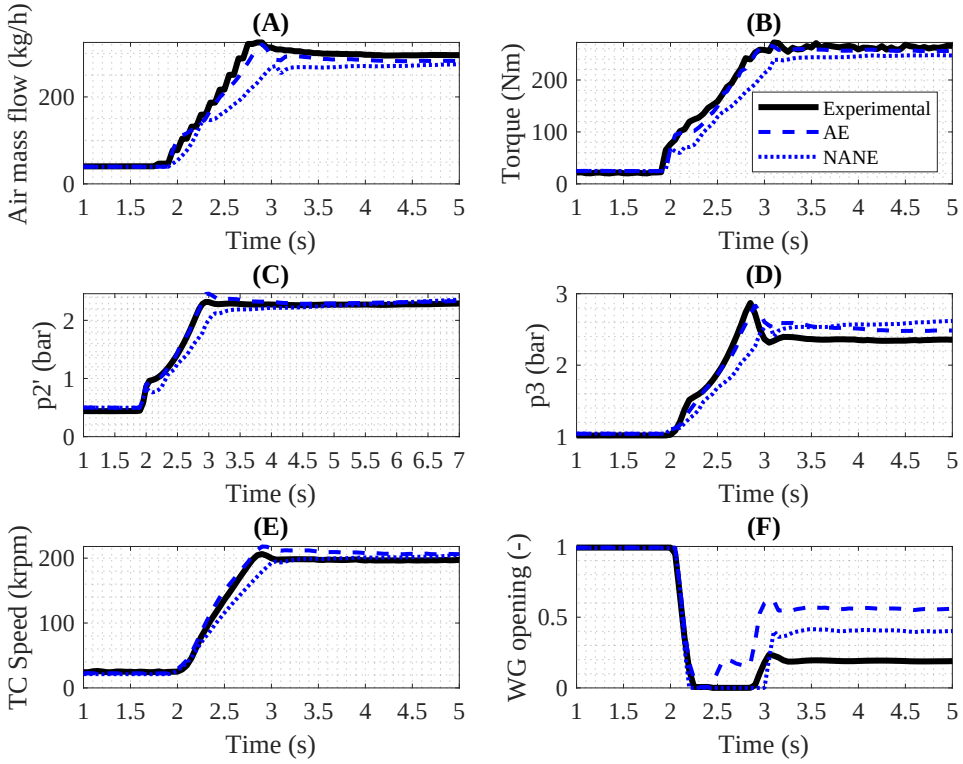

Figure 3.45: WG, 3000rpms sudden tip-in, continuous series corresponds to experimental, dashed corresponds to model results with AE turbocharger maps, and dotted corresponds to NANE maps

Moving to the lower engine speed (1500rpm) transient, same variables are shown as for the higher speed one. VGT-1 results can be found in Figure 3.46, VGT-2 in Figure 3.47 and WG Figure 3.48.

It is the low-end, where turbocharger maps modelling accuracy is more relevant, as in the full loads was evidenced. The main explanation is the one that follows: turbine and/or compressor wrong modelling practice, leads to big differences in terms of VGT closure, to compensate for the lack of boost pressure (attributed to the lack of turbocharger efficiency). Particularly, in the lower engine speeds, one of the main benefits of the VGT, is the nozzle section variation to provide a better turbine-engine matching. However, an excessive VGT closure implies a p3 $>$ p2, which is an undesirable situation,

which, under relatively low mass flow ratios (as in the low engine speeds) may impede achieving the proper air mass flow. This was concluded in the full load's validation, see Figure 3.36 and Figure 3.37 for this analysis, and it is again taking its role in the low-speed transient.

See how none of the NANE series along Figure 3.46(A)(B), Figure 3.47(A)(B) and Figure 3.48(A)(B) properly achieves air mass flow and torque, because of the lack of boost pressure during the transient itself, see Figure 3.46(C), Figure 3.47(C) and Figure 3.48(C). By contrast, AE maps in any TC unit, perform accurately in terms of air mass flow and torque, since boost pressure is properly achieved in any case, at any time.

In the case of the VGT-1 NANE series, after second four, p3 stays almost steady, below the experimental value, see Figure 3.46(D), this happens since there is no increase in boost pressure/air mass.... Under the AE maps approach, there is a slight error in terms of p3 prediction, however, this error hardly impacts torque evolution. What is more, in the AE series, at the end of the transient, hardly any error in terms of p3 is committed.

Moving to VGT-2, the extremely closed VGT predicted position using the NANE series, leads to a 0.4 bar exhaust manifold pressure over-estimation, as in Figure 3.47(D) is shown. The previous issue with p3 directly impacts average engine variables and the engine torque evolution. In AE maps, it is evidenced a p3 under-prediction, which again, is not directly impacting air mass flow/engine torque. This p3 under-prediction is attributed to the excess of turbocharger initial speed, during the low-load initial steady state. The same could be stated for VGT-1. This statement is confirmed afterwards in this section.

In the case of the WG, experimentally there is no margin to further close the by-pass valve, hence, the model is limited in by-pass closure terms, at least until second five. As far as the boost pressure built is under-predicted by the NANE series, p3 in Figure 3.48(D), is kept below the experimental one. AE maps perform extraordinarily accurately under the complete engine test. Particularly, aiming to evaluate the turbocharger modelling, turbocharger speed and p3 are called to question, resulting in hardly any noticeable error, even considering initial turbocharger speed at the initial low-load steady state.

In all, in the NANE series, as far as boost pressure is not achieved, the VGTs mechanisms further close the nozzle area, however, the situation gets

even worse, since turbine efficiency and/or volumetric efficiency decreases. As described, in the case of the WG, there was no possibility for further closing the WG orifice to compensate for the lack of turbine and compressor efficiencies. To back up the previous, compressor and turbine efficiencies for VGT-1, VGT-2 and WG are depicted in Figure 3.49. It is evidenced that systematically, compressor efficiencies for AE series are higher at any time. The same could be said for the turbines. Particularly, for the VGT-2, compressor efficiencies differences between series are the smallest (even if the compressor evolution is considerably different), while turbine series differences are the largest.

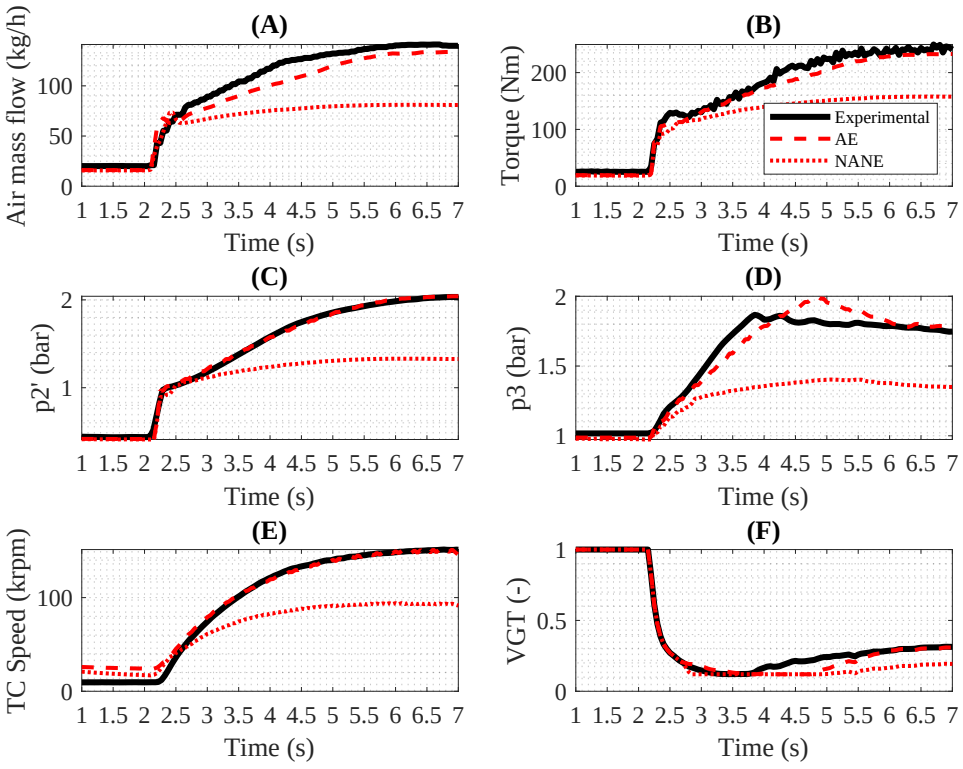

Figure 3.46: VGT-1, 1500rpms sudden tip-in, continuous series corresponds to experimental, dashed corresponds to model results with AE turbocharger maps, and dotted corresponds to NANE maps

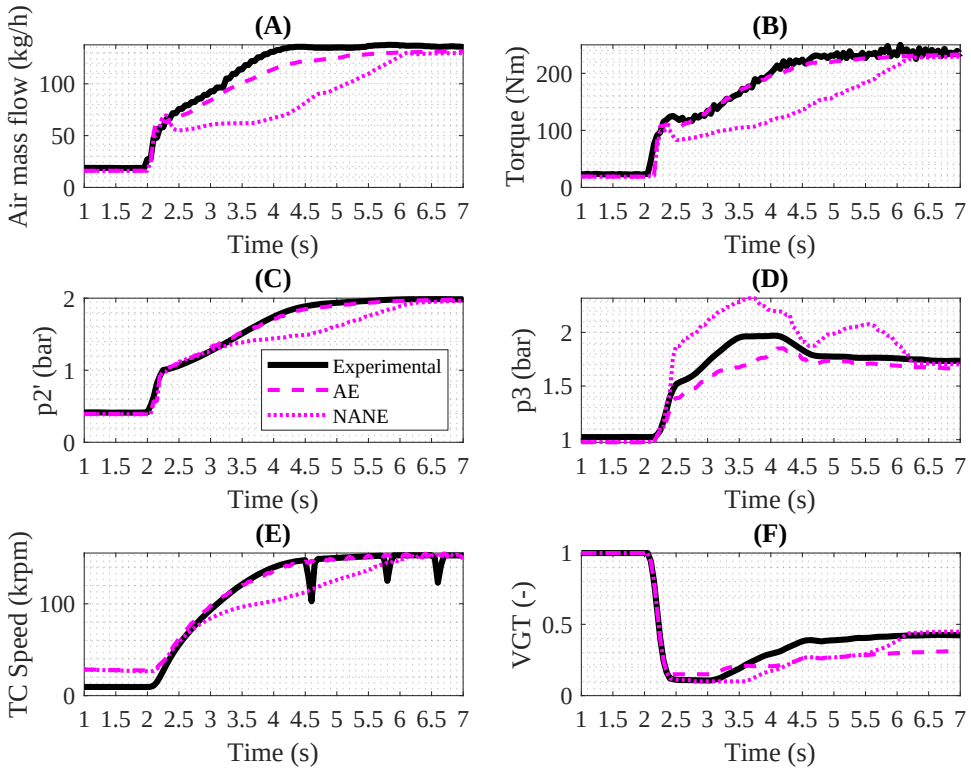

Figure 3.47: VGT-2, 1500rpms sudden tip-in, continuous series corresponds to experimental, dashed corresponds to model results with AE turbocharger maps, and dotted corresponds to NANE maps

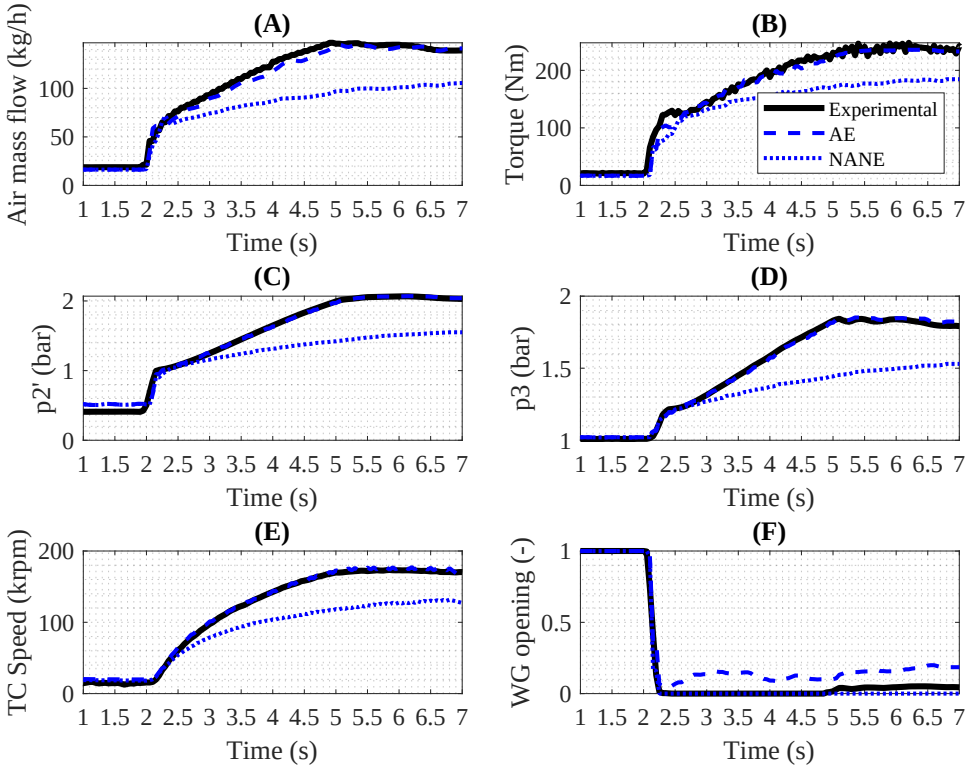

Figure 3.48: WG, 1500rpms sudden tip-in, continuous series corresponds to experimental, dashed corresponds to model results with AE turbocharger maps, and dotted corresponds to NANE maps

Large differences happen in terms of compressor efficiencies and effective turbine efficiency "ETE", see Figure 3.49. It shall be highlighter the main difference between both series efficiencies lies in the fact that NANE series are affected by heat transfer, as it was deeply discussed in subsection 3.3.2. Taking as an example the compressor efficiencies in Figure 3.49(A), NANE efficiency is wrongly considered as an isentropic one, since comes directly from an experimental campaign in which heat transfer influences the maps and it is defined in Equation 3.13, while AE one comes from Equation 3.14, and it is isentropic indeed.

Figure 3.49(B) deals with "ETE" instead of turbine efficiency. However it shall be highlighted that for the NANE series, the "ETE" considered is

the "$ETE_{experimental}$", which corresponds to the one in Equation 3.7, which is influenced by heat transfer as it has been previously discussed in subsection 3.3.2. On the contrary, the "ETE" in the AE series is calculated making usage of Equation 3.18, which differs from Equation 3.7 in the sense that has no heat transfer effects, since the isentropic efficiency in the turbine side, it is the adiabatic one: "$\eta_{turbine}^{isentropic-adiabatic}$".

$$ETE_{adiabatic} = \eta_{turbine}^{isentropic-adiabatic}\eta_{mechanic} \tag{3.18}$$

NANE maps present a systematically lower efficiency, which allows for a better prediction in terms of initial turbocharger speed: the turbine produces less power, while the compressor consumes more, in balance, the TC decelerates and finds equilibrium in terms of energy balance, in a lower speed working point. In all, it is confirmed that the initial TC over-speed in the AE series (at least for the VGTs) is attributed to the unmeasured (out-of-design) turbocharger maps areas, where efficiency is wrongly extrapolated and over-predicted.

Finally, it shall also be pointed out that for a proper WG-to-VGT comparison, the "ETE" shown for the WG series, corresponds to the mass-averaged "ETE" with which the turbine mass flow is expanded, assigning a value of zero to the "ETE" corresponding the by-passed mas flow. This is done according to Equation 3.19 for both WG series (AE and NANE), and it is the information depicted in Figure 3.49. In summary, Equation 3.19 calculates "$ETE_{total-mass}$", which is obtained as the product of the turbine mass flow efficiency "$ETE_{turbine-mass}$" times the turbine mass flow ratio with respect to the total amount of exhaust gases. The turbine mass flow ratio can be obtained as the unit minus the portion of by-passed gasses.

Special care shall be taken at this point since simulation codes give as output the turbine efficiency considering only the mass flow through the turbine "$ETE_{turbine-mass}$". However, when comparing WG turbines against technologies where there is no by-passed mass flow (as in VGTs), it is necessary to consider the term "$ETE_{total-mass}$" rather than the term "$ETE_{turbine-mass}$". To illustrate the expected differences between both efficiency definition values, Figure 3.50 shows for the WG, both "ETE" definition evolution for the 1500rpm transient for AE and NANE.

$$ETE_{total-mass} = ETE_{turbine-mass}(1 - \frac{\%_{by-passed-mass}}{100}) \tag{3.19}$$

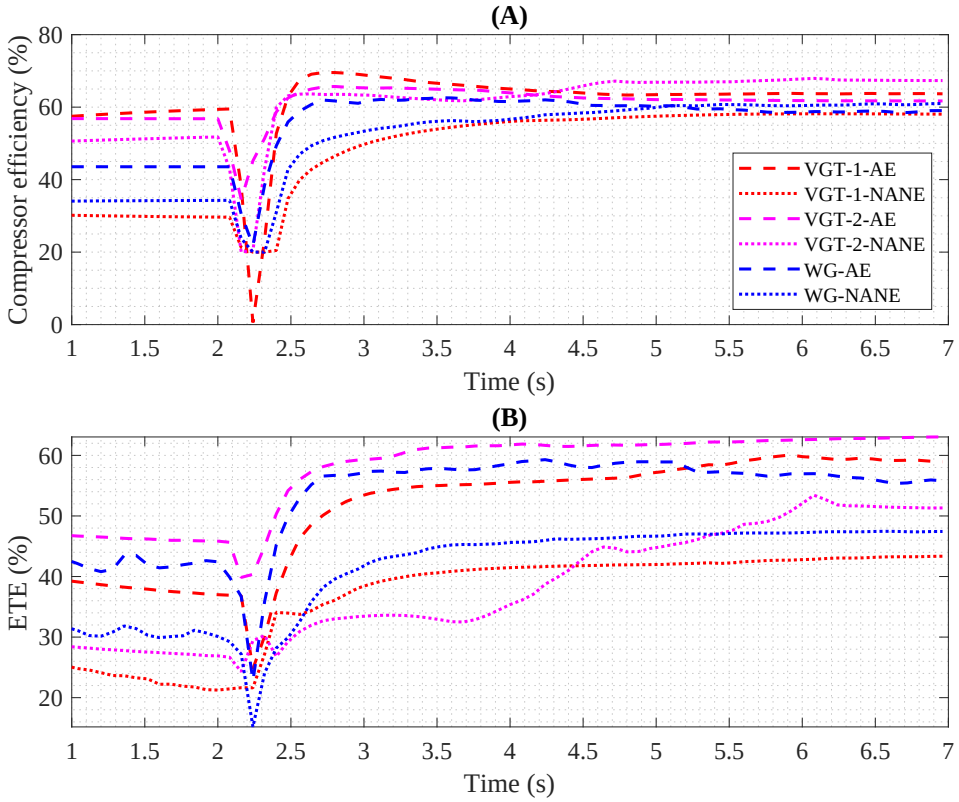

Figure 3.49: 1500rpm transients' efficiencies. (A) Deals with compressor efficiencies, (B) with turbine efficiencies. Dotted series correspond to NANE series, dashed series corresponds to AE series

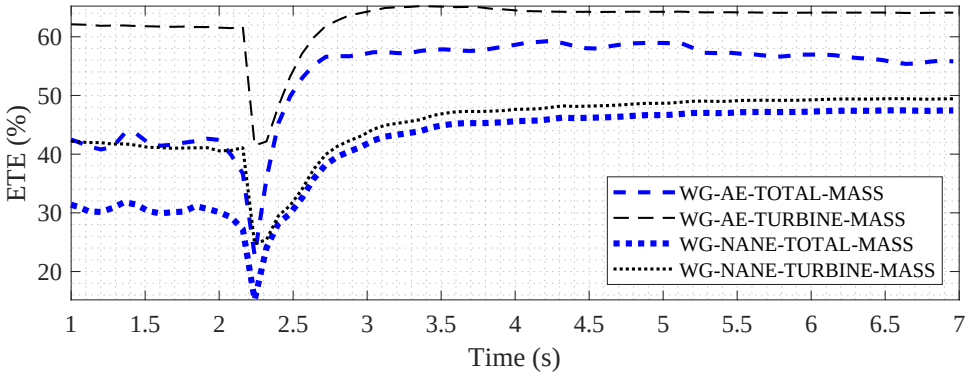

Figure 3.50: 1500rpm transients' WG efficiency. Thin black series correspond the expanded gasses efficiency, thicker blue series, to the averaged efficiency, with respect to the total exhaust gasses

As in subsubsection 3.2.1.3 was detailed, VGT-1 for the 1500rpm speed is the only database in which low inertia thermocouples were assembled, for exhaust gasses thermal evolution recording.

Figure 3.51(A) deals with experimental and model information for T3 and Figure 3.51(B) deals with T4. During the transient itself, AE configuration accurately predicts both T3 and T4. It is only in the low load initial steady-state (2bar BMEP) where an error of -45ºC in T4 is committed. This error in T4 is attributed to the over-predicted turbine efficiency in the low-load initial steady condition, which goes in hand with the turbocharger speed over-prediction at that operative area: Since turbine efficiency is over-predicted, the power balance along the TC leads to a higher speed to reach the energy equilibrium condition. The proper prediction of T3 (which goes in hand with the rest of the variables already discussed), allows us to further validate the NNW performance as well as the heat transfer multiplier in the exhaust manifold. The 10-20ºC under-prediction in the earliest stages of the sudden demand could be attributed to several uncertainty sources, such as combustion prediction in highly transient working points, exhaust thermal inertia or slight lack on p3, as in Figure 3.46(D) was shown.

T4 is never well-predicted in the NANE configuration. In the initial working point, there is a slight over-prediction in terms of T4, even though, the accuracy is even higher than the one from the AE maps in the initial steady-

state point. Following with the NANE results analysis, even if T3 is under-predicted along the transient itself, (aspect directly attributed to the lack of air, fuel...) T4 is highly over-predicted, which is purely explained by the poorly turbine efficiency prediction.

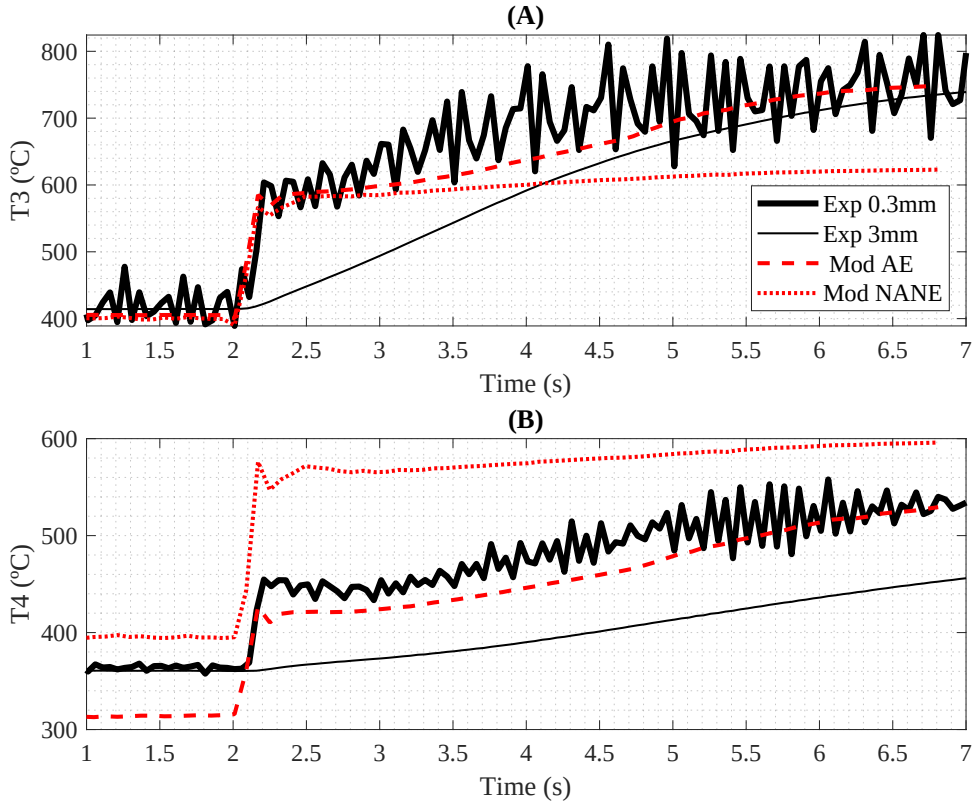

Figure 3.51: Low inertia and high inertia thermocouples response for VGT-1 1500 sudden tip-in. (A) Corresponds to T3 and (B) corresponds to T4. Experimental and model information included

Chapter 3 Bibliography

[1] J. R. Serrano, F. J. Arnau, L. M. García-Cuevas, A. Gómez-Vilanova, S. Guilain, and S. Batard. "A Methodology for Measuring Turbocharger Adiabatic Maps in a Gas-Stand and Its Usage for Calibrating Control Oriented and One-Dimensional Models at Early ICE Design Stages".

Journal of Energy Resources Technology 143.(4) (2021), pp. 1–11. ISSN: 0195-0738. DOI: 10.1115/1.4048229 (cit. on pp. xii, 25, 105).

[5] J. R. Serrano, F. J. Arnau, J. De la Morena, A. Gómez-Vilanova, S. Guilain, and S. Batard. "A methodology to calibrate Gas-Dynamic Models of turbocharged petrol egines with variable geometry turbines and with focus on dynamics prediction during tip-in load transient tests". In: *Volume 8: Industrial and Cogeneration; Manufacturing Materials and Metallurgy; Marine; Microturbines, Turbochargers, and Small Turbomachines*. Vol. 2020-june. American Society of Mechanical Engineers, 2020, pp. 22–26. ISBN: 978-0-7918-8419-5. DOI: 10.1115/GT2020-15169. URL: https://asmedigitalcollection.asme.org/GT/proceedings/GT2020/84195/Virtual,Online/1095133 (cit. on pp. xii, 25, 105).

[6] J. R. Serrano, F. J. Arnau, L. M. G.-C. González, A. Gómez-Vilanova, and S. Guilain. "Impact of a holistic turbocharger model in the prediction of engines performance in transient operation and in steady state with LP-EGR". In: *Volume 2: Emissions Control Systems; Instrumentation, Controls, and Hybrids; Numerical Simulation; Engine Design and Mechanical Development*. San Diego, California, USA: American Society of Mechanical Engineers, 2018, pp. 1–16. ISBN: 978-0-7918-5199-9. DOI: 10.1115/ICEF2018-9550. URL: https://asmedigitalcollection.asme.org/ICEF/proceedings/ICEF2018/51999/SanDiego,California,USA/273145 (cit. on pp. xiii, 34, 36, 51, 64).

[7] J. R. Serrano, F. J. Arnau, L. M. G.-C. González, A. Gómez-Vilanova, and S. Guilain. "An experimental methodology and model for characterizing radial centrifugal compressors of turbocharged engines from diathermal perspective". In: *Advances in Mechanism and Machine Science*. Krakow, Poland: Springer International Publishing, 2019, pp. 883–892. ISBN: 978-3-030-20130-2. DOI: 10.1007/978-3-030-20131-9_88. URL: https://link.springer.com/chapter/10.1007/978-3-030-20131-9_88 (cit. on pp. xiii, 23, 37, 38, 98).

[52] Society of Automotive Engineers. *Turbocharger Gas Stand Test Code - SAE Standards*. 1995. DOI: 10.4271/J1826_199503. URL: http://standards.sae.org/wip/j1826/ (cit. on pp. 21, 22, 84, 110).

[53] SAE J1723. *Supercharger testing standard*. 1995. DOI: J1723_199508. URL: https://saemobilus.sae.org/content/J1723_199508 (cit. on pp. 21, 89, 91, 105).

[54] B. Sirakov and M. Casey. "Evaluation of Heat Transfer Effects on Turbocharger Performance". *Journal of Turbomachinery* 135.(2) (2012). ISSN: 0889504X. DOI: 10.1115/1.4006608 (cit. on pp. 21, 97).

[55] A. Romagnoli and R. Martinez-Botas. "Heat transfer analysis in a turbocharger turbine: An experimental and computational evaluation". *Applied Thermal Engineering* 38 (2012), pp. 58–77. ISSN: 13594311. DOI: 10.1016/j.applthermaleng.2011.12.022. URL: http://dx.doi.org/10.1016/j.applthermaleng.2011.12.022 (cit. on pp. 21, 97).

[59] S. Marelli, G. Marmorato, M. Capobianco, and A. Rinaldi. "Heat Transfer Effects on Performance Map of a Turbocharger Compressor for Automotive Application". In: *SAE Technical Papers*. Vol. 2015-April. April. 2015. DOI: 10.4271/2015-01-1287. URL: http://papers.sae.org/2015-01-1287/ (cit. on pp. 22, 84, 97).

[61] J. R. Serrano, P. Olmeda, F. J. Arnau, M. A. Reyes-Belmonte, and H. Tartoussi. "A study on the internal convection in small turbochargers. Proposal of heat transfer convective coefficients". *Applied Thermal Engineering* 89 (2015), pp. 587–599. ISSN: 13594311. DOI: 10.1016/j.applthermaleng.2015.06.053 (cit. on pp. 23, 84).

[62] J. R. Serrano, P. Olmeda, F. J. Arnau, A. Dombrovsky, and L. Smith. "Turbocharger heat transfer and mechanical losses influence in predicting engines performance by using one-dimensional simulation codes". *Energy* 86 (2015), pp. 204–218. ISSN: 03605442. DOI: 10.1016/j.energy.2015.03.130 (cit. on pp. 23, 25, 39, 51).

[69] S. Zhu, K. Deng, and S. Liu. "Modeling and extrapolating mass flow characteristics of a radial turbocharger turbine". *Energy* 87 (2015), pp. 628–637. ISSN: 03605442. DOI: 10.1016/j.energy.2015.05.032. URL: http://dx.doi.org/10.1016/j.energy.2015.05.032 (cit. on pp. 27, 98).

[70] F. Payri, J. R. Serrano, P. Fajardo, M. A. Reyes-Belmonte, and R. Gozalbo-Belles. "A physically based methodology to extrapolate performance maps of radial turbines". *Energy Conversion and Management* 55 (2012), pp. 149–163. ISSN: 01968904. DOI: 10.1016/j.enconman.2011.11.003 (cit. on pp. 27, 98).

[74] J. Galindo, A. Tiseira, R. Navarro, D. Tarí, H. Tartoussi, and S. Guilain. "Compressor Efficiency Extrapolation for 0D-1D Engine Simulations". In: *SAE Technical Papers*. 2016. DOI: 10.4271/2016-01-0554 (cit. on pp. 27, 98).

[75] J. R. Serrano, P. Olmeda, A. Tiseira, L. M. García-Cuevas, and A. Lefebvre. "Theoretical and experimental study of mechanical losses inautomotive turbochargers". *Energy* 55 (2013), pp. 888–898. ISSN: 03605442. DOI: 10.1016/j.energy.2013.04.042. URL: http://dx.doi.org/10.1016/j.energy.2013.04.042 (cit. on pp. 30, 84, 97).

[76] J. R. Serrano, P. Olmeda, A. Tiseira, L. M. García-Cuevas, and A. Lefebvre. "Importance of Mechanical Losses Modeling in the Performance Prediction of Radial Turbochargers under Pulsating Flow Conditions". In: *SAE International Journal of Engines*. Vol. 6. 2. 2013, pp. 729–738. DOI: 10.4271/2013-01-0577. URL: http://saeeng.saejournals.org/content/6/2/729\%5Cnhttp://saeeng.saejournals.org/content/6/2/729.abstract (cit. on pp. 30, 84, 97).

[91] G. Ericsson, H. E. Angstrom, and F. Westin. "Optimizing the transient of an SI-engine equipped with variable cam timing and variable turbine". In: *SAE Technical Papers*. Vol. 3. 1. 2010, pp. 903–915. DOI: 10.4271/2010-01-1233 (cit. on pp. 33, 63, 163, 165).

[93] B. Pla, J. De la Morena, P. Bares, and I. Jiménez. "Cycle-to-cycle combustion variability modelling in spark ignited engines for control purposes". *International Journal of Engine Research* 21.(8) (2020), pp. 1398–1411. ISSN: 20413149. DOI: 10.1177/1468087419885754 (cit. on p. 55).

[94] J. R. Serrano, P. Olmeda, F. J. Arnau, A. Dombrovsky, and L. Smith. "Methodology to characterize heat transfer phenomena in small automotive turbochargers: Experiments and modelling based analysis". In: *Proceedings of the ASME Turbo Expo*. Vol. 1B. February. 2014. ISBN: 9780791845585. DOI: 10.1115/GT2014-25179. URL: http://proceedings.asmedigitalcollection.asme.org/proceeding.aspx?doi=10.1115/GT2014-25179 (cit. on pp. 84, 97).

Chapter 4

Turbocharged 4-S ICE analysis prospective modelling

Contents

4.1 Introduction

The present chapter deals with the SI 1.3 L engine described in chapter 3. The difficulties of a direct turbine technology comparison with merely experimental data are widely discussed here, since, for example, boundary conditions may affect somehow the engine-turbocharger output. However, it is not only the test boundary conditions but also the ECU calibration and the compressor side of each single turbocharger unit that may imply severe differences, especially under extreme working conditions.

In all, the previous variables become out-of-control influencing parameters and allow to state that purely experimental data is not suitable for solely turbine technologies comparison. The aforementioned difficulties are analysed in this chapter, taking advantage of the experimental campaign carried out in the engine and carefully described in chapter 3, in combination with the results coming from the modelling of the aforementioned phenomena.

To obtain a comparison between turbine technologies with the minimum possible bias, it was decided to make use of a 1-D complete engine model on the GT-Suite platform. Hence, the experimental campaign which was taken as the basis for the calibration of the engine model is not taken as a comparative basis.

Having reached this point, a sensibility study is assessed, in which the several "out-of-control" variables' impact is evaluated in the context of the engine-turbocharger. The previous is followed by a specific modelling methodology campaign for turbine technologies comparison, overcoming any experimental uncertainty. As deeply analysed in section 3.4 more realistic and accurate results are expected from the use of adiabatic turbocharger maps (AE). Therefore, in this chapter, all the presented modelling results deal with AE maps simulations. This is not specified in all the plots for the sake of readiness. NANE calculations are not presented in this chapter after having evidenced the expected poorer performance in predicting the turbocharger output.

A set of full, partial loads and transient simulations are carried out. In these simulations, the same engine boundaries, defined by altitude and engine speed at full-load, and compressor map for all turbines are kept. With this approach, a clear comparison between the VGT and WG technologies is provided. Differences between technologies are presented and carefully analysed

in section 4.3.

Furthermore, in the last section of this chapter, a set of optimization calculations are developed for the VGT, to explore the potential of this technology, being coupled to the SI-ICE: First of all, the VVT is optimized in the full load curve, while lambda control, governs T3, secondly, lambda=1 is fixed while VVT is optimized simultaneously, and the same procedure is followed for the partial loads. Finally, a methodology for the VGT control during heavy transient tip-ins is developed.

4.2 Out-of-control experimental differences

In this section, some "out-of-control experimental differences" that may impede obtaining a “solely turbines comparison” are described and their impact is analysed. In all, the identified main three differences are test-cell boundaries, engine controlling unit (ECU) calibration and compressor side of each turbocharger.

4.2.1 Boundaries differences

Despite having tested the engine in the same location, daily temperature, pressure and humidity variations are present in the experimental campaigns which were carried out. As an example of the previous, T1 and p1, are shown in Figure 4.1(A) and Figure 4.1(B) for VGT-1 and VGT-2 full loads from 1250 to 5000 engine rpm.

In order to show the potential effect on the compressor pressure ratio, p2 shown in Figure 4.1(C) at 3500rpm working point is discussed: first of all, the same boost pressure was achieved for both turbocharger units. Thus, it is more evident the influence of compressor inlet pressure in the averaged compressor pressure ratio. In all, the compressor pressure ratio for VGT-1 is about 2.68 while for VGT-2 is about 2.74 (+0.06 in comparison to VGT-1). Figure 4.1(D) has been included to show that the p3 difference for the same point (3500rpm) between VGT-1 and VGT-2 is about 0.11bar in consequence, at a first sight, the error in 0.06 in terms of compressor pressure ratio may be considered when comparing both turbines-engine output.

The importance of any variable could be an object of forward analysis, however, it is out of the scope of this thesis. Just to provide an idea of the magnitude of the potential impact, the developed model is taken advantage of to evaluate the impact of environmental pressure variations. The way to proceed is the one that follows:

- VGT-2 AE full load curve calculated and presented in Figure 3.38 is taken as the reference for this sensibility study. These results are labelled as VGT-2(ref) series in Figure 4.2 and correspond to the x-axis in Figure 4.3 for this sensibility study.
- A second full load curve is calculated for the VGT-2, in which test-cell pressure is offset -25mbar with respect to the values in VGT-2(ref). This series is labelled as VGT-2(-25mbar), and Figure 4.2 reveals that it can be expected a %VGT opening difference between a 1.5-8% depending on the engine working point.

  Afterwards, this series is added to Figure 4.3, and placing the series VGT-2(-25mbar) in the y-axis, one can see the differences between VGT-2(ref) and VGT-2(-25mbar) for several variables (each point corresponds to the location of the same engine speed and full load operative point). In terms of torque, one can see that differences are inexistent, however in terms of turbocharger speed, T2, and p3, the barrier of the +/-3% is reached, and in some cases, it is surpassed.
- Thirdly, aiming to clarify if the impact of the boundaries may be comparable to the expected difference between turbocharger units, VGT-1(ref) is added to Figure 4.3. VGT-1(ref), corresponds to a calculation in which the same reference boundaries, targetted boost-pressure, mixture enrichment, VVT... in all, any variable is set up as in VGT-2(ref) series. This way, one can appreciate the differences between two turbocharger units, under similar boundaries. The same methodology is applied for the WG(ref) series. VGT-1(ref), as well as WG(ref), are added in the y-axes in Figure 4.3.
- In fourth place, looking at the results, one can conclude that (in the analysed range), in terms of torque, boundaries impact (from VGT-2(reference) vs. VGT-2(-25mbar) comparison) are neglectable, see Figure 4.3(A). However, in terms of turbocharger speed, differences originated by boundaries dispersion, is in the same order of the expected

differences when comparing different turbochargers, and the same could be stated for the T2, see Figure 4.3(B) and Figure 4.3(C) respectively.

To conclude with this analysis: On the one hand, it is shown that daily or monthly pressure dispersion may imply differences in the same order of the ones expected between turbines with the same technology (VGT i.e). On the other hand, different technologies (VGT vs. WG i.e) lead to greater discrepancies in terms of engine and turbocharger variables. So comparing different turbochargers (with different technologies), by merely using the experimental campaign, can be only taken as a first approximation.

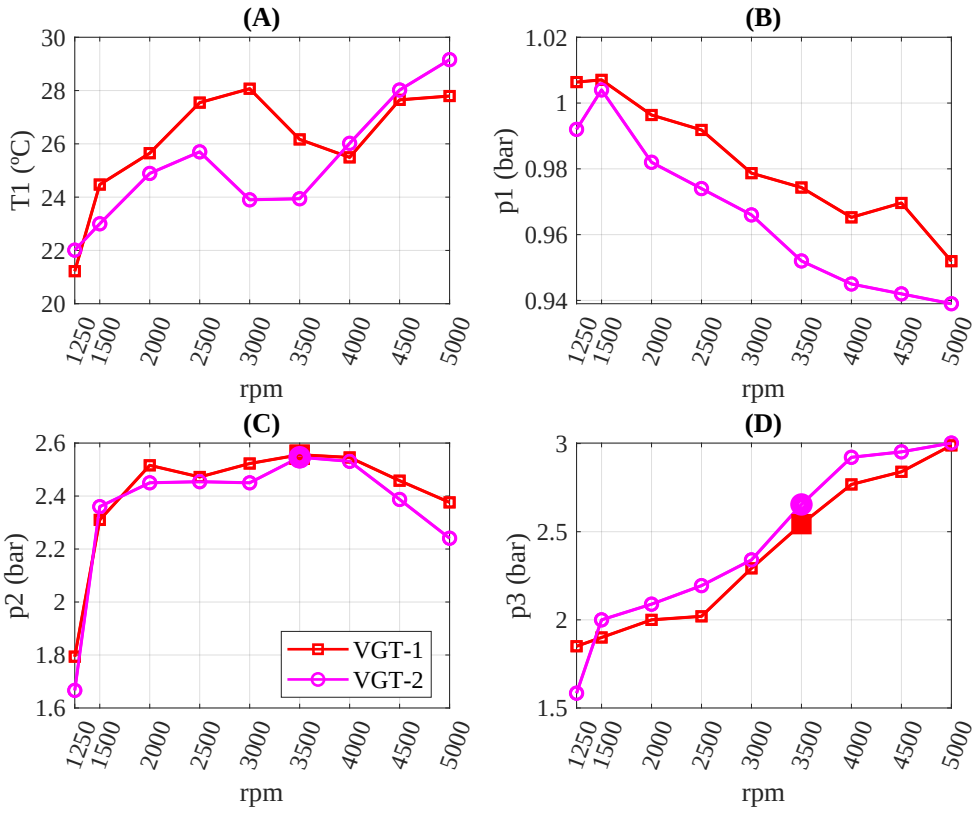

Figure 4.1: Experimental variables in full load tests for VGT-1 and VGT-2

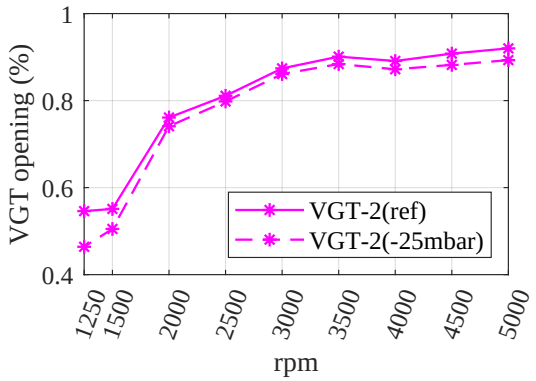

Figure 4.2: Sensibility study for pressure effect impact: VGT-2 position differences when boundary pressure differs -25mbar from reference value

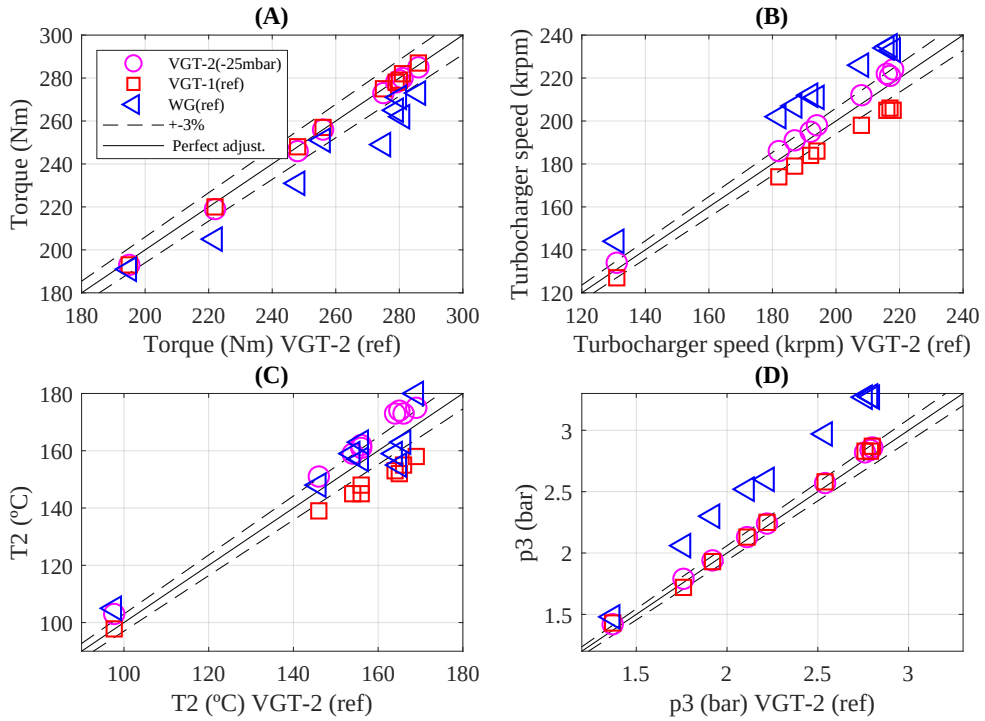

Figure 4.3: Sensibility study for pressure effect impact: VGT-2(ref) vs. VGT-2(-25 mbar), VGT-2(ref) vs. VGT-1(ref) and VGT-2(ref) vs. WG(ref)

4.2.2 ECU calibration

For the studied engine, the engine controlling unit was originally calibrated while the WG turbocharger unit was assembled to the engine. Among other parameters, VVT, as well as turbine inlet temperature control (through air-to-fuel-ratio management), are governed through the ECU and optimized for the WG turbocharger. In consequence, one may expect an under-optimized performance of the ECU, when the WG unit is overridden by any other turbocharger, especially if the turbocharger matching is substantially different. As an example, it is shown, from the experimental campaign, how T3 in Figure 4.4(A) is considerably higher for the engine-WG combination. This is almost purely attributed to the mixture enrichment management for T3 control, which is closer to 1 (stoichiometric) in the case of the WG turbocharger, see Figure 4.4(B).

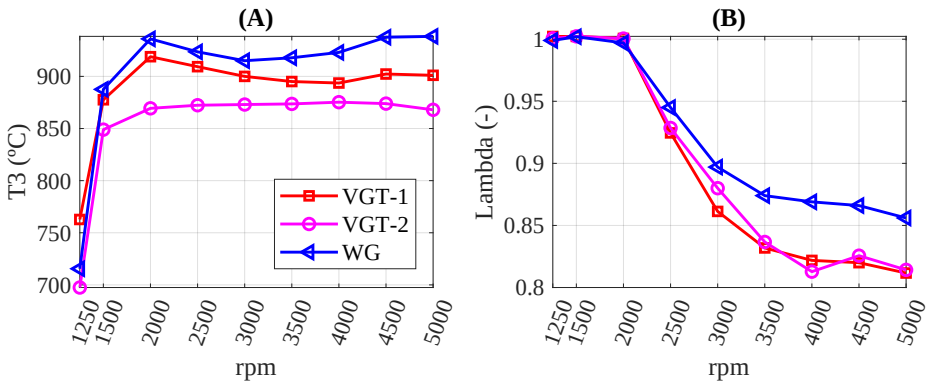

Figure 4.4: Turbine inlet temperature and Lambda for WG, VGT-1 and VGT-2

The impact in fuel enrichment is evidenced in Figure 4.5. Again, it is taken the VGT-2(ref) series, which corresponds to the x-axis, and it is the result of the modelling of the experimental full load curve. In the y-axis, it is presented the information coming from modelling the VGT-2 but imposing the AFR values coming from the WG experimental campaign. In other words, the Lambda values from Figure 4.4(B), specifically from the WG series, are taken and imposed in the VGT-2 simulation. Particularly in Figure 4.5, the engine speed range is constraint from 2500-5000rpm, since for the lower range, in any case, the engine operated under stoichiometric conditions, as in Figure 4.4 is depicted. The interest in this comparison lies in analysing the ECU

management of AFR dispersion, as a consequence of TC models differences.

Regarding torque, differences reach the 3% of difference in terms of engine torque output. However, the variable affected to a deeper degree is the BSFC, where differences reach 11.5% in relative terms. This difference is mainly caused by the excess of injected fuel. In other words, working under reach mixture conditions leads to a partial burnt of the fuel and with a direct impact on the resulting BSFC. Having said that, it is noticeable from Figure 4.5(C), the higher T3 values in the VGT-2(AFR-WG) series, in some cases, overcoming the barrier of the 3%.

Even though in terms of p3, no differences take place when comparing both series of data, in consequence, pumping losses are not altered by the AFR un-equal control.

In all, AFR dispersions lead up to 45ºC at the exhaust temperature and 11.5% of BSFC differences.

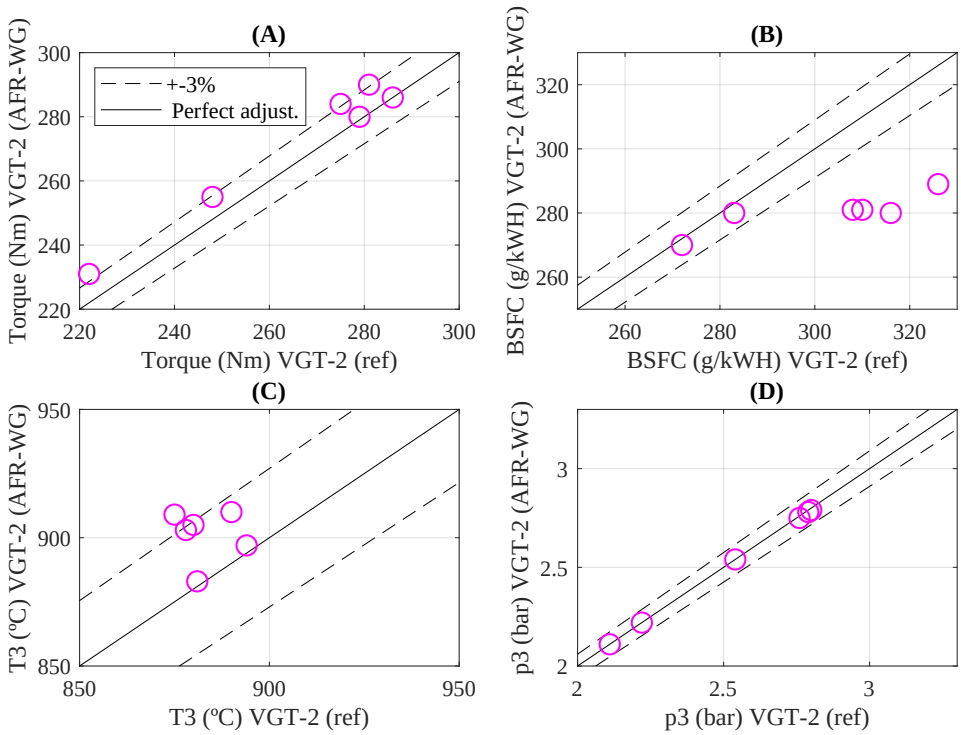

Figure 4.5: VGT-2(ref) vs. VGT-2(AFR-WG) to evidence lambda differences and its implications in torque, BSFC, T3 as well as turbine inlet pressure

About VVT management, the ECU is responsible for the set-up at each operative point, as a function of engine load and engine speed. To provide with an idea of the set-up range, Figure 4.6 shows the intake and exhaust valves, both extreme positions in which maximum Figure 4.6(A) and minimum Figure 4.6(B) valve overlap can be set up. The optimum position combination for the intake and exhaust VVT depends on the engine working point, but also on the turbocharger which is coupled to the engine itself: since p2'/p3 is one of the main parameters for the VVT set-up.

To summarize, the employed VVT set-up for each engine working point, corresponds to the ECU estimation, according to a calibration, which was performed with the engine coupled to the WG. The last does not necessarily imply a "close-to-optimum" set-up for any engine-turbocharger combination.

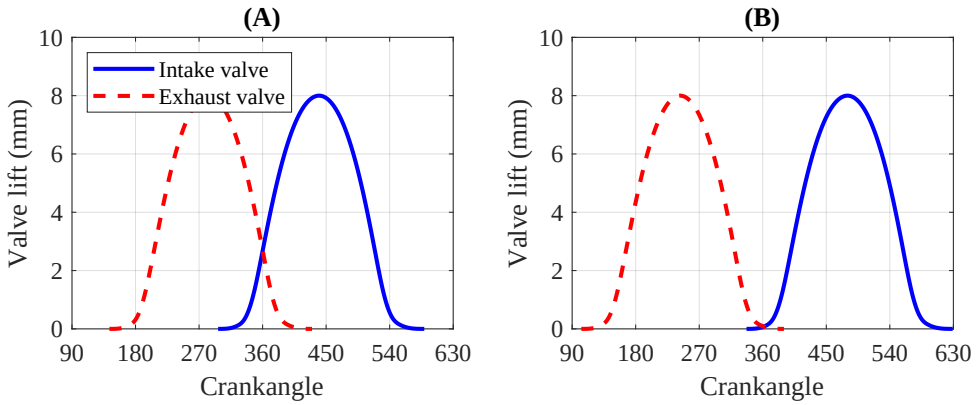

Figure 4.6: VVT extreme positions, (A) corresponds to maximum valve overlap and (B) to minimum valve overlap

4.2.3 Compressor differences

It is not only boundaries and ECU calibration the variables that imply some bias for turbines comparison. Unless the compressor sides of the respective turbines are the same, differences in terms of compressor efficiencies, surge line and mass flow maps, may lead to concluding turbine differences, which take origin at the compressor side.

In other to show the differences between all three compressors corresponding to the analysed turbochargers, Figure 4.7, Figure 4.8 and Figure 4.9 (for WG, VGT-1 and VGT-2 respectively) show the compressor efficiency contours in the pressure ratio-reduced mass flow map. Same reduced mass flow, pressure ratio and compressor efficiency contours range are selected for every figure, to evidence the differences between compressor maps. In addition, the compressor operative cycle for several engine speeds is presented in each compressor map. The points (from left to right in each figure) deal with 1250, 1500, 3000 4000 and 5000 engine rpm and full loads. These engine points in the compressor map correspond to the black line series, which includes the complete engine cycle (720 crank-angle degrees) instantaneous compressor historic.

Therefore, it can be stated that VGT-1 shows a higher compressor efficiency, especially in the high-end (see the point of 5000rpm), where VGT-1 compressor efficiency is above 70%, the WG is between 70% and 65%, and the

VGT-2 lower limit is below the 65% efficiency. 3000 and 4000rpm in the VGT-1 work under compressor efficiencies between 75% and 80%, while VGT-2 and WG are in the context of 70% (±5%) for the same points.

In the low-end (1250-1500rpm) the most remarkable difference is the pressure ratio (PR) difference between the different compressor units, especially at 1250rpm, where the VGT-1 almost reaches a PR of about two, while VGT-2 is about 1.7 and WG hardly overcomes the value of 1.5. These differences between both VGTs are mainly governed by surge line differences: during the experimental campaign, in the case of the VGTs, it was compressor surge the limitation for further boosting, and this is confirmed from Figure 4.8 and Figure 4.9 for VGT-1 and VGT-2 respectively.

In the case of the WG experimental full loads, compressor surge was not detected in the low-end torque, it was the turbine by-pass valve the limitation, however, one can realize that surge limit was not very far from being reached in the low-end. Compressor side differences are evidenced, as well as the may impact on the turbocharger/engine performance.

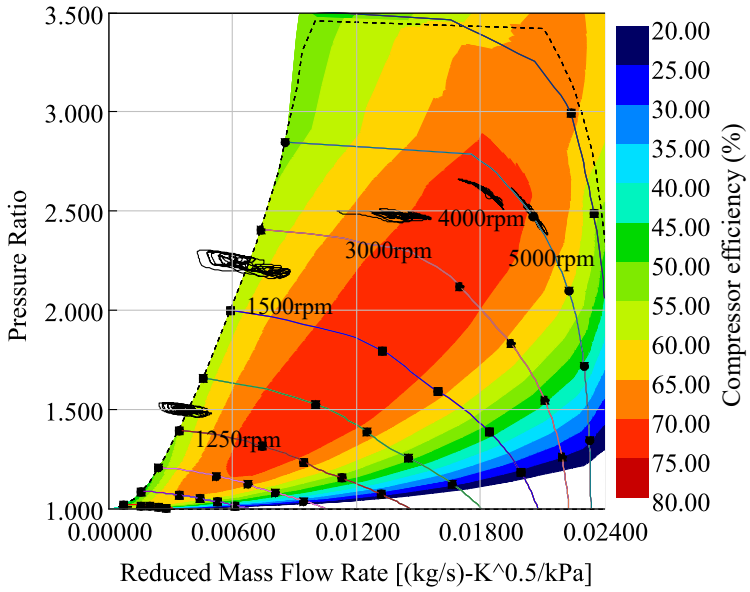

Figure 4.7: WG compressor efficiency map contours and full load working points

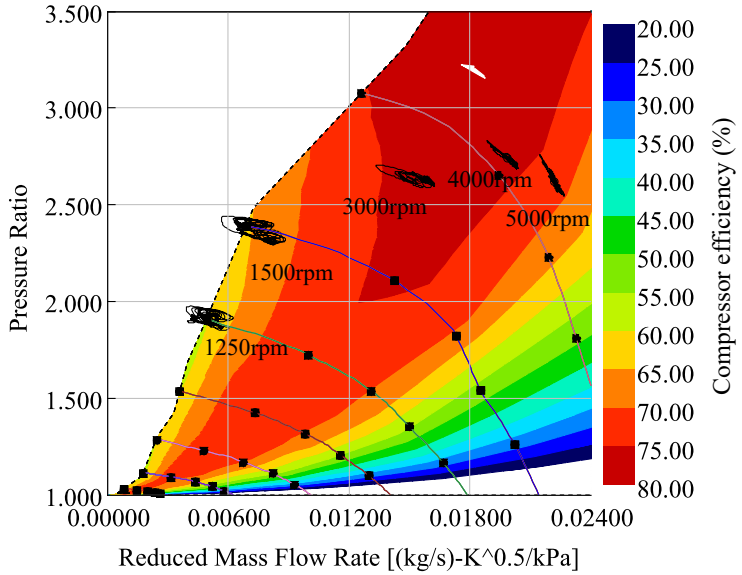

Figure 4.8: VGT-1 compressor efficiency map contours and full load working points

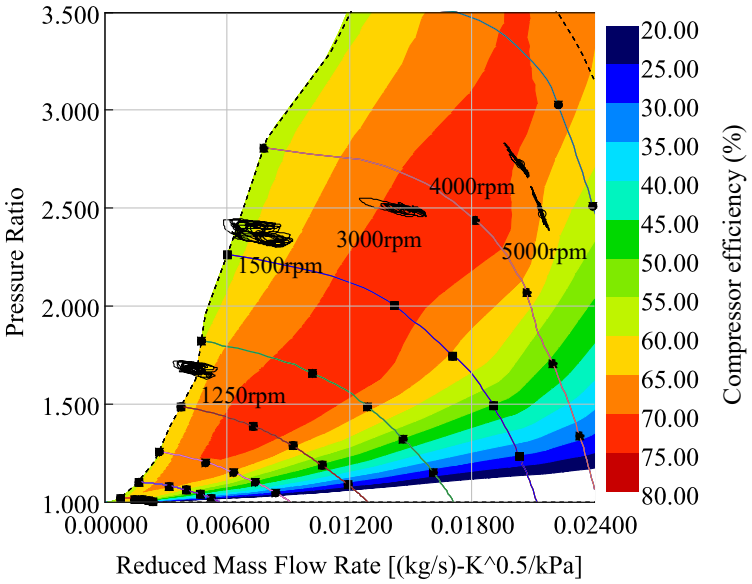

Figure 4.9: VGT-2 compressor efficiency map contours and full load working points

It is clear from Figure 4.7, Figure 4.8 and Figure 4.9, how close the compressor surge limits were reached (specially at 1250 and 1500). In these cases, it is ensured that no surge was reached at all, since the compressor operative points, come from the experimental data. The previous can be stated, even if there were some incursions beyond the surge limit. Indeed at this stage, it was of high value having collected the experimental data since surge detection is one of the main limitations of 0D/1D codes.

4.2.4 Prospective modelling methodology

In other to overcome the aforementioned variables that may hinder a comparison between turbine technologies performance in the context of SI ICE, the following steps are followed:

- Same engine intake and exhaust boundaries are set up for every simulated working point, with the aim of neglecting the possible bias caused by means of the test-cell temperature and pressure variations with the normal daily or monthly evolution.
- The same compressor map is used in combination with the three used turbines. Particularly in this work, it was chosen the compressor associated with VGT-2 since it was the one in which higher speeds were recorded.
- It is guaranteed that in any case, thermo-mechanical limits are equally reached in any case. In other to guarantee the accomplishment of this point, the model is monitored, and several actuators are regulated so that thermo-mechanical limits are reached (not overcome). These limits are gathered in Table 4.1.

  It shall be highlighted that the issue with experimental T3 differences previously presented, is solved by means of a PID which controls the mixture richness. The PID targets the T3 limit by comparing this limit against the estimated turbine inlet temperature.

  Particularly, from the modelling perspective, the engine and turbocharger suppliers stated that the WG turbine is capable of withstanding temperatures up to 1020ºC, while for VGTs the limit is 990ºC. These new limits do not correspond to the ones in previous chapter 3, in which

the experimental limit was set up to 950ºC. The lower limit in the experimental campaign is justified by the motivation of staying on the side of the safety testing practice, since later on, with ECU calibration and components dispersion, the experimental value of 950ºC may be exceeded eventually. However, in this chapter, with the aim of exploring the complete turbine capabilities, the new higher limits are the one's set-up.

Table 4.1: Turbocharger thermo-mechanic limits for modelling activities

Variable	**Limit**	**Controlled by**
Maximum compressor outlet temperature	175ºC	WG or VGT
Maximum boost pressure	2.55bar	WG or VGT
Maximum TC speed	250krpm	WG or VGT
Maximum turbine inlet temperature (WG)	1020ºC	AFR or WG
Maximum turbine inlet temperature (VGT)	990ºC	AFR or VGT
Maximum turbine inlet pressure	3bar	WG or VGT

4.3 Turbines comparison

In this section, the calibrated model, the trained NNW as well as the validated, adiabatized and extrapolated turbocharger maps are taken for the turbine technologies comparison. Following the key points on subsection 4.2.4, results dealing with full loads calculations at sea level and several altitude working conditions (1300 and 2500m), as well as in partial loads are presented. The target here in this section of the work is to clarify the differences when comparing the WG and the VGT technologies when iso-working conditions and thermo-mechanical limits are reached.

4.3.1 Full loads at sea level

Figure 4.10 shows the full-load results for the main engine variables. Each engine or turbocharger limit is shown as a horizontal black line on the corresponding chart. The first remarkable fact in Figure 4.6(A) is the higher mass flow in the high-end (4000-5000 rpm) for both VGTs. Figure 4.10(B) shows the resulting torque, which is systematically higher for the VGTs as well. The

main reason for the previously presented air mass flow and torque differences are analysed depending on the working area as it follows:

- Taking a look into the high-end torque (4000-5000 RPM), for both technologies, p3 limit is reached and represents the limiting parameter for higher power achievement, see Figure 4.10(C), where the 3 bar continuous black series is reached as stated. However, even if both technologies reach the maximum allowed p3, a higher boost is achieved with the VGTs. The rest of limits are not reached, or kept under control, such as maximum boost pressure, T2, neither the turbocharger speed, as Figure 4.10(C), Figure 4.10(D), Figure 4.10(E) and Figure 4.10(F) show. In other words, the WG lower efficiency values in the high-end torque imply a p3 limitation that constrains the engine output more than in the case of VGTs. This is confirmed by taking a look at turbine efficiency in Figure 4.10(G).

  As far as only adiabatic maps are being used in this study, Figure 4.10(G) deals with purely isentropic turbine efficiency, which, as deeply discussed in section 3.3, consider purely aerodynamic turbine performance information. Particularly the WG series appeals to the turbine isentropic efficiency, considering as zero the waste-gated gas efficiency. This consideration was applied in subsection 3.4.2, in Equation 3.19, for the ETE analysis. Now, this idea is applied to the isentropic efficiency for the WG, in Equation 4.1. "$\eta_{turbine,t-s}^{total-mass}$" corresponds to the turbine isentropic efficiency, considering the efficiency with which the gas flowing through the rotor is expanded "$\eta_{turbine,t-s}^{turbine-mass}$", but discounting the by-passed mass flow "$\%_{by-passed-mass}$".

$$\eta_{turbine,t-s}^{total-mass} = \eta_{turbine,t-s}^{turbine-mass}(1 - \frac{\%_{by-passed-mass}}{100}) \tag{4.1}$$

  Figure 4.10(H) reveals the VGT and WG mechanisms opening, very similar positions are predicted by the model, for both VGT in the high-end. Finally, Figure 4.10(I) deals with the mixture enrichment for the T3 control. It is evidenced by the fact that no enrichment is required in the case of the WG TC, while some it is required for the VGTs. The reason is the p3 limitation, which at the same time leads to lower values of air mass flow (consequently injected fuel) in comparison to the VGT. In addition, the fact of considering the actual limit of 1020ºC (not 950ºC as

in the experimental campaign) contributed to the stoichiometric mixture resulting in the high-end for the WG.

- In the middle engine speed range (2000-3500 rpm), torque differences are associated with the systematically lower p3 requirement to reach the targetted boost pressure. This is again purely attributed to higher VGTs efficiency. In any case, p3 is not a limitation, hence the maximum p2' is always achieved by all three turbochargers. It is remarkable the PID in charge of T3 control: in the points where T3 limitation is an issue, it is confirmed that mixture enrichment regulation does not benefit one turbocharger or another. As it can be seen in Figure 4.10(D), more enrichment is required for the VGTs, being attributed to two different reasons: the higher amount of fresh air and the more restrictive T3 limitation (990ºC dashed line, which corresponds to VGTs T3 limit).

- In the low-end torque (1250-1500 rpm), the WG orifice is almost completely closed see Figure 4.10(G). In other words, the turbine effective area is on the limit for the operative air mass flow range corresponding to the low-end. In any case, all three turbocharger units can reach the targetted boost pressure in the low-end torque, which is limited by the compressor surge. Anyway, the p3 requirement to fulfil boost pressure is always higher in the case of the WG.

The aforementioned conclusions go in hand with the ones found in previous studies. Tang et al. [95] already observed the over-sized effect of fixed geometry turbines for the low-end torque, as well as the under-sized effect in the high-speed range, were identified.

In the current study, the WG turbocharger main drawback against the VGTs lies from 1500 to 5000rpm, where the lower efficiency implies lower torque and at some point (from 4000rpm in advance) a boost pressure limitation. Tang et al. [95] claimed that VGT technology showed benefits from 5 to 22% in the low-end torque, and 3 to 13% in the high-end compared to the WG. Here differences are gathered in Table 4.2. Values in Table 4.2 are calculated according to Equation 4.2. Even if low-end torque differences are lower than the ones expected by other researchers in the field, torque differences are in the same order. On the contrary, middle-range and high-end torque expected differences are very close to the ones proposed by previous researchers.

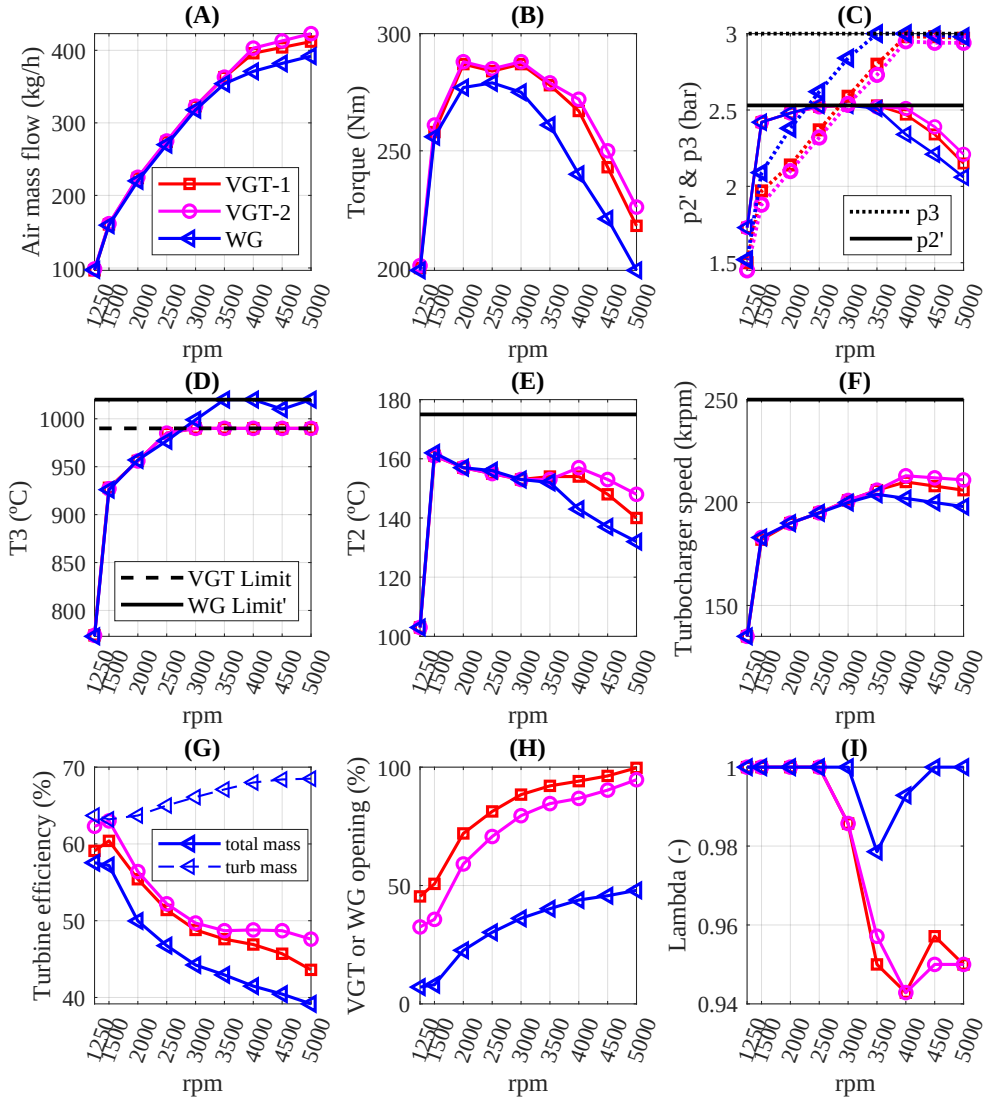

Figure 4.10: Sea level predicted performance from 1250 to 5000rpm, considering VGT-1, VGT-2 and WG. Black horizontal series correspond to the specified limits on each chart

Table 4.2: VGT torque differences for each engine speed, with respect to WG turbocharger (in %)

rpm	**1250**	**1500**	**2000**	**2500**	**3000**	**3500**	**4000**	**4500**	**5000**
VGT-1	0.5	0.8	3.6	1.8	4.4	6.5	11.3	10	9.5
VGT-2	1	2	4	2.2	4.7	6.9	13.3	13.1	13.6

Table 4.3 deals with BSFC differences in the same way as for torque are presented in Table 4.2. From 1250 to 3500, the lower p3 requirement for the same boost pressure is intimately linked to the higher engine torque as previously discussed. This explains the BSFC improvements (reduction) for the VGT when compared to the WG. The positive differences found in the range of 4000-5000 imply a higher BSFC for the VGT, in comparison to the WG. The last is directly attributed to the higher mixture enrichment requirement for the VGTs, to keep the T3 within the limit specified by the TC suppliers. However, the higher torque is still guaranteed at the full load curve.

Table 4.3: VGT BSFC differences for each engine speed, with respect to WG turbocharger (in %)

rpm	**1250**	**1500**	**2000**	**2500**	**3000**	**3500**	**4000**	**4500**	**5000**
VGT-1	-0.7	-0.2	-1.4	-0.2	-1.2	-0.9	0.6	0.6	0.7
VGT-2	0.4	-0.7	-1.6	-0.4	-1.3	-1.2	0.8	0.8	0.2

$$Difference = \frac{Variable_i^{VGT-X} - Variable_i^{WG}}{Variable_i^{WG}} * 100 \tag{4.2}$$

To reinforce the predicted higher efficiency of the VGTs, Figure 4.11 and Figure 4.12, show turbine isentropic efficiency maps, including the operative area in black continuous line series for VGT-2 and WG turbines, in the 4000 rpm working points. Just taking a look into both figures, higher efficiency is predicted in the WG turbine, however, it shall be reminded that here, only the "turbine mass flow" is being taken into account. The total exhaust mass flow, as well as the turbine and by-passed mass flows, are plotted in Figure 4.13. The turbine isentropic efficiency in Figure 4.11 it is only referred to the black series in Figure 4.13.

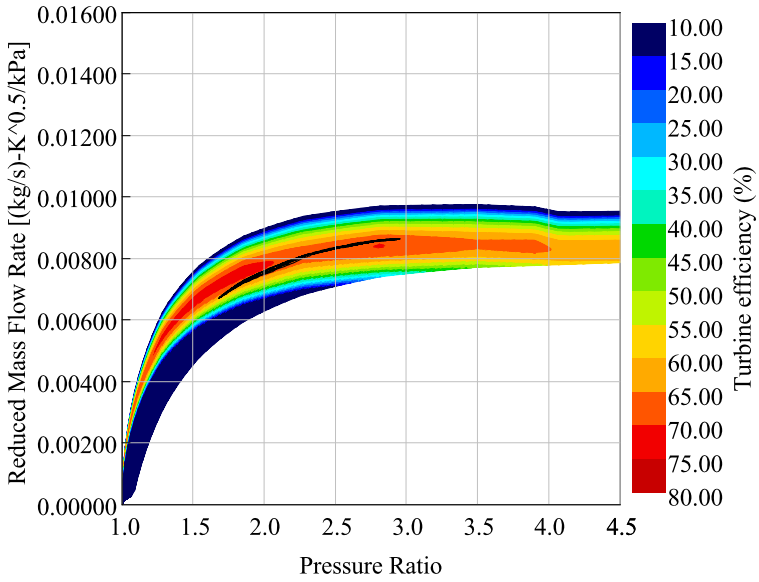

Figure 4.11: WG efficiency-PR turbine map and 4000 rpm operative area

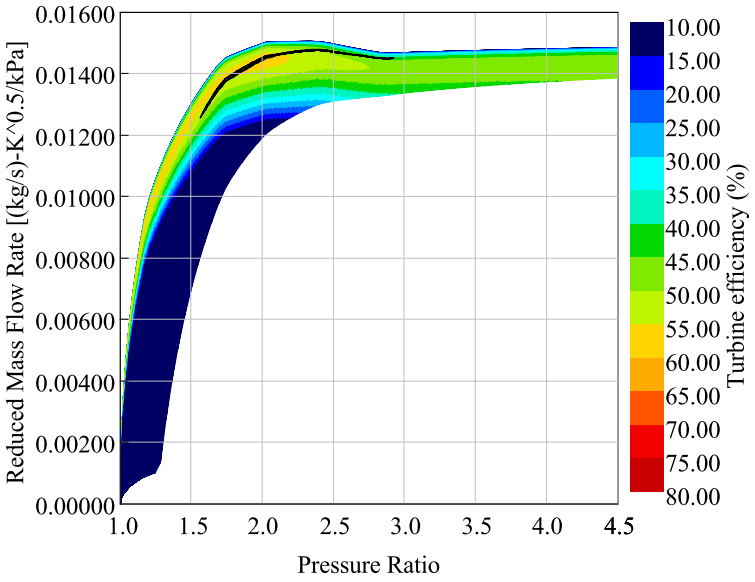

Figure 4.12: VGT-2 efficiency-PR turbine map and 4000 rpm operative area

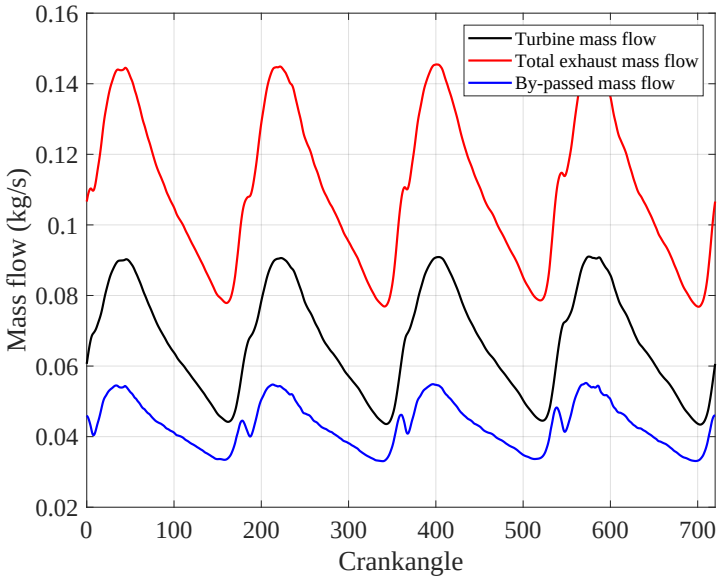

Figure 4.13: 4000 rpm instantaneous exhaust mass flow through the complete crankangle. Turbine and by-passed mass flows are also included

It is called to question whether the compressor map chosen is it better matched to one or other of the turbine unit. To clarify this point, the analysis is focused on the 2000rpm working point. Two main aspects are analysed:

- First, from Figure 4.10(C) it is evidenced that boost pressure is the same for all three turbocharger series. However, it is also shown how a different p3 is required for each turbocharger series. Hence, it can be analysed the impact of the p3 variability (attributed to the turbine) in the compressor map. For this purpose, Figure 4.14 shows for all three series, the 2000rpm compressor operative point. As it can be seen, the compressor operative point differences are almost negligible. From the last, one can conclude that p3 variability resulting from different turbine technologies, do not imply a negative or positive impact on the compressor map. In conclusion, it is the engine timing system (intake and exhaust valves), the element governing the compressor operative point, rather than the turbine side of the turbocharger itself.
- As it has been previously stated, in the 2000rpm point, p3 differences are found. First of all, as has been previously discussed, the compressor

operative working point is mainly governed by the engine timing system itself, rather than the turbine. Following this line, it is then the compressor side, the one that "imposes the TC speed" to satisfy the boost pressure and mass flow demand from the engine block. Simultaneously on the turbine side, the controlling mechanism (WG/VGT) is adapted to satisfy the energy balance in the turbocharger, to assure the desired boost pressure. Consequently, the turbine operative area is the one resulting from the engine-compressor matching and the compressor power requirements. In consequence, it is also expected that one compressor may favour more one or another turbine unit (as for the compressor-turbine matching). This may happen if the blade-to-speed-ratio (BSR) range of the turbine is far from the optimum (having accepted that compressor and engine determine the turbine operative area). To analyse this effect all three turbine maps have been plotted, in combination with the 2000rpm working point turbine operative area. VGT-1, VGT-2 and WG, turbine PR-BSR maps are included in Figure 4.15, Figure 4.16 and Figure 4.17 respectively. From these plots, one can understand that all three turbine units are operating around the optimum BSR and no significant matching benefit is found for any of the analysed turbine units. From the previous, one can deduce that compressor maps do not damage/show favour for any of the analysed turbine maps. Carefully analysing the maximum pressure ratio at which the WG unit is operated, the black series in Figure 4.17, is slightly better centred in the efficiency map (in comparison to the VGTs). The efficiency corresponding to the maximum pressure ratio at which the VGTs are operated, is around 50 to 55%, while for the WG, it is between 60 and 65%. Furthermore, the WG peak efficiency is higher than the one in the VGT units (75% and 70% respectively). However, the WG diameter opening corresponds to an orifice diameter of about 9mm. As a result, the corresponding efficiency for the amount of flow through the waste-gate valve is zero, hence, lowering the averaged efficiency shown in Figure 4.17. In conclusion, it is shown that qualitatively, the compressor selected is not more or less suitable for one or other turbine units. The operative area of the different turbines is almost equally centred in the maps, and efficiency differences are related to the turbine technology differences: on the one hand, the WG shows higher efficiency, since the by-passed gasses can not be taken into account in the maps. On the other hand, the VGTs show lower efficiencies, but there is no waste-gated mass flow.

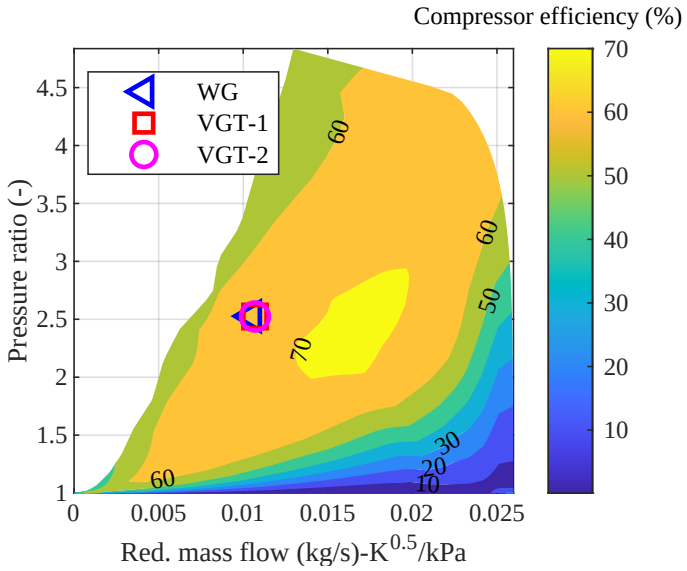

Figure 4.14: Compressor map and operative point of engine 2000rpm. Undetectable differences between the three included series: WG, VGT-1 and VGT-2

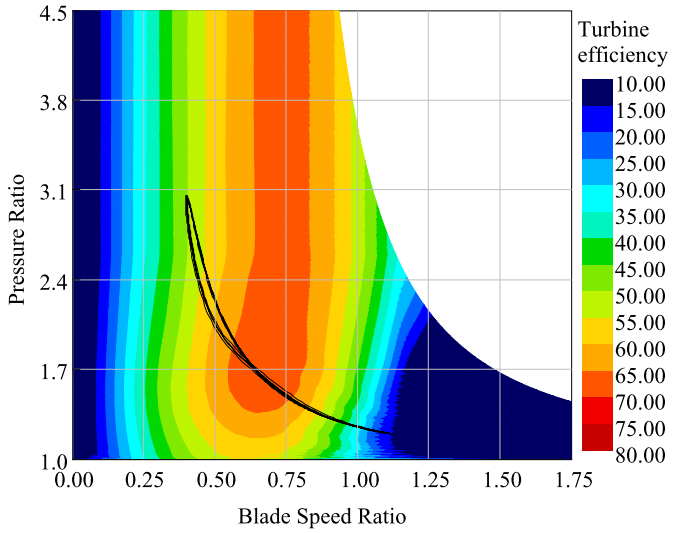

Figure 4.15: VGT-1 turbine map (72% opening): Pressure ratio vs BSR and iso-efficiency contours. In black, the operative area over the complete engine cycle (720º) for the 2000 rpm

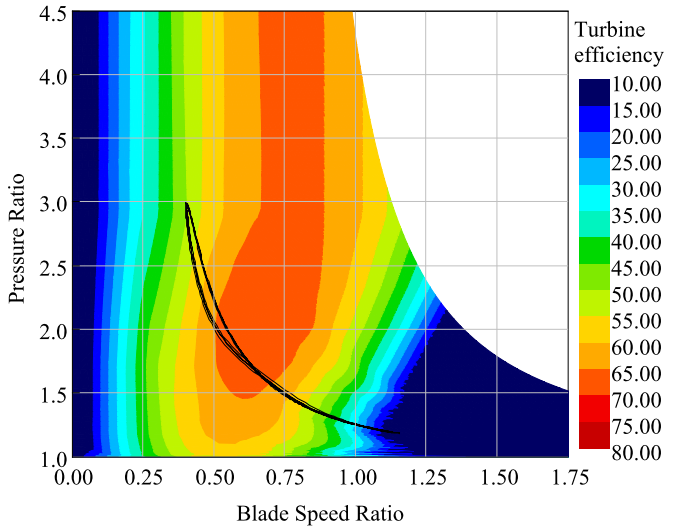

Figure 4.16: VGT-2 turbine map (59% opening): Pressure ratio vs BSR and iso-efficiency contours. In black, the operative area over the complete engine cycle (720º) for the 2000 rpm

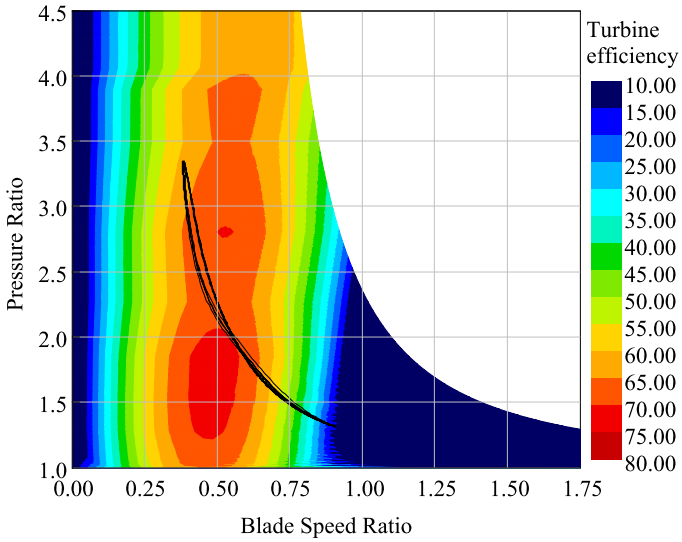

Figure 4.17: WG turbine map: Pressure ratio vs BSR and iso-efficiency contours. In black, the operative area over the complete engine cycle (720º) for the 2000 rpm. WG opening of 9mm during this simulation

4.3.2 Full loads at 1300m and 2500m of altitude

Aiming to further analyse the WG vs VGT technology, full load curves have been simulated at 1300 m of altitude, which corresponds to the homologating extended altitude for the real drive emissions (RDE) cycle. Results for all three analysed turbochargers are depicted in Figure 4.18.

Again the main conclusion from these calculations is the higher air mass flow and torque provided by the VGTs, see Figure 4.18(A) and Figure 4.18(B). The explanation is very similar to the one provided for the "sea level" calculations:

- In the high-end torque (4000-5000 rpm), WG reaches the maximum p3 value, see Figure 4.18(C), while this does not happen for the VGTs in any case. It is in fact compressor outlet temperature the main limitation for the VGT series (both of them), see Figure 4.18(D) it is in this area, where some extra TC speed is achieved in the VGTs, see Figure 4.18(E), but in any case, far from the limit. The combination of higher boost and lower p3 leads to higher air mass flow and torque values for the VGTS.

  Furthermore, in the WG series, the T3 limit is never reached, see Figure 4.18(F), as a consequence, the model predicts stoichiometric working conditions, see Figure 4.18(G). On the contrary, the T3 limit is achieved by the VGTs, leading to a subtle mixture enrichment, in any case, lower than at sea level.

- In the middle range (2000-3500 rpm) it is compressor outlet temperature the main limitation that prevents further boost level. The lower external boundary pressure, associated with the altitude simulation, implies higher pressure ratios that lead to higher compressor outlet temperatures. It shall be pointed out that the lower p3 taking place in the VGTs, leads to some extra torque in the VGT technology.

- In the low-end torque (1250-1500 rpm) the WG mechanism is fully closed, while there is still some margin for the compressor surge (as well as for higher boost level). In the VGTs, the surge limit is reached, while there is still some extra closure available. In other words, at 1300m, the WG is limited in terms of turbine minimum effective section while in the case of the VGTs the low-end torque limitation is governed by the

compressor surge as it was concluded in [87]. In any case, the VGTs provide with higher torque output, since a higher boost is achieved.

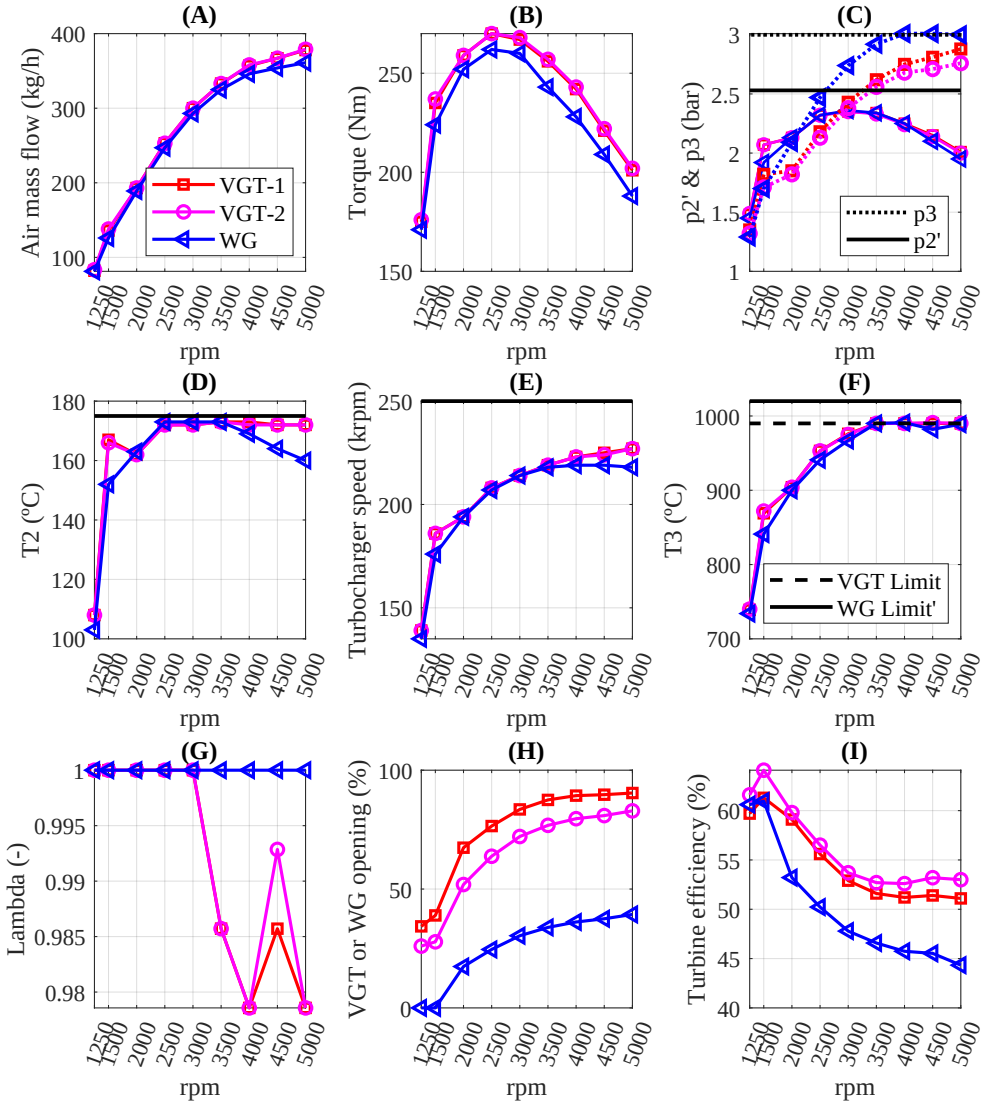

Figure 4.18: 1300m altitude and full load predicted performance from 1250 to 5000rpm, considering VGT-1, VGT-2 and WG. Black horizontal series correspond to the specified limits on each chart

To sum up, Table 4.4 and Table 4.5 gather torque and BSFC differences receptively, making usage of Equation 4.2. Broadly, torque differences have already been discussed, while BSFC shows in general terms an improvement, even in the high-end torque, where lambda control in the VGT, still requires some mixture enrichment, contrary to the WG. It is only in 1500 rpm, where VGT BSFC is higher than for the WG, but this happens simultaneously with the torque improvement. On average, at 1500, a 5.4% of torque improvement and a 2.75% of extra BSFC is expected. The VGTs drawback in terms of BSFC is directly associated with the retarded predicted combustion: the NNW compensates the higher boost pressure in the VGTs series with some spark retard, looking for knock avoidance.

Table 4.4: 1300m altitude over the sea level, VGT torque differences for each engine speed, with respect to WG turbocharger (in %)

rpm	**1250**	**1500**	**2000**	**2500**	**3000**	**3500**	**4000**	**4500**	**5000**
VGT-1	1.8	5.0	2.8	2.8	2.9	5.2	5.9	5.4	6.8
VGT-2	2.6	5.8	3	3	3.2	5.6	6.4	5.8	7.5

Table 4.5: 1300m altitude over the sea level, VGT BSFC differences for each engine speed, with respect to WG turbocharger (in %)

rpm	**1250**	**1500**	**2000**	**2500**	**3000**	**3500**	**4000**	**4500**	**5000**
VGT-1	-0.9	2.6	-0.6	-0.3	-0.7	-1.4	-0.4	-0.3	0.3
VGT-2	0	2.9	-0.6	-0.5	-0.9	-1.6	-0.7	-1.3	-0.2

The same conclusions are obtained for 2500m of altitude, where low-end torque differences, see Figure 4.19(A) are even bigger than the ones at 1300m. The key point is that at 1300m WG mechanism was at its maximum closed position, while the VGTs still had some margin to further compensate the environment air density decrease (while the same cannot be stated for the VGT). See Figure 4.19(B) for VGT and rack position. On the contrary, surge limit is reached for the VGTs from 1250-1500 rpm.

For the rest of the engine range (2000-5000 rpm), T2 is the limit for the VGTs, see Figure 4.19(C). Both p2 and p3 are far from their respective limits, as in Figure 4.19(D) is depicted.

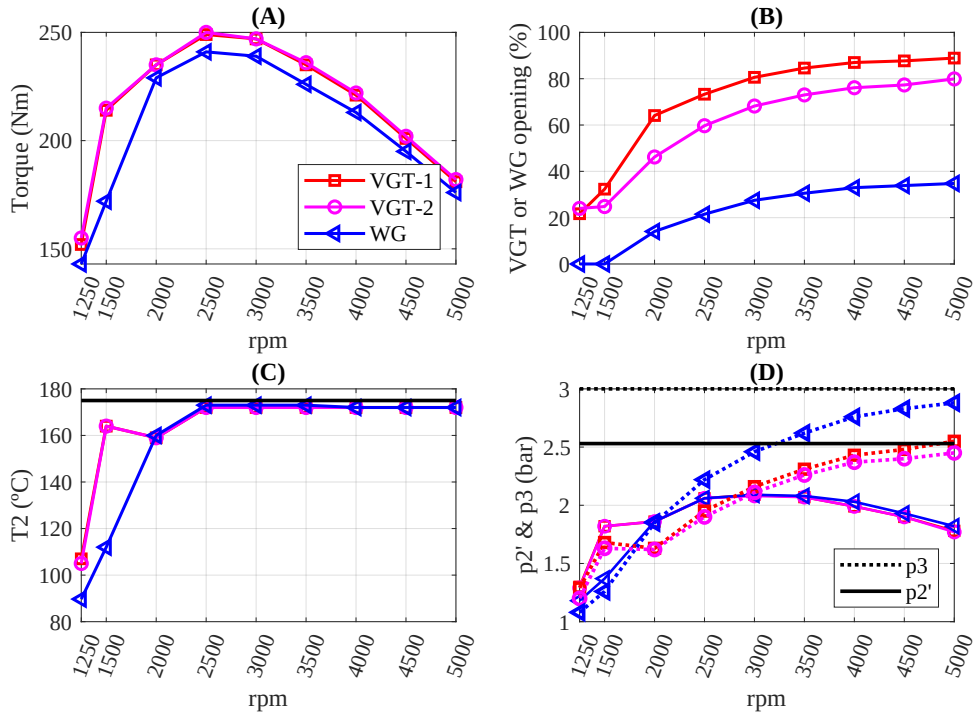

Figure 4.19: 2500m altitude and full load predicted performance from 1250 to 5000rpm, considering VGT-1, VGT-2 and WG. Black horizontal series correspond to the specified limits on each chart

4.3.3 Partial loads (12bar BMEP)

The engine speed range in this study goes from 2000 to 4000 rpm. The simulation strategy was to target a given torque value corresponding to the area of the engine operation where the transition from throttled to boosted operation is performed. As it can be seen in Figure 4.20(A), no significant BSFC differences are observed. BSFC difference is calculated according to Equation 4.2.

The VGT technology implies higher restriction to the air mass flow circulation. As a result, higher p3 is generated, Figure 4.20(B). Even though, there is no penalty in terms of BSFC or pumping losses, in Figure 4.20(A) and Figure 4.20(C). The reason is that even if p3 is around 0.04 bar higher for the VGT technology, the throttle body compensates the extra p3 with some extra

p2', see dotted series in Figure 4.20(E), to guarantee the requested torque.

The CNN can predict further combustion advance with increasing engine speed. This is why slight differences are observed in terms of CA50 Figure 4.20(F).

In previous studies such as in the one from Kapoor et al. [96], turbine maps were optimized for each engine operative area. They concluded that for the partial load working points the differences induced by turbine maps were almost negligible (hardly reaching values of 0.9 g/kWh). Similar results were obtained and concluded in this study since BSFC differences reached a maximum value of 1.1 g/kWh.

The most important difference lies in the fact that the VGTs keep the TC speeding higher than the WG does, this may imply some benefits from the transient perspective. It is evident the higher turbocharger speed (around 22 krpm systematically, whatever working point). In addition, the pressure in the routing between the throttle and the compressor is also higher. This means that after the sudden throttle opening a higher torque delivery may be expected, at least in the very early cycles, which are the most critical ones in the transient response of highly turbocharged engines.

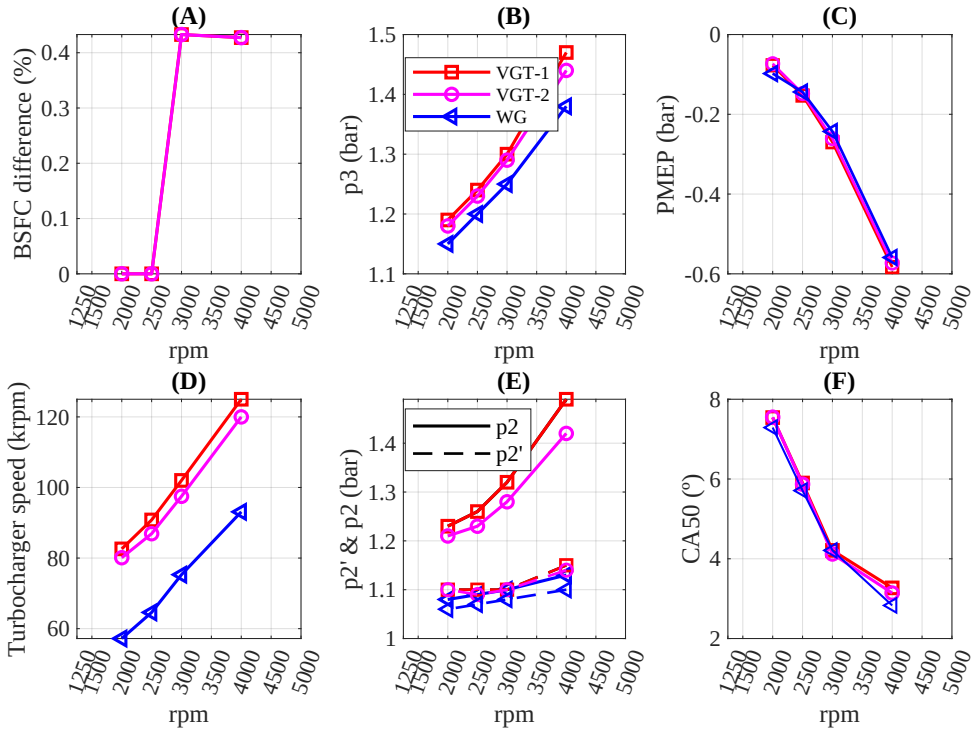

Figure 4.20: 12 bar BMEP working points for VGT-1, VGT-2 and WG

4.4 VGT-SI Model usage for VVT optimization

In this work, it is made usage of the engine model, coupled to VGT-2, to identify, study and evaluate the potential benefits that one could expect from the usage of VGT technology. In this work the VVT is adjusted with the motivation of collecting the synergies between both: VVT and VGT as in [91] was studied. In other words, both, intake and exhaust valves setup have a certain degree of freedom, as in Figure 4.6 was shown for both (intake and exhaust).

However, the optimum position for each working point may vary depending on the p2'/p3 resulting as a function of the turbocharger performance (among other parameters). In consequence, the model covers all the possible combinations in terms of the VVT setting, looking for the most suitable combination.

As an example, for the full loads, it is the torque the target variable to be optimized (maximized in particular).

Some special care is taken into account regarding the engine trapping ratio "TR", which in any case shall be kept above the value of 97% to guarantee proper operation of the 3-ways catalyst. "TR" is defined in Equation 4.3, as the ratio between the retained fresh air "$\sum_{i=1}^{n-cylinder} m_{retained}$" and the total amount of fresh air going through the engine "$\int \dot{m}_{inlet}$".

$$TR = \frac{\sum_{i=1}^{n-cylinder} m_{retained}}{\sum_{i=1}^{n-cylinder} \int \dot{m}_{inlet}} \tag{4.3}$$

Furthermore, lambda=1 working conditions in full loads would be studied and compared against the baseline lambda control and WG turbocharger configuration. In other words, it is evaluated whether VGT working under stoichiometric working conditions may provide with similar output as the WG coupled to the standard engine control strategy.

Also, a study regarding the VVT configuration, looking for the improvement of the BSFC in the partial loads is assessed.

In all, the results in this section attempt to provide an idea of how much potential can be expected from the VGT in comparison to the WG, when the VVT is purposely adjusted for the first technology, as well as exploring the stoichiometric operation in the complete engine map, to see the limitations that this may imply.

4.4.1 Full loads VVT optimization

In this section of the study, lambda control guarantees the accomplishment of the T3 thermo-mechanical limit, while the VGT position controls the boost pressure. Accordingly, lambda control would tend to force stoichiometric conditions, unless T3 limitation is overcome. In terms of VGT position, it is the turbocharger speed, turbine inlet pressure and compressor outlet pressure and temperature, the variables that would limit the mechanism closure and boost pressure in all. This is the normal operative strategy followed by the ECU in any case.

In the calculations, the VVT is varied in several discretization steps be-

tween the extreme VVT positions for both: the intake and exhaust valves. Each VVT configuration case is attempted to maximize the engine torque output since torque (or power) represents the most interesting engine variable in the full load's operative area. In other studies, VVT and VGT simultaneous management were studied to optimize the engine output under transient conditions for example [91].

Parallelly to torque maximization, the accomplishment of the 97% of trapping ratio becomes a new constraint limit. In other words, the VVT setup combination providing maximum torque, is necessarily the selected one, except TR is not constricted between the values of 0.97-1 (97-100% respectively).

1250 rpm results for the VVT optimization technique are depicted in Figure 4.21 and Figure 4.22, showing the resulting torque and TR respectively. The x-axis corresponds to the intake valve opening (IVO), and the y-axis to the exhaust valve closing (EVC). An EVC of 0º implies that valve closure occurs at the TDC. For the IVO, the same could be said. If the IVO is configured before the TDC, and the EVC takes place afterwards, then some valve overlap happens.

See how in Figure 4.21 and Figure 4.22 the information from the model has been arranged into iso-torque areas, as well as iso-trapping efficiency areas. After examining the possible configurations, the model can find the areas in which the maximum engine output performance (which is the objective variable to be optimized). The black asterisks in Figure 4.21 and Figure 4.22 correspond to the ECU calibration that takes place for each specified point. See how for the 1250rpm case, it is evidenced how the ECU calibration agrees with the models' optimum solution in terms of torque. However, it is identified that in terms of TR, a value around 94.5% is expected, which is not in the desired range. Furthermore, the model provides very valuable information: by just advancing the EVC a few degrees (-5º in this particular case) torque is kept while TR is improved to the desired 97%.

Figure 4.23 and Figure 4.24 show the same information but for 2000 rpm (torque and TR). See how for the 2000 rpm there is still some torque improving margin by just retarding the EVC, in other words, increasing the valve overlap. The last can be justified by the fact that systematically, "more favourable" p2/p3 ratios result from the VGTs (in comparison to the WG). Hence, retarding the EVC does not diminish the volumetric efficiency (as for the back-flows arising). The torque increase here goes in hand with the aug-

mented engine expansion stroke, before the gas exchange process, in addition to the increased amount of air mass flow rate. Figure 4.23 back dashed line, shows the required modification (from the black asterisk to the red circle) to find the most optimum VVT configuration for torque improvement while keeping the TR within the desired range at the same time. The same evolution is depicted in Figure 4.23.

Figure 4.25 shows how during the valve overlap, still p2/p3>1 is guaranteed during most of the valve overlap. The last is of high importance from the volumetric efficiency perspective. Since VGT presents higher p2/p3 ratio values than the WG does, it is logical that some extra valve overlap does not worsen the results, when moving from WG to VGT technology.

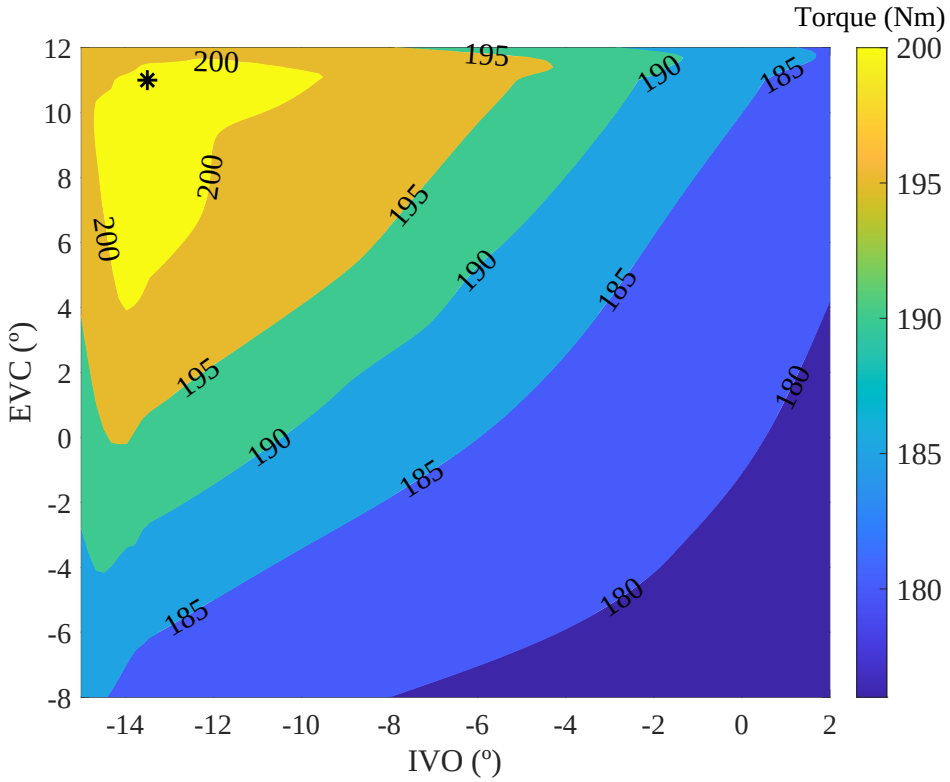

Figure 4.21: 1250 rpm VVT model torque optimization results. Asterisk corresponds to ECU calibration

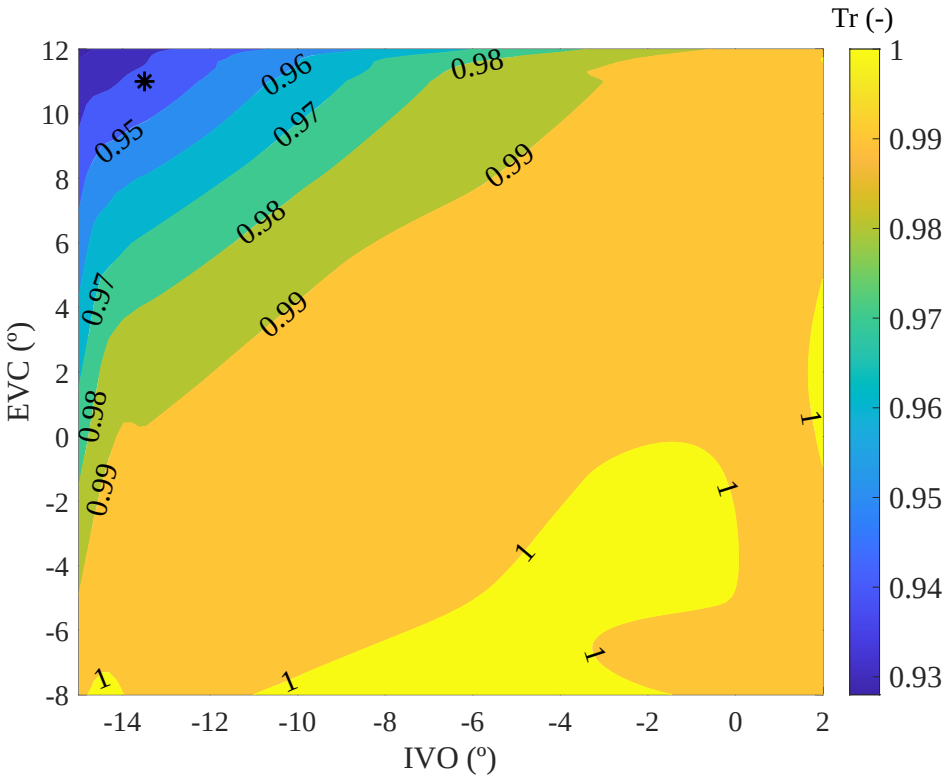

Figure 4.22: 1250 rpm VVT model torque optimization, trapping ratio results. Asterisk corresponds to ECU calibration

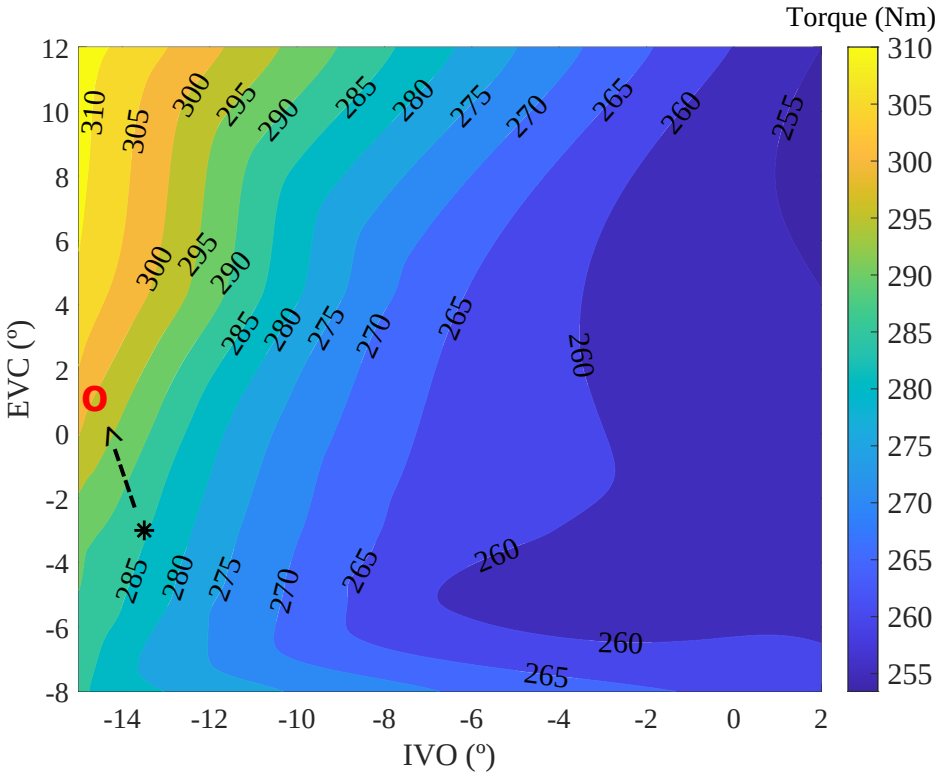

Figure 4.23: 2000 rpm VVT model torque optimization results. Asterisk corresponds to ECU calibration

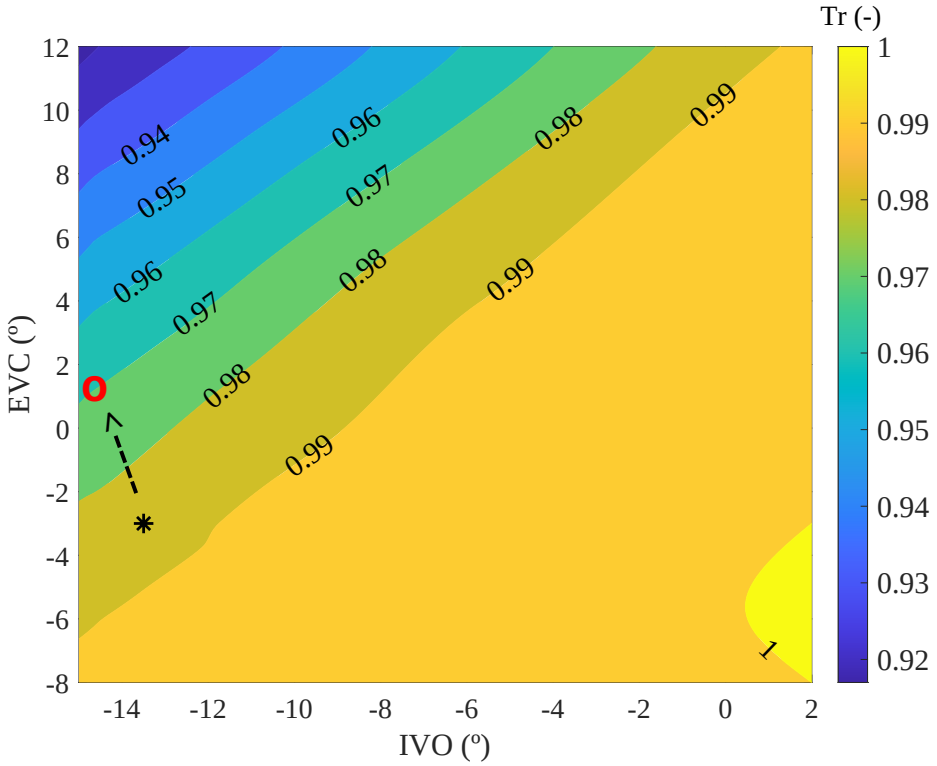

Figure 4.24: 2000 rpm VVT model torque optimization, trapping ratio results. Asterisk corresponds to ECU calibration

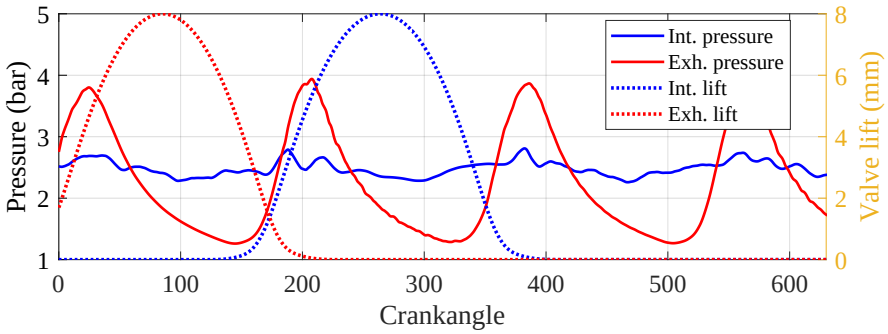

Figure 4.25: 2000 rpm, intake manifild and exhaust manifold pressure as well as intake and exhaust valve lifts

Finally, to show the consistency of the methodology, Figure 4.26 shows the torque optimization results for the 4000 rpm working point for any VVT combination. There is still some margin in terms of IVO. Torque can be improved by about 5Nm (1.8%). Furthermore, in Figure 4.27 the higher p3 (in comparison to p2') implies a TR>0.98 and is almost insensitive to the selected combination. See the black dashed arrow going from the black asterisk to the red circle, which evidences the aforementioned improvement.

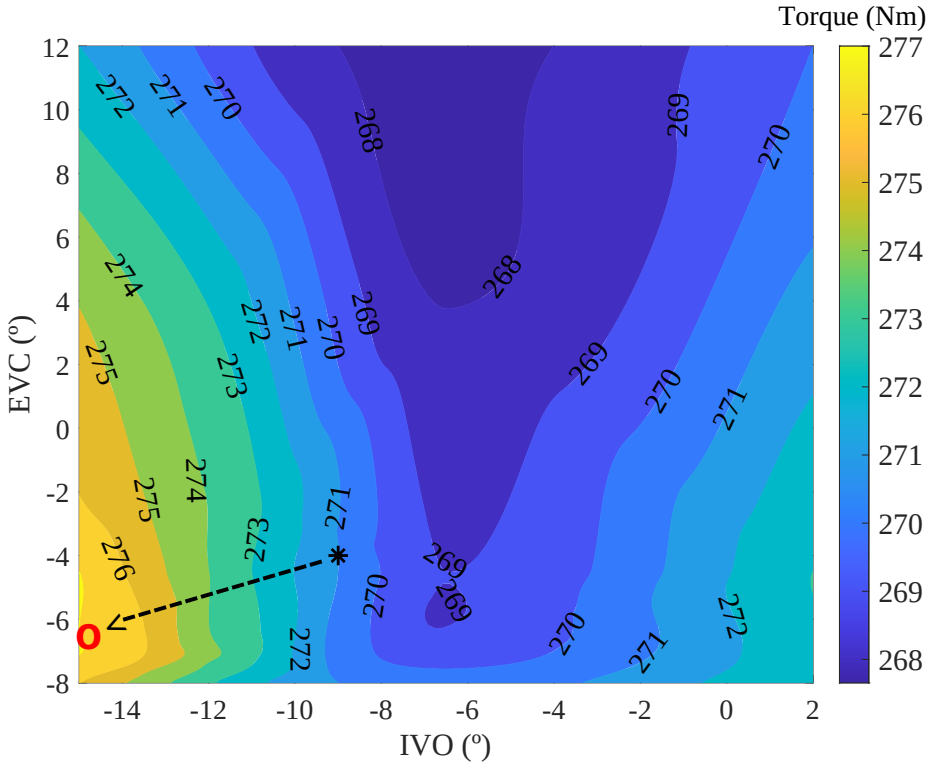

Figure 4.26: 4000 rpm VVT model torque optimization results. Asterisk corresponds to ECU calibration

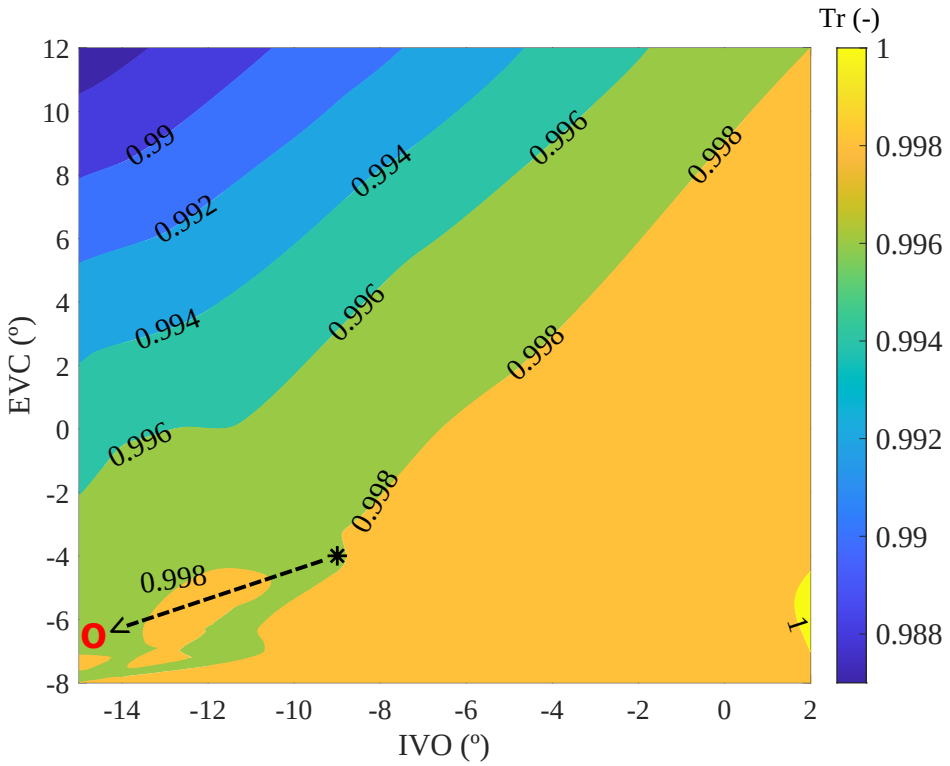

Figure 4.27: 4000 rpm VVT model torque optimization, trapping ratio results. Asterisk corresponds to ECU calibration

Finally, in order to appreciate the VVT optimization potential in full load operative area, Figure 4.28 shows two series of data:

- VGT-2 not-optimized VVT, corresponding to the ECU calibration of the VVT (VGT-2-ECU).
- VGT-2 optimized VVT (VGT-2-OPT). The selected VVT combination in this series of data corresponds to the one that, providing with the maximum torque output, accomplishes with all the aforementioned limits, including the TR.

As previously stated, in the results included in Figure 4.28, the same compressor and same boundaries, are imposed, as well as the same fitted engine

1-D model. The unique difference lies in the VVT combination.

In comparison to VGT-2-ECU from Figure 4.28(A), air mass flow differences are only detectable in the range of 2500-3500rpm, while for the rest of the engine range, differences are not noticeable at all. However, in terms of torque, VGT-2-OPT output increase is much more noticeable, in the range of 1500-4000, while some slight improvement is achieved in the high-end torque, see Figure 4.28(B).

It is only in the 1250 rpms working point, where there is no benefit in terms of torque, however, the VVT optimization has been able to improve the engine TR, to the desired 97%. These working conditions were not being guaranteed with the ECU calibration, where the TR was about 94.1%, see Figure 4.28(C).

For the engine range between 2000-4000 rpm, the trapping ratio has decreased when is compared against the original ECU calibration, since some more valve-overlap is found to be a better solution. T3 has diminished as a consequence of both: the slight higher short-circuited fresh mixture, as well as the retard in terms of EVC, as for 2000rpm was previously discussed and depicted in Figure 4.23. In this line, the lower T3, leads to a slightly higher p3, to achieve the desired boost pressure, see Figure 4.28(D) and Figure 4.28(E) respectively. However, this is not an issue, since p3 is not a limitation in this range.

Particularly, for the 3000-4000rpm area, after the optimization, the mixture enrichment is less. The previous is attributed to the lower TR, and the retard in terms of EVC, both contribute to the task of diminishing T3, hence, the engine works under leaner conditions, see Figure 4.28(F).

Specifically in 4500-5000rpm, a slightly higher p2' is achieved in the optimized series, see Figure 4.28(G), as a consequence of the EVC advance and its influence in the instantaneous turbine inlet manifold boundaries. To further evidence the previous, p3 oscillation and exhaust mass flow are included in Figure 4.29(A) and Figure 4.29(B) respectively for the 5000 rpm point. In all, the variation in the EVC, and its implications on the turbine map operative area, lead to higher efficiency as in Figure 4.28(H) is observed in averaged terms, and in Figure 4.29(C) specifically for 5000rpm instantaneous evolution.

Finally, the resulting impact on the engine output, as a consequence of the VVT optimization, leads to a more powerful and efficient engine, see Fig-

ure 4.28(I), where the BSFC results only in improvements for the VGT. In all, the VGTS' BSFC reduction, in comparison to the WG, fluctuates in the range of 1-20g/kWh depending on the working point.

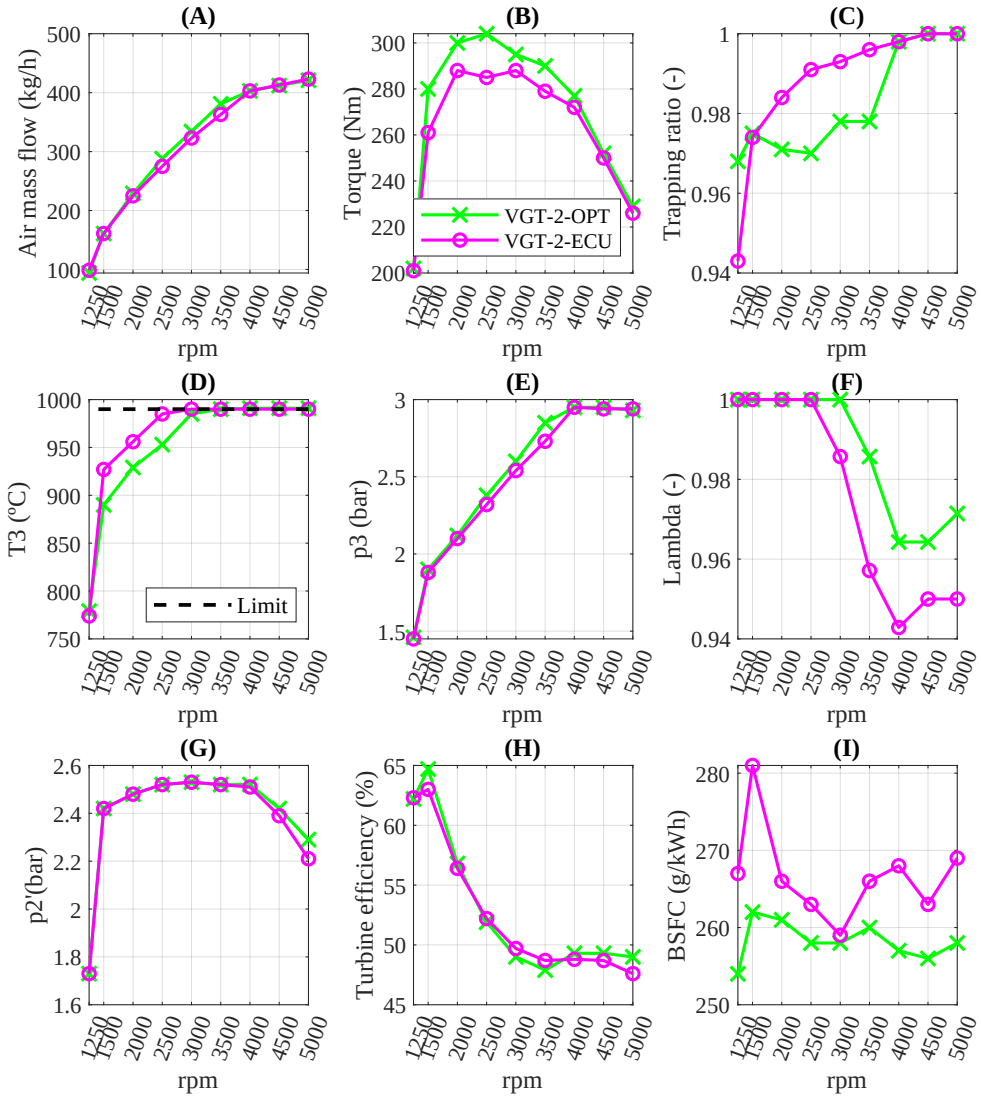

Figure 4.28: Full loads at sea level including VGT-2 with ECU calibration of the VVT as well as VGT-2 optimized according to maximum engine power criteria

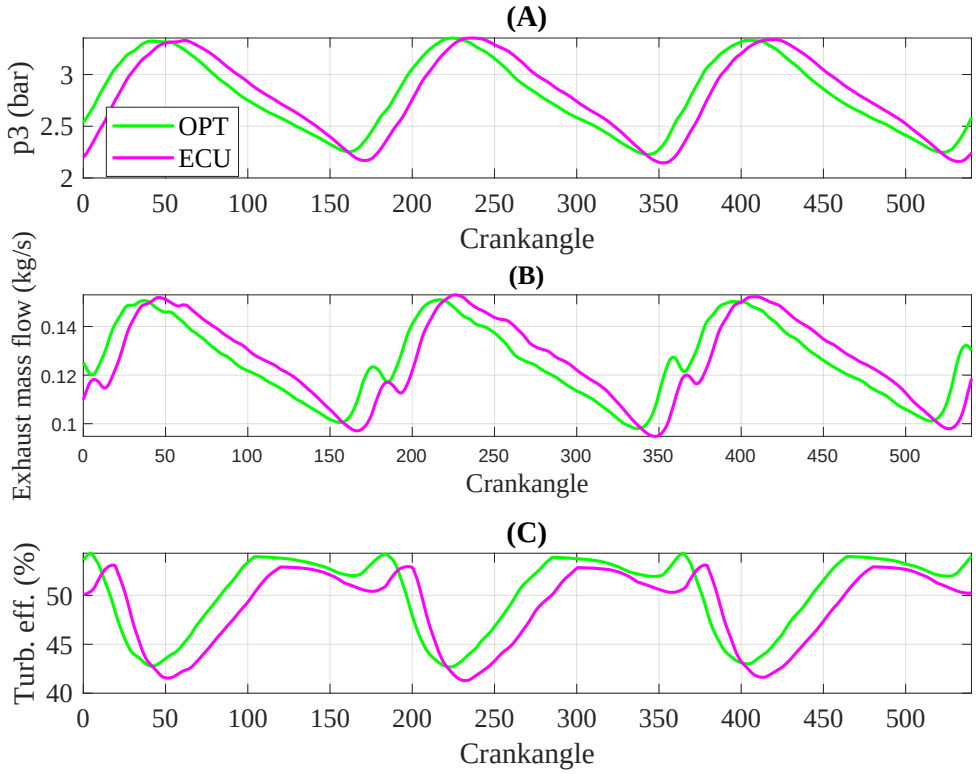

Figure 4.29: 5000rpm engine speed. (A) corresponds to p3 oscillation through the complete engine cycle of 720º

A summary of the VVT optimization in terms of EVC and IVO is included in Table 4.6. Where negative values imply further advance in crank angle degrees, taking as a basis the ECU calibration. As an example, 5000rpm found solution implies advancing the EVC by 9 crank angle degrees, as well as the IVO by 11 crank angle degrees.

Table 4.6: VVT variation in crankangle degrees with respect to ECU calibration. EVC and IVO included

rpm	**5000**	**4500**	**4000**	**3500**	**3000**	**2500**	**2000**	**1500**	**1250**
EVC CAD delay	-9º	-2º	-2.7º	12º	8.5º	8.5º	3.8º	-6.8º	-4.8º
IVO CAD delay	-11º	-6º	-6º	-5.5º	-1.5º	-1.2º	-0.8º	-6º	-0.4º

4.4.2 Full load results: VVT optimization and lambda=1

In this section, lambda control pursues the stoichiometric conditions in the complete full load engine curve, even if the T3 limitation is overcome. It is then, VGT position, the actuator that is regulated to assure the T3 limitation, in addition to turbocharger speed, turbine inlet pressure, compressor outlet pressure and temperature. In other words, boost pressure is limited by the PID governing the VGT, which is assuring the T3 limit not to be overcome. The target in these simulations is to explore the potential of working under stoichiometric working conditions in the complete operative area and quantify the expected engine performance.

As well as for the cases shown in the optimized series shown in Figure 4.28, here, the VVT is again optimized accordingly, with the target of maximizing the engine output while keeping any variable under the thermo-mechanic limit.

Results are included in Figure 4.30 and only includes the range of 3500-5000. The series in this study correspond to VGT-2 and are labelled as VGT-2-ECU and VGT-OPT-STOICH, as for: not optimized VVT and optimized VVT under stoichiometric mixture control respectively. From 1250 to 3000, in the first optimization stage in subsection 4.4.1, the model already predicted stoichiometric operation as the most optimum one, so the analysis in the aforementioned speed range was already discussed.

As the main conclusion, from Figure 4.30(A), one can see the evident decrease of air mass flow from 4000 up to 5000rpm, which is the main reason for the torque decrease going from 22Nm (at 4000rpm) to 11Nm (at 5000rpm), see Figure 4.30(B).

The main reason for the previous results is the lack of boost pressure since T3 becomes a limitation for the boost pressure: the imposed stoichiometric mixture leads to higher temperatures, hence, the limitation of 990ºC limit is guaranteed through some VGT extra opening, to lower the boost pressure, as in Figure 4.30(C) it is shown. However, it shall be recalled that 3000rpm working engine torque is slightly improved, while T3 was effectively kept around 990ºC for the complete studied range.

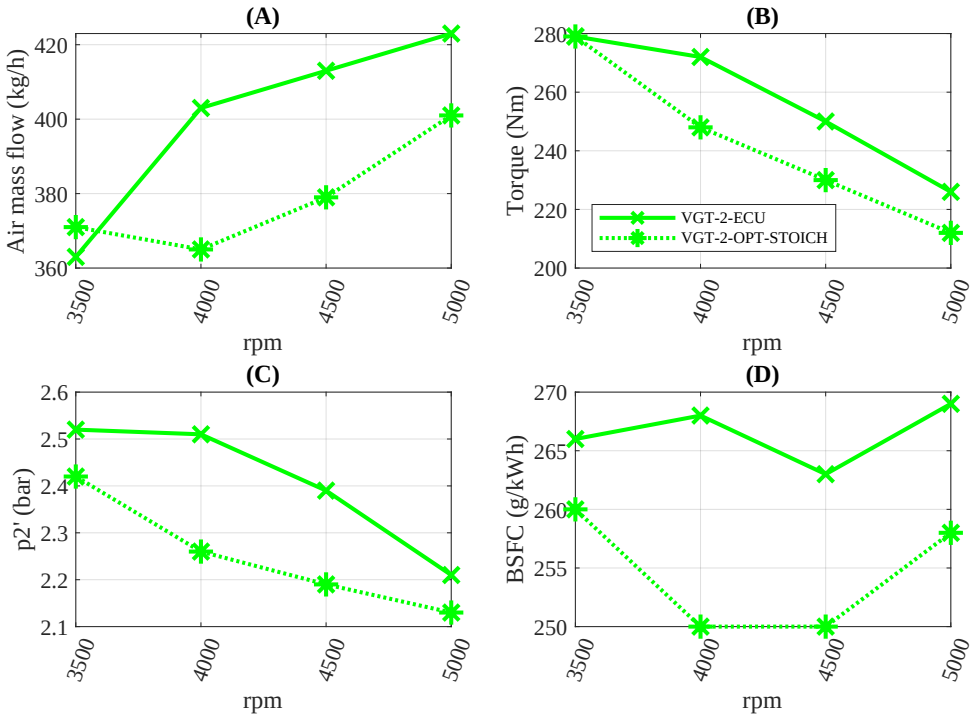

Figure 4.30: Full loads at sea level including: VGT-2 with VVT management governed by ECU calibration and VGT-2 optimized according to maximum engine power criteria under stoichiometric mixture

The interest of this control strategy lies in the fact that the EGR technique could be omitted. EGR main motivation lies in the T3 control [97]. Furthermore, other advantages have been found such as the overall BSFC improvement through the pumping losses reduction as well as spark centring [98]. Other studies analysed the capabilities of cooled EGR in reducing the soot emission [99] and increasing volumetric efficiency [100].

However, the EGR technique implies an extra freedom degree parameter, which adds more complexity in terms of engine control and hardware, as well as some penalty in terms of transient response. By switching from WG to VGT and optimizing the VVT, keeping in mind the T3 limitation, the stoichiometric mixture can also be kept, without the usage of EGR. The previous may lead to a more compact, simpler, cheaper and more responsive engine layout. Limiting the T3 by just opening the VGT (hence, limiting boost) is possible as in this

study is shown.

Figure 4.31 shows the complete engine full load curve (from 1250 to 5000rpm) for both series of data: VGT-2-OPT-SHOICH and the WG-ECU. The first one was already described, the second one corresponds to the WG turbocharger, in combination with the standard ECU calibration for the VVT control, and fuel enrichment strategy for the T3 limitation (WG-ECU). Figure 4.31(A) deals with torque and as it can be appreciated, VGT-2-OPT-SHOICH shows a great benefit in terms of torque especially from 1500-3500rpm.

Above 4000rpm, the torque advantage is reduced but still present in favour of the VGT. The explanation for the previous torque benefit limitation it is directly attached to the lower boost pressure, see Figure 4.31(B) in the VGT-2-OPT-SHOICH, as a consequence of the T3 control strategy: While in the WG-ECU, it is Lambda, the variable in charge of this duty, in the VGT-2-OPT-SHOICH it is boost pressure. TC speed differences Figure 4.31(C) are not relevant and far from the limit of 250krpm.

Even though, the lower value of p3 in the VGT series, see Figure 4.31(D), contributes to the slight torque benefit in favour of the VGT technology in the high-end range.

T3 is a constraint within the TC supplier limits, and it is evidenced, that by opening the VGT close to its maximum rack position, it is possible to successfully control T3, see Figure 4.31(E) and Figure 4.31(F). Particularly at 5000, VGT is completely open while T3 is about 992^{o}C, it is then of high relevance, the proper selection of the VGT maximum opening option.

In terms of trapping ratio, differences can be appreciated in Figure 4.31(G). As a general conclusion, VGT-2-OPT-SHOICH series is a constraint within the 0.97-1, while in the case of the WG, at 1250, the estimated TR is about 0.95. From 1500-3500, the expected values for the VGT-2-OPT-SHOICH is slightly lower than in the WG-ECU, motivated by the more favourable p2'-to-p3 ratio.

Finally, in terms of lambda, differences are only found at 3500 and 4000 engine rpm, see Figure 4.31(H). The previous difference in lambda prediction, coupled to the more favourable p2'-to-p3 ratio (the last, leading to higher torque) explains BSFC differences identified in Figure 4.31(I).

Concluding, not only torque figures are systematically better for the VGT-2-OPT-SHOICH, but the model also claims more favourable BSFC figures, as

well as a leaner operation, since there is no excess of injected fuel. Furthermore, it is possible to control T3 by just means of the VGT opening control strategy.

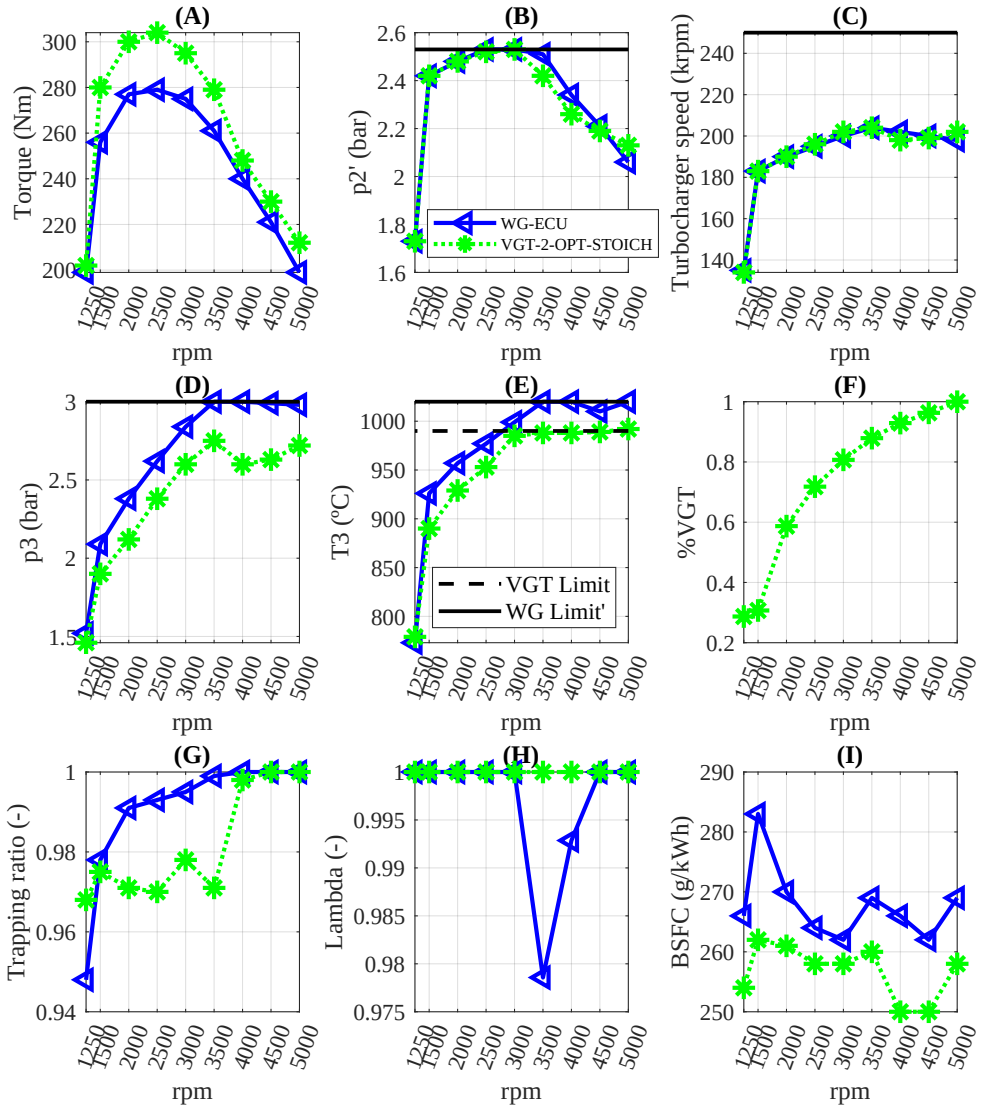

Figure 4.31: Full loads at sea level including: WG with VVT management governed by ECU calibration and VGT-2 with VVT optimized according to maximum engine power criteria under imposed stoichiometric mixture

4.4.3 Partial loads (12bar) BMEP VVT optimization

Here, again the VVT was optimized but in order to optimize the BSFC. Here, in the 12bar BMEP, the speed range from 2000-4000 was evaluated and corresponds to the operative area where the VGT mechanism is completely open, while the throttle controls the boost pressure. T3, as well as the rest of engine thermo-mechanic limitations, are far from being reached, so there is no restriction to be taken into account.

In summary, it was found that for the operative range, where there is some throttle actuation, there is no margin for BSFC improvement. Equation 4.4 is used for the BSFC difference calculation in relative terms, after the optimization procedure. Sub-index "i" in Equation 4.4 corresponds to each evaluated engine speed. Results are included in Table 4.7, and differences do not reach the 0.2% improvement if one takes as comparison basis the ECU calibration for the WG turbocharger.

$$Difference = \frac{BSFC_i^{VGT-2-OPT} - BSFC_i^{VGT-2-ECU}}{BSFC_i^{VGT-2-ECU}} * 100 \tag{4.4}$$

Table 4.7: BSFC improvement after VVT optimization for the 12 BMEP working points

rpm	**4000**	**3000**	**2500**	**2000**
BSFC difference (%)	-0.195	-0.130	-0.079	-0.157

4.5 Transient response

In this section of the document, the already deeply discussed 1D model is used to develop a methodology to manage the VGT position under heavy transient conditions. Particularly in this section, the methodology has only been followed and applied for the VGT-2 TC unit, as well as the AE maps were the ones selected.

Dealing with the VGT control, from the experimental campaign, a try-and-error methodology was performed, in which several of the control parameters

were varied in discrete steps, pursuing the best engine torque evolution. As a result, a "close-to-optimum" VGT control for boost-pressure built (hence, torque) is obtained.

In the evaluated transient tests, which consist of sudden load demands, under constant speed: the target is to achieve the maximum engine torque output in the minimum possible time. For this target, a control system is specifically developed, taking advantage of the developed model. The key point here lies in the fact that from the engine 1-D model, one can collect as much information as required for the VGT management predictive control.

In section subsection 3.4.2, the procedure to model the VGT position consisted in correlating the experimental VGT signal to the turbine maps, so that the turbine VGT position maps, matched the actual mechanism position definition. Thus, one could take the experimental VGT position as a reference during the complete engine transient. With this, it was shown that it is possible to reproduce the boost pressure evolution. However, in this section, the target is to predict the desired (optimum) VGT evolution on each time step, targeting the fastest possible engine response (while keeping any variable within the accepted limits for components protection).

Regarding the VVT management, it was selected the ECU standard calibration for the transient tests evolution, since complete VVT optimized maps were not generated. Lambda control was, in any case, guaranteeing the stoichiometric mixture, since for the evaluated transients, T3 limitation was never reached. Furthermore, the combustion prediction task was carried out utilizing the CNN for CA50, CA90 and TOC prediction along with the complete simulation.

Consequently, the only variable that requires further control, is the VGT mechanism, which, as it was shown in Figure 3.6, represents one of the main transient response governing variables. The control architecture to "decide" at each time-step, the selected VGT position, follows the next structure and order:

- First of all, it is required to estimate the final state desired turbocharger speed. In the example analysed in this work, this can be directly extracted from the full loads modelling or experimental campaign: For example, at 3000rpms, it is known that the turbocharger speed is about 187krpms, and for 1500 engine rpm, the TC speed is about 152krpm.

- Secondly, two turbocharger rotational accelerations are calculated simultaneously:
  - The TC "acceleration requirement" to cover the difference between the final desired speed (187krpm for example) and the modelled speed at each analysed instant of the simulation, in a time-lapse of one complete engine cycle. In other words, with the "acceleration requirement", it is pretended to evaluate at each engine complete cycle, which is the TC required acceleration, so that the final desired TC speed is achieved by the next cycle. Equation 4.5 shows how the "acceleration requirement" "$\dot{n}_{i-required}$" is calculated at each engine cycle (i), as the difference between the final targetted speed "n_{final}" and the modelled speed every engine turn "n_i", divided by the time taken by the engine to cover a complete engine turn "t_{720}".

$$\dot{n}_{i-required} = \frac{n_{final} - n_i}{t_{720}} \tag{4.5}$$

  - The other calculated acceleration is the maximum possible turbocharger rotational acceleration. This acceleration corresponds to the maximum one that could be achieved, without reaching any of the engine-TC limits. The way to proceed with this acceleration, it is to consider the maximum allowed or achievable p3 according to the effective turbine area and the flow going through the turbine at the analysed time step.
    Afterwards, assuming the estimated maximum p3 and collecting from the model, the turbine inlet temperature, as well the gasses mass flow one can calculate the reduced mass flow Equation 4.6. The combination of the reduced air mass flow, TC reduced speed and pressure ratio (for which p4 is required, and known from the model), gives back the VGT that matches the calculated conditions. The turbine efficiency can also be known (directly taken from the turbine map), and by means of Equation 4.7 it is calculated the maximum power achievable by the turbine at the calculated given time.

$$\dot{m}_{turb}^{reduced} = \frac{\dot{m}\sqrt{T_3}}{p_3} \tag{4.6}$$

$$\dot{W}_{turbine} = \dot{m}_{turb} T_3 c_p \eta_{turbine} [1 - (\frac{p4}{p3})^{(\gamma-1)/\gamma}] \tag{4.7}$$

In other words, the turbine map is used as an inverse look-up table to identify a given VGT position. An example of the previous can be found in the diagram shown in Figure 4.32, where after having estimated the maximum achievable p3, and the corresponding reduced mass flow and speed, it is possible to identify the VGT position. In "standard" simulations, the VGT represents the input instead of the output.

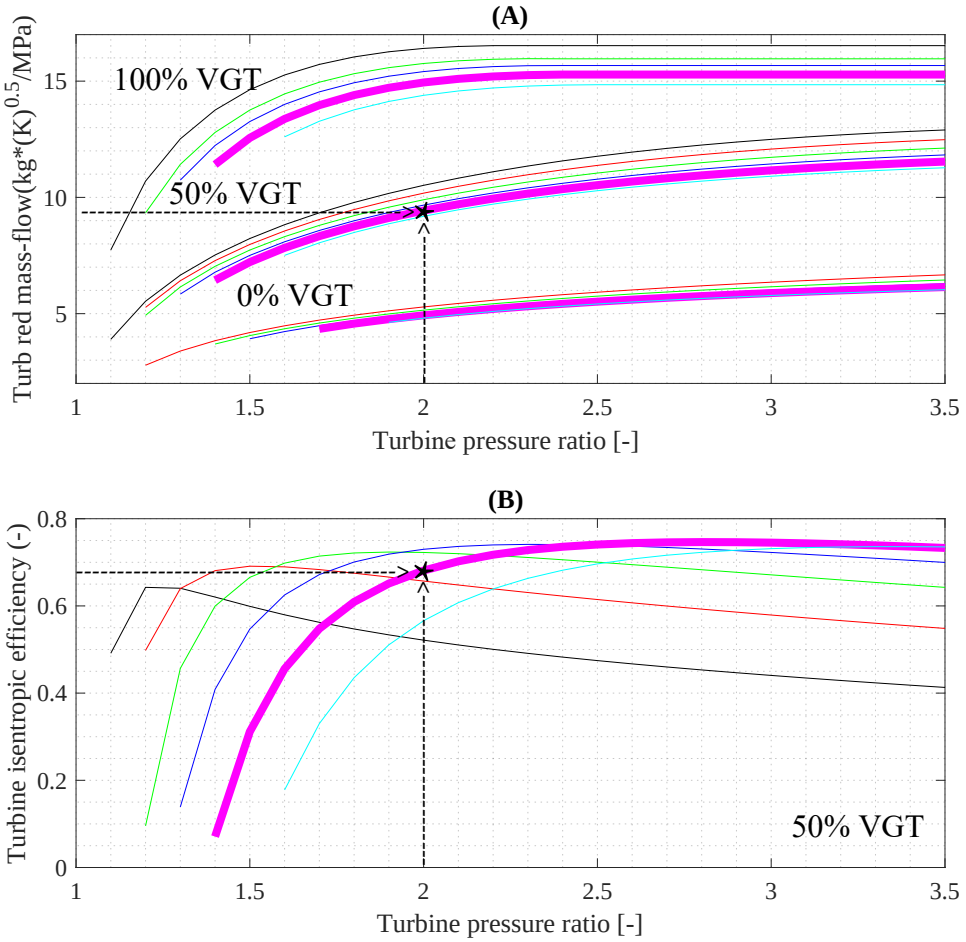

Figure 4.32: (A) Diagram for VGT position obtention and (B) once the VGT required is obtained, from the maps, it is possible to obtain the turbine isentropic efficiency

Finally, from the model, it is also known the compressor power consumption, the friction losses, as well as the TC shaft speed. The last, in combination with the actual TC moment of inertia, allows predicting, through the power balance in the TC shaft, the maximum possible acceleration as in Equation 4.8 it is shown. Notice that all the implied power sources are included in the energy balance.

$$\dot{w}_{i-max} = \frac{\dot{W}_{TURB} - \dot{W}_{COMP} - \dot{W}_{FRICTION}}{I_{TC} * n} \tag{4.8}$$

- Thirdly, the lowest of both previously calculated accelerations is chosen: if the "acceleration requirement" is lower than the maximum possible one, then, the first acceleration is chosen, otherwise, the maximum possible acceleration is chosen. This criterion ensures that if the targeted speed is unachievable for the subsequent engine cycle, then the chosen acceleration (hence, expected speed by next cycle) is the "maximum possible acceleration". On the opposite scenario, if the acceleration required to achieve the desired final speed is lower than the maximum possible acceleration, then the chosen acceleration is the "required". Figure 4.33(A) shows both previously described accelerations (maximum possible and required for instant response). Observe how in Figure 4.33(A), at the very first stages, the desired acceleration is higher than the maximum. Nevertheless, as the transient evolves, there is a moment when the required acceleration is lower than the maximum achievable (around second 2.85).

- In fourth place, whatever the selected acceleration, it is added to the TC speed at the analysed time-step and provides with the "predicted trajectory in Figure 4.33(B), for the example of 3000rpm sudden tip-in. This sequence is repeated during the modelling itself. Figure 4.33(B) also shows the desired TC speed (the one desirable if an instantaneous response could be achieved).

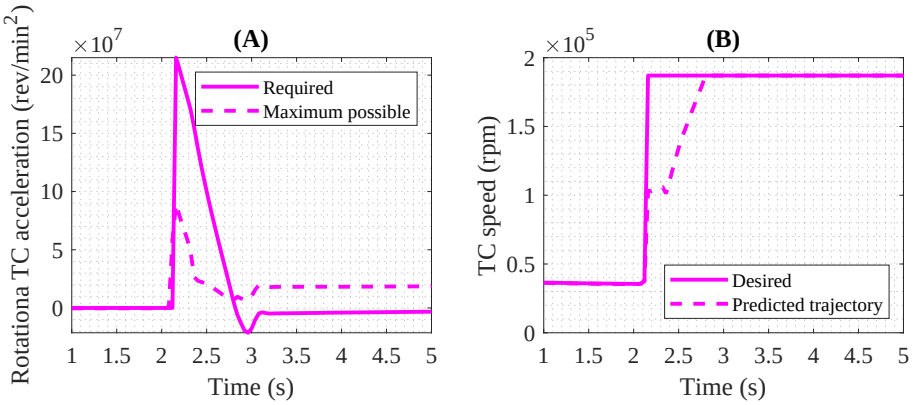

Figure 4.33: (A) Shows the maximum possible acceleration and the acceleration required. (B) Shows the TC speed predicted (fastest possible trajectory) and the desired (instantaneous) evolution

- Fifth, if the chosen acceleration is the maximum one, the corresponding prediction of the VGT position signal is sent to the turbine element, hence, providing the maximum acceleration possible.

  If by chance, the desired acceleration is the "required" one, it is proceeding to identify first, the required power demand, and afterwards, the pressure ratio that would satisfy this power demand to the turbine side.

  To obtain the required turbine power, Equation 4.8 is re-arranged to calculate the term "$\dot{W}_{TURB}$" since all the rest can be extracted from the simulation directly at the analysed instant. Hence, re-arranging Equation 4.7, one can obtain the required pressure ratio that fits the turbine power.

  With all the previous calculated information, one can also estimate the turbine reduced mas flow, (which, in combination with the pressure ratio) can provide the suitable VGT position that satisfies the power demand for the desired acceleration. The idea here is following the same procedure as for the "maximum possible acceleration" was followed in Figure 4.32. The efficiency term for the desired VGT is also taken from the turbine AE maps.

- Afterwards, the speed trajectory generated as the "predicted trajectory", which presumably is the fastest possible, is compared against the speed

trajectory resulting by the complete 1D modelling: in short, after managing the predicted VGT evolution along with the complete transient simulation. The differences taking place are damped by a PID, which applies a limited correction over the predicted VGT profile.

This correction (closed loop stage of the control) is required to compensate for several assumptions or simplifications done during the open loop VGT prediction. An example of the previous is the consideration of constant T3 during each complete engine cycle. Another aspect for the closed loop requirement is the highly pulsating behaviour of the exhaust manifold mass flow, and its impact on the turbine efficiency fluctuation during the engine complete cycle (while in the VGT management model, a constant efficiency is taken from the map for each engine turn).

- Finally it is of high relevance to identify the maximum gradient at which the VGT mechanism opening can be actuated. As an example, in Figure 4.34, two different predicted VGT trajectories are shown for the 3000rpm tip-in: the series labelled as "Non-limited" calls for the results in which the VGT control is as fast as the model refreshment of the predicted VGT position (once per complete engine turn, corresponding to 0.04s for the analysed engine speed). Furthermore, the opening or closing rate has no limitation. This may lead to unrealistic results since the VGT mechanism is managed faster than it is possible to be pretended actually. From the experimental campaign, it is obtained the maximum opening or closing rate and imposed on the simulation accordingly, giving as a result, the "Limited" series. For reference, the black series corresponds to the experimental tip-in VGT signal. As it is evidenced, during the sudden tip-in demand and corresponding VGT closing (between second 2.2 and second 2.4), both: the "limited" and the experimental series, show a very similar trend.

Figure 4.35 clarifies the VGT control strategy, in order to clarify the followed procedure. Both, the open and closed loop are included, as well as the filtering of the VGT predicted position.

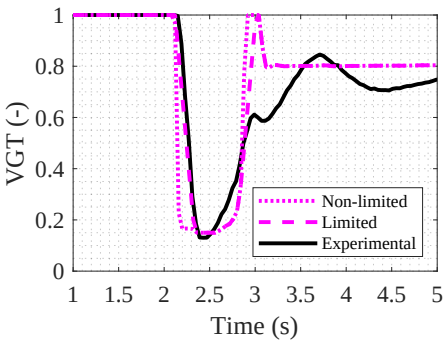

Figure 4.34: 3000rpm tip-in VGT position: experimental and two modelled series: with and without maximum VGT rate limitation

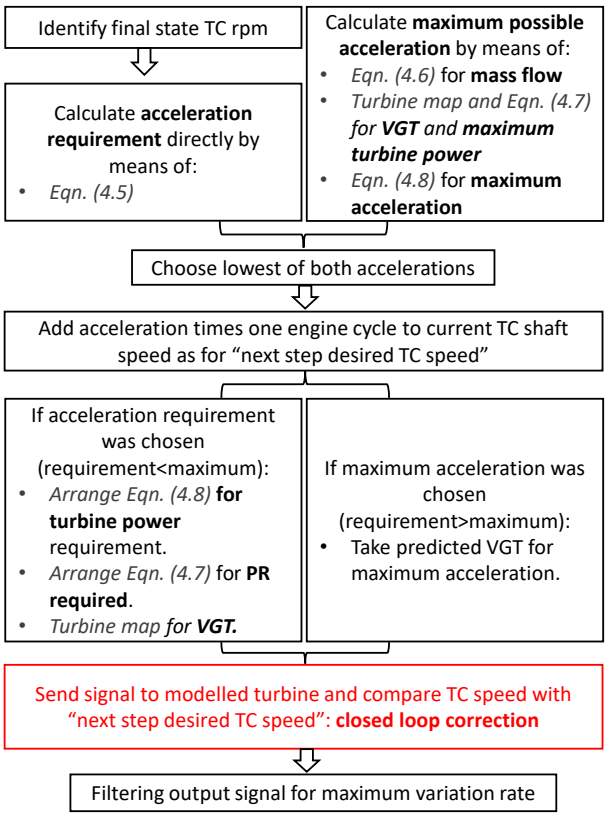

Figure 4.35: VGT control strategy diagram repeated each time step. Open loop corresponds to black boxes and closed loop to the red box

As an example to lighten the procedure performance, the obtained transient evolution for 3000 rpm is compared against the experimental most-optimum engine response. In Figure 4.36 is included the air mass flow, torque, TC speed, boost pressure and exhaust manifold pressure as well as turbocharger speed and VGT position.

Looking at the results, it is found a relevant improvement in terms of transient response: The air mass flow evolution in the model follows a faster evolution than the one followed in the experimental campaign. As a result, the model reduces the time to achieve the final desired torque around (0.25s of benefit in the context of a transient that takes around 1.2s). The last is attributed to the boost pressure faster evolution, especially from second 2.5 in advance. The benefit in terms of boost pressure (and TC speed) is directly attributed to the higher turbine inlet pressure, which simultaneously results from the VGT management differences. As it can be induced, from second 2.5, the predictive VGT control model keeps the turbine in a closer position than the experiment, looking for the maximum acceleration criteria. After second 2.85, more VGT opening is required to compensate for this effect and avoid an over-oscillation in the engine response. Turbine inlet pressure surpasses the limit of 3bar (by 0.15bar) during 0.1 seconds. If this situation was attempted to be avoided, the control could be more restrictive to compensate for this aspect.

The key point here lies in the fact that the proposed methodology for the VGT control has been able to provide a faster response and afterwards, has achieved a stable torque output.

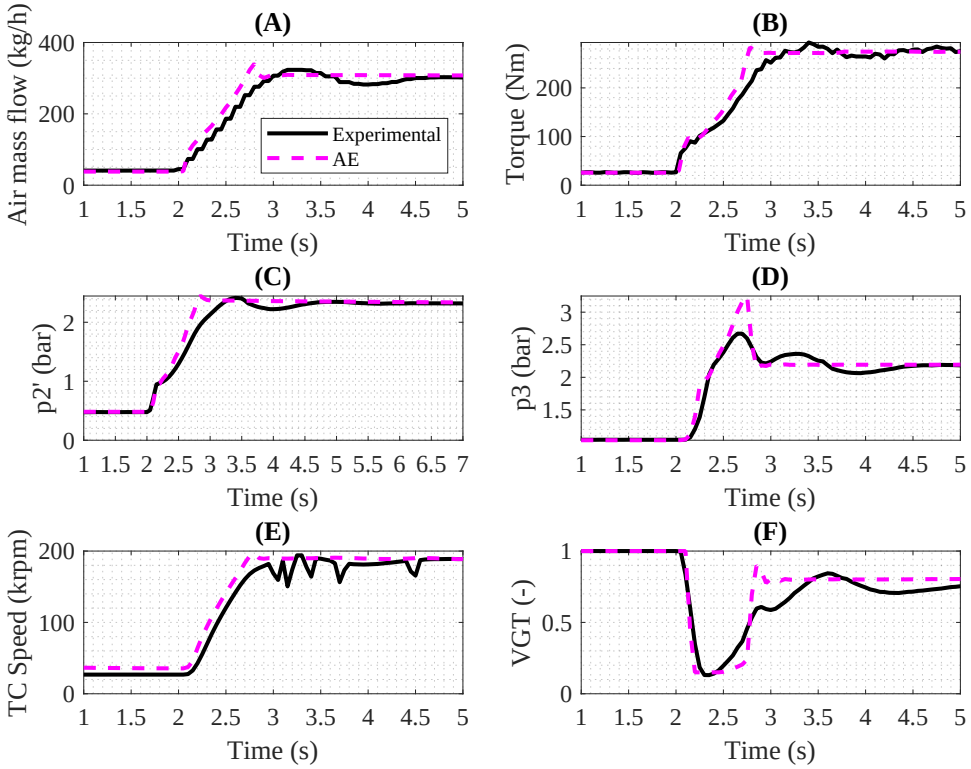

Figure 4.36: 3000rpm transient tip-in. Two series as included: experimental data and predicted transient after VGT prediction procedure

Finally, it is shown the following example for the 1500rpm engine sudden tip-in in Figure 4.37. Here it is also shown the best tip-in that was obtained after the complete experimental campaign, in which several trials were performed. As well Figure 4.37 includes the model predicted performance during the same tip-in. Here, it is evidenced that both series provide very similar values in terms of air mass flow, torque and boost pressure evolution. The last happens since the VGT has no margin for further closure during the major part of the transient, thus, leading to very similar performance.

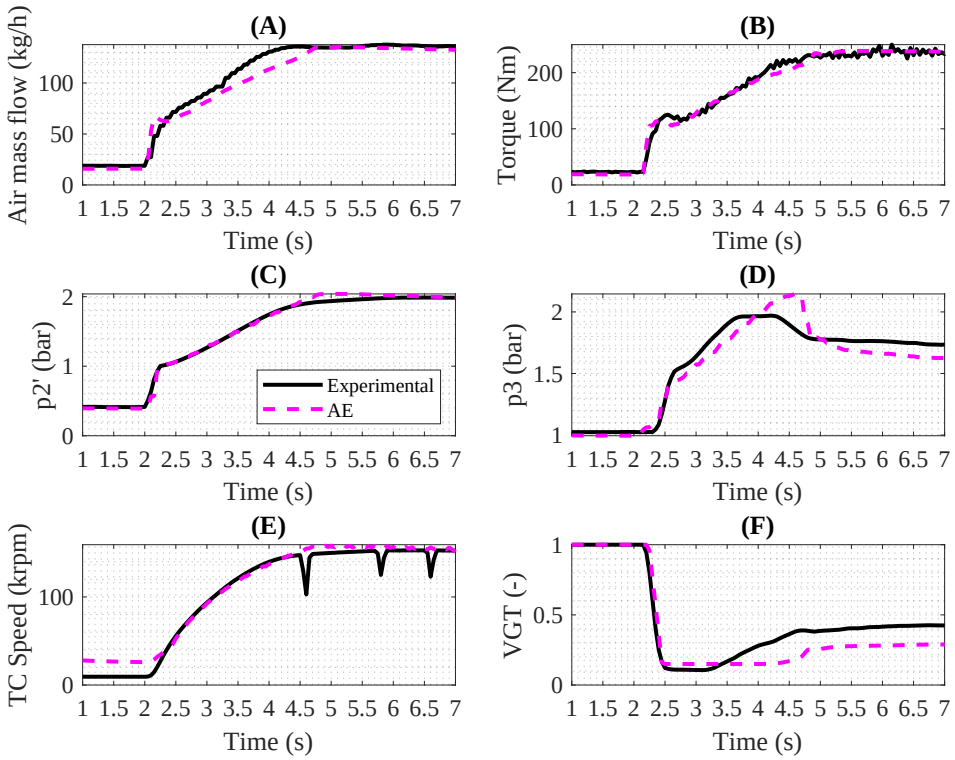

Figure 4.37: 1500rpm transient tip-in. Two series as included: experimental data and predicted transient after VGT prediction procedure

One of the main limitations at the 1500rpm full load operative point is the presence of compressor surge. Since surge is not predicted in the 1-D model it is required to check its absence during the complete simulation. Figure 4.38 shows the iso-efficiency contours in the compressor map (pressure ratio-reduced mass flow rate map). The black dotted series corresponds to the area through which the compressor is operated along with the 1500rpm transient. The operation evolution goes from very low compressor speed to almost 160krpm. It can be confirmed that even if the surge limit was close to being reached, it was successfully avoided.

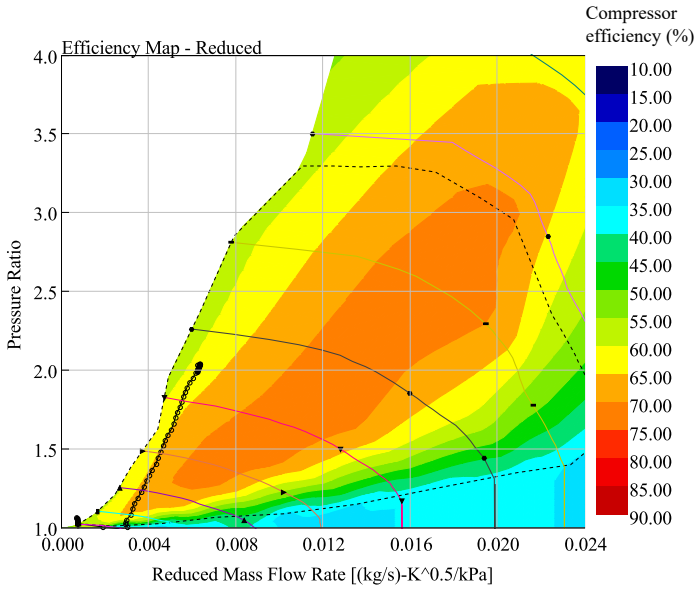

Figure 4.38: Compressor iso-efficiency contours in pressure ratio-Reduced mass flow map. 1500rpm transient tip-in operative area for surge check

In conclusion, it has been found a technique that provides the same or better engine transient response than the one that was achieved after an extensive experimental campaign. Thus, it has been developed a flexible tool that may be used to explore new controlling methodologies to improve the transient response. Furthermore, this tool can be taken advantage of, in order to proceed with further comparison and benchmarking of different TC technologies or units.

Chapter 4 Bibliography

[87] J. Andersen, E. Karlsson, and A. Gawell. "Variable turbine geometry on SI engines". In: *SAE Technical Papers*. Vol. 2006. 724. 2006, pp. 776–790. DOI: 10.4271/2006-01-0020 (cit. on pp. 33, 158).

[91] G. Ericsson, H. E. Angstrom, and F. Westin. "Optimizing the transient of an SI-engine equipped with variable cam timing and variable turbine". In: *SAE Technical Papers*. Vol. 3. 1. 2010, pp. 903–915. DOI: 10.4271/2010-01-1233 (cit. on pp. 33, 63, 163, 165).

[95] H. Tang, A. Pennycott, S. Akehurst, and C. J. Brace. "A review of the application of variable geometry turbines to the downsized gasoline engine". *International Journal of Engine Research* 16.(6) (2015), pp. 810–825. ISSN: 20413149. DOI: 10.1177/1468087414552289 (cit. on p. 150).

[96] P. Kapoor, A. W. Costall, N. Sakellaridis, J. Hooijer, R. Lammers, H. Tartoussi, and S. Guilain. "Adaptive Turbo Matching: Radial Turbine Design Optimization through 1D Engine Simulations with Meanline Model in-the-Loop". *SAE Technical Papers* 2018-April (2018), pp. 1–15. ISSN: 01487191. DOI: 10.4271/2018-01-0974 (cit. on p. 162).

[97] J. M. Luján, H. Climent, R. Novella, and M. E. Rivas-Perea. "Influence of a low pressure EGR loop on a gasoline turbocharged direct injection engine". *Applied Thermal Engineering* 89 (2015), pp. 432–443. ISSN: 13594311. DOI: 10.1016/j.applthermaleng.2015.06.039 (cit. on p. 176).

[98] T. Alger, T. Chauvet, and Z. Dimitrova. "Synergies between high EGR operation and GDI systems". *SAE International Journal of Engines* 1.(1) (2009), pp. 101–114. ISSN: 19463936. DOI: 10.4271/2008-01-0134 (cit. on p. 176).

[99] T. Li, T. Yin, and B. Wang. "Anatomy of the cooled EGR effects on soot emission reduction in boosted spark-ignited direct-injection engines". *Applied Energy* 190 (2017), pp. 43–56. ISSN: 03062619. DOI: 10.1016/j.apenergy.2016.12.105. URL: http://dx.doi.org/10.1016/j.apenergy.2016.12.105 (cit. on p. 176).

[100] H. Wei, T. Zhu, G. Shu, L. Tan, and Y. Wang. "Gasoline engine exhaust gas recirculation - A review". *Applied Energy* 99 (2012), pp. 534–544. ISSN: 03062619. DOI: 10.1016/j.apenergy.2012.05.011. URL: http://dx.doi.org/10.1016/j.apenergy.2012.05.011 (cit. on p. 176).

Chapter 5

Concluding remarks

Contents

5.1 Introduction

Following the trend of downsizing, the implementation of VGT in SI-ICE becomes more interesting to engine developers. Furthermore, variable geometry turbine technology implementation in gasoline engines is possible, among other reasons, thanks to the advances in materials technology and active turbine cooling. Hence, developing a methodology for complete engine-turbochargers 1-D modelling may result in high interest, with the purpose of well-understanding the implications of the VGT implementation in SI engines.

One of the most controversial issues when modelling turbocharged engines, is the turbocharger unit itself, since merely experimental information it is not representative of the turbochargers integral performance, as it has been widely studied in the literature and clarified in this work.

The previous, justify the proposal of a methodology, specifically developed in order to cope with the aforementioned issues and overcoming the so-called TC maps. Accordingly, making usage of the proposed holistic methodology, it is evidenced the high-quality results that allow for deeper studies, comparisons and prospective modelling of the complete ICE-TC system.

The main conclusions of the thesis are gathered into four different sections:

- Engine modelling.
- Turbocharger maps procedure.
- Complete SI-ICE model validation.
- Model usage for prospective analysis.

Finally, some proposals for future works are made, in order to solve the most relevant identified issues, as well as for optimizing some of the developed procedures/methodologies.

5.2 Engine modelling

A methodology is proposed to obtain well-calibrated 1-D engine codes. For this purpose, first of all, a complete experimental campaign is performed for

a SI 1.3 litres ICE. Three TC units were tested in the SI ICE at several working conditions, such as steady-state full and partial loads as well as tip-ins consisting of a sudden (constant speed load-demand).

Having collected all the experimental data, an engine model was developed and fitted (or calibrated) in GT-Power software. During the calibration procedure, several coefficients were adjusted in order to well-predict the different engine phenomena. Also, TC itself was decoupled (the turbine side from the compressor side) during the fitting simulations to avoid any TC maps uncertainty: this way, intake and exhaust manifold pressures are semi-independently governed by different actuators in the model (turbocharger speed and VGT position respectively). It is remarkable that this methodology decouples the energy balance between turbine and compressor, hence, energy unbalance is allowed to take place at this stage since the interest at this point lies in the reciprocating engine model calibration.

A neural network for combustion prediction is trained during this procedure, since all the experimental variables are assured during the fitting, the instantaneous cylinder pressure evolution is reproduced by modifying the combustion parameters accordingly. Then, it is possible to correlate combustion parameters with some modelled variables (deeply related to combustion timing), in such a way that combustion could be predicted in forwarding simulations.

Aspects such as proper injection timing modelling and its impact on other engine variables are evaluated, particularly in the instantaneous cylinder pressure evolution. Finally, since any engine variable is converged to the experimental campaign, the FMEP map is obtained.

Having reached this point, the complete engine (except the TC unit) is fitted. Tables dealing with the obtained fitted coefficients are included.

However, when the turbine and compressor sides are re-coupled to each other, unsatisfactory predictions are obtained, especially in the low-end torque, high-end torque as well as heavy load transients. This wrong modelling practice was attributed to the TC maps since it is the only not-fitted element. Hence, it is called into question the accuracy of modelling TC with hot maps, deeply discussed to be affected by heat transfer effects and heat losses.

The previous is the main motivation for the proposed methodology for validated TC maps procedure.

5.3 Turbocharger maps procedure

Heat transfer and mechanical losses have been proved to take an important role in automotive turbochargers. The effects of the aforementioned phenomena are considered to represent the discrepancies in the modelling activities previously carried out.

To solve the previous issue, properly calibrating heat transfer and mechanical losses properties becomes of high interest for proper engine simulations. A carefully designed gas stand experimental procedure and data processing methodology have been disclosed. Different sets of experimental information (adiabatic, hot insulated, and hot exposed) were necessary to perform a proper calibration of the HT-ML-TCM developed by the university research institute CMT-Motores Térmicos. The model calibration is constituted by three main steps, each one with special interest for one/several sub-models:

- Almost-adiabatic tests were necessary to provide the turbocharger model with enough data for the aerodynamic maps fitting and extrapolation and friction losses model calibration. If almost-adiabatic data is pretended to be directly used as the turbocharger maps, special care should be taken with the stabilization criteria. It would be preferable to wait until all the mean working fluids temperatures are totally stabilized. Furthermore, here, since thermal gradients are highly reduced, the heat transfer phenomena's importance is diminished. The previous allows focusing the model calibration effort on mechanical losses and the SAE standard maps (for turbine and compressor).

- Hot insulated cases allowed for the internal heat transfer model calibration. External insulation enables to (almost) avoid the external heat transfer losses, proof of this, it is the energy balance agreement in this test typologies, that allow neglecting external heat losses. The previous permits focusing the efforts on the internal heat transfer (internal conductances specifically).

- Hot exposed tests allowed for external heat transfer model calibration. At this point, since the previous sub-models are already validated, the only remaining uncertainty lies on the external heat losses model, which is then adjusted to the experimental campaign results.

Having obtained the purely adiabatic maps, the in-house TC holistic model (HT-ML-TCM) is also used for the maps extrapolation.

5.4 Complete SI-ICE model validation

Afterwards, the TC hot maps which were evidenced to provide with poor performance, are overridden by the developed adiabatic and extrapolated TC maps. At this stage, it a remarkable fact that the TC maps are the only aspect of the engine model which has been modified.

Full load simulations were performed and better results were systematically obtained with the usage of the new set of maps configuration. Low-end and high-end torque are successfully predicted (contrary to the hot maps' configuration).

Other variables directly related to the accuracy of the TC system modelling are evaluated, such as temperature drop across the turbine. The same engine and turbocharger limits found during the experiments were reached during the simulations: T3, TC speed, T2 and compressor surge.

As a final validation, two different constant speeds (1500 and 3000 rpm) sudden load demands were modelled. The obtained results in these simulations were in line with the steady states: adiabatic maps performed accurately and it was possible to reproduce the transient without any problem. When trying to reproduce the transients, making usage of the hot maps, the lack of turbocharger efficiency leads to a lack of boost pressure (and air mass flow, injected fuel, torque...).

The aforementioned conclusions are obtained for both analysed VGTs as well as the WG turbocharger, which is the baseline TC of the analysed engine unit.

The main problem which was identified to happen in the adiabatic maps engine simulations is the one that follows: an excess of approximately 10 krpm takes place at the initial very low load steady-state before the transient itself. This error. The reason for the initial TC rpms error is attributed to the lack of TC information in the very low-speed range (<50 krpm). In conclusion, it would be highly interesting to record the TC maps including a wider operative range.

What is more, compressor pressure ratios below 1, take place in the analysed tip-ins. Thus, it would be of high interest to gather information dealing with the compressor operative area below PR=1, to improve the model prediction in such working conditions.

For the rest of the variables, the higher accuracy of the AE maps is remarkable, not only dealing with the impact on the main engine variables, but also with T3 and T4 evolution.

5.5 Model usage for prospective analysis

Having accepted the TC adiabatic and extrapolated maps, as well as having validated the rest of the engine model under several working conditions, several prospective studies are assessed:

- Firstly, a sensibility analysis on the impact of the called "out-of-control" testing variables is developed. These variables are mainly the test cell pressure and temperature, ECU management of the AFR and compressor performance differences.
- Secondly, it is proposed a methodology to consistently analyse the impact of different turbine technologies for gasoline direct injection engines. It is then presented a comparison of WG vs. VGT at several working points. The methodology consists of performing full and partial (throttled) loads under iso-boundary working conditions, guaranteeing (unlike in the experimental campaign) that the engine performance is limited by at least one thermo-mechanical barrier.

  Besides, the simulations were performed at iso-compressor configuration, since the compressor side performance may lead to p3, T2, TC-RPM differences as well as imply some bias in terms of surge limitation. Finally, the proposed methodology guarantees T3 limitation for each turbine technology, unlike in the experimental campaign, where the ECU managed unequally the T3 control. It is then, considered that maximum turbine inlet temperature is lower for the VGT, but at least, the supplier specified limit was achieved.

  The results evidenced that VGT provides a systematically higher torque output and presents fewer limitations in terms of p3. With altitude

working conditions, differences are mode evident in the low-end torque, and slightly lower in the rest of the engine range, since T2 limitation becomes the new barrier, and this does not depend on the turbine technology. However, the systematic lower p3 in the case of the VGT implies an advantage in terms of engine torque.

Under partial loads (throttled conditions), very few differences are identified between turbine technologies.

- Finally, it is made usage of the model to explore the potential benefits of the VGT. For this purpose, the VVT is optimized, with the target of maximizing torque, while keeping the engine working under the desired limits. At this stage, for the sake of readiness and to ease the view of the plots, only VGT-2 was submitted to study. Conclusions here can be divided into several points:

  - Under standard engine operation: lambda is controlled as a function of T3, while VGT position governs boost pressure, it was found that in comparison to the ECU calibration of the VVT, the model tent to increase the valve overlap, as for VGTs. The motivation for this strategy lies in the fact that p2/p3, results in a higher ratio than for the WG, hence, increasing the valve overlap (by retarding EVC and/or advancing IVO) lead to a more favourable configuration regarding engine torque output.

    In all, it was found that when comparing VGT-2 with vs. without VVT optimization, it is expected a benefit up to 19.5Nm in some cases. Furthermore, the BSFC is substantially reduced as far as the engine is operated under a closer-to stoichiometric mixture because of the T3 reduction caused by the VVT management.

  - A second engine study at full load was pretended, but in this case, simultaneously to the VVT optimization, stoichiometric AFR control was imposed. As a consequence, the boost pressure is limited by T3. A severe torque reduction is found in the range where some mixture enrichment was originally required to limit T3.

    It is then concluded that: comparing VGT-2 with vs. without lambda=1, nor VVT optimization, up to 22Nm can be lost. However, up to 27g/kWh of benefit in terms of BSFC can be expected.

    With respect to the WG and the standard T3 control strategy of mixture enrichment, the VGT associated with a lambda=1 (plus

the VVT optimization) shows an improvement over the complete engine range, even for the high-end torque. BSFC figures are also better for the VGT as well.

  - In terms of partial loads, 12 bar of BMEP points' VVT configuration was attempted to be optimized, but the benefits were almost undetectable (below the 0.2%).

- To finish, a methodology to manage the VGT position under transient conditions has been developed. This methodology calls for the validated model and TC maps, to predict the fastest possible engine output, by means of optimizing the VGT mechanism control criteria. As a result, the best experimental transients were matched or even improved for low and high-speed sudden tip-ins. Furthermore, this tool can be taken advantage of, to proceed with further comparison and benchmarking of different TC technologies or units.

  Finally, the physically-based principles of this control, allow for its application in diverse thermochemical systems where transient response optimization is of high interest.

5.6 Future works

As future works, it is proposed several activities that may provide this study with higher consistency and may contribute in the understating on the VGT technology and its impact in modern SI-ICE:

- For the consistency of the study, it would be interesting to repeat this study for at least another WG and VGT turbocharger. This way, conclusions would be backed up by more information and lead to more robust statements.

- Repeat the methodology described for the turbine technologies comparison, but with another compressor unit, again, seeking the robustness of the study.

- Apply the predictive VGT control methodology to the VGT-1 as well as adapt the idea to the WG TC. With this, the control would be further validated and deeper conclusions could be achieved by comparing the

three TC results. In addition, some other studies attempting to improve the transient may be performed, such as optimizing the VVT during transient operation, targeting the fastest possible response.

- Exploring the impact of the VGT in comparison to the WG in the after-treatment warm-up. On the one hand, in the case of the WG technology, during a cold start, most of the exhaust gas bypasses the turbine itself (both: volute and rotor). On the other hand, in the case of the VGT the exhaust gas, necessarily goes across the turbine. The last may present some disadvantages in terms of the 3-way-catalyst light-off temperature achievement for the VGT, since the turbine thermal inertia as well as the turbine pressure ratio, may slow down the thermal transient.

- Increasing the experimental information to feed the NNW for combustion prediction with more variety of working conditions. The same could be applied to the FMEP map.

- Exploring new engine configurations, for example a 3-Cylinder version of the engine, EGR usage for T3 control and BSFC improvement.

- Take advantage of the model to explore other arising TC technologies, such as variable compressor geometries, ball-bearing technologies as well as twin and double-entry VGT configurations for example.

Global bibliography

[1] J. R. Serrano, F. J. Arnau, L. M. García-Cuevas, A. Gómez-Vilanova, S. Guilain, and S. Batard. "A Methodology for Measuring Turbocharger Adiabatic Maps in a Gas-Stand and Its Usage for Calibrating Control Oriented and One-Dimensional Models at Early ICE Design Stages". *Journal of Energy Resources Technology* 143.(4) (2021), pp. 1–11. ISSN: 0195-0738. DOI: 10.1115/1.4048229 (cit. on pp. xii, 25, 105).

[2] J. R. Serrano, P. Piqueras, J. De la Morena, A. Gómez-Vilanova, and S. Guilain. "Methodological analysis of variable geometry turbine technology impact on the performance of highly downsized spark-ignition engines". *Energy* 215 (2021). ISSN: 03605442. DOI: 10.1016/j.energy.2020.119122 (cit. on p. xii).

[3] J. R. Serrano, F. J. Arnau, P. Bares, A. Gomez-Vilanova, J. Garrido-Requena, M. J. Luna-Blanca, and F. J. Contreras-Anguita. "Analysis of a novel concept of 2-stroke rod-less opposed pistons engine (2S-ROPE): Testing, modelling, and forward potential". *Applied Energy* 282.(PA) (2021), p. 116135. ISSN: 03062619. DOI: 10.1016/j.apenergy.2020.116135. URL: https://doi.org/10.1016/j.apenergy.2020.116135 (cit. on pp. xii, 8).

[4] J. R. Serrano, R. Payri, B. Tormos, and A. Gómez-Vilanova. "¿ Por qué es necesario seguir desarrollando motores de combustión para luchar contra la crisis climática global desde la perspectiva del transporte?" *Dyna Ingeniería e Industria* (2019), pp. 48–54. DOI: 10.23800/10329 (cit. on p. xii).

[5] J. R. Serrano, F. J. Arnau, J. De la Morena, A. Gómez-Vilanova, S. Guilain, and S. Batard. "A methodology to calibrate Gas-Dynamic Models of turbocharged petrol egines with variable geometry turbines

and with focus on dynamics prediction during tip-in load transient tests". In: *Volume 8: Industrial and Cogeneration; Manufacturing Materials and Metallurgy; Marine; Microturbines, Turbochargers, and Small Turbomachines*. Vol. 2020-june. American Society of Mechanical Engineers, 2020, pp. 22–26. ISBN: 978-0-7918-8419-5. DOI: 10.1115/GT2020-15169. URL: https://asmedigitalcollection.asme.org/GT/proceedings/GT2020/84195/Virtual,Online/1095133 (cit. on pp. xii, 25, 105).

[6] J. R. Serrano, F. J. Arnau, L. M. G.-C. González, A. Gómez-Vilanova, and S. Guilain. "Impact of a holistic turbocharger model in the prediction of engines performance in transient operation and in steady state with LP-EGR". In: *Volume 2: Emissions Control Systems; Instrumentation, Controls, and Hybrids; Numerical Simulation; Engine Design and Mechanical Development*. San Diego, California, USA: American Society of Mechanical Engineers, 2018, pp. 1–16. ISBN: 978-0-7918-5199-9. DOI: 10.1115/ICEF2018-9550. URL: https://asmedigitalcollection.asme.org/ICEF/proceedings/ICEF2018/51999/SanDiego,California,USA/273145 (cit. on pp. xiii, 34, 36, 51, 64).

[7] J. R. Serrano, F. J. Arnau, L. M. G.-C. González, A. Gómez-Vilanova, and S. Guilain. "An experimental methodology and model for characterizing radial centrifugal compressors of turbocharged engines from diathermal perspective". In: *Advances in Mechanism and Machine Science*. Krakow, Poland: Springer International Publishing, 2019, pp. 883–892. ISBN: 978-3-030-20130-2. DOI: 10.1007/978-3-030-20131-9_88. URL: https://link.springer.com/chapter/10.1007/978-3-030-20131-9_88 (cit. on pp. xiii, 23, 37, 38, 98).

[8] J. R. Serrano. "Imagining the future of the internal combustion engine for ground transport in the current context". *Applied Sciences (Switzerland)* 7.(10) (2017). ISSN: 20763417. DOI: 10.3390/app7101001 (cit. on p. 2).

[9] T. Gnann, P. Plötz, S. Funke, and M. Wietschel. "What is the market potential of plug-in electric vehicles as commercial passenger cars? A case study from Germany". *Transportation Research Part D: Transport and Environment* 37.(2015) (2015), pp. 171–187. ISSN: 13619209. DOI: 10.1016/j.trd.2015.04.015. URL: http://dx.doi.org/10.1016/j.trd.2015.04.015 (cit. on p. 2).

[10] S. Bobeth and I. Kastner. "Buying an electric car: A rational choice or a norm-directed behavior?" *Transportation Research Part F: Traffic Psychology and Behaviour* 73 (2020), pp. 236–258. ISSN: 13698478. DOI: 10.1016/j.trf.2020.06.009. URL: https://doi.org/10.1016/j.trf.2020.06.009 (cit. on p. 2).

[11] C. Brand. "Beyond 'Dieselgate': Implications of unaccounted and future air pollutant emissions and energy use for cars in the United Kingdom". *Energy Policy* 97 (2016), pp. 1–12. ISSN: 03014215. DOI: 10.1016/j.enpol.2016.06.036. URL: http://dx.doi.org/10.1016/j.enpol.2016.06.036 (cit. on p. 2).

[12] M. Neaimeh, S. D. Salisbury, G. A. Hill, P. T. Blythe, D. R. Scoffield, and J. E. Francfort. "Analysing the usage and evidencing the importance of fast chargers for the adoption of battery electric vehicles". *Energy Policy* 108.(December 2016) (2017), pp. 474–486. ISSN: 03014215. DOI: 10.1016/j.enpol.2017.06.033 (cit. on p. 2).

[13] M. E. López-Lambas, A. Monzón, and G. Pieren. "Analysis of using electric car for urban mobility, perceived satisfaction among university users." *Transportation Research Procedia* 27 (2017), pp. 524–530. ISSN: 23521465. DOI: 10.1016/j.trpro.2017.12.132. URL: https://doi.org/10.1016/j.trpro.2017.12.132 (cit. on p. 2).

[14] L. Tang, G. Rizzoni, and A. Cordoba-Arenas. "Battery Life Extending Charging Strategy for Plug-in Hybrid Electric Vehicles and Battery Electric Vehicles". *IFAC-PapersOnLine* 49.(11) (2016), pp. 70–76. ISSN: 24058963. DOI: 10.1016/j.ifacol.2016.08.011. URL: http://dx.doi.org/10.1016/j.ifacol.2016.08.011 (cit. on p. 3).

[15] I. Bloom et al. "An accelerated calendar and cycle life study of Li-ion cells". *Journal of Power Sources* 101.(2) (2001), pp. 238–247. ISSN: 03787753. DOI: 10.1016/S0378-7753(01)00783-2 (cit. on p. 3).

[16] B. Jones, R. J. Elliott, and V. Nguyen-Tien. "The EV revolution: The road ahead for critical raw materials demand". *Applied Energy* 280.(April) (2020), p. 115072. ISSN: 03062619. DOI: 10.1016/j.apenergy.2020.115072. URL: https://doi.org/10.1016/j.apenergy.2020.115072 (cit. on p. 3).

[17] J. Zhao, X. Xi, Q. Na, S. Wang, S. N. Kadry, and P. M. Kumar. "The technological innovation of hybrid and plug-in electric vehicles for environment carbon pollution control". *Environmental Impact Assessment*

Review 86.(October 2020) (2021). ISSN: 01959255. DOI: 10.1016/j.eiar.2020.106506 (cit. on p. 3).

[18] G. Milev, A. Hastings, and A. Al-Habaibeh. "The environmental and financial implications of expanding the use of electric cars - A Case study of Scotland". *Energy and Built Environment* 2.(2) (2021), pp. 204–213. ISSN: 26661233. DOI: 10.1016/j.enbenv.2020.07.005. URL: https://doi.org/10.1016/j.enbenv.2020.07.005 (cit. on p. 3).

[19] H. Ritchie and M. Roser. "Energy". *Our World in Data* (2020). URL: https://ourworldindata.org/energy (cit. on p. 3).

[20] V. Smil. *Energy Transitions: Global and National Perspectives (Expanded and updated edition)*. 2nd ed. Vol. 30. 4. Praeger; 2 edition (Dec 31 2016), 2017, p. 297. ISBN: 144085324X. URL: http://vaclavsmil.com/2016/12/14/energy-transitions-global-and-national-perspectives-second-expanded-and-updated-edition/ (cit. on p. 3).

[21] BP. *Statistical Review of World Energy globally consistent data on world energy markets . and authoritative publications in the field of energy The Statistical Review world of World Energy and data on world energy markets from is The Review has been providing.* Tech. rep. BP, 2020, p. 66. URL: https://www.bp.com/content/dam/bp/business-sites/en/global/corporate/pdfs/energy-economics/statistical-review/bp-stats-review-2020-full-report.pdf (cit. on pp. 3, 8).

[22] C. Buchal, H.-D. Karl, and H.-W. Sinn. "Kohlemotoren, Windmotoren und Dieselmotoren: Was zeigt die CO2-Bilanz?" *ifo Schnelldienst* 8.(April) (2019), pp. 40–54. URL: ifosd-v72-y2019-i08-p40-54.pdf (cit. on p. 4).

[23] Maarten Messagie. "Life Cycle Analysis of the Climate Impact of Electric Vehicles". *Transport and Environment* (2017), p. 14 (cit. on p. 4).

[24] H. Ritchie and M. Roser. "CO and Greenhouse Gas Emissions". *Our World in Dat* (2020). URL: https://ourworldindata.org/co2-and-other-greenhouse-gas-emissions (cit. on p. 5).

[25] R. Kawamoto, H. Mochizuki, Y. Moriguchi, T. Nakano, M. Motohashi, Y. Sakai, and A. Inaba. "Estimation of CO2 Emissions of internal combustion engine vehicle and battery electric vehicle using LCA". *Sus-*

tainability (Switzerland) 11.(9) (2019). ISSN: 20711050. DOI: 10.3390/su11092690 (cit. on pp. 6, 7).

[26] E. Massaguer, A. Massaguer, T. Pujol, M. Comamala, L. Montoro, and J. R. Gonzalez. "Fuel economy analysis under a WLTP cycle on a mid-size vehicle equipped with a thermoelectric energy recovery system". *Energy* 179 (2019), pp. 306–314. ISSN: 03605442. DOI: 10.1016/j.energy.2019.05.004. URL: https://doi.org/10.1016/j.energy.2019.05.004 (cit. on p. 7).

[27] J. Pavlovic, B. Ciuffo, G. Fontaras, V. Valverde, and A. Marotta. "How much difference in type-approval CO2 emissions from passenger cars in Europe can be expected from changing to the new test procedure (NEDC vs. WLTP)?" *Transportation Research Part A: Policy and Practice* 111.(October 2017) (2018), pp. 136–147. ISSN: 09658564. DOI: 10.1016/j.tra.2018.02.002 (cit. on p. 7).

[28] K. Kurtyka and J. Pielecha. "The evaluation of exhaust emission in RDE tests including dynamic driving conditions". *Transportation Research Procedia* 40 (2019), pp. 338–345. ISSN: 23521465. DOI: 10.1016/j.trpro.2019.07.050. URL: https://doi.org/10.1016/j.trpro.2019.07.050 (cit. on p. 7).

[29] R. Suarez-Bertoa, P. Mendoza-Villafuerte, F. Riccobono, M. Vojtisek, M. Pechout, A. Perujo, and C. Astorga. "On-road measurement of NH3 emissions from gasoline and diesel passenger cars during real world driving conditions". *Atmospheric Environment* 166 (2017), pp. 488–497. ISSN: 18732844. DOI: 10.1016/j.atmosenv.2017.07.056. URL: http://dx.doi.org/10.1016/j.atmosenv.2017.07.056 (cit. on p. 7).

[30] A. Zare et al. "Cold-start NOx emissions: Diesel and waste lubricating oil as a fuel additive". *Fuel* 286.(P2) (2021). ISSN: 00162361. DOI: 10.1016/j.fuel.2020.119430. URL: https://doi.org/10.1016/j.fuel.2020.119430 (cit. on p. 7).

[31] J. Pavlovic, G. Fontaras, S. Broekaert, B. Ciuffo, M. A. Ktistakis, and T. Grigoratos. "How accurately can we measure vehicle fuel consumption in real world operation?" *Transportation Research Part D: Transport and Environment* 90.(December 2020) (2021). ISSN: 13619209. DOI: 10.1016/j.trd.2020.102666. URL: https://doi.org/10.1016/j.trd.2020.102666 (cit. on p. 7).

[32] R. Novella, J. Gomez-Soriano, P. J. Martinez-Hernandiz, C. Libert, and F. Rampanarivo. "Improving the performance of the passive pre-chamber ignition concept for spark-ignition engines fueled with natural gas". *Fuel* 290.(November 2020) (2021). ISSN: 00162361. DOI: 10.1016/j.fuel.2020.119971. URL: https://doi.org/10.1016/j.fuel.2020.119971 (cit. on p. 7).

[33] T. Kegl, A. Kovač Kralj, B. Kegl, and M. Kegl. "Nanomaterials as fuel additives in diesel engines: A review of current state, opportunities, and challenges". *Progress in Energy and Combustion Science* 83 (2021). ISSN: 03601285. DOI: 10.1016/j.pecs.2020.100897 (cit. on p. 7).

[34] J. Galindo, J. R. Serrano, L. M. García-Cuevas, and N. Medina. "Using a CFD analysis of the flow capacity in a twin-entry turbine to develop a simplified physics-based model". *Aerospace Science and Technology* 112 (2021). ISSN: 12709638. DOI: 10.1016/j.ast.2021.106623. URL: https://doi.org/10.1016/j.ast.2021.106623 (cit. on p. 7).

[35] F. Dong and K. Yamazaki. "The Pt-Pd alloy catalyst and enhanced catalytic activity for diesel oxidation". *Catalysis Today* (July) (2020). ISSN: 09205861. DOI: 10.1016/j.cattod.2020.08.019. URL: https://doi.org/10.1016/j.cattod.2020.08.019 (cit. on p. 7).

[36] A. F. Abdul-Manan, H. W. Won, Y. Li, S. M. Sarathy, X. Xie, and A. A. Amer. "Bridging the gap in a resource and climate-constrained world with advanced gasoline compression-ignition hybrids". *Applied Energy* 267.(April) (2020), p. 114936. ISSN: 03062619. DOI: 10.1016/j.apenergy.2020.114936. URL: https://doi.org/10.1016/j.apenergy.2020.114936 (cit. on p. 7).

[37] H. Dong, J. Fu, Z. Zhao, Q. Liu, Y. Li, and J. Liu. "A comparative study on the energy flow of a conventional gasoline-powered vehicle and a new dual clutch parallel-series plug-in hybrid electric vehicle under NEDC". *Energy Conversion and Management* 218.(March) (2020). ISSN: 01968904. DOI: 10.1016/j.enconman.2020.113019. URL: https://doi.org/10.1016/j.enconman.2020.113019 (cit. on p. 7).

[38] J. R. Serrano, A. García, J. Monsalve-Serrano, and S. Martínez-Boggio. "High efficiency two stroke opposed piston engine for plug-in hybrid electric vehicle applications: Evaluation under homologation and real driving conditions". *Applied Energy* 282.(October 2020) (2021). ISSN: 03062619. DOI: 10.1016/j.apenergy.2020.116078 (cit. on p. 8).

[39] Q. Tang, J. Fu, J. Liu, B. Boulet, L. Tan, and Z. Zhao. "Comparison and analysis of the effects of various improved turbocharging approaches on gasoline engine transient performances". *Applied Thermal Engineering* 93 (2016), pp. 797–812. ISSN: 13594311. DOI: 10.1016/j.applthermaleng.2015.09.063 (cit. on p. 9).

[40] W. Geng, D. Lou, C. Wang, and T. Zhang. "A cascaded energy management optimization method of multimode power-split hybrid electric vehicles". *Energy* 199 (2020), p. 117224. ISSN: 03605442. DOI: 10.1016/j.energy.2020.117224. URL: https://doi.org/10.1016/j.energy.2020.117224 (cit. on p. 9).

[41] H. Hiereth and P. Prenninger. *Charging the Internal Combustion Engine*. Springer, Vienna, 2007, pp. 1–268. ISBN: 978-3-211-47113-5. DOI: 10.1007/978-3-211-47113-5 (cit. on pp. 9, 32).

[42] A. J. Feneley, A. Pesiridis, and A. M. Andwari. "Variable Geometry Turbocharger Technologies for Exhaust Energy Recovery and Boosting-A Review". *Renewable and Sustainable Energy Reviews* 71.(September 2015) (2017), pp. 959–975. ISSN: 18790690. DOI: 10.1016/j.rser.2016.12.125. URL: http://dx.doi.org/10.1016/j.rser.2016.12.125 (cit. on pp. 10, 32).

[43] N. Brinkert, S. Sumser, S. Weber, K. Fieweger, A. Schulz, and H.-J. Bauer. "Understanding the Twin Scroll Turbine: Flow Similarity". *Journal of Turbomachinery* 135.(2) (2012), p. 021039. ISSN: 0889-504X. DOI: 10.1115/1.4006607 (cit. on p. 10).

[44] Y. Mingyang, M. botas Ricardo, D. Kangyao, Z. Yangjun, and Z. Xinqian. "Unsteady influence of Self Recirculation Casing Treatment (SRCT) on high pressure ratio centrifugal compressor". *International Journal of Heat and Fluid Flow* 58 (2016), pp. 19–29. ISSN: 0142727X. DOI: 10.1016/j.ijheatfluidflow.2015.12.004 (cit. on p. 10).

[45] D. Zeppei, S. Koch, and A. Rohi. "Ball Bearing Technology for Passenger Car Turbochargers". *MTZ worldwide* 77.(11) (2016), pp. 26–31. DOI: 10.1007/s38313-016-0109-z (cit. on pp. 10, 31).

[46] S. Rajoo, A. Romagnoli, and R. F. Martinez-Botas. "Unsteady performance analysis of a twin-entry variable geometry turbocharger turbine". *Energy* 38.(1) (2012), pp. 176–189. ISSN: 03605442. DOI: 10.1016/j.energy.2011.12.017. URL: http://dx.doi.org/10.1016/j.energy.2011.12.017 (cit. on p. 10).

[47] B. Lee, D. Jung, D. Assanis, and Z. Filipi. "Dual-stage turbocharger matching and boost control options". In: *Proceedings of the Spring Technical Conference of the ASME Internal Combustion Engine Division*. January. 2008, pp. 267–277. ISBN: 0791848132. DOI: 10.1115/ICES2008-1692 (cit. on p. 10).

[48] H. Dong, Z. Zhao, J. Fu, J. Liu, J. Li, K. Liang, and Q. Zhou. "Experiment and simulation investigation on energy management of a gasoline vehicle and hybrid turbocharger optimization based on equivalent consumption minimization strategy". *Energy Conversion and Management* 226.(August) (2020). ISSN: 01968904. DOI: 10.1016/j.enconman.2020.113518. URL: https://doi.org/10.1016/j.enconman.2020.113518 (cit. on p. 10).

[49] Z. Ding, W. Zhuge, Y. Zhang, H. Chen, R. Martinez-Botas, and M. Yang. "A one-dimensional unsteady performance model for turbocharger turbines". *Energy* 132 (2017), pp. 341–355. ISSN: 03605442. DOI: 10.1016/j.energy.2017.04.154. URL: http://dx.doi.org/10.1016/j.energy.2017.04.154 (cit. on pp. 20, 32).

[50] F. Bozza, V. De Bellis, and L. Teodosio. "Potentials of cooled EGR and water injection for knock resistance and fuel consumption improvements of gasoline engines". *Applied Energy* 169 (2016), pp. 112–125. ISSN: 03062619. DOI: 10.1016/j.apenergy.2016.01.129. URL: http://dx.doi.org/10.1016/j.apenergy.2016.01.129 (cit. on p. 20).

[51] O. R. Sandoval, M. V. Fonda, V. R. Roso, R. B. R. da Costa, R. M. Valle, and J. G. Baêta. "Computational technique for turbocharger transient characterization using real driving conditions data". *Energy* 186 (2019). ISSN: 03605442. DOI: 10.1016/j.energy.2019.07.152 (cit. on p. 20).

[52] Society of Automotive Engineers. *Turbocharger Gas Stand Test Code - SAE Standards*. 1995. DOI: 10.4271/J1826_199503. URL: http://standards.sae.org/wip/j1826/ (cit. on pp. 21, 22, 84, 110).

[53] SAE J1723. *Supercharger testing standard*. 1995. DOI: J1723_199508. URL: https://saemobilus.sae.org/content/J1723_199508 (cit. on pp. 21, 89, 91, 105).

[54] B. Sirakov and M. Casey. "Evaluation of Heat Transfer Effects on Turbocharger Performance". *Journal of Turbomachinery* 135.(2) (2012). ISSN: 0889504X. DOI: 10.1115/1.4006608 (cit. on pp. 21, 97).

[55] A. Romagnoli and R. Martinez-Botas. "Heat transfer analysis in a turbocharger turbine: An experimental and computational evaluation". *Applied Thermal Engineering* 38 (2012), pp. 58–77. ISSN: 13594311. DOI: 10.1016/j.applthermaleng.2011.12.022. URL: http://dx.doi.org/10.1016/j.applthermaleng.2011.12.022 (cit. on pp. 21, 97).

[56] G. Tanda, S. Marelli, G. Marmorato, and M. Capobianco. "An experimental investigation of internal heat transfer in an automotive turbocharger compressor". *Applied Energy* 193 (2017), pp. 531–539. ISSN: 03062619. DOI: 10.1016/j.apenergy.2017.02.053. URL: http://dx.doi.org/10.1016/j.apenergy.2017.02.053 (cit. on p. 21).

[57] R. D. Burke, C. R. Vagg, D. Chalet, and P. Chesse. "Heat transfer in turbocharger turbines under steady, pulsating and transient conditions". *International Journal of Heat and Fluid Flow* 52 (2015), pp. 185–197. ISSN: 0142727X. DOI: 10.1016/j.ijheatfluidflow.2015.01.004. URL: http://dx.doi.org/10.1016/j.ijheatfluidflow.2015.01.004 (cit. on p. 21).

[58] G. Salameh, G. Goumy, and P. Chesse. "Water cooled turbocharger heat transfer model initialization: Turbine and compressor quasi-adiabatic maps generation". *Applied Thermal Engineering* 185.(June 2020) (2021). ISSN: 13594311. DOI: 10.1016/j.applthermaleng.2020.116430. URL: https://doi.org/10.1016/j.applthermaleng.2020.116430 (cit. on p. 21).

[59] S. Marelli, G. Marmorato, M. Capobianco, and A. Rinaldi. "Heat Transfer Effects on Performance Map of a Turbocharger Compressor for Automotive Application". In: *SAE Technical Papers*. Vol. 2015-April. April. 2015. DOI: 10.4271/2015-01-1287. URL: http://papers.sae.org/2015-01-1287/ (cit. on pp. 22, 84, 97).

[60] L. Huang, C. Ma, Y. Li, J. Gao, and M. Qi. "Applying neural networks (NN) to the improvement of gasoline turbocharger heat transfer modeling". *Applied Thermal Engineering* 141.(November 2017) (2018), pp. 1080–1091. ISSN: 13594311. DOI: 10.1016/j.applthermaleng.2018.06.062 (cit. on p. 22).

[61] J. R. Serrano, P. Olmeda, F. J. Arnau, M. A. Reyes-Belmonte, and H. Tartoussi. "A study on the internal convection in small turbochargers. Proposal of heat transfer convective coefficients". *Applied Thermal En-*

gineering 89 (2015), pp. 587–599. ISSN: 13594311. DOI: 10.1016/j.applthermaleng.2015.06.053 (cit. on pp. 23, 84).

[62] J. R. Serrano, P. Olmeda, F. J. Arnau, A. Dombrovsky, and L. Smith. "Turbocharger heat transfer and mechanical losses influence in predicting engines performance by using one-dimensional simulation codes". *Energy* 86 (2015), pp. 204–218. ISSN: 03605442. DOI: 10.1016/j.energy.2015.03.130 (cit. on pp. 23, 25, 39, 51).

[63] F. Payri, P. Olmeda, F. J. Arnau, A. Dombrovsky, and L. Smith. "External heat losses in small turbochargers: Model and experiments". *Energy* 71 (2014), pp. 534–546. ISSN: 03605442. DOI: 10.1016/j.energy.2014.04.096. URL: http://dx.doi.org/10.1016/j.energy.2014.04.096 (cit. on p. 23).

[64] J. R. Serrano, P. Olmeda, A. Páez, and F. Vidal. "An experimental procedure to determine heat transfer properties of turbochargers". *Measurement Science and Technology* 21.(3) (2010). ISSN: 13616501. DOI: 10.1088/0957-0233/21/3/035109 (cit. on p. 23).

[65] A. Romagnoli, A. Manivannan, S. Rajoo, M. S. Chiong, A. Feneley, A. Pesiridis, and R. F. Martinez-Botas. *A review of heat transfer in turbochargers*. 2017. DOI: 10.1016/j.rser.2017.04.119. URL: http://dx.doi.org/10.1016/j.rser.2017.04.119 (cit. on p. 25).

[66] J. R. Serrano, A. Tiseira, L. M. García-Cuevas, L. B. Inhestern, and H. Tartoussi. "Radial turbine performance measurement under extreme off-design conditions". *Energy* 125 (2017), pp. 72–84. ISSN: 03605442. DOI: 10.1016/j.energy.2017.02.118 (cit. on p. 27).

[67] Z. Liu and C. Copeland. "New method for mapping radial turbines exposed to pulsating flows". *Energy* 162 (2018), pp. 1205–1222. ISSN: 03605442. DOI: 10.1016/j.energy.2018.08.107. URL: https://doi.org/10.1016/j.energy.2018.08.107 (cit. on p. 27).

[68] G. Salameh, P. Chesse, and D. Chalet. "Mass flow extrapolation model for automotive turbine and confrontation to experiments". *Energy* 167 (2019), pp. 325–336. ISSN: 03605442. DOI: 10.1016/j.energy.2018.10.183. URL: https://doi.org/10.1016/j.energy.2018.10.183 (cit. on p. 27).

[69] S. Zhu, K. Deng, and S. Liu. "Modeling and extrapolating mass flow characteristics of a radial turbocharger turbine". *Energy* 87 (2015), pp. 628–637. ISSN: 03605442. DOI: 10.1016/j.energy.2015.05.032. URL: http://dx.doi.org/10.1016/j.energy.2015.05.032 (cit. on pp. 27, 98).

[70] F. Payri, J. R. Serrano, P. Fajardo, M. A. Reyes-Belmonte, and R. Gozalbo-Belles. "A physically based methodology to extrapolate performance maps of radial turbines". *Energy Conversion and Management* 55 (2012), pp. 149–163. ISSN: 01968904. DOI: 10.1016/j.enconman.2011.11.003 (cit. on pp. 27, 98).

[71] J. R. Serrano, F. J. Arnau, L. M. García-Cuevas, and L. B. Inhestern. "An innovative losses model for efficiency map fitting of vaneless and variable vaned radial turbines extrapolating towards extreme off-design conditions". *Energy* 180 (2019), pp. 626–639. ISSN: 03605442. DOI: 10.1016/j.energy.2019.05.062 (cit. on p. 27).

[72] J. R. Serrano, A. Tiseira, L. M. García-Cuevas, and T. R. Usaquén. "Adaptation of a 1-D tool to study transient thermal in turbocharger bearing housing". *Applied Thermal Engineering* 134.(June 2017) (2018), pp. 564–575. ISSN: 13594311. DOI: 10.1016/j.applthermaleng.2018.01.085. URL: https://doi.org/10.1016/j.applthermaleng.2018.01.085 (cit. on p. 27).

[73] J. Galindo, R. Navarro, L. M. García-Cuevas, D. Tarí, H. Tartoussi, and S. Guilain. "A zonal approach for estimating pressure ratio at compressor extreme off-design conditions". *International Journal of Engine Research* 20.(4) (2019), pp. 393–404. ISSN: 20413149. DOI: 10.1177/1468087418754899 (cit. on p. 27).

[74] J. Galindo, A. Tiseira, R. Navarro, D. Tarí, H. Tartoussi, and S. Guilain. "Compressor Efficiency Extrapolation for 0D-1D Engine Simulations". In: *SAE Technical Papers*. 2016. DOI: 10.4271/2016-01-0554 (cit. on pp. 27, 98).

[75] J. R. Serrano, P. Olmeda, A. Tiseira, L. M. García-Cuevas, and A. Lefebvre. "Theoretical and experimental study of mechanical losses inautomotive turbochargers". *Energy* 55 (2013), pp. 888–898. ISSN: 03605442. DOI: 10.1016/j.energy.2013.04.042. URL: http://dx.doi.org/10.1016/j.energy.2013.04.042 (cit. on pp. 30, 84, 97).

[76] J. R. Serrano, P. Olmeda, A. Tiseira, L. M. García-Cuevas, and A. Lefebvre. "Importance of Mechanical Losses Modeling in the Performance Prediction of Radial Turbochargers under Pulsating Flow Conditions". In: *SAE International Journal of Engines*. Vol. 6. 2. 2013, pp. 729–738. DOI: 10.4271/2013-01-0577. URL: http://saeeng.saejournals.org/content/6/2/729\%5Cnhttp://saeeng.saejournals.org/content/6/2/729.abstract (cit. on pp. 30, 84, 97).

[77] M. Deligant, P. Podevin, and G. Descombes. "Experimental identification of turbocharger mechanical friction losses". *Energy* 39.(1) (2012), pp. 388–394. ISSN: 03605442. DOI: 10.1016/j.energy.2011.12.049. URL: http://dx.doi.org/10.1016/j.energy.2011.12.049 (cit. on p. 30).

[78] P. Novotný, M. Jonák, and J. Vacula. "Evolutionary Optimisation of the Thrust Bearing Considering Multiple Operating Conditions in Turbomachinery". *International Journal of Mechanical Sciences* 195.(September 2020) (2021). ISSN: 00207403. DOI: 10.1016/j.ijmecsci.2020.106240 (cit. on p. 30).

[79] P. Novotný and J. Hrabovský. "Efficient computational modelling of low loaded bearings of turbocharger rotors". *International Journal of Mechanical Sciences* 174.(September 2019) (2020). ISSN: 00207403. DOI: 10.1016/j.ijmecsci.2020.105505 (cit. on p. 30).

[80] L. Smolík and Š. Dyk. "Towards efficient and vibration-reducing full-floating ring bearings in turbochargers". *International Journal of Mechanical Sciences* 175.(January) (2020). ISSN: 00207403. DOI: 10.1016/j.ijmecsci.2020.105516 (cit. on p. 30).

[81] A. Torregrosa, F. Arnau, P. Piqueras, M. Reyes-Belmonte, M. Knutsson, and J. Lennblad. "Acoustic one-dimensional compressor model for integration in a gas-dynamic code". In: *SAE Technical Papers*. 2012. DOI: 10.4271/2012-01-0834. URL: http://papers.sae.org/2012-01-0834/ (cit. on p. 32).

[82] J. Galindo, P. Fajardo, R. Navarro, and L. M. García-Cuevas. "Characterization of a radial turbocharger turbine in pulsating flow by means of CFD and its application to engine modeling". *Applied Energy* 103 (2013), pp. 116–127. ISSN: 03062619. DOI: 10.1016/j.apenergy.2012.09.013. URL: http://dx.doi.org/10.1016/j.apenergy.2012.09.013 (cit. on p. 32).

[83] J. Galindo, F. J. Arnau, L. M. García-Cuevas, and P. Soler. "Experimental validation of a quasi-two-dimensional radial turbine model". *International Journal of Engine Research* 21.(6) (2020), pp. 915–926. ISSN: 20413149. DOI: 10.1177/1468087418788502 (cit. on p. 32).

[84] K. Song, B. Zhao, H. Sun, and W. Yi. "A physics-based zero-dimensional model for the mass flow rate of a turbocharger compressor with uniform/distorted inlet condition". *International Journal of Engine Research* 20.(6) (2019), pp. 624–639. ISSN: 20413149. DOI: 10.1177/1468087418773673 (cit. on p. 32).

[85] N. Watson and M. Janota. *Turbocharging the Internal Combustion Engine*. Basingstok. Macmillan, 1982. ISBN: 0333242904 (cit. on p. 32).

[86] M. Sjerić, I. Taritaš, R. Tomić, M. Blažić, D. Kozarac, and Z. Lulić. "Efficiency improvement of a spark-ignition engine at full load conditions using exhaust gas recirculation and variable geometry turbocharger – Numerical study". *Energy Conversion and Management* 125 (2016), pp. 26–39. ISSN: 01968904. DOI: 10.1016/j.enconman.2016.02.047 (cit. on p. 33).

[87] J. Andersen, E. Karlsson, and A. Gawell. "Variable turbine geometry on SI engines". In: *SAE Technical Papers*. Vol. 2006. 724. 2006, pp. 776–790. DOI: 10.4271/2006-01-0020 (cit. on pp. 33, 158).

[88] K. Shimizu, W. Sato, H. Enomoto, and M. Yashiro. "Torque control of a small gasoline engine with a variable nozzle turbine turbocharger". In: *SAE Technical Papers*. 2009, pp. 1–7 (cit. on p. 33).

[89] M. Noga. "Application of VNT turbocharger in spark ignition engine with additional expansion of exhaust gases". *Tehnicki Vjesnik* 25.(6) (2018), pp. 1575–1580. ISSN: 18486339. DOI: 10.17559/TV-20160211230747 (cit. on p. 33).

[90] H. Tang, C. Copeland, S. Akehurst, C. Brace, P. Davies, L. Pohorelsky, L. Smith, and G. Capon. "A novel predictive semi-physical feed-forward turbocharging system transient control strategy based on mean-value turbocharger model". *International Journal of Engine Research* 18.(8) (2017), pp. 765–775. ISSN: 20413149. DOI: 10.1177/1468087416670052 (cit. on p. 33).

[91] G. Ericsson, H. E. Angstrom, and F. Westin. "Optimizing the transient of an SI-engine equipped with variable cam timing and variable turbine". In: *SAE Technical Papers*. Vol. 3. 1. 2010, pp. 903–915. DOI: 10.4271/2010-01-1233 (cit. on pp. 33, 63, 163, 165).

[92] Y. Wang, G. Conway, J. McDonald, and A. Birckett. "Predictive GT-power simulation for VNT matching to EIVC strategy on a 1.6 L turbocharged gdi engine". In: *SAE Technical Papers*. Vol. 2019-April. April. 2019, pp. 1–12. DOI: 10.4271/2019-01-0192 (cit. on p. 33).

[93] B. Pla, J. De la Morena, P. Bares, and I. Jiménez. "Cycle-to-cycle combustion variability modelling in spark ignited engines for control purposes". *International Journal of Engine Research* 21.(8) (2020), pp. 1398–1411. ISSN: 20413149. DOI: 10.1177/1468087419885754 (cit. on p. 55).

[94] J. R. Serrano, P. Olmeda, F. J. Arnau, A. Dombrovsky, and L. Smith. "Methodology to characterize heat transfer phenomena in small automotive turbochargers: Experiments and modelling based analysis". In: *Proceedings of the ASME Turbo Expo*. Vol. 1B. February. 2014. ISBN: 9780791845585. DOI: 10.1115/GT2014-25179. URL: http://proceedings.asmedigitalcollection.asme.org/proceeding.aspx?doi=10.1115/GT2014-25179 (cit. on pp. 84, 97).

[95] H. Tang, A. Pennycott, S. Akehurst, and C. J. Brace. "A review of the application of variable geometry turbines to the downsized gasoline engine". *International Journal of Engine Research* 16.(6) (2015), pp. 810–825. ISSN: 20413149. DOI: 10.1177/1468087414552289 (cit. on p. 150).

[96] P. Kapoor, A. W. Costall, N. Sakellaridis, J. Hooijer, R. Lammers, H. Tartoussi, and S. Guilain. "Adaptive Turbo Matching: Radial Turbine Design Optimization through 1D Engine Simulations with Meanline Model in-the-Loop". *SAE Technical Papers* 2018-April (2018), pp. 1–15. ISSN: 01487191. DOI: 10.4271/2018-01-0974 (cit. on p. 162).

[97] J. M. Luján, H. Climent, R. Novella, and M. E. Rivas-Perea. "Influence of a low pressure EGR loop on a gasoline turbocharged direct injection engine". *Applied Thermal Engineering* 89 (2015), pp. 432–443. ISSN: 13594311. DOI: 10.1016/j.applthermaleng.2015.06.039 (cit. on p. 176).

[98] T. Alger, T. Chauvet, and Z. Dimitrova. "Synergies between high EGR operation and GDI systems". *SAE International Journal of Engines* 1.(1) (2009), pp. 101–114. ISSN: 19463936. DOI: 10.4271/2008-01-0134 (cit. on p. 176).

[99] T. Li, T. Yin, and B. Wang. "Anatomy of the cooled EGR effects on soot emission reduction in boosted spark-ignited direct-injection engines". *Applied Energy* 190 (2017), pp. 43–56. ISSN: 03062619. DOI: 10.1016/j.apenergy.2016.12.105. URL: http://dx.doi.org/10.1016/j.apenergy.2016.12.105 (cit. on p. 176).

[100] H. Wei, T. Zhu, G. Shu, L. Tan, and Y. Wang. "Gasoline engine exhaust gas recirculation - A review". *Applied Energy* 99 (2012), pp. 534–544. ISSN: 03062619. DOI: 10.1016/j.apenergy.2012.05.011. URL: http://dx.doi.org/10.1016/j.apenergy.2012.05.011 (cit. on p. 176).

"Mathematics is the language in which God has written the Universe."

Galileo Galilei.